Spin Correlations in Top Quark Production at e^+e^- Linear Colliders

Takashi Nasuno

Dept. of Physics, Hiroshima University
Higashi-Hiroshima 739-8526, Japan

March, 1999*, Thesis*

ACKNOWLEDGMENT

It is a great pleasure to thank the many people who have contributed to the completion of this thesis, through their knowledge, guidance, support and friendship. First of all, I would like to thank my thesis supervisor, Jiro Kodaira, for many discussions, his assistances and enlightening comments on my works over years. My understanding of physics have been improved by his enthusiasm and practical viewpoints. Moreover he gave me many chances to meet impressive physicists and opportunities to discuss with them. First, thanks to his supports, I could take part in the 24th SLAC Summer Institute (SSI) on Particle Physics, August 19-30, 1996, where I studied new aspects of physics and felt the passion of many physicists. After SSI, I had a nice meet with Stephen Parke and got a chance to collaborate with him. Second, the International Symposium on "QCD Corrections and New Physics", he held at Hiroshima in 1997, led me to deep understanding of physics which became a base of this thesis. Again I would like to express my heartfelt thanks to Jiro Kodaira.

Stephen Parke constantly stimulated my interest, not only in top quark physics, but in many other branches of physics, and kindly provided me with modern calculations of the polarized $t\bar{t}$ cross-sections. His supports are greatly acknowledged from my heart.

I wish to express my gratitude to Haruo Ui, Taizo Muta and Michihiro Hirata for many valuable instructions. Their supports encouraged me and made me possible to complete this thesis. I also benefited from discussions with Tetsuya Onogi, Takuya Morozumi, Yuichiro Kiyo and Michihiro Hori. Tetsuya Onogi and Takuya Morozumi helped me understand the implications of top quark physics. And I would like to thank Yuichiro Kiyo and Michihiro Hori for their friendship and the countless discussions till far into the night. They were good collaborators for me to get a new understanding of physics. I also thank Hideko Masuda and Mami Kohno for their assistances. Without their help, I probably would not spend a good time in Hiroshima University. I would like to express my deepest gratitude to Tsuneo Uematsu in Kyoto University and Kazuhiro Tanaka in Juntendo University. I was always encouraged by their physics and the discussion with them.

Finally in my personal side, I would like to thank my parents and my sister for their

continuous supports and encouragements which made me possible to continue my researches.

ABSTRACT

The object of this thesis is to study the spin-spin correlations for top quark productions and their decay at polarized e^+e^- linear colliders. For the analyses of the spin-spin correlations in top quark production, we introduce a generic spin basis and show which spin basis is the most optimal. We discuss the spin-angular correlations for the top quark decay, and demonstrate that the directions of electro-weak decay products of polarized top quarks are strongly correlated to the top quark spin. We also explain how to measure the top quark spin using decay products. The spin correlations using the generic spin basis are extensively studied at the next to leading order of QCD for top quark productions at e^+e^- colliders. The radiative corrections induce an anomalous γ/Z magnetic moment for the top quarks and allow for real gluon emissions. Therefore they might change the leading order analyses. We show that higher order effects on the top quark spin orientation are very small. The final results are that the top (or anti-top) quarks are produced in an essentially unique spin configuration for a particular spin basis even after including the $\mathcal{O}(\alpha_s)$ QCD corrections. Our results imply that measuring the spin correlation for top quarks is very promising to reveal new aspects of the Standard Model, as well as new physics beyond the Standard Model.

"Truth emerges more readily from error than confusion."

-Francis Bacon-

Contents

List of Figures

List of Tables

Chapter 1

Introduction

High-energy e^+e^- colliders have been essential instruments to search for the fundamental constituents of matter and their interactions. Merged with the experimental observations at hadron colliders, the structures and properties of the "fundamental"particles are adequately described by the Standard Model. The matter particles, which are leptons and quarks, can be classified into three generations with identical symmetries. It has been known that the electro-weak and strong forces are described by gauge field theories. The strong force is described by the $\mathrm{SU}(3)_c$ gauge theory, which is called Quantum Chromo Dynamics (QCD) [1]. The vector bosons of this model are grouped into eight colored massless gluons which mediate the strong interactions. The QCD has only one arbitrary or free parameter, Λ_{QCD}. Nevertheless, it explains, all hadronic dynamics including confinement, asymptotic freedom, nucleon structure, and baryon and meson spectroscopy. On the other hand, the electro-weak theory has many arbitrary parameters and is described with the gauge group of $\mathrm{SU}(2)_L \otimes \mathrm{U}(1)_Y$ [2], where $\mathrm{SU}(2)_L$ is the weak isospin group, acting on left-handed fermions, and $\mathrm{U}(1)_Y$ is the hypercharge group. At "low" energy (at the scale $\sim$ 250 GeV), the $\mathrm{SU}(2)_L \otimes \mathrm{U}(1)_Y$ symmetry is spontaneously broken. This mechanism is referred to as Higgs mechanism [3], which induces mass of gauge bosons, $W^{\pm}, Z$, and other fermions. The heavy gauge bosons, $W^{\pm}, Z$, were discovered at CERN in the middle of 1980's. Thanks to these impressive successes, the gauge theory with the group $\mathrm{SU}(3)_c \otimes \mathrm{SU}(2)_L \otimes \mathrm{U}(1)_Y$ has been called the "Standard Model".

The Standard Model has been tested and checked through precision experiments with remarkable accuracy during the past few decades. With those numerous data, the Standard Model has been successful in describing the properties of particles and the structure of their basic interactions. Despite this success, however, the Standard Model has not been considered as the final theory of nature. As a matter of fact, the Higgs mechanism is still hypothetical and

has not been established experimentally. The properties of the latest member of the matter, top quark, have not yet been fully revealed. To make a further progress and to step on to a new stage, we must investigate both the "strengths" and the "weaknesses" of the Standard Model and must understand it in detail. There are two complementary and sometimes mutually related strategies to explore the new aspects of the Standard Model and to reveal signals of new physics beyond it. The first is to look for "new" phenomena at high energy collider facilities, the e^+e^- colliders LEP II, the ep colliders HERA, $p\bar{p}$ colliders TEVATRON, the pp colliders LHC and e^+e^- linear colliders JLC. The high energy colliders bring us a good chance to have a clue to new physics. The second is to utilize good probes, which might be Higgs particle and top quarks. Precision studies of these heavy particles also may reveal new aspects of the Standard Model and clues to the physics beyond the Standard Model, since these particles are considered to have important information on the mechanism of breaking of the electro-weak symmetry. In this thesis, we will focus on the top quark as a fascinating probe. A high energy e^+e^- linear collider provides a very impressive tool to carry out detailed studies of top quarks.

The first stage of top quark physics was opened with its discovery at FNAL [4, 5]. The top quark with a very large mass 173.8 ± 5.2 GeV [6] makes us expect that the top quark plays a special role in particle physics. It might contain a hint of new physics beyond the Standard Model. The presence of Higgs boson and its Yukawa coupling to fermions play a fundamental role in the Standard Model, and the Yukawa coupling is proportion to the fermion mass. Therefore the top quark will likely offer a possibility for its direct measurement, which has not yet been established experimentally. Among many other possibilities, for instance, T or CP violation in the top quark sector and the possibility of the presence of anomalous couplings have been discussed in many papers [7]. The very heavy top quark will provide us with a unique opportunity to understand nature deeply.

Now, the following fact is typical to heavy top quarks that the top quark rapidly decays through electro-weak interactions before hadronization effects [8, 9] come in. Therefore there are significant angular correlation between the decay products of the top quark and the spin of the top quark [10]. This implies that if the produced top and anti-top quarks correlate their spins, there will be a sizable angular correlations between all the particles, both incoming and outgoing, in these events. There are many papers on the angular correlations for top quark events [11, 12] produced at both e^+e^- colliders [13] and hadron colliders [14]. In most of these works, the top quark spin is decomposed in the helicity basis. For ultra-relativistic particles,

this approach is appropriate. However, in general, the helicity basis is not a unique choice for massive particles. It may depend on the energy (speed) of the produced quark which spin basis is the most optimal to study the spin correlations. Mahlon and Parke [15] have considered various decompositions of the top quark spin which result in a large asymmetry at hadron colliders. Parke and Shadmi [16] extended this study to the e^+e^- annihilation process at the leading order in the perturbation theory and found that the "off-diagonal" basis is the most efficient decomposition of the top (anti-top) quark spin. In this spin basis, the top quarks are produced in an essentially unique spin configuration. This result is of great interest and importance from both theoretical and phenomenological viewpoints. However, it is of crucial importance to estimate the radiative corrections to this process which are dominated by QCD. The radiative corrections, in general, add two effects to the leading order analysis: the first is that a new vertex structure (anomalous γ/Z magnetic moment) is induced by the loop corrections to the tree level vertex, the second is that a (hard) real gluon emission from the final quarks can flip the spin and change the momentum of parent quarks. Therefore, compared to the radiative corrections to physical quantities which are spin independent, it is possible that spin-dependent quantities may be particularly sensitive to the effects of QCD radiative corrections. The analytical study of QCD radiative corrections to heavy quark production was pioneered in Ref. [17] (see *e.g.* Ref. [18] for a recent article). Polarized heavy quark productions, in helicity basis, have been calculated by many authors[19, 20]. Recently, the polarized cross-sections for not only longitudinally but also transversely polarized heavy quarks have been investigated [21] at the next to leading order of QCD corrections. Meanwhile, polarization phenomena in top quark productions near threshold have also been analyzed [22].

The main part of this thesis is a discussion on the polarized top quark production at the QCD one-loop level. We focus on the issue of what is the optimal decomposition of the top quark spin for e^+e^- colliders. (The physics of top quark production at muon colliders and e^+e^- colliders is identical provided the energy is not tuned to the Higgs boson resonance.) We calculate the cross-section in a "generic" spin basis which includes the helicity basis as a special case.

The thesis is organized as follows. In Section 2, we review some techniques for calculating helicity amplitudes, since these techniques are useful and effective to investigate, in particular, the spin dependent amplitudes. One can see that these calculational methods are indispensable techniques to analyze the spin correlations. In Section 3, we discuss the spin-spin correlations in top quark pair productions and the spin-angular correlations in the decay process of top

quarks at the leading order in perturbation theory. The measurement of top quark spin is also discussed. We demonstrate that top quark pairs are produced in an essentially unique spin configuration in polarized e^+e^- linear colliders, and that the angular distribution of top quark decay products is strongly correlated to the direction of top quark spin axis. In section 4, we examine the QCD corrections to the polarized top (anti-top) quark production, and present our analytic calculations of one-loop corrections to the polarized top quark production in a generic spin basis. We also give the numerical results both in the helicity, beam-line and the off-diagonal bases. We compare the full one-loop results with those in the leading order and soft gluon approximations. The final chapter contains a summary. In Appendices, the notations, conventions and some useful formulae for the helicity amplitude we use in this thesis are included. The phase space integrals which are needed in Section 4 are summarized. The unpolarized total cross-section for top pair production, using our results, is also given as a cross check.

Chapter 2

Spinor Helicity Method

With the progress of precision in experimental data, we must calculate higher order Feynman diagrams in the perturbation theory in order to refine the theoretical predictions. For scattering process with more than two particles in the final state, the spin projection operator methods quickly become unwieldy. This difficulty is overcome by employing the spinor helicity method, which is a powerful technique for computing helicity amplitudes for multi particle process involving spin 1/2 and spin 1 particles.

The technique of helicity amplitudes in the high-energy limit (which corresponds to massless limit) was pioneered in the paper by Bjorken and Chen [23], and later was extended to the massless gauge theories by the CALKUL collaboration [24]. Xu, Zhang and Chang [25] had proposed a new definition of the polarization vector of the gauge boson based on the helicity spinor basis and the decomposition of amplitudes into gauge-invariant subsets. They generalized the helicity amplitude techniques developed by the CALKUL collaboration to the non-abelian case. Meanwhile, a technique [26], which utilizes the super symmetry connecting vector particle scattering with scalar particle scattering, was suggested, and the combined use of these techniques was shown to be more advantageous by Parke and Taylor. The helicity amplitude method, which is useful in the calculation of cross-sections for processes with many final state particles, is reviewed in the article [27] by Parke and Mangano. After these developments, these techniques for massless particles were extended to the case of massive particles by Kleiss and Stirling and other authors [28]. This useful extension makes us possible to analyze and calculate the processes involving massive particles more easily.

These techniques enable us to obtain easily analytically compact expressions for various amplitudes, so they are extremely useful for the analysis of the process we are interested in. We use these techniques for top quark pair productions and their decay. In this chapter, we

present a brief introduction to the spinor helicity method following Ref. [27].

2.1 Massless Spinor States

In this section, we derive and summarize expressions for the spinor products [25, 27, 29] for massless fermions. The spinor helicity method utilizing the spinor products is extremely efficient for QCD with only massless quarks, and the massless case is a basis for the extension to the massive spinor case. We demonstrate an example using this technique in the next section. The extension of this technique to massive fermions is discussed in Sec. 2.3.

We will begin with massless helicity spinors and denote their chiral projection by,

$$\begin{array}{rcl} |p\pm\rangle & \equiv & u_\pm(p) = v_\mp(p) = \frac{1\pm\gamma_5}{2}u(p), \\ \langle p\pm| & \equiv & \bar{u}_\pm(p) = \bar{v}_\mp(p). \end{array} \tag{2.1}$$

These massless spinors have the following properties.

1. Dirac Equation:

$$\hat{p}\,|p\pm\rangle = \langle p\pm|\,\hat{p} = 0, (\hat{p} \equiv \gamma^\mu p_\mu). \tag{2.2}$$

2. Chirality Conditions:

$$\begin{array}{rcl} (1\pm\gamma_5)\,|p\mp\rangle & = & 0, \\ \langle p\pm|\,(1\pm\gamma_5) & = & 0. \end{array} \tag{2.3}$$

3. Normalization and Completeness:

$$\langle p\pm|\,\gamma^\mu\,|p\pm\rangle = 2p^\mu, \tag{2.4}$$

$$|p+\rangle\langle p+| + |p-\rangle\langle p-| = \hat{p}. \tag{2.5}$$

4. Massless Spinor Relations:

$$|p\pm\rangle\langle p\pm| = \frac{1\pm\gamma_5}{2}\hat{p}, \tag{2.6}$$

$$\langle p+|q+\rangle = \langle p-|q-\rangle = 0, \tag{2.7}$$

$$\langle p-|q+\rangle = -\langle q-|p+\rangle, \tag{2.8}$$

$$\langle p-|p+\rangle = \langle p+|p-\rangle = 0. \tag{2.9}$$

5. Chisholm Identity:

$$\langle p\pm|\,\gamma^\mu\,|q\pm\rangle\,[\gamma_\mu] = 2[|q\pm\rangle\langle p\pm| + |p\mp\rangle\langle q\mp|]. \tag{2.10}$$

Equations (2.7)∼(2.9) show that most of spinor products vanish, and only a few spinor products become non-zero. Therefore, it is convenient to introduce the following notation for spinor products:

$$\begin{array}{rcrcl} \langle pq\rangle & \equiv & \langle p-|q+\rangle & = & -\langle qp\rangle\,, \\ [pq] & \equiv & \langle p+|q-\rangle & = & -[qp]\,. \end{array} \tag{2.11}$$

These spinor products satisfy

$$\langle pq\rangle^* = -[pq]\,, \tag{2.12}$$

where all spinors are assumed to have positive energy. The squared spinor products become

$$|\langle pq\rangle|^2 \;=\; |[pq]|^2 \;=\; 2p\cdot q. \tag{2.13}$$

The spinor product $\langle p\ q\rangle$ plays a fundamental role in this paper. Other properties of the spinor products are summarized in the Appendix D.

2.2 Circular Polarizations of Massless Bosons

We shall explain how to construct the polarization vector of massless gauge bosons by employing the spinor techniques [24, 27, 29]. The polarization vectors, $\varepsilon^\mu_\pm(k)$, corresponding to states of definite helicity, satisfy,

$$\varepsilon_\pm(k)\cdot k \;=\; 0, \tag{2.14}$$

$$\varepsilon^\mu_\mp(k) \;=\; [\varepsilon^\mu_\pm(k)]^*, \tag{2.15}$$

$$\varepsilon_\lambda(k)\cdot\varepsilon^*_{\lambda'}(k) \;=\; -\delta_{\lambda\lambda'}, \tag{2.16}$$

where k^μ is the momentum of massless gauge boson, and the subscripts λ, λ' denote the helicity states ($\pm$).

In the four dimensions, the physical Hilbert space of massless vector is isomorphic to the physical Hilbert space of massless spinor, since they both lie in the one-dimensional representations of SO(2). This isomorphism is realized through a linear transformation which relates the vector states to like-helicity fermion states:

$$\begin{array}{rcl} \varepsilon^\mu_-(k) & = & N\,\langle k+|\,\gamma^\mu\,|p+\rangle\,, \\ \varepsilon^\mu_+(k) & = & N^*\,\langle k-|\,\gamma^\mu\,|p-\rangle\,, \end{array} \tag{2.17}$$

where $\varepsilon^\pm_\mu(k)$ is the polarization vector of an incoming massless gauge boson, the momentum p is a light-like arbitrary reference momentum and assumed to be not parallel to the momentum

k. The factor N is a normalization constant. The factor N is determined from Eqn.(2.16):

$$\varepsilon^-(k)\cdot\varepsilon^+(k) \;=\; -2|N|^2 p\cdot k = -1. \tag{2.18}$$

Therefore, the polarization vectors of massless gauge bosons are given by

$$\varepsilon^\mu_-(k) \;=\; \frac{e^{i\phi(k,p)}}{\sqrt{2}}\frac{\langle k+|\,\gamma^\mu\,|p+\rangle}{\langle pk\rangle}, \tag{2.19}$$

$$\varepsilon^\mu_+(k) \;=\; -\frac{e^{-i\phi(k,p)}}{\sqrt{2}}\frac{\langle k-|\,\gamma^\mu\,|p-\rangle}{[pk]}, \tag{2.20}$$

where $e^{i\phi(k,p)}$ is a phase factor which depends on the momentum k, and the reference momentum p. In this thesis, we set this phase factor unity and we obtain the polarization vector:

$$\varepsilon^\mu_\mp(k) \;=\; \mp\frac{1}{\sqrt{2}}\frac{\langle k\mp|\,\gamma^\mu\,|p\mp\rangle}{\langle p\pm|k\mp\rangle}. \tag{2.21}$$

In Eqn. (2.21), the reference momentum p can be chosen freely in a convenient way because of gauge invariance of the theory. The proof proceeds in the following way. By changing the reference momentum p in Eqn.(2.21) to another reference momentum q, we have

$$\varepsilon^\mu_\pm(k,p) \;=\; \varepsilon^{\mu,q}_\pm + \beta_\pm(p,q,k)k^\mu, \tag{2.22}$$

$$\beta_-(p,q,k) \;=\; \frac{\sqrt{2}\,\langle qp\rangle}{\langle qk\rangle\,\langle pk\rangle}, \tag{2.23}$$

$$\beta_+(p,q,k) \;=\; (\beta_+)^*. \tag{2.24}$$

When the polarization vector $\varepsilon^\mu_\pm(k)$ is replaced by its momentum k, the scattering amplitude $\mathcal{M}$ should vanish:

$$\mathcal{M} \;=\; \mathcal{M}_\mu\varepsilon^\mu_\pm \;\to\; \mathcal{M}_\mu k^\mu \;=\; 0. \tag{2.25}$$

Therefore the second term in the Eqn.(2.22) does not contribute to the helicity amplitude. This implies that we can choose a different reference momentum p for each polarization vector in the process, and furthermore different reference momentum for each gauge invariant subset of the full amplitude, without worrying about the relative phase.

Now we show an application of these techniques to a real process [27, 29]. The process we consider as an example is the photon-photon scattering process:

$$\gamma(k_1,\lambda_1)+\gamma(k_2,\lambda_2) \;\to\; q(p_1,\lambda_3)+\bar{q}(p_2,\lambda_4),$$

where k_1, k_2 are the momenta of real photons, p_1, p_2 are the momenta of final massless quarks, and $\lambda_i, (i=1,2,3,4)$ denotes the helicity state $(\pm)$. Two diagrams contribute to this process at the leading order, t channel (Fig.2.1 (a)) and u channel fermion (Fig.2.1 (b)) exchanges.

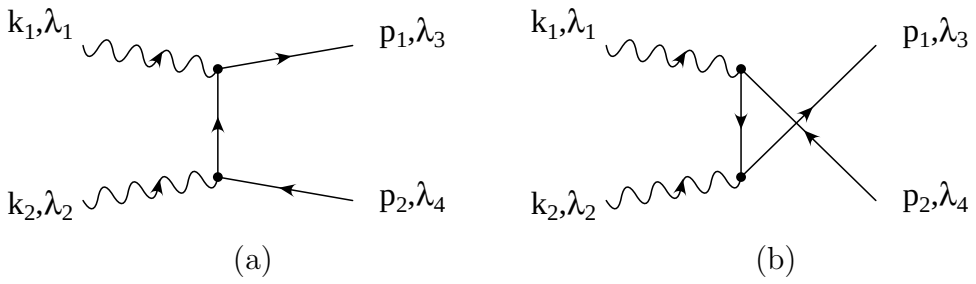

Figure 2.1: The tree level contributions to the $\gamma\gamma \to q\bar{q}$ process

The corresponding amplitudes are

$$\begin{aligned}
\mathcal{M}(\lambda_3,\lambda_4;\lambda_1,\lambda_2) &= \mathcal{M}_t(\lambda_3,\lambda_4;\lambda_1,\lambda_2) + \mathcal{M}_u(\lambda_3,\lambda_4;\lambda_1,\lambda_2)\ , \qquad (2.26)\\
\mathcal{M}_t(\lambda_3,\lambda_4;\lambda_1,\lambda_2) &= -e^2Q_q^2\bar{u}(p_1,\lambda_3)\Big[\hat{\varepsilon}_1(k_1,\lambda_1)\frac{\hat{p}_1-\hat{k}_1}{(p_1-k_1)^2}\hat{\varepsilon}_2(k_2,\lambda_2)\Big]v(p_2,\lambda_4),\\
\mathcal{M}_u(\lambda_3,\lambda_4;\lambda_1,\lambda_2) &= -e^2Q_q^2\bar{u}(p_1,\lambda_3)\Big[\hat{\varepsilon}_2(k_2,\lambda_2)\frac{\hat{p}_1-\hat{k}_2}{(p_1-k_2)^2}\hat{\varepsilon}_1(k_1,\lambda_1)\Big]v(p_2,\lambda_4),
\end{aligned}$$

where Q_q is the quark charge in the unit of electron charge e. It is easy to show that the helicity amplitudes with $\lambda_1 = \lambda_2$, and with $\lambda_3 = \lambda_4$ vanish. Therefore, only four helicity amplitudes corresponding to,

$$\mathcal{M}(\lambda_3,\lambda_4;\lambda_1,\lambda_2) = \mathcal{M}(\pm,\mp;+,-), \mathcal{M}(\pm,\mp;-,+), \qquad (2.27)$$

should be considered. Here we consider the amplitude $\mathcal{M}(+,-;-,+)$, and use the photon polarization vectors,

$$\begin{aligned}
\hat{\varepsilon}(k_1,-1) &= \frac{1}{\sqrt{2}\,\langle p_2\ k_1\rangle}\,\langle k_1 + |\gamma^\mu| p_2+\rangle\,\gamma_\mu\\
&= \frac{\sqrt{2}}{\langle p_2\ k_1\rangle}(|k_1-\rangle\,\langle p_2-| + |p_2+\rangle\,\langle k_1+|)\ , \qquad (2.28)\\
\hat{\varepsilon}(k_2,+1) &= -\frac{1}{\sqrt{2}\,[p_1\ k_2]}\,\langle k_2 - |\gamma^\mu| p_1-\rangle\,\gamma_\mu\\
&= -\frac{\sqrt{2}}{[p_1\ k_2]}(|k_2+\rangle\,\langle p_1+| + |p_1-\rangle\,\langle k_2-|)\ , \qquad (2.29)
\end{aligned}$$

where the reference momentum of the polarization vector for the photon with momentum k_1/k_2 has been chosen to be the momentum p_2/p_1. We obtain,

$$\mathcal{M}_t(+,-;-,+) = e^2Q_q^2\frac{\langle p_1\ k_1\rangle\,\langle p_2\ k_1\rangle\,[k_1\ p_1]\,\langle k_2\ p_2\rangle}{(p_1\cdot k_1)\,\langle p_2\ k_1\rangle\,[p_1 k_2]}$$

$$
\begin{aligned}
&= -2e^2Q_q^2\frac{[k_1\ p_1]\,\langle k_2\ p_2\rangle}{\langle k_1\ p_1\rangle^*\,\langle p_1\ k_2\rangle} \\
&= -2e^2Q_q^2 e^{i\phi(k_1,p_1)}\frac{\langle k_2\ p_2\rangle}{\langle p_1\ k_2\rangle}, \\
\mathcal{M}_u(+,-;-,+) &= e^2Q_q^2\frac{\langle p_1\ p_1\rangle\,\langle p_2\ k_1\rangle\,\langle k_2-|\,(\hat{p}_1-\hat{k}_2)\,|p_1-\rangle\,\langle p_2\ p_2\rangle}{(p_1\cdot k_2)\,\langle p_2\ k_1\rangle\,[p_1k_2]} \\
&= 0,
\end{aligned}
$$

where $e^{i\phi(k_1,p_1)}$ is the phase factor and given by $e^{i\phi(k_1,p_1)} = [k_1\ p_1]\,/\,\langle k_1\ p_1\rangle^*$. The amplitude $\mathcal{M}_u$ gives zero, because $\langle p_2 p_2\rangle = \langle p_1 p_1\rangle = 0$. Thus we immediately arrive at the final result,

$$
|\mathcal{M}(+,-;-,+)|^2 = 4e^4Q_q^4\frac{k_2\cdot p_2}{k_1\cdot p_2}. \tag{2.30}
$$

By using the invariance under the CP transformation, the remaining non-zero helicity amplitudes are,

$$
|\mathcal{M}(+,-;-,+)|^2 = |\mathcal{M}(-,+;+,-)|^2 = 4e^4Q_q^4\frac{k_2\cdot p_2}{k_2\cdot p_1}, \tag{2.31}
$$

$$
|\mathcal{M}(+,-;+,-)|^2 = |\mathcal{M}(-,+;-,+)|^2 = 4e^4Q_q^4\frac{k_1\cdot p_2}{k_1\cdot p_1}. \tag{2.32}
$$

This example shows the efficiency of the spinor helicity method to calculate the cross-section. The squared amplitude for $\gamma\gamma \to q\bar{q}$ process, averaged over initial spins and summed over final and colors ($N_C = 3$) reads,

$$
|\mathcal{M}|^2 = 2N_C e^4 Q_q^4\left(\frac{t^2+u^2}{ut}\right). \tag{2.33}
$$

Here we use the Mandelstam valuables, $t = (k_1 - p_1)^2$ and $u = (k_1 - p_2)^2$.

2.3 Massive Spinor States

We consider, in this section, massive spinor states and show that the massive spinor states also can be described in terms of massless spinor states [23, 27]. At first, we summarize the properties of the massive spinors $u(p,s),\ v(p,s)$ with momentum p and polarization s.

1. Dirac Equation:

$$(\hat{p}-m)u(p,s) \ = \ 0, \quad \bar{u}(p,s)(\hat{p}-m) \ = \ 0, \tag{2.34}$$

$$(\hat{p}+m)v(p,s) \ = \ 0, \quad \bar{v}(p,s)(\hat{p}+m) \ = \ 0. \tag{2.35}$$

2. Normalization, Orthogonality and Completeness:

$$\begin{aligned} \bar{u}(p,s1)\ u(p,s2) &= 2m\delta_{s1,s2}, \\ \bar{v}(p,s1)\ v(p,s2) &= -2m\delta_{s1,s2}, \end{aligned} \tag{2.36}$$

$$\begin{aligned} \bar{u}(p,s1)\ v(p,s2) &= 0, \\ \bar{v}(p,s1)\ u(p,s2) &= 0, \end{aligned} \tag{2.37}$$

$$\begin{aligned} \textstyle\sum_s u(p,s)\ \bar{u}(p,s) &= \hat{p}+m, \\ \textstyle\sum_s v(p,s)\ \bar{v}(p,s) &= \hat{p}-m. \end{aligned} \tag{2.38}$$

The spin vector s^μ of massive fermion has the form in the fermion's rest frame:

$$s^\mu \ = \ (0,\ \boldsymbol{s}), \tag{2.39}$$

with $\boldsymbol{s}\cdot\boldsymbol{s} \ = \ 1$. The spin vector, when the fermion is moving with momentum p, become

$$s^\mu \ = \ \left(\frac{\boldsymbol{p}\cdot\boldsymbol{s}}{m},\ \boldsymbol{s}+\frac{\boldsymbol{p}\ (\boldsymbol{p}\cdot\boldsymbol{s})}{m(E+m)}\right), \tag{2.40}$$

where $p=(E,\ \boldsymbol{p})$ and spin vector satisfies $p\cdot s \ = \ 0, s\cdot s \ = \ -1$. The projection operators [30] are given by

$$u(p,s)\bar{u}(p,s) \ = \ (\hat{p}+m)\frac{1+\gamma_5\hat{s}}{2}\ u(p), \tag{2.41}$$

$$v(p,s)\bar{v}(p,s) \ = \ (\hat{p}-m)\frac{1+\gamma_5\hat{s}}{2}\ v(p). \tag{2.42}$$

Therefore, the polarized fermion states are projected as,

$$u(p,\uparrow) \ = \ \frac{1+\gamma_5\hat{s}}{2}\ u(p), \tag{2.43}$$

$$u(p,\downarrow) \ = \ \frac{1-\gamma_5\hat{s}}{2}\ u(p), \tag{2.44}$$

$$v(p,\uparrow) \ = \ \frac{1+\gamma_5\hat{s}}{2}\ v(p), \tag{2.45}$$

$$v(p,\downarrow) \ = \ \frac{1-\gamma_5\hat{s}}{2}\ v(p), \tag{2.46}$$

where spin states, $\uparrow/\downarrow$ refers to fermions with spin in $+\boldsymbol{s}/-\boldsymbol{s}$ direction in their rest frame. Now, we rewrite Eqns.(2.43)$\sim$(2.46) in terms of massless helicity spinor states and show how to describe the massive spinor states in terms of massless helicity states. Let us consider, for example, the state $u(p,\uparrow)$ and rewrite it using properties satisfied by gamma matrices,

$$\begin{aligned} u(p,\uparrow) &= \frac{1+\gamma_5}{2}\frac{1+\gamma_5\hat{s}}{2}\,u(p) + \frac{1-\gamma_5}{2}\frac{1+\gamma_5\hat{s}}{2}\,u(p), \\ &= \frac{1+\gamma_5}{2}\frac{1+\hat{s}}{2}\,u(p) + \frac{1-\gamma_5}{2}\frac{1-\hat{s}}{2}\,u(p). \end{aligned} \tag{2.47}$$

In Eqn.(2.47), the quantities $[(1\pm\hat{s})/2]\;u(p)$ can be identified with massless spinors having momentum $(p\pm ms)/2$ due to the following reasons [31]

1. Dirac Equation: At first, note that the momentum p_i $(i=1,2)$ is light-like,

$$p_1 \equiv \frac{p+ms}{2}, \quad (p_1^2 = 0), \tag{2.48}$$

$$p_2 \equiv \frac{p-ms}{2}, \quad (p_2^2 = 0), \tag{2.49}$$

and simple relations between $p_i,\ p$ and s,

$$p = p_1 + p_2, \tag{2.50}$$

$$ms = p_1 - p_2. \tag{2.51}$$

Next it is easy to show,

$$\hat{p}_1\frac{1+\hat{s}}{2}u(p) = \hat{p}_2\frac{1-\hat{s}}{2}u(p) = 0.$$

Therefore, the quantities $[(1\pm\hat{s})/2]\;u(p)$ are proportional to the massless spinors $Q(p_1)$, $Q(p_2)$ respectively.

$$Q(p_1) = A\frac{(1+\hat{s})}{2}u(p)\ , \tag{2.52}$$

$$Q(p_2) = B\frac{(1-\hat{s})}{2}u(p)\ , \tag{2.53}$$

$$\tag{2.54}$$

where factors $A,\ B$ are normalization constant.

2. Projection Property: The normalization factors A and B will be fixed by constructing the projection operators, which read

$$\begin{aligned} Q(p_1)\bar{Q}(p_1) &= |A|^2\hat{p}_1, \\ Q(p_2)\bar{Q}(p_2) &= |B|^2\hat{p}_2, \end{aligned}$$

Therefore, we conclude that $[(1 \pm \hat{s})/2]\ u(p)$ are the massless spinors $Q(p_i)$ except for phase factors. Above consideration tells us

$$\begin{aligned} u(p,\uparrow) &= \frac{1+\gamma_5}{2}\,Q(p_1) + e^{i\phi(p_1,p_2)}\,\frac{1-\gamma_5}{2}\,Q(p_2), \\ &\equiv |p_1+\rangle + e^{i\phi(p_1,p_2)}\,|p_2-\rangle\,. \end{aligned} \tag{2.55}$$

Here, we have chosen the overall phase factor such that there is no phase in front of $|p_1+\rangle$. Therefore, $\phi(p_1,p_2)$ represents the relative phase between the states $|p_1+\rangle$ and $|p_2-\rangle$, This phase factor can be determined by the normalization condition for $u(p,\uparrow)$ in Eqn.(2.36). It is not difficult to obtain,

$$e^{i\phi} = \frac{\langle p_2\ p_1\rangle}{m}, \tag{2.56}$$

where we have used the relation:

$$|\,\langle p_2\ p_1\rangle\,|^2 = 2\,p_1\cdot p_2 = m^2. \tag{2.57}$$

In this way, all massive spinor states can be written in terms of massless chiral spinors as (for the anti-fermions, we use the superscript "bar"for their momenta),

$$u(p,\uparrow) = |p_1+\rangle + |p_2-\rangle\,\frac{\langle p_2\ p_1\rangle}{m}, \tag{2.58}$$

$$u(p,\downarrow) = |p_1-\rangle + |p_2+\rangle\,\frac{[p_2\ p_1]}{m}, \tag{2.59}$$

$$\bar{u}(p,\uparrow) = \langle p_1+| + \frac{[p_1\ p_2]}{m}\,\langle p_2-|\,, \tag{2.60}$$

$$\bar{u}(p,\downarrow) = \langle p_1-| + \frac{\langle p_1\ p_2\rangle}{m}\,\langle p_2+|\,, \tag{2.61}$$

$$v(\bar{p},\uparrow) = |\bar{p}_1-\rangle - |\bar{p}_2+\rangle\,\frac{[\bar{p}_2\ \bar{p}_1]}{m}, \tag{2.62}$$

$$v(\bar{p},\downarrow) = |\bar{p}_1+\rangle - |\bar{p}_2-\rangle\,\frac{\langle\bar{p}_2\ \bar{p}_1\rangle}{m}, \tag{2.63}$$

$$\bar{v}(\bar{p},\uparrow) = \langle\bar{p}_1-| - \frac{\langle\bar{p}_1\ \bar{p}_2\rangle}{m}\,\langle\bar{p}_2+|\,, \tag{2.64}$$

$$\bar{v}(\bar{p},\downarrow) = \langle\bar{p}_1+| - \frac{[\bar{p}_1\ \bar{p}_2]}{m}\,\langle\bar{p}_2-|\,. \tag{2.65}$$

The light like momenta p_1, p_2, $\bar{p}_1$ and $\bar{p}_2$ are defined by,

$$p_1 \equiv \frac{p+ms_p}{2},\quad p_2 \equiv \frac{p-ms_p}{2}, \tag{2.66}$$

$$\bar{p}_1 \equiv \frac{\bar{p}+ms_{\bar{p}}}{2},\quad \bar{p}_2 \equiv \frac{\bar{p}-ms_{\bar{p}}}{2}. \tag{2.67}$$

For the convenience of later calculations, let us write down p_i explicitly in the rest and moving frame of the massive fermions. In the rest frame, the four momentum of the massive fermion and the spin vector take

$$p = (m,\ \mathbf{0}), \tag{2.68}$$

$$s_p = (0,\ \boldsymbol{\omega}),\quad (|\boldsymbol{\omega}|^2 = 1). \tag{2.69}$$

So, the light like momenta $p_1,\ p_2$ are

$$p_1 = \frac{m}{2}(1,\ \boldsymbol{\omega}),\quad p_2 = \frac{m}{2}(1,\ -\boldsymbol{\omega}). \tag{2.70}$$

These equations show that the direction of the particle's spin is in the same direction of the spatial part of p_1 or in the opposite direction of the spatial part of p_2. For the moving fermion, $p = (E,\ \mathcal{P}\boldsymbol{n})$, $(|\boldsymbol{n}|^2 = 1)$, p_i are obtained by boosting Eqn.(2.69)$\sim$(2.70). The spin vector and decomposed light-like momenta $p_1,\ p_2$ become

$$s_p = \Big(\mathcal{P}\frac{(\boldsymbol{n}\cdot\boldsymbol{\omega})}{m}, \boldsymbol{\omega} + \frac{\mathcal{P}^2(\boldsymbol{n}\cdot\boldsymbol{\omega})\ \boldsymbol{n}}{m(m+E)}\Big), \tag{2.71}$$

$$p_1 = \frac{1}{2}\Big(E + \mathcal{P}\ (\boldsymbol{n}\cdot\boldsymbol{\omega}), \mathcal{P}\ \boldsymbol{n} + m\ \boldsymbol{\omega} + \frac{\mathcal{P}^2(\boldsymbol{n}\cdot\boldsymbol{\omega})\ \boldsymbol{n}}{(m+E)}\Big), \tag{2.72}$$

$$p_2 = \frac{1}{2}\Big(E - \mathcal{P}\ (\boldsymbol{n}\cdot\boldsymbol{\omega}), \mathcal{P}\ \boldsymbol{n} - m\ \boldsymbol{\omega} - \frac{\mathcal{P}^2\ (\boldsymbol{n}\cdot\boldsymbol{\omega})\ \boldsymbol{n}}{(m+E)}\Big). \tag{2.73}$$

Here we consider the familiar helicity state, that is, the spin of massive particle is projected along its direction of motion,

$$\boldsymbol{n} = \boldsymbol{\omega}, \tag{2.74}$$

$$p_1 = \frac{1}{2}\Big(E + \mathcal{P}, \Big[\mathcal{P} + m + \frac{\mathcal{P}^2}{(m+E)}\Big]\boldsymbol{n}\Big), \tag{2.75}$$

$$p_2 = \frac{1}{2}\Big(E - \mathcal{P}, \Big[\mathcal{P} - m - \frac{\mathcal{P}^2}{(m+E)}\Big]\boldsymbol{n}\Big). \tag{2.76}$$

In the large momentum limit (which is equivalent to the massless limit), $p_1 = p$, $p_2 = 0$. Then, the spinors become the chiral eigenstates:

$$u(p,R) \to |p_1+\rangle\,,\ u(p,L) \to |p_1-\rangle\ , \tag{2.77}$$

$$v(\bar{p},R) \to |\bar{p}_1-\rangle\,,\ v(\bar{p},L) \to |\bar{p}_1+\rangle\ , \tag{2.78}$$

$$\bar{u}(p,R) \to \langle p_1-|\,,\ \bar{u}(p,L) \to \langle p_1+|\ , \tag{2.79}$$

$$\bar{v}(\bar{p},R) \to \langle \bar{p}_1+|\,,\ \bar{v}(\bar{p},L) \to \langle \bar{p}_1-|\ , \tag{2.80}$$

where we have labeled helicity states by R (L) instead of $\uparrow$ ($\downarrow$). This demonstrates the relation between the right-handed (left-handed) helicity state, $u(p, R)$ ($u(p, L)$), in the massless limit and the right-handed (left-handed) chiral state.

2.4 Circular Polarizations of Massive Bosons

The polarization vectors for massive gauge boson [28, 27, 32] can also be described in terms of massless spinors. Transversely polarized states satisfy Eqns.(2.14) $\sim$ (2.16) in Sec.2.2. For massive gauge boson, we must also take into account the longitudinally polarized state. Let $\varepsilon^\mu_\pm$ denote transversely polarized states and ε^μ_0 is the longitudinally one. The properties of polarization vectors for a massive gauge boson with momentum k and mass m are

$$\begin{aligned} \varepsilon_\lambda(k)\cdot k &= 0, && (2.81)\\ \varepsilon_\lambda(k)\cdot\varepsilon^*_{\lambda'}(k) &= -\delta_{\lambda\lambda'}, && (2.82)\\ \sum_\lambda \varepsilon^\mu_\lambda(k)\varepsilon^{\nu *}_\lambda(k) &= -g^{\mu\nu}+\frac{k^\mu k^\nu}{m^2}, && (2.83) \end{aligned}$$

where λ and λ' denote $+,-$ and 0.

Let s be the spin vector associated with the massive vector boson, which satisfies,

$$k\cdot s \;=\; 0, \quad (k^2 \;=\; m^2). \tag{2.84}$$

Here three polarization vectors ε_λ are defined such that in the vector boson rest frame, the boson has the spin projection $\lambda=(+,0,-)$ with respect to the spatial part of the spin vector s. Three polarization vectors $\varepsilon^\mu_\lambda(k)$ are given in terms of two light-like vectors,

$$\begin{aligned} k^\mu_1 &= \frac{k^\mu - m s^\mu}{2}, && (2.85)\\ k^\mu_2 &= \frac{k^\mu + m s^\mu}{2}. && (2.86) \end{aligned}$$

Then, we get polarization vectors for the incoming gauge boson:

$$\begin{aligned} \varepsilon^\mu_\pm &= \frac{\langle k_1\pm|\,\gamma^\mu\,|k_2\pm\rangle}{\sqrt{2}m}, && (2.87)\\ \varepsilon^\mu_0 &= \frac{\langle k_1+|\,\gamma^\mu\,|k_1+\rangle - \langle k_2+|\,\gamma^\mu\,|k_2+\rangle}{2m} \;=\; \frac{k^\mu_1-k^\mu_2}{m}. && (2.88) \end{aligned}$$

In this expressions, the helicity basis is given by choosing the spatial part of the spin vector s to be in the same direction as the spatial part of the momentum vector k.

Chapter 3

Spin Correlations at Leading Order

In 1994, the top quark was discovered by the CDF and D0 collaborations [4, 5]. The measured top quark mass is approximately 175 GeV, which is nearly twice the mass scale of electro-weak symmetry breaking. Thus the top quark with large mass brings a good opportunity to understand electro-weak symmetry breaking and to reveal physics beyond the Standard Model. The top quark decays electroweakly before hadronizing because its width is much greater than the hadronization timescale set by Λ_{QCD} [9]. Therefore, there are significant angular correlations between the decay products of the top quark and the spin of the top quark. These angular correlations depend sensitively on the top quark couplings to the Z^0 boson and photon, and to the W boson and b quark. These angular distributions are considered as good information to constrain the couplings of top quarks in the Standard Model. Most works [11, 12] are performed by using top quark spin decomposed in the helicity basis. In the case of ultra-relativistic particles, this decomposition is appropriate. However this basis is not necessarily optimal to investigate the spin correlations since the produced top quarks are non-relativistic at realistic linear colliders: *e.g.* $\beta = v/c \sim 0.5$ for a 400 GeV collider. As a matter of fact, Mahlon and Parke [15] have shown that this decomposition in helicity basis is far from the optimal decomposition for top quark productions at hadron colliders. Parke and Shadmi [16] have extended these analyses to lepton colliders.

In this chapter, we discuss the spin-spin correlations for the top quark pair production at polarized e^+e^- linear colliders at the leading order in perturbation theory. We introduce the "generic spin basis" and investigate which decomposition of top quark spin is optimal to study spin correlations for moderate energies. The spin-angular correlations for the top (anti-top) quark decay are also discussed.

3.1 Spin-Spin Correlations for Top Pair production

In this section, we derive the leading order spin dependent differential cross-sections for top quark pair productions in a generic spin basis. We find the most optimal spin decomposition for top and anti-top quark to study spin correlations. The one-loop analyses will be given in the next chapter.

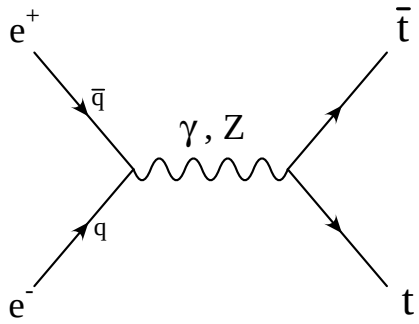

Figure 3.1: The tree level contributions to the $e^-e^+ \to t\bar{t}$ process

The Feynman graph for the $e^+e^- \to t\bar{t}$ process at the leading order in perturbation theory is given in Fig.3.1. We calculate the amplitude using the spinor helicity method. The momenta of electron, positron, top quark and anti-top quark are labeled by q, $\bar{q}$, t and $\bar{t}$ respectively, and s_t ($s_{\bar{t}}$) represents the spin vector of top (anti-top) quark. As explained in the previous chapter, we decompose the top (anti-top) quark momentum t ($\bar{t}$) into a sum of two massless momenta t_1, t_2 ($\bar{t}_1, \bar{t}_2$),

$$t = t_1 + t_2, \ (\bar{t} = \bar{t}_1 + \bar{t}_2), \tag{3.1}$$

$$ms_t = t_1 - t_2, \ (ms_{\bar{t}} = \bar{t}_1 - \bar{t}_2). \tag{3.2}$$

The amplitudes for $e^-_L e^+_R$ ($e^-_R e^+_L$) scattering processes are obtained to be,

$$\begin{aligned}
&\mathcal{M}(e^-_L e^+_R \to t_{s_t}\bar{t}_{s_{\bar{t}}}) \\
&= \frac{4\pi\alpha}{s} \langle \bar{q}- | \gamma^\mu_L | q- \rangle \, \bar{u}(t, s_t)\gamma_\mu \left[f_{LL}\gamma_L + f_{LR}\gamma_R \right] v(\bar{t}, s_{\bar{t}}) \ , \qquad (3.3) \\
&\mathcal{M}(e^-_R e^+_L \to t_{s_t}\bar{t}_{s_{\bar{t}}}) \\
&= \frac{4\pi\alpha}{s} \langle \bar{q}+ | \gamma^\mu_R | q+ \rangle \, \bar{u}(t, s_t)\gamma_\mu \left[f_{RL}\gamma_L + f_{RR}\gamma_R \right] v(\bar{t}, s_{\bar{t}}) \ , \qquad (3.4)
\end{aligned}$$

where e^-_L/e^+_L (e^-_R/e^+_R) means the electron/positron with left-handed (right-handed) helicity state. We have neglected the electron (positron) mass. The quantity α is the fine structure

constant $\alpha = e^2/(4\pi)$, and s is the total energy, $\gamma^\mu_{R/L} \equiv \gamma^\mu\gamma_{R/L}$, $\gamma_{R/L} \equiv (1 \pm \gamma_5)/2$. The quantities f_{IJ}'s are the sum of photon and Z^0 boson couplings to fermions (electron and top quark) including the propagator and are given by

$$f_{IJ} = -Q_t + Q_e^I Q_t^J \frac{1}{\sin^2\theta_W} \frac{s}{s - M_Z^2 + iM_Z\Gamma_Z} \ .$$

Here M_Z is the Z boson mass, Γ_Z is the width of Z boson, θ_W is the Weinberg angle and $I, J \in (L, R)$. The parameter $Q_t = 2/3$ is the electric charge of the top quark in the unit of electron charge e. The electron couplings to the Z boson are given by

$$Q_e^L = \frac{2\sin^2\theta_W - 1}{2\cos\theta_W} \quad , \quad Q_e^R = \frac{\sin^2\theta_W}{\cos\theta_W} \ . \tag{3.5}$$

The top quark couplings to the Z boson are given by

$$Q_t^L = \frac{3 - 4\sin^2\theta_W}{6\cos\theta_W} \quad , \quad Q_t^R = -\frac{2\sin^2\theta_W}{3\cos\theta_W} \ . \tag{3.6}$$

The squared amplitude for $e_L^- e_R^+$ scattering reads

$$\begin{aligned}
&|\mathcal{M}(e_L^- e_R^+ \to t_\uparrow \bar{t}_\uparrow)|^2 \\
&= 4\left(\frac{4\pi\alpha}{s}\right)^2 \Big[|f_{LL}|^2 (2q\cdot t_1)(2\bar{q}\cdot\bar{t}_2) + |f_{LR}|^2 (2\bar{q}\cdot t_2)(2q\cdot\bar{t}_1) \\
&\qquad + \frac{1}{m^2}\{f_{LL}f_{LR}^* \mathrm{Tr}[\gamma_L q t_1 t_2 \bar{q}\bar{t}_2\bar{t}_1] + c.c\}\Big] \ , \qquad (3.7) \\
&|\mathcal{M}(e_L^- e_R^+ \to t_\uparrow \bar{t}_\downarrow)|^2 \\
&= 4\left(\frac{4\pi\alpha}{s}\right)^2 \Big[|f_{LL}|^2 (2q\cdot t_1)(2\bar{q}\cdot\bar{t}_1) + |f_{LR}|^2 (2\bar{q}\cdot t_2)(2q\cdot\bar{t}_2) \\
&\qquad + \frac{1}{m^2}\{f_{LL}f_{LR}^* \mathrm{Tr}[\gamma_L q t_1 t_2 \bar{q}\bar{t}_1\bar{t}_2] + c.c\}\Big] \ , \qquad (3.8) \\
&|\mathcal{M}(e_L^- e_R^+ \to t_\downarrow \bar{t}_\uparrow)|^2 \\
&= 4\left(\frac{4\pi\alpha}{s}\right)^2 \Big[|f_{LL}|^2 (2q\cdot t_2)(2\bar{q}\cdot\bar{t}_2) + |f_{LR}|^2 (2\bar{q}\cdot t_1)(2q\cdot\bar{t}_1) \\
&\qquad + \frac{1}{m^2}\{f_{LL}f_{LR}^* \mathrm{Tr}[\gamma_L q t_2 t_1 \bar{q}\bar{t}_2\bar{t}_1] + c.c\}\Big] \ , \qquad (3.9) \\
&|\mathcal{M}(e_L^- e_R^+ \to t_\downarrow \bar{t}_\downarrow)|^2 \\
&= 4\left(\frac{4\pi\alpha}{s}\right)^2 \Big[|f_{LL}|^2 (2q\cdot t_2)(2\bar{q}\cdot\bar{t}_1) + |f_{LR}|^2 (2\bar{q}\cdot t_1)(2q\cdot\bar{t}_2) \\
&\qquad + \frac{1}{m^2}\{f_{LL}f_{LR}^* \mathrm{Tr}[\gamma_L q t_2 t_1 \bar{q}\bar{t}_1\bar{t}_2] + c.c\}\Big] \ , \qquad (3.10)
\end{aligned}$$

where all momenta, p, under the "Tr" operator are understood to be $\hat{p}$. The squared amplitude for $e_R^- e_L^+$ scattering are given by interchanging $L,\ R$ as well as $\uparrow,\ \downarrow$ in Eqn.(3.7)$\sim$(3.10).

Before discussing the spin basis, let us fix the coordinate system. In the center of mass (CM) frame, we take the production plane to be $x-z$ plane and set the direction of the motion of the top quark to be $+z$ direction (see Fig.3.2).

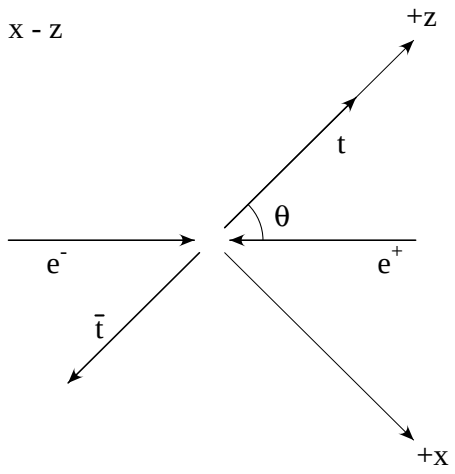

Figure 3.2: $e^-e^+ \to t\bar{t}$ process in the center of mass frame.

Now, the generic spin basis we consider here is based on the following facts: First, CP is conserved in the Standard Model. Hence the spins of top and ant-top quark can be defined to be back-to-back. Second, there is no transverse polarization of the top (anti-top) quark at the tree level in the Standard Model. Here the "transverse" means the direction normal to the production plane[33]. Hence, the spin vectors are on the production plane and they are parametrized by one parameter. We define the generic basis in the following way; For top quark, we got to its rest frame and its spin is decomposed along the direction $\mathbf{s}_t$ in the rest frame of the top quark which makes an angle ξ with the anti-top quark momentum in the clockwise direction. Similarly, the anti-top quark spin states are defined in the anti-top rest frame along the direction $\mathbf{s}_{\bar{t}}$ having the same angle ξ from the direction of the top quark momentum (see Fig.3.3).

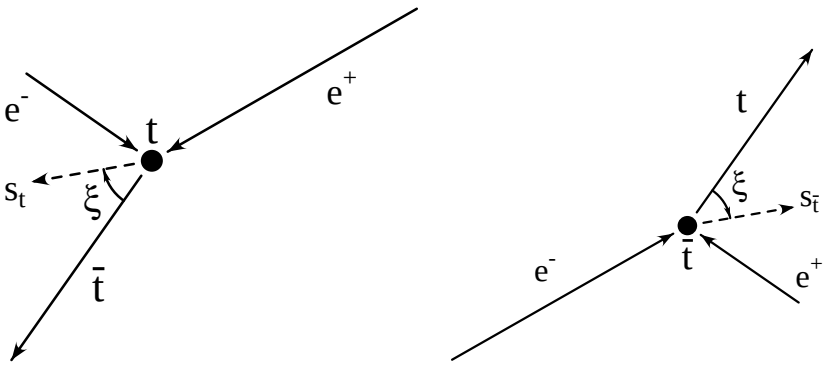

Figure 3.3: The generic spin basis for the top (anti-top) quark in its rest frame. $\mathbf{s}_t$ ($\mathbf{s}_{\bar{t}}$) is the top (anti-top) spin axis.

In the top (anti-top) quark rest frame, the top (anti-top) quark momentum t_{RF}, ($\bar{t}_{RF}$) and the spin vector become s_t^{RF} ($s_{\bar{t}}^{RF}$) as,

$$\begin{array}{rcl@{\qquad}rcl} t^\mu_{RF} &=& m(1,0,0,0), & \bar{t}^\mu_{RF} &=& m(1,0,0,0), \\ (s_t^{RF})^\mu &=& (0,-\sin\xi,0,-\cos\xi), & (s_{\bar{t}}^{RF})^\mu &=& (0,\sin\xi,0,\cos\xi). \end{array} \tag{3.11}$$

Now let us decompose the top (anti-top) quark momentum t_{RF} ($\bar{t}_{RF}$) in terms of massless momenta t_1^{RF} and t_2^{RF} ($\bar{t}_1^{RF}$ and $\bar{t}_2^{RF}$),

$$t_{RF} = t_1^{RF} + t_2^{RF}, \quad m s_t^{RF} = t_1^{RF} - t_2^{RF}, \tag{3.12}$$

$$\bar{t}_{RF} = \bar{t}_1^{RF} + \bar{t}_2^{RF}, \quad m s_{\bar{t}}^{RF} = \bar{t}_1^{RF} - \bar{t}_2^{RF}. \tag{3.13}$$

From these relations, the four massless momenta are expressed as

$$(t_1^{RF})^\mu = \frac{m}{2}(1,-\sin\xi,0,-\cos\xi), \tag{3.14}$$

$$(t_2^{RF})^\mu = \frac{m}{2}(1,\sin\xi,0,\cos\xi), \tag{3.15}$$

$$(\bar{t}_1^{RF})^\mu = \frac{m}{2}(1,\sin\xi,0,\cos\xi), \tag{3.16}$$

$$(\bar{t}_2^{RF})^\mu = \frac{m}{2}(1,-\sin\xi,0,-\cos\xi). \tag{3.17}$$

To get back to the CM frame, we boost back all quantities in the $+z$ ($-z$) direction with the top (anti-top) quark speed $\beta = \sqrt{1-4m^2/s}$. The momenta of particles in the CM frame are given by,

$$t^\mu = m\gamma(1,0,0,\beta), \quad \bar{t}^\mu = m\gamma(1,0,0,-\beta), \tag{3.18}$$

$$q^\mu = m\gamma(1,\sin\theta,0,\cos\theta)\ , \quad \bar{q}^\mu = m\gamma(1,-\sin\theta,0,-\cos\theta)\ , \tag{3.19}$$

$$t_1^\mu = \frac{m}{2}(\gamma(1-\beta\cos\xi), -\sin\xi, 0, \gamma(\beta-\cos\xi)) \ , \tag{3.20}$$

$$t_2^\mu = \frac{m}{2}(\gamma(1+\beta\cos\xi), -\sin\xi, 0, \gamma(\beta+\cos\xi)) \ , \tag{3.21}$$

$$\bar{t}_1^\mu = \frac{m}{2}(\gamma(1-\beta\cos\xi), -\sin\xi, 0, -\gamma(\beta-\cos\xi)) \ , \tag{3.22}$$

$$\bar{t}_2^\mu = \frac{m}{2}(\gamma(1+\beta\cos\xi), -\sin\xi, 0, -\gamma(\beta+\cos\xi)) \ , \tag{3.23}$$

where $\gamma = 1/\sqrt{1-\beta^2}$ and θ is the scattering angle of the top quark with respect to the electron in the CM frame [see Fig.3.2].

Let us write down the squared amplitudes using kinematical variables in the CM frame. Since each term in Eqn.(3.7) reads as

$$\begin{aligned}&(2q\cdot t_1)(2\bar{q}\cdot\bar{t}_2)\\ &= m^4\gamma^4[(1-\beta\cos\theta)^2 - \{(\cos\theta-\beta)\cos\xi - \sqrt{1-\beta^2}\sin\theta\sin\xi\}^2] \ ,\end{aligned} \tag{3.24}$$

$$\begin{aligned}&(2q\cdot\bar{t}_1)(2\bar{q}\cdot t_2)\\ &= m^4\gamma^4[(1+\beta\cos\theta)^2 - \{(\beta+\cos\theta)\cos\xi + \sqrt{1-\beta^2}\sin\theta\sin\xi\}^2] \ ,\end{aligned} \tag{3.25}$$

$$\begin{aligned}&\mathrm{Tr}[\gamma_L q t_1 t_2 \bar{q}\bar{t}_2\bar{t}_2] \ = \ \mathrm{Tr}[\gamma_R q t_1 t_2 \bar{q}\bar{t}_2\bar{t}_2]\\ &= m^6\gamma^4[1-\beta^2 - \{\sqrt{1-\beta^2}\cos\theta\cos\xi + \sin\theta\sin\xi\}^2] \ ,\end{aligned} \tag{3.26}$$

the squared amplitude becomes

$$|\mathcal{M}(e_L^- e_R^+ \to t_\uparrow \bar{t}_\uparrow)|^2 = 16\pi^2\alpha^2 |A_{LR}\cos\xi - B_{LR}\sin\xi|^2, \tag{3.27}$$

where the quantities A_{LR} and B_{LR} are defined by

$$A_{LR} = \Big[(f_{LL}+f_{LR})\sqrt{1-\beta^2}\,\sin\theta\Big]/2 \ , \tag{3.28}$$

$$B_{LR} = \Big[f_{LL}(\cos\theta+\beta) + f_{LR}(\cos\theta-\beta)\Big]/2. \tag{3.29}$$

Similarly, other squared amplitudes are

$$|\mathcal{M}(e_L^- e_R^+ \to t_\downarrow \bar{t}_\downarrow)|^2 = 16\pi^2\alpha^2 |A_{LR}\cos\xi - B_{LR}\sin\xi|^2 \ , \tag{3.30}$$

$$|\mathcal{M}(e_L^- e_R^+ \to t_\uparrow \bar{t}_\downarrow \text{ or } t_\downarrow \bar{t}_\uparrow)|^2 = 16\pi^2\alpha^2 |A_{LR}\sin\xi + B_{LR}\cos\xi \pm D_{LR}|^2 \ , \tag{3.31}$$

with

$$D_{LR} = \Big[f_{LL}(1+\beta\cos\theta) + f_{LR}(1-\beta\cos\theta)\Big]/2 \ . \tag{3.32}$$

The differential cross-section is given by

$$\frac{d\sigma}{d\cos\theta} = \frac{1}{32\pi}\frac{\beta}{s}\sum_{N_C}|\mathcal{M}|^2 \ ,$$

where N_c is the color degree of freedom, $N_c = 3$ and s is the total energy. Thus, we arrive at the final expression of the polarized cross-sections for the top quark production,

$$\begin{aligned}
\frac{d\sigma}{d\cos\theta}(e^-_L e^+_R \to t_\uparrow \bar{t}_\uparrow) &= \frac{d\sigma}{d\cos\theta}(e^-_L e^+_R \to t_\downarrow \bar{t}_\downarrow) \\
&= \frac{3\pi\alpha^2}{2s}\beta|A_{LR}\cos\xi - B_{LR}\sin\xi|^2, \qquad (3.33) \\
\frac{d\sigma}{d\cos\theta}(e^-_L e^+_R \to t_\uparrow \bar{t}_\downarrow \text{ or } t_\downarrow \bar{t}_\uparrow) &= \frac{3\pi\alpha^2}{2s}\beta|A_{LR}\sin\xi + B_{LR}\cos\xi \pm D_{LR}|^2,
\end{aligned}$$

Now, consider numerical behavior of the parameter f_{IJ}. The production threshold for top quarks is far above the Z boson mass. The contribution of the Z boson width to f_{IJ} is suppressed by a factor

$$\frac{M_Z\Gamma_Z}{(s-M_Z^2)^2 + (M_Z\Gamma_Z)^2} \sim (0.0015) ,$$

when $\sqrt{s} = 400$ GeV, $M_Z = 91$ GeV, $\Gamma_Z = 2.49$ GeV. Therefore, in our discussions bellow, we neglect the Z boson width. We use the values for the parameters of the standard model in Table 3.1.

m	M_Z	α	$\sin^2\theta_W$
175 [GeV]	91.187 [GeV]	1/128	0.2315

Table 3.1: Input parameters of the Standard Model.

We show the β dependence of f_{IJ}'s in Fig.3.4.

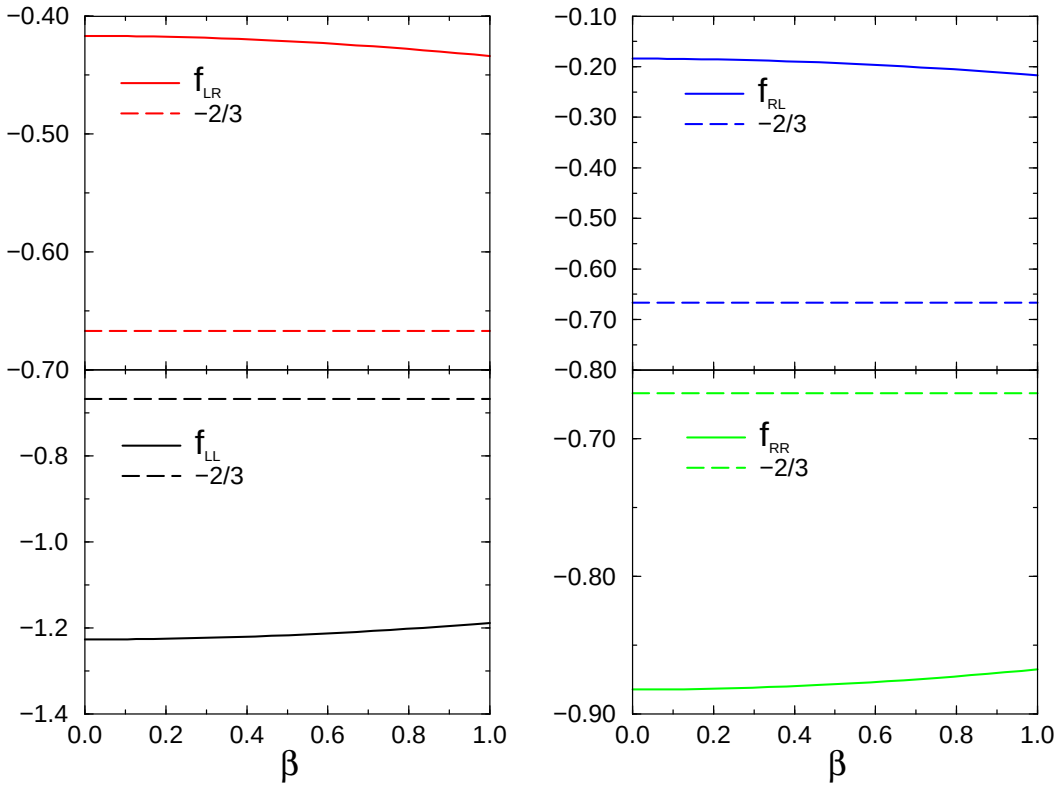

Figure 3.4: Top quark speed, β, dependence of f_{LL}, f_{LR}, f_{RL} and f_{RR}.

For the top quark production, f_{IJ} have a weak β dependence and are given by

$$-1.23 \leq f_{LL} \leq -1.19 \quad , \quad -0.882 \leq f_{LR} \leq -0.867 \ ,$$
$$-0.433 \leq f_{RR} \leq -0.417 \quad , \quad -0.217 \leq f_{RL} \leq -0.184 \ .$$

When fermions do not couple to Z boson and couple only to the photon, all parameters f_{IJ}'s go to $-2/3$. The difference, $f_{IJ} - (-2/3)$, shows the contribution from the Z boson, and we can investigate their effects in all energy region.

Since we are interested in maximizing the spin correlations of top quark pairs, we vary the spin angle, ξ, to find an appropriate spin basis. Following the articles [15, 16], we introduce "helicity", "beamline" and "off-diagonal" bases and derive the polarized cross-sections in these bases from Eqn.(3.33).

1. Helicity basis

   The helicity basis, the most familiar spin basis, is given by

$$\cos\xi \ = \ \pm 1, \tag{3.34}$$

for which the top quark spin is defined along its direction of motion. It is noted that the helicity basis can not be used in the threshold energy region, because the top (anti-top) quark momentum is undefined in this region. Substituting Eqn.(3.34) to the general polarized cross-section in Eqn.(3.33), we can obtain the well known polarized cross-section:

$$\begin{aligned}
\frac{d\sigma}{d\cos\theta}(e^-_L e^+_R \to t_L\bar{t}_L) &= \frac{d\sigma}{d\cos\theta}(e^-_L e^+_R \to t_R\bar{t}_R) \\
&= \frac{3\pi\alpha^2}{8s}\beta|f_{LL}+f_{LR}|^2(1-\beta^2)\sin^2\theta, \qquad (3.35)\\
\frac{d\sigma}{d\cos\theta}(e^-_L e^+_R \to t_R\bar{t}_L \text{ or } t_L\bar{t}_R) &= \frac{3\pi\alpha^2}{8s}\beta|f_{LL}(1\mp\beta)+f_{LR}(1\pm\beta)|^2(1\mp\cos\theta)^2.
\end{aligned}$$

Here t_L (t_R) state corresponds to $t_\uparrow$ ($t_\downarrow$) state with $\cos\xi = +1$.

2. Beamline basis

In the rest frame of top quark, there are three natural choices for the direction of the top quark spin; direction of the electron, the positron or the anti-top quark momentum. In the threshold region, the anti-top quark momentum direction, which is undefined, is excluded leaving only the electron or positron momentum directions. The situation is the same for the anti-top quark spin. The natural choice (see the discussion at the end of this section)is that the top (anti-top) quark spin is in the direction of the positron (electron) momentum in its rest frame. This spin basis is called "beamline basis "[15, 16, 34], The spin angle ξ is determined by

$$\cos\xi = \frac{\cos\theta+\beta}{1+\beta\cos\theta}. \qquad (3.36)$$

The polarized cross-sections in the beamline basis are

$$\begin{aligned}
\frac{d\sigma}{d\cos\theta}(e^-_L e^+_R \to t_\uparrow\bar{t}_\uparrow) &= \frac{d\sigma}{d\cos\theta}(e^-_L e^+_R \to t_\downarrow\bar{t}_\downarrow) \\
&= \left(\frac{3\pi\alpha^2}{2s}\beta\right)|f_{LR}|^2\frac{\beta^2(1-\beta^2)\sin^2\theta}{(1+\beta\cos\theta)^2}, \\
\frac{d\sigma}{d\cos\theta}(e^-_L e^+_R \to t_\downarrow\bar{t}_\uparrow) &= \left(\frac{3\pi\alpha^2}{2s}\beta\right)|f_{LR}|^2\frac{\beta^4\sin^4\theta}{(1+\beta\cos\theta)^2}, \qquad (3.37)\\
\frac{d\sigma}{d\cos\theta}(e^-_L e^+_R \to t_\uparrow\bar{t}_\downarrow) &= \left(\frac{3\pi\alpha^2}{2s}\beta\right)\left|f_{LL}(1+\beta\cos\theta)+f_{LR}\frac{(1-\beta)^2}{(1+\beta\cos\theta)}\right|^2.
\end{aligned}$$

3. Off-diagonal basis

There exists the third possibility called "off-diagonal" basis which makes the contributions from the like-spin configuration vanish [16]. The spin angle, ξ, is determined by

$$\tan\xi = \frac{A_{LR}}{B_{LR}} = \frac{(f_{LL}+f_{LR})\sqrt{1-\beta^2}\,\sin\theta}{f_{LL}(\cos\theta+\beta)+f_{LR}(\cos\theta-\beta)}\ . \tag{3.38}$$

In this basis, we obtain the polarized cross-sections,

$$\begin{aligned}
&\frac{d\sigma}{d\cos\theta}(e^-_Le^+_R\to t_\uparrow\bar{t}_\uparrow) \;=\; \frac{d\sigma}{d\cos\theta}(e^-_Le^+_R\to t_\downarrow\bar{t}_\downarrow) \;\equiv\; 0 \qquad , \\
&\frac{d\sigma}{d\cos\theta}(e^-_Le^+_R\to t_\uparrow\bar{t}_\downarrow \text{ or } t_\downarrow\bar{t}_\uparrow) \\
&= \left(\frac{3\pi\alpha^2}{2s}\beta\right)\left(\sqrt{A^2_{LR}+B^2_{LR}}\mp D_{LR}\right)^2 \\
&= \left(\frac{3\pi\alpha^2}{8s}\beta\right)\Big[f_{LL}(1+\beta\cos\theta)+f_{LR}(1-\beta\cos\theta) \\
&\mp\sqrt{[f_{LL}(1+\beta\cos\theta)+f_{LR}(1-\beta\cos\theta)]^2-4f_{LL}f_{LR}\beta^2\sin^2\theta}\Big]^2 \quad .
\end{aligned} \tag{3.39}$$

It is to be noted that we can consider another "off-diagonal " basis,

$$\tan\xi = \frac{A_{RL}}{B_{RL}} = \frac{(f_{RR}+f_{RL})\sqrt{1-\beta^2}\,\sin\theta}{f_{RR}(\cos\theta+\beta)+f_{RL}(\cos\theta-\beta)}\,, \tag{3.40}$$

which makes the contributions from the like-spin configuration vanish in the $e^-_Re^+_L$ scattering process. So, we can consider two "off-diagonal " bases for top quark pair production because $f_{LR}/f_{LL} \neq f_{RL}/f_{RR}$. However, the difference between f_{LR}/f_{LL} and f_{RL}/f_{RR} is not large numerically (see Fig.3.4). Therefore we call the basis defined by Eqn.(3.38) as "off-diagonal" basis in the following discussions.

Let us consider the difference between above three bases. In Fig.3.5, we plot the dependence of the spin angle ξ on the scattering angle θ for the helicity, beamline and off-diagonal bases at $\beta = 0$ (threshold), $\beta = 0.5$ ($\sqrt{s} \sim 400$ GeV) and $\beta = 1$ (ultra high energy).

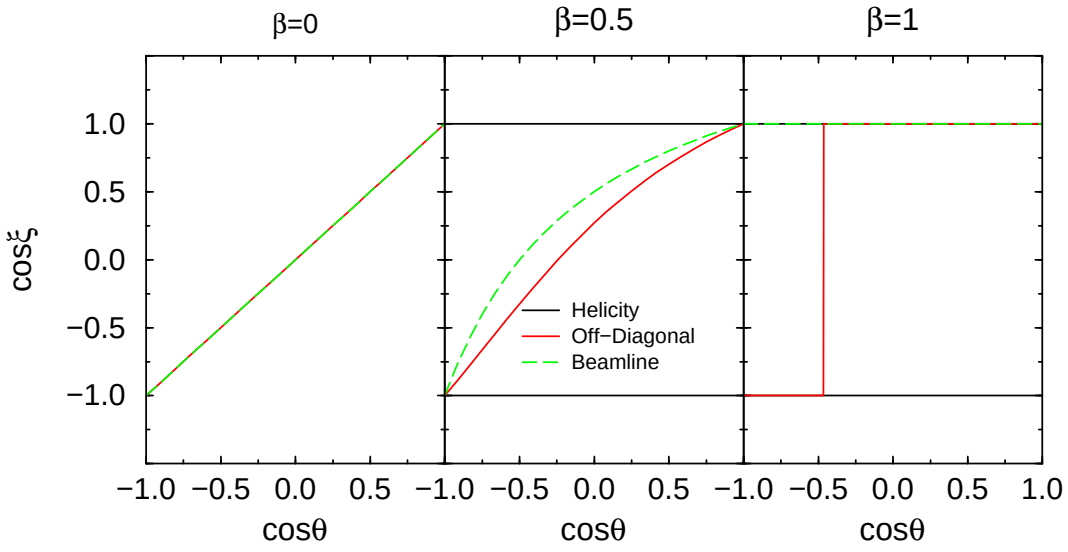

Figure 3.5: The dependence of the spin angle, ξ on the scattering angle θ in helicity, beamline and off-diagonal bases at $\beta = 0, 0.5$ and 1. It is noted that the off-diagonal basis at $\beta = 1$ changes from $\cos\xi = -1$ to $\cos\xi = +1$ at $\cos\theta = -(f_{LL} - f_{LR})/(f_{LL} + f_{LR})$.

When β is zero, the helicity basis can not be defined. However, the beamline and off-diagonal bases are defined also at threshold and they are given by the same equation, $\xi = \theta$. This fact says that it is correct that the top (anti-top) quark spin decomposes into the direction of positron (electron) momentum in the threshold region. When $\beta = 0.5$, we can see apparently the difference among these three bases. In particular, for the central region in which $\cos\theta \simeq 0$, there are remarkable differences between the three bases. However, the difference between the beamline basis and off-diagonal basis are small for all scattering angle compared to the helicity basis. The beamline and off-diagonal bases become close to the helicity basis with $\cos\xi = \pm 1$ near $\cos\theta = \pm 1$. When $\beta = 1$, the beamline basis coincides with the helicity basis with $\cos\xi = +1$. While, the off-diagonal basis is equal to the helicity basis with $\cos\xi = -1$ from $\cos\theta = -1$ to $\cos\theta = -(f_{LL} - f_{LR})/(f_{LL} + f_{LR})$, and equal to the helicity basis with $\cos\xi = +1$ form $\cos\theta = -(f_{LL} - f_{LR})/(f_{LL} + f_{LR})$ to $\cos\theta = +1$. The off-diagonal basis corresponds to the different helicity bases at $\cos\theta \simeq 1$ and $\cos\theta \simeq -1$.

Now we will show the polarized cross-sections for the helicity, the beamline and the off-diagonal bases in Fig.3.6 at $\sqrt{s} = 400$ GeV.

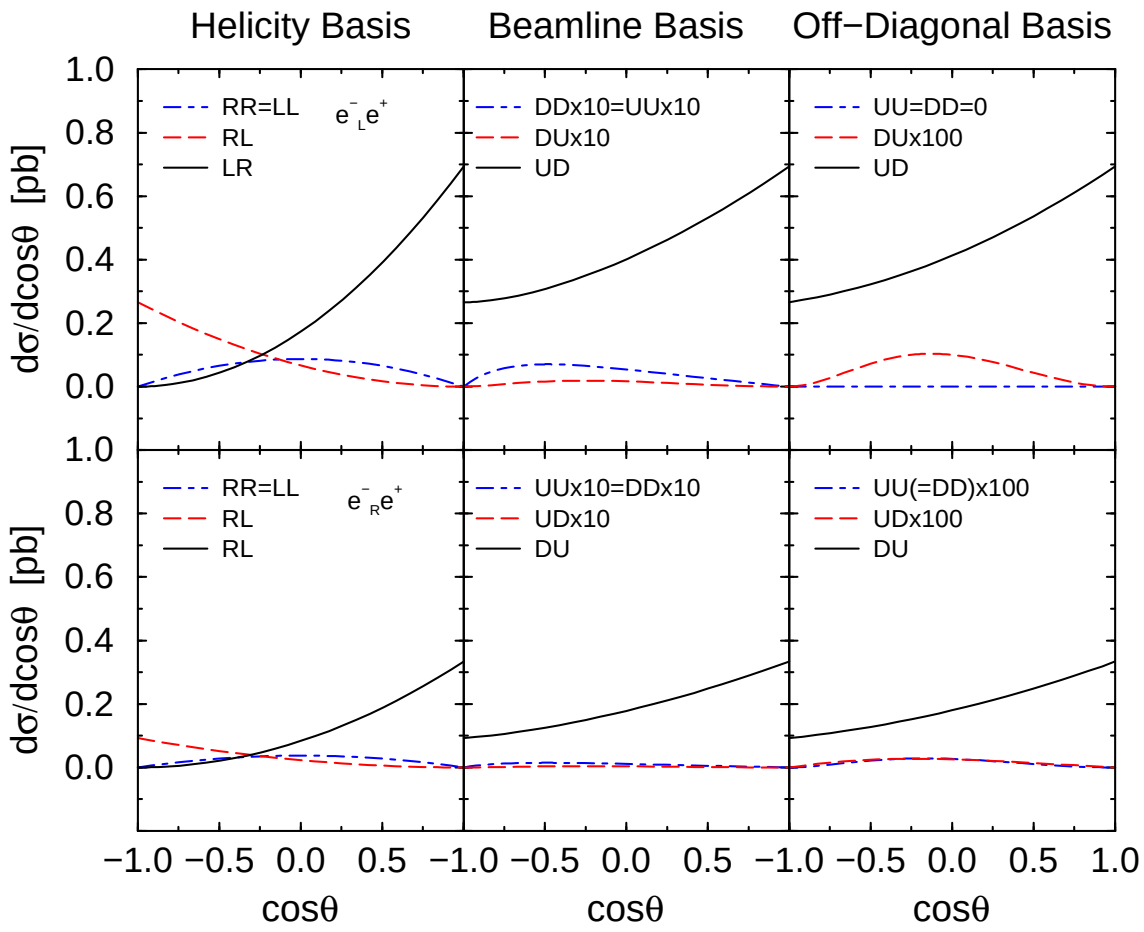

Figure 3.6: The polarized differential cross-sections in the helicity, beamline and off-diagonal bases at $\sqrt{s} = 400$ GeV for the $e^-_L e^+ (e^-_R e^+) \to t\bar{t}$ process. We plot the $t_L\bar{t}_L$ (LL), $t_R\bar{t}_R$ (RR), $t_R\bar{t}_L$ (RL), $t_R\bar{t}_L$ (RL) productions for the helicity basis and $t_\uparrow\bar{t}_\downarrow$ (UD), $t_\downarrow\bar{t}_\uparrow$ (DU), $t_\uparrow\bar{t}_\uparrow$ (UU) and $t_\downarrow\bar{t}_\downarrow$ (DD) productions for the beamline and the off-diagonal bases. Note that the sub-dominant and sub-sub-dominant configurations for both $e^-_L e^+$ and $e^-_R e^+$ process are amplified by the factor of 10 in the beamline basis and by the factor of 100 in the off-diagonal basis.

$e^-_L e^+$	Helicity	Beamline	Off-Diagonal
Dominant Frac.	0.5305 (LR)	0.97846 (UD)	0.99876 (UD)
Sub-Dominant Frac.	0.2033 (RL)	0.00964 (UU,DD)	0.00124 (DU)
$e^-_R e^+$	Helicity	Beamline	Off-Diagonal
Dominant Frac.	0.5804 (RL)	0.98979 (DU)	0.99744 (DU)
Sub-Dominant Frac.	0.1608 (LR)	0.00457 (UU,DD)	0.00089 (UU,DD)

Table 3.2: The fraction of $e^-_{L/R} e^+$ cross-sections for the dominant and the sub-dominant spin configurations in the helicity, beamline and off-diagonal bases at $\sqrt{s} = 400$ GeV.

The dominant component for the helicity basis is $t_L\bar{t}_R$ (LR) for $e_L^-e^+$ scattering and $t_R\bar{t}_L$ (RL) for $e_R^-e^+$ scattering at $\sqrt{s} = 400$ GeV. This dominant component occupies 53% of the total cross-section for $e_L^-e^+$ scattering and 58% of the total cross-section for $e_R^-e^+$ as shown in Table 3.2. Other components make up more than 40% of the total cross-section. Thus, the helicity basis does not show strong spin correlations for the polarized cross-sections at this energy. In contrast, in the beamline and the off-diagonal bases, only one component dominates the total cross-section. The dominant component for the beamline and the off-diagonal bases is $t_\uparrow\bar{t}_\downarrow$ (UD) and makes up more than 97% of the total cross-section for $e_L^-e^+$ scattering. For $e_R^-e^+$ scattering, the dominant contribution in the beamline and off-diagonal bases is $t_\downarrow\bar{t}_\uparrow$ (DU) component and make up more than 98% of the total cross-section. Other components give almost zero contribution. Apparently the top (anti-top) quark spin is strongly correlated with positron (electron) spin in the beamline and off-diagonal bases.

Here we focus on the beamline and off-diagonal bases and try to explain (1)*why the top (anti-top) quark spin is associated with the positron (electron) spin* and (2)*why the polarized cross-section in the beamline and off-diagonal bases show similar behaviors*. To answer these questions, recall the expression Eqn.(3.3) for $e_L^-e^+ \to t_{s_t}\bar{t}_{s_{\bar{t}}}$.

$$\begin{aligned}
&\mathcal{M}(e_L^-e_R^+ \to t_{s_t}\bar{t}_{s_{\bar{t}}}) \\
&= \frac{4\pi\alpha}{s}\,\langle\bar{q}-|\,\gamma_L^\mu\,|q-\rangle\,\bar{u}(t,s_t)\gamma_\mu\left[f_{LL}\gamma_L + f_{LR}\gamma_R\right]v(\bar{t},s_{\bar{t}}).
\end{aligned} \tag{3.41}$$

Using Fierz transformations in Eqn.(3.41), we obtain,

$$\begin{aligned}
\mathcal{M}(e_L^-e_R^+ \to t_{s_t}\bar{t}_{s_{\bar{t}}}) &= \frac{8\pi\alpha}{s}f_{LL}\Big[\,\bar{u}(t,s_t)\,|\bar{q}+\rangle\,\langle q+|\,v(\bar{t},s_{\bar{t}}) \\
&\quad + \frac{f_{LR}}{f_{LL}}\,\bar{u}(t,s_t)\,|q-\rangle\,\langle\bar{q}+|\,v(\bar{t},s_{\bar{t}})\,\Big].
\end{aligned} \tag{3.42}$$

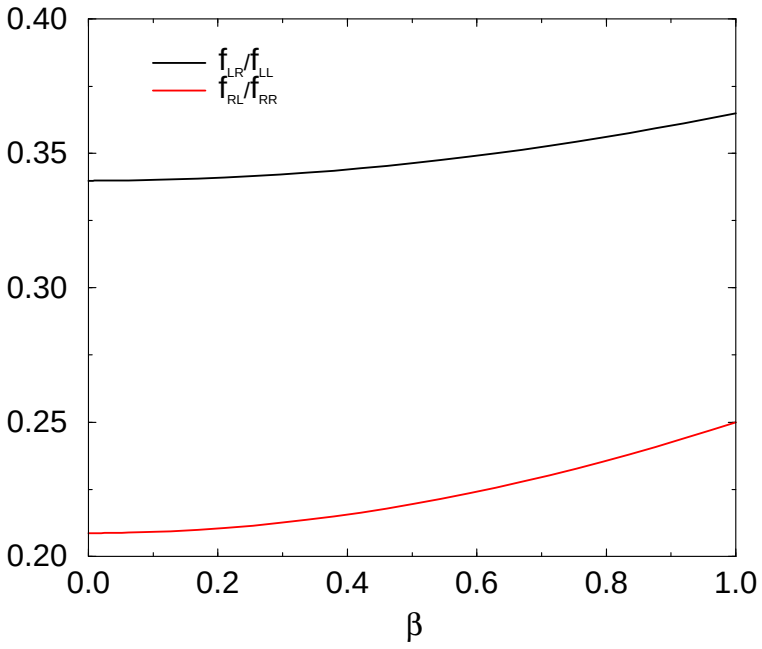

Figure 3.7: Top quark speed, β, dependence of ratios, f_{LR}/f_{LL} and f_{RL}/f_{RR}.

Figure (3.7) shows the top quark speed β dependence of the ratio f_{IJ}'s. For the top quark production, the f_{IJ}'s have a weak energy dependence; Numerically the parameters f_{IJ} fall in the range,

$$0.34 \leq \frac{f_{LR}}{f_{LL}} \leq 0.37, \tag{3.43}$$

$$0.21 \leq \frac{f_{RL}}{f_{RR}} \leq 0.25. \tag{3.44}$$

Because the ratio $|f_{LR}/f_{LL}|$ is less than 1, the first term of Eqn.(3.42) is dominant. This implies that the top (ant-top) quark spin is associated with positron (electron) spin.

We now come to the question (2). Now remember the definition of the spin angle ξ in the beamline and the off-diagonal bases in Eqns.(3.36) and (3.38). The spin angle ξ for the beamline basis is obtained from Eqn.(3.38) with $f_{LR} = 0$. Then we focus on the factor f_{LR} to answer the question (2). Since the factor $|f_{LR}|$ is smaller than $|f_{LL}|$, let us take an approximation of $f_{LR} = 0$ in Eqns.(3.37) and (3.39). The polarized cross-sections in the beamline and off-diagonal bases become the same expressions as

$$\begin{aligned} \frac{d\sigma}{d\cos\theta}(e^-_L e^+_R \to t_\uparrow \bar{t}_\uparrow) &= \frac{d\sigma}{d\cos\theta}(e^-_L e^+_R \to t_\downarrow \bar{t}_\downarrow) = 0, \\ \frac{d\sigma}{d\cos\theta}(e^-_L e^+_R \to t_\downarrow \bar{t}_\uparrow) &= 0, \end{aligned} \tag{3.45}$$

$$\frac{d\sigma}{d\cos\theta}(e_L^- e_R^+ \to t_\uparrow \bar{t}_\downarrow) \;=\; \left(\frac{3\pi\alpha^2}{2s}\beta\right)|f_{LL}|^2(1+\beta\cos\theta)^2.$$

Thus the difference between the polarized cross-sections in the beamline and the off-diagonal bases is $\mathcal{O}(|f_{LR}/f_{LL}|)$. The subdominant contributions, (UU, DD, DU), come from the $\mathcal{O}(|f_{LR}/f_{LL}|)$ corrections. This is the reason why polarized cross-sections in the beamline basis behaves like that in the off-diagonal basis.

Finally we discuss the top quark speed β dependence of the polarized cross-sections in the helicity, beamline and off-diagonal bases. We define the fraction $\sigma(e_L^- e^+ \to t_{s_t} t_{s_{\bar{t}}})/\sigma_T$ of top pair productions for each spin configurations, where σ_T is the total cross-section for the process, $e_L^- e^+ \to t\bar{t}$ and the suffix s_t ($s_{\bar{t}}$) represents the spin of top (anti-top) quark. We present the fraction in the helicity, beamline and off-diagonal bases in Fig.3.8.

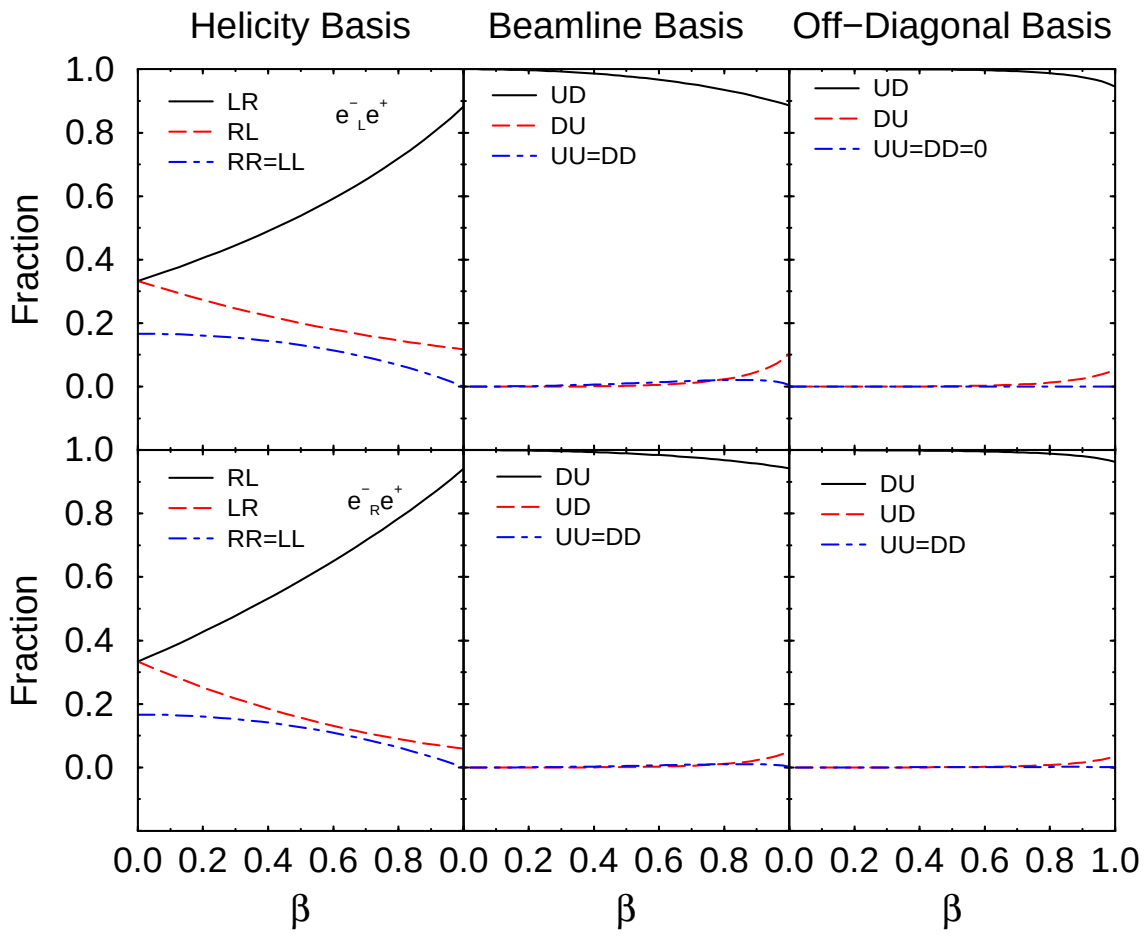

Figure 3.8: The fraction of top quark pairs in the helicity, beamline and off-diagonal bases, as a function of the top quark speed, β.

In the helicity basis, as the CM energy get larger, the spin correlation becomes stronger for $e^-_L e^+$ and $e^-_R e^+$ scattering. The polarized cross-sections in the beamline basis coincide with those in the helicity basis in the limit β to 1. This is in agreement with the fact that the helicity and beamline bases become identical in the limit of β to 1 (see the discussion on Fig.3.5). In the beamline and off-diagonal bases, the UD ($t_\uparrow \bar{t}_\downarrow$) channel dominates for $e^-_L e^+$ process for all values β as shown in Fig.3.8. (The DU ($t_\downarrow \bar{t}_\uparrow$) channel for $e^-_R e^+$ gives the dominant fraction in the beamline and off-diagonal bases.) However, there is a slight difference between in the beamline basis and in the off-diagonal basis near $\beta = 1$. This is due to the fact that the off-diagonal basis corresponds to the helicity basis with either $\cos\xi = +1$ or with $\cos\xi = -1$, depending on the scattering angle, while the beamline basis coincides the helicity basis with $\cos\xi = 1$ in the limit β to 1.

3.2 Top Quark Decays at Leading Order

In the previous section, we have shown that the top quark pairs are produced in an unique spin configurations at polarized e^+e^- linear colliders in a appropriate basis. We discuss in this section the spin-angular correlations for the top quark decay and measurement of the top quark spin. Because of the heavy mass of top quark, the width of top quark amounts to nearly 1.57 GeV [10]. In consequence, the top quark decays rapidly through the electro-weak interaction before the hadronization (which is governed by the scale Λ_{QCD}) take place. Therefore, we can obtain information of the top quark spin by measuring its decay products without being suffered from the complicated hadronization effects [35]. We show the electro-weak decay products of polarized top quark are strongly correlated to its spin axis at the leading order in perturbation theory of the Standard Model.

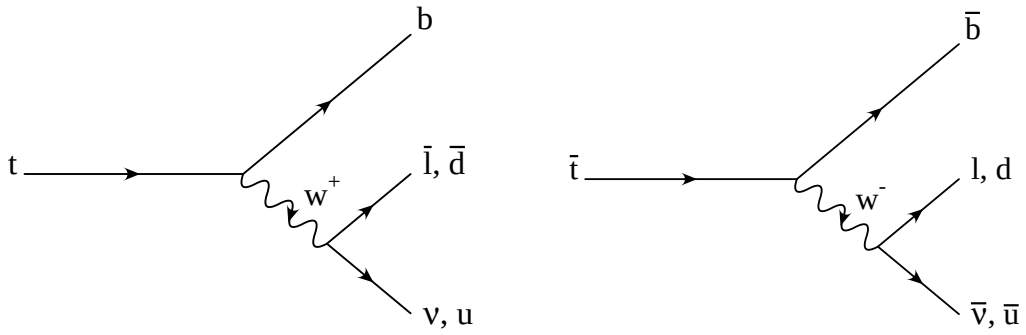

Figure 3.9: The hadronic and semi-leptonic decay process of top (anti-top) quark

The top (anti-top) quarks decay dominantly,

$$t \;\rightarrow\; W^+b,\; \bar{t} \;\rightarrow\; W^-\bar{b}. \tag{3.46}$$

For the W^+ (W^-) decay, there are hadronic decay and leptonic decay modes (see Fig. 3.9);

$$\begin{array}{lllllll} W^+ & \rightarrow & u\bar{d} \text{ or } c\bar{s}, & W^- & \rightarrow & d\bar{u} \text{ or } s\bar{c}, \\ W^+ & \rightarrow & \bar{l}\,\nu_l, & W^- & \rightarrow & l\,\bar{\nu}_l. \end{array} \tag{3.47}$$

Now let us calculate the decay distribution for the top quark decay. (The anti-top quark decay can be calculated similarly.) Momenta of the particles are assigned by its symbol, and we decompose the top momentum t into a sum of two massless momenta t_1 and t_2,

$$t \;=\; t_1 + t_2.$$

The spin vector of top quark is related to the momenta $t_1,\ t_2$ by the following relation,

$$s_t \ = \ \frac{1}{2m}(t_1 - t_2).$$

The amplitudes for $t_\uparrow/t_\downarrow \to b\bar{l}\nu_l$ are given by,

$$\mathcal{M}(t_\uparrow \to b\bar{l}\nu_l) \ = \ -g^2 \frac{V_{tb}\,\langle b\ \nu\rangle\,[\bar{l}\ t_2]}{(t-b)^2 - M_W^2 + iM_W\Gamma_W}\frac{\langle t_2\ t_1\rangle}{m}\ , \tag{3.48}$$

$$\mathcal{M}(t_\uparrow \to b\bar{l}\nu_l) \ = \ -g^2 \frac{V_{tb}\,\langle b\ \nu\rangle\,[\bar{l}\ t_1]}{(t-b)^2 - M_W^2 + iM_W\Gamma_W}\ . \tag{3.49}$$

The mass and the width of W boson are M_W and Γ_W, and SU(2) coupling g is related to the electro-magnetic coupling through $g = e/\sin\theta_W$. V_{tb} is the Cabibbo-Kobayashi-Maskawa (CKM) matrix element. For the hadronic decay of the top quark, one should replace $\bar{l}$ with $\bar{d}$ and ν with u in Eqns.(3.48) and (3.49). The squared matrix elements for the top (anti-top) quark decay, $t \to b\bar{l}\nu_l$, are given by

$$|\mathcal{M}(t_\uparrow \to b\bar{l}\nu_l)|^2 \ = \ \frac{4g^4|V_{tb}|^2}{[(\bar{l}+\nu)^2 - M_W^2]^2 + M_W^2\Gamma_W^2}(b\cdot\nu)(\bar{l}\cdot t_2)\ , \tag{3.50}$$

$$|\mathcal{M}(t_\downarrow \to b\bar{l}\nu_l)|^2 \ = \ \frac{4g^4|V_{tb}|^2}{[(\bar{l}+\nu)^2 - M_W^2]^2 + M_W^2\Gamma_W^2}(b\cdot\nu)(\bar{l}\cdot t_1)\ . \tag{3.51}$$

To calculate the decay distributions, we take the top (anti-top) quark rest frame in which the direction of top quark spin axis coincides with the $z-$axis. The kinematical variables for top quark decay process are,

$$\begin{aligned} s_t^\mu \ &= \ (0,\mathbf{s}_t) \ = \ (0,0,0,1)\ , \\ t^\mu \ &= \ m(1,0,0,0)\ , \\ t_1 \ &= \ (m/2)(1,0,0,1)\ , \\ t_2 \ &= \ (m/2)(1,0,0,-1)\ , \\ \bar{l}^\mu \ &= \ E_{\bar{l}}(1,\sin\theta_{\bar{l}}\cos\phi,\sin\theta_{\bar{l}}\sin\phi,\cos\theta_{\bar{l}})\ . \end{aligned} \tag{3.52}$$

Here the lepton mass is neglected, and the energy of lepton is denoted by $E_{\bar{l}}$. The variables $\theta_{\bar{l}},\ \phi$ are angles to specify the orientation of top quark spin as in Fig.3.10.

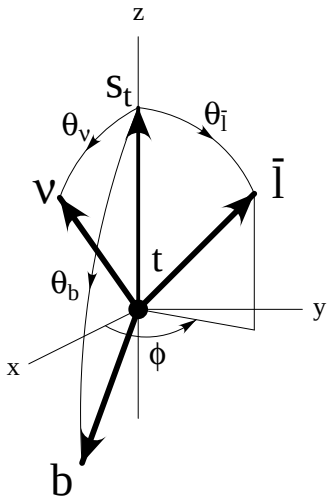

Figure 3.10: The momentum configurations for decay products, lepton and neutrino, in the top quark rest frame. The direction of top quark spin is defined by the direction of $+z$ axis.

It is convenient to introduce the scaled variables, $w, y, \bar{y}, x_{\bar{l}}$ and x_ν.

$$\begin{aligned} w^2 &= (\bar{l}+\nu)^2,\ y = \frac{w^2}{m^2},\ \bar{y} = \frac{M_W^2}{m^2}, \\ \gamma &= \frac{\Gamma_W}{M_W},\ x_{\bar{l}} = \frac{2E_{\bar{l}}}{m},\ x_\nu = \frac{2E_\nu}{m}. \end{aligned}$$

The three particle phase space integral can be parametrized in terms of scaled variables $x_{\bar{l}}$, y, and the angles $\theta_{\bar{l}}$, ϕ.

$$\begin{aligned} \int (PS)_3 &= \int \frac{d^3b}{(2\pi)^3(2b^0)} \frac{d^3\bar{l}}{(2\pi)^3(2\bar{l}^0)} \frac{d^3\nu}{(2\pi)^3(2\nu^0)} (2\pi)^4\delta^4(t-b-\bar{l}-\nu), \\ &= \frac{m^2}{2(4\pi)^4} \int_0^1 dx_{\bar{l}} \int_0^{x_{\bar{l}}} dy \int d\cos\theta_{\bar{l}} d\phi. \end{aligned} \tag{3.53}$$

The differential distribution for the lepton, $\bar{l}$, in the decay of the polarized top quark can be written as

$$\frac{d\Gamma(s_t)}{dx_{\bar{l}} dy d\cos\theta_{\bar{l}}}(t \to b\bar{l}\nu_l) = \frac{mg^4}{16(4\pi)^3} \left(\frac{|V_{tb}|^2}{\bar{y}^2}\right) \frac{F_0(s_t)}{(1-y/\bar{y})^2+\gamma^2}, \tag{3.54}$$

where s_t denotes top quark spin states ($\uparrow$ or $\downarrow$), and the function $F_0(s_t)$ is given by

$$\begin{aligned} F_0(\uparrow) &= x_{\bar{l}}(1-x_{\bar{l}})(1+\cos\theta_{\bar{l}}), \\ F_0(\downarrow) &= x_{\bar{l}}(1-x_{\bar{l}})(1-\cos\theta_{\bar{l}}). \end{aligned} \tag{3.55}$$

After integrating over variable y in Eqn.(3.54), we obtain the double differential $(x_{\bar{l}} - \theta_{\bar{l}})$ distribution.

$$\frac{d\Gamma(s_t)}{dx_{\bar{l}} d\cos\theta_{\bar{l}}}(t \to b\bar{l}\nu_l) \;=\; \frac{mg^4}{16(4\pi)^3}\left(\frac{1}{\bar{y}\gamma}\right) F_0(s_t)\arctan\left[\frac{\gamma x_{\bar{l}}}{(1+\gamma^2)\bar{y} - x_{\bar{l}}}\right]. \tag{3.56}$$

This result shows that the double differential distribution in written in a factrized form, the energy distribution and the angular distribution.

The above formula Eqn.3.56 will be reduced to a simple form if we take into account that the W boson propagator in Eqn.(3.54) can be approximated as for the process $t \to b\bar{l}\nu$.

$$\frac{1}{(1-y/\bar{y})^2 + \gamma^2} \;=\; \frac{\pi}{\gamma}\delta\left(1 - \frac{y}{\bar{y}}\right) \;+\; \mathcal{O}(\gamma)\ .$$

In fact, the value of γ is small, ~ 0.02 and we can neglect the contribution from terms of order $\mathcal{O}(\gamma)$ (the narrow width approximation). In the narrow width approximation for W boson, $\gamma \to 0$, Eqn.(3.56) is reduced to,

$$\frac{1}{\Gamma_T}\frac{d\Gamma}{dx_{\bar{l}}\; d\cos\theta_{\bar{l}}} \;=\; \frac{1}{2}\mathcal{F}(x_{\bar{l}})\left[1 + \alpha_{\bar{l}}\cos\theta_{\bar{l}}\right], \tag{3.57}$$

$$\mathcal{F}(x_{\bar{l}}) \;=\; \frac{3x_{\bar{l}}(1-x_{\bar{l}})}{(1-\bar{y})^2(1+2\bar{y})}\ , \tag{3.58}$$

with the region of kinematical valuable $x_{\bar{l}}$,

$$\bar{y} \;\le\; x_{\bar{l}} \;\le\; 1. \tag{3.59}$$

Here Γ_T is the total decay width, and the parameter $\alpha_{\bar{l}}$ ($\alpha_{\bar{l}} = 1$ for the $\uparrow$ quark spin state and $\alpha_{\bar{l}} = -1$ for the $\downarrow$ state.) denotes the strength of correlation between the momentum direction of decay particle $\bar{l}$ and the direction of top quark spin axis.

In the same way, we can calculate the differential distribution for any decay product i ($i = b,\ \bar{l},\ \nu,\ u,\ \bar{d},\ W$). The differential angular distribution, in general, is written as after integrating over x_i [36, 37, 38],

$$\frac{1}{\Gamma_T}\frac{d\Gamma}{d\cos\theta_i} \;=\; \frac{1+\alpha_i\cos\theta_i}{2}, \tag{3.60}$$

where θ_i denotes the angle between the top quark spin axis $\mathbf{s}_t$ and the direction of motion of decay product i ($i = b,\ \bar{l},\ \nu,\ u,\ \bar{d}$, W). The correlation coefficient α_i may be computed from the squared matrix elements (3.50)$\sim$(3.51). (see Refs.[36, 37] for the details.)

i	α_i	α_i
l or d	1	1.00
ν or u	$\frac{(\bar{y}-1)(2\bar{y}^2+11\bar{y}-1)-12\bar{y}^2\ln\bar{y}}{(2\bar{y}+1)(\bar{y}-1)^2}$	-0.318
W^+	$-\frac{\bar{y}-2}{\bar{y}+2}$	0.406
b	$\frac{\bar{y}-2}{\bar{y}+2}$	-0.406

Table 3.3: Correlation coefficients α_i for the polarized top quark decay in the narrow width approximation for W boson. The b quark mass is neglected, and the values $m = 175.0$ GeV and $M_W = 80.41$ GeV are used.

For the spin-up top quark, the correlation coefficients α_i are given in Table.3.3. For the spin-down top quark, the correlation coefficients have the opposite sign.

Using the values in Table.3.3, we plot the single particle spin-angular correlation Eqn.(3.60) in Fig.3.11.

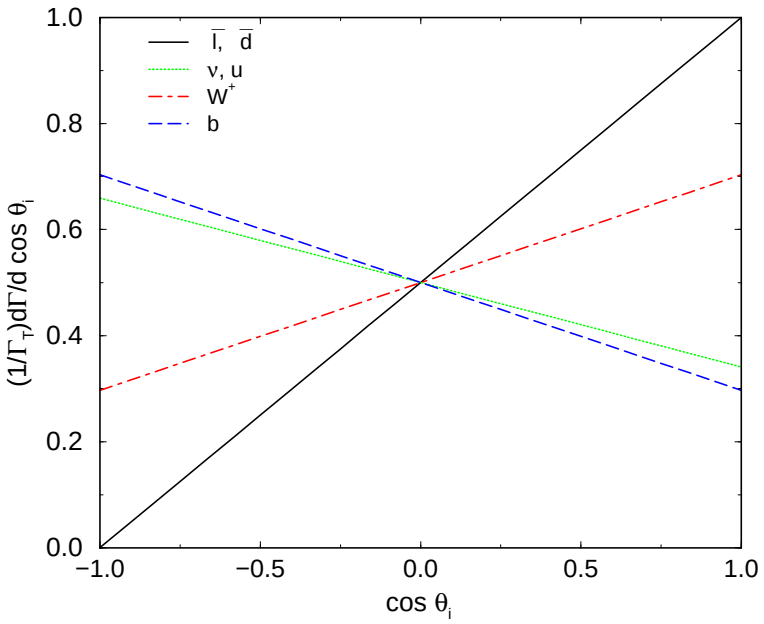

Figure 3.11: The angular distributions of decay products i, ($\bar{l}, \bar{d}, u, \nu_l, b$ and W^+), in the top quark decay process. The θ_i is the angle between the direction of top quark spin and the moving direction of decay product i.

The lepton and d-type quark are maximally correlated with the top quark spin axis compared

with other particles, u, ν_l, b and W^+. It is surprising that the charged lepton or d-type quark come from the decay of the W boson which is less correlated with the top quark spin.

Here it might be interesting and instructive to investigate spin component of W boson contributes to the decay process, $(t \to b\bar{l}\nu)$. To answer this question, we consider the top quark cascade decay $t \to bW^+ \to b\bar{l}\nu$ [16, 34, 39]. The differential decay distribution of a polarized top quark depends on three angles. First is the angle, χ_W^t, which specifies the moving direction of the W boson with respect to the top quark spin in the top quark rest frame. Second is the angle, $\pi - \chi_l^W$, between the direction of motion of b quark and lepton in the W boson rest frame. Finally the azimuthal angle, Φ, between the lepton and top quark spin around the direction of W boson. The differential decay distribution is

$$\begin{aligned}
&\frac{1}{\Gamma_T}\frac{d^3\Gamma}{d\cos\chi_W^t d\cos\chi_l^W d\Phi} \\
&= \frac{3}{16\pi(m^2+2M_W^2)}\Big[m^2(1+\cos\chi_W^t)\sin^2\chi_l^W + M_W^2(1-\cos\chi_W^t)(1-\cos\chi_l^W)^2 \\
&\qquad + 2mM_W(1-\cos\chi_l^W)\sin\chi_W^t\sin\chi_l^W\cos\Phi\Big] . \qquad (3.61)
\end{aligned}$$

In Eqn.(3.61), the first and the second terms are contributions from the longitudinal and transverse W boson, and the third term represents the interference between the longitudinal and transverse W boson. The contribution of the transverse W boson is suppressed by the factor M_W^2/m^2, and the interference contribution, by the factor $2M_W/m$ compared to the contribution of the longitudinal W. Note that the interference term does not contribute to the total decay width because of the factor $\cos\Phi$.

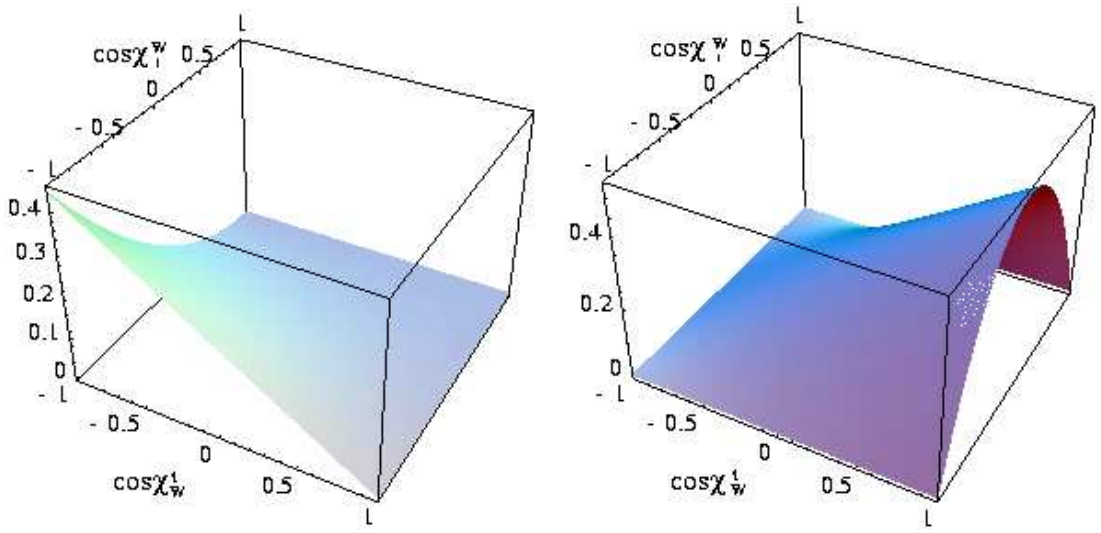

(a) (b)

Figure 3.12: The 3-dimensional plot of the top quark differential angular distribution, $\frac{1}{\Gamma_T}\frac{d^2\Gamma}{d\cos\chi_l^W d\cos\chi_W^t}$. (a) is the contribution from the longitudinal W boson and (b) from the transverse W boson (b).

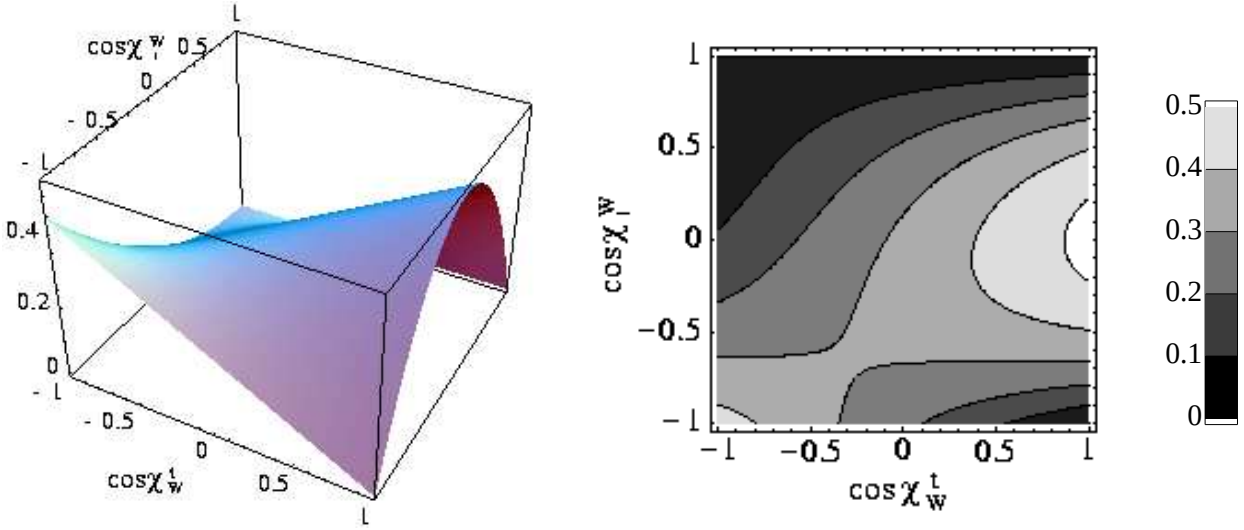

Figure 3.13: The 3-dimensional and contour plot of the top quark differential angular distribution, $\frac{1}{\Gamma_T}\frac{d^2\Gamma}{d\cos\chi_l^W d\cos\chi_W^t}$. Each contour-line shows the angular distribution with the values $0.1, 0.2, 0.3, 0.4, 0.5$.

We plot the 3-dimensional differential angular distribution in $\cos\chi_l^W$ verses $\cos\chi_W^t$ in Fig.3.12. Fig.3.12(a) presents the contribution of longitudinal W boson, Fig.3.12(b) shows the transverse W boson. Fig.3.13 shows 3-dimensional and contour plots of the differential angular distribution in $\cos\chi_l^W$ verses $\cos\chi_W^t$. When the W boson momentum is parallel to the top quark spin $\cos\chi_W^t = 1$, only the longitudinal W boson contributes to the angular distribution. When the W boson momentum is anti-parallel to the top quark spin $\cos\chi_W^t = -1$, the transverse W boson purely contributes. In the region, $-1 \leq \cos\chi_W^t \leq 1$, both the longitudinal and the transverse W boson contribute and significantly. Although the contribution of transverse W boson to the total decay width is small, $\sim 30\%$, the transverse W boson has a significant impact on the angular distribution of the top quark decay products.

Now we move the to the discussion on the measurement [27, 40] of the top quark spin. As mentioned before, there are two top quark decay modes, hadronic decay and semi-leptonic decay. The rate of the hadronic decay mode is approximately 9 times larger than the rate of each leptonic decay mode. However, we must take into account the efficiency to identify the d-type quark from u-type (or vice versa) in order to utilize the hadronic decay products. Therefore, we consider the the semi-leptonic decay mode of the top (anti-top) quark to simplify our discussions. From Eqn.(3.60), we can obtain the probability $P(\uparrow \mid \text{in the cone})$ that the top quark has spin up when we pick up events which satisfy the condition $\cos\theta_i > y$,

$$P(\uparrow \mid \text{in the cone}) \;=\; \frac{(1+\langle s_t\rangle)\,(2+\alpha_i(1+y))}{4+2\,\langle s_t\rangle\,\alpha_i(1+y)}, \tag{3.62}$$

where the probability function $P(A|B)$ denotes the conditional probability of the event A, and $\langle s_t\rangle$ denotes the average value of the top quark spin defined by

$$\langle s_t\rangle = \sum_{s_t=-1,1} s_t \times P(s_t). \tag{3.63}$$

$P(s_t)$ is the probability that the top quarks with spin s_t are produced.

It is straightforward to extend this analysis to the top pair production process. The double decay distribution for the decay product "i" from the top quark and the decay product "$\bar{i}$" from the anti-top quark is given by

$$\begin{aligned}\frac{d^2\Gamma}{d\cos\theta_i d\cos\theta_{\bar{i}}} \;&\simeq\; \frac{1}{4}\{1+\alpha_i\langle s_t\rangle\cos\theta_i+\alpha_{\bar{i}}\langle s_{\bar{t}}\rangle\cos\theta_{\bar{i}} \\ &\quad +\alpha_i\alpha_{\bar{i}}\langle s_t s_{\bar{t}}\rangle\cos\theta_i\cos\theta_{\bar{i}}\}\,,\end{aligned} \tag{3.64}$$

where θ_i ($\theta_{\bar{i}}$) is the angle between the direction of the top (anti-top) quark spin and the momentum of decay product i ($\bar{i}$) in the top (anti-top) quark rest frame. As can be seen

in the above expression, it is obvious how the spin correlation between the top and anti-top quarks is related to the distribution of their decay products.

When we collect events for which the charged lepton i from the top quark lies in the cone defined by $\cos\theta_i > y$, the effective α in the expression Eqn.(3.60) for anti-top quark becomes,

$$\alpha_{\bar{i}}^{eff} = \frac{\{2\langle s_{\bar{t}}\rangle + \alpha_i \langle s_t s_{\bar{t}}\rangle (1+y)\}}{2 + \alpha_i \langle s_t\rangle (1+y)} \times \alpha_{\bar{i}}, \tag{3.65}$$

which determine the $\bar{i}$ distribution under the condition mentioned above. Then the distribution of the decay product $\bar{i}$ from the anti-top quark is given by

$$\frac{1}{\Gamma_T}\frac{d\Gamma}{d\cos\theta_{\bar{i}}} = \frac{1+\alpha_{\bar{i}}^{eff}\cos\theta_{\bar{i}}}{2}. \tag{3.66}$$

By observing this distribution, we can obtain the averaged value of the spin $\langle s_t\rangle$ and the spin correlation $\langle s_t s_{\bar{t}}\rangle$ between the top and anti-top quarks.

Chapter 4

QCD Corrections to Spin Correlations

A basic consequence of the large top quark mass is its short lifetime. The top quark lifetime is $\tau \sim 10^{-24}$ second and top quark decays very rapidly to the b quark and the W boson before QCD long distance effects come in. Therefore, top quarks are produced essentially as unbounded fermion. However they still feel the strong interactions and will radiate gluons. Especially, there are two "new" effects, which are caused by the QCD radiative correction. First, the QCD corrections induce the new structure to $\gamma/Z - t - \bar{t}$ vertex. Second, the emission of a real gluon with spin 1 leads to the spin-flip effects. Thus it is important and urgent to study how the tree level picture will be affected by QCD correction. The QCD $\mathcal{O}(\alpha_s)$ corrections to the top quark productions have been studied in several papers [19, 20], including analyses of the effects on the production angle distributions and their polarization. However, in these works, the top quark spin is decomposed in the helicity basis. In previous chapter, we studied that the top quark spin decomposition in the helicity basis is not appropriate at moderate energies, and the "off-diagonal" basis is optimal spin decomposition in this energy region at the leading order.

In this chapter, we present the differential cross-sections for top quark productions in the "generic" spin basis at QCD one-loop level, and investigate which is the optimal decomposition of top quark spin at QCD one-loop level at the energy far above the threshold for top quarks. We quantitatively analyze spin-spin correlations for top quarks, and examine the spin flip effects caused by the QCD radiative corrections.

4.1 Vertex Corrections and Soft Gluon Case

In this section, we derive the QCD correction at $\mathcal{O}(\alpha_s)$ to the spin dependent differential cross-section for top quark pair production in the soft gluon approximation (SGA) [41, 42]. In

this approximation, only the QCD vertex corrections modify the spin correlations of the top quarks. Therefore, in order to investigate a new structure induced by the QCD corrections, it is instructive to consider the soft gluon approximation. We give analytic expressions for the polarized cross-sections at QCD one-loop level in the soft-gluon approximation using the generic spin basis.

4.1.1 QCD Corrections to Vertex $\gamma/Z - t - \bar{t}$

The QCD corrections to the cross-sections are given by the interference between the tree and the one-loop vertex diagram in Fig.4.1.

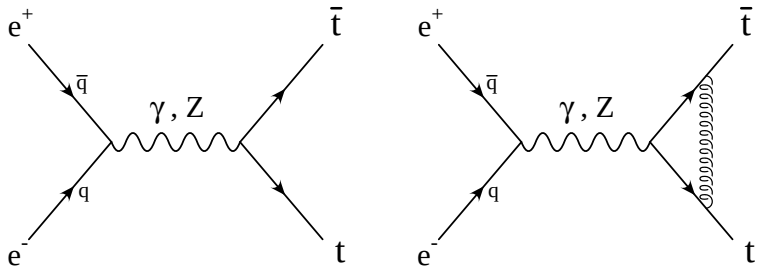

Figure 4.1: The tree level and the QCD one-loop contributions to the $e^-e^+ \to t\bar{t}$ process.

There are both infrared and ultra-violet singularities in the one-loop integrals of the virtual corrections. We treat the ultra-violet singularities within the frame work of dimensional regularization in $D = 4 - 2\varepsilon$, and introduce an infinitesimal mass for the gluon to avoid infrared singularities.

At the one-loop level, the $\gamma - t - \bar{t}$ and $Z - t - \bar{t}$ vertex functions can be written in terms of three form factors A_0, B_0, C_0 as follows:

$$\Gamma^{\gamma}_{\mu} = eQ_t \left[(1 + A_0)\,\gamma_\mu + B_0\,\frac{t_\mu - \bar{t}_\mu}{2m} \right] , \tag{4.1}$$

$$\begin{aligned} \Gamma^{Z}_{\mu} = \frac{e}{\sin\theta_W} \Big[& \left\{ Q_t^L\,(1 + A_0) + (Q_t^L - Q_t^R)\,B_0 \right\} (\gamma_L)_\mu \\ & + \left\{ Q_t^R\,(1 + A_0) - (Q_t^L - Q_t^R)\,B_0 \right\} (\gamma_R)_\mu \\ & + \frac{Q_t^L + Q_t^R}{2}\,B_0\,\frac{t_\mu - \bar{t}_\mu}{2m} + \frac{Q_t^L - Q_t^R}{2}\,C_0\,\frac{t_\mu + \bar{t}_\mu}{2m}\gamma_5 \Big] , \end{aligned} \tag{4.2}$$

where Q_t, θ_W, m and $t_\mu\,(\bar{t}_\mu)$ have been defined in the previous chapter. The form factor A_0 represents the enhancement effect to the tree vertex structure. So, this factor does not change

the tree-level results except for the multiplicative enhancement. Meanwhile, the factors B_0, C_0 are the coefficients of new vertex structures induced by the QCD corrections. In particular, the factor C_0 represents the contribution from only the QCD corrected $Z-t-\bar{t}$ vertex.

$$\begin{aligned} A_0 &= \hat{\alpha}_s\Bigg[C_{UV} - \ln\frac{m^2}{\mu^2} + 3\beta\ln\left(-\frac{1+\beta}{1-\beta}\right) + \frac{1+\beta^2}{\beta}\Big\{\ln\left(-\frac{1+\beta}{1-\beta}\right)\ln\frac{\lambda^2}{m^2} \\ &+ \frac{1}{2}\ln\left(-\frac{1-\beta^2}{4\beta^2}\right)\ln\left(-\frac{1+\beta}{1-\beta}\right) + \mathrm{Li}_2\left(\frac{1+\beta}{2\beta}\right) - \mathrm{Li}_2\left(-\frac{1-\beta}{2\beta}\right)\Big\}\Bigg], \qquad (4.3) \\ B_0 &= \hat{\alpha}_s\frac{1-\beta^2}{\beta}\ln\left(-\frac{1+\beta}{1-\beta}\right), \qquad (4.4) \\ C_0 &= \hat{\alpha}_s\left[(2+\beta^2)\frac{1-\beta^2}{\beta}\ln\left(-\frac{1+\beta}{1-\beta}\right) - 2(1-\beta^2)\right], \qquad (4.5) \end{aligned}$$

with

$$\begin{aligned} C_{UV} &= \frac{1}{\varepsilon} + \ln 4\pi - \gamma_E\ , \qquad (4.6) \\ \beta &= \sqrt{1-\frac{4m^2}{s+i\epsilon}}\ . \qquad (4.7) \end{aligned}$$

where $\varepsilon = 2 - D/2$, D is the space-time dimension, $\gamma_E \simeq 0.57721$ is the Euler constant, β is the speed of the produced top (anti-top) quark and the strong coupling constant is $\hat{\alpha}_s \equiv \frac{C_2(R)}{4\pi}\alpha_s = \frac{C_2(R)}{(4\pi)^2}g^2$ with $C_2(R) = 4/3$ for SU(3) color.

We have introduced an infinitesimal mass λ for the gluon to avoid infrared singularities. The wave function renormalization factor z_2 in the one-shell renormalization scheme is calculated to be,

$$z_2 = 1 + \hat{\alpha}_s\left(-C_{UV} + \ln\frac{m^2}{\mu^2} - 4 - 2\ln\frac{\lambda^2}{m^2}\right). \qquad (4.8)$$

After multiplying the wave function renormalization factor, the "renormalized" form factors A, B and C read

$$\begin{aligned} A &= A_R + A_I \\ &= \hat{\alpha}_s\Bigg[\left(\frac{1+\beta^2}{\beta}\ln\frac{1+\beta}{1-\beta} - 2\right)\ln\frac{\lambda^2}{m^2} - 4 + 3\beta\ln\frac{1+\beta}{1-\beta} + \frac{1+\beta^2}{\beta} \\ &\quad\times\left\{\frac{1}{2}\ln^2\frac{1+\beta}{1-\beta} + \ln^2\frac{1+\beta}{2\beta} - \ln^2\frac{1-\beta}{2\beta} + 2\mathrm{Li}_2\left(\frac{1-\beta}{1+\beta}\right) + \frac{2}{3}\pi^2\right\}\Bigg] \\ &\quad + i\pi\hat{\alpha}_s\left[-3\beta - \frac{1+\beta^2}{\beta} - \Big(\ln\frac{1-\beta}{2\beta} + \ln\frac{1+\beta}{2\beta}\Big) - \frac{1+\beta^2}{\beta}\ln\Big(\frac{\lambda^2}{m^2}\Big)\right], \qquad (4.9) \\ B &= B_R + B_I \end{aligned}$$

$$= \hat{\alpha}_s \frac{1-\beta^2}{\beta} \ln\frac{1+\beta}{1-\beta} - i\pi\hat{\alpha}_s \frac{1-\beta^2}{\beta} \ , \tag{4.10}$$

$$C = C_R + C_I$$

$$= \hat{\alpha}_s \left[(2+\beta^2)\frac{1-\beta^2}{\beta} \ln\frac{1+\beta}{1-\beta} - 2(1-\beta^2) \right] - i\pi\hat{\alpha}_s \frac{2+\beta^2}{\beta} \ , \tag{4.11}$$

where suffices R, I stand for the real part and the imaginally part of the form factors A, B, C respectively. In the above expressions, we take only the real part of the form factors. The reasons are (1) The contribution of Z boson width is negligible in the region of CM energy $\sqrt{s}$ far above the production threshold for top quarks. (2) We do not consider the transverse top quark polarization normal to the scattering plane, since we are interested in how QCD corrections modify the tree level spin correlations and which spin basis is the most effective for spin correlation studies (Although it is known [12, 21] that the transverse top quark polarization becomes non-zero when the higher order QCD corrections are included and this transverse polarization is very important and related to the phenomena of CP violation, we do not consider transverse polarization of the top quarks).

We get the amplitudes for the $e^-_{L/R}e^+_{R/L} \to t_{s_t}\bar{t}_{s_{\bar{t}}}$ process using above renormalized vertex:

$$\begin{aligned}
&\mathcal{M}(e^-_L e^+_R \to t_{s_t}\bar{t}_{s_{\bar{t}}}) \\
&= \left(\frac{4\pi\alpha}{s}\right) \langle \bar{q}-| \left(\gamma_L\right)_\mu |q-\rangle \, \bar{u}(t,s_t) \Big[\Big\{ f_{LL}(1+A_R+B_R) - f_{LR}B_R \Big\}\gamma^\mu_L \\
&\qquad + \Big\{ f_{LR}(1+A_R+B_R) - f_{LL}B_R \Big\}\gamma^\mu_R \\
&\qquad + \frac{B_R}{2}(f_{LL}+f_{LR})\frac{t^\mu - \bar{t}^\mu}{2m} \\
&\qquad + \frac{C_R}{2}(f_{LL}-f_{LR})\frac{t^\mu + \bar{t}^\mu}{2m}\gamma_5 \Big] v(\bar{t}, s_{\bar{t}}),
\end{aligned} \tag{4.12}$$

$$\begin{aligned}
&\mathcal{M}(e^-_R e^+_L \to t_{s_t}\bar{t}_{s_{\bar{t}}}) \\
&= \left(\frac{4\pi\alpha}{s}\right) \langle \bar{q}+| \left(\gamma_R\right)_\mu |q+\rangle \, \bar{u}(t,s_t) \Big[\Big\{ f_{RR}(1+A_R+B_R) - f_{RL}B_R \Big\}\gamma^\mu_R \\
&\qquad + \Big\{ f_{RL}(1+A_R+B_R) - f_{RR}B_R \Big\}\gamma^\mu_L \\
&\qquad + \frac{B_R}{2}(f_{RR}+f_{RL})\frac{t^\mu - \bar{t}^\mu}{2m} \\
&\qquad + \frac{C_R}{2}(f_{RR}-f_{RL})\frac{t^\mu + \bar{t}^\mu}{2m}\gamma_5 \Big] v(\bar{t}, s_{\bar{t}}),
\end{aligned} \tag{4.13}$$

where the electron (positron) mass is neglected. Note that the contribution from C_R vanish because it is proportion to the electron mass in the amplitudes.

Since we do not consider the transverse polarization of top quark, we can define the spin of top and anti-top quark in the production plane. We use the generic spin basis defined in

Chapter 3 and again, we decompose the top (anti-top) quark momentum t ($\bar{t}$) into the two massless momenta $t_1,\ t_2$ ($\bar{t}_1,\ \bar{t}_2$).

Using spinor helicity method, we can easily obtain the squared amplitudes at one-loop level,

$$
\begin{aligned}
&|\mathcal{M}(e_L^- e^+ \to t_\uparrow \bar{t}_\uparrow)|^2 \\
&= \left(\frac{4\pi\alpha}{s}\right)^2 \Bigg[4\Big\{|f_{LL}|^2(1+2A_R+2B_R) - 2f_{LL}f_{LR}B_R\Big\}(2q\cdot t_1)(2\bar{q}\cdot \bar{t}_2) \\
&\quad +4\Big\{|f_{LR}|^2(1+2A_R+2B_R) - 2f_{LL}f_{LR}B_R\Big\}(2q\cdot \bar{t}_1)(2\bar{q}\cdot t_2) \\
&\quad +\frac{4}{m^2}\Big\{f_{LL}f_{LR}(1+2A_R+2B_R) - 2f_{LL}f_{LR}B_R\Big\}\mathrm{Tr}[q t_1 t_2 \bar{q}\bar{t}_2\bar{t}_1] \\
&\quad +\frac{B_R}{2m^2}(f_{LL}+f_{LR})f_{LL}\mathrm{Tr}[q(t-\bar{t})\bar{q}\bar{t}_2(t_2-\bar{t}_1)t_1] \\
&\quad +\frac{B_R}{2m^2}(f_{LL}+f_{LR})f_{LR}\mathrm{Tr}[q(t-\bar{t})\bar{q}t_2(t_1-\bar{t}_2)\bar{t}_1]\Bigg] , \qquad (4.14)
\end{aligned}
$$

$$
\begin{aligned}
&|\mathcal{M}(e^+ e^- \to t_\uparrow \bar{t}_\downarrow)|^2 \\
&= \left(\frac{4\pi\alpha}{s}\right)^2 \Bigg[4\Big\{|f_{LL}|^2(1+2A_R+2B_R) - 2f_{LL}f_{LR}B_R\Big\}(2q\cdot t_1)(2\bar{q}\cdot \bar{t}_1) \\
&\quad +4\Big\{|f_{LR}|^2(1+2A_R+2B_R) - 2f_{LL}f_{LR}B_R\Big\}(2q\cdot \bar{t}_2)(2\bar{q}\cdot t_2) \\
&\quad +\frac{4}{m^2}\Big\{f_{LL}f_{LR}(1+2A_R+2B_R) - 2f_{LL}f_{LR}B_R\Big\}\mathrm{Tr}[q t_1 t_2 \bar{q}\bar{t}_1\bar{t}_2] \\
&\quad +\frac{B_R}{2m^2}(f_{LL}+f_{LR})f_{LL}\mathrm{Tr}[q(t-\bar{t})\bar{q}\bar{t}_1(t_2-\bar{t}_2)t_1] \\
&\quad +\frac{B_R}{2m^2}(f_{LL}+f_{LR})f_{LR}\mathrm{Tr}[q(t-\bar{t})\bar{q}t_2(t_1-\bar{t}_1)\bar{t}_2]\Bigg] , \qquad (4.15)
\end{aligned}
$$

$$
\begin{aligned}
&|\mathcal{M}(e^+ e^- \to t_\downarrow \bar{t}_\uparrow)|^2 \\
&= \left(\frac{4\pi\alpha}{s}\right)^2 \Bigg[4\Big\{|f_{LL}|^2(1+2A_R+2B_R) - 2f_{LL}f_{LR}B_R\Big\}(2q\cdot t_2)(2\bar{q}\cdot \bar{t}_2) \\
&\quad +4\Big\{|f_{LR}|^2(1+2A_R+2B_R) - 2f_{LL}f_{LR}B_R\Big\}(2q\cdot \bar{t}_1)(2\bar{q}\cdot t_1) \\
&\quad +\frac{4}{m^2}\Big\{f_{LL}f_{LR}(1+2A_R+2B_R) - 2f_{LL}f_{LR}B_R\Big\}\mathrm{Tr}[q t_2 t_1 \bar{q}\bar{t}_2\bar{t}_1] \\
&\quad +\frac{B_R}{2m^2}(f_{LL}+f_{LR})f_{LL}\mathrm{Tr}[q(t-\bar{t})\bar{q}\bar{t}_2(t_1-\bar{t}_1)t_2] \\
&\quad +\frac{B_R}{2m^2}(f_{LL}+f_{LR})f_{LR}\mathrm{Tr}[q(t-\bar{t})\bar{q}t_1(t_2-\bar{t}_2)\bar{t}_1]\Bigg] , \qquad (4.16)
\end{aligned}
$$

$$
\begin{aligned}
&|\mathcal{M}(e^+ e^- \to t_\downarrow \bar{t}_\downarrow)|^2 \\
&= \left(\frac{4\pi\alpha}{s}\right)^2 \Bigg[4\Big\{|f_{LL}|^2(1+2A_R+2B_R) - 2f_{LL}f_{LR}B_R\Big\}(2q\cdot t_2)(2\bar{q}\cdot \bar{t}_1) \\
&\quad +4\Big\{|f_{LR}|^2(1+2A_R+2B_R) - 2f_{LL}f_{LR}B_R\Big\}(2q\cdot \bar{t}_2)(2\bar{q}\cdot t_1)
\end{aligned}
$$

$$
\begin{aligned}
&+\frac{4}{m^2}\Big\{f_{LL}f_{LR}(1+2A_R+2B_R)-2f_{LL}f_{LR}B_R\Big\}\mathrm{Tr}[qt_2t_1\bar{q}\bar{t}_1\bar{t}_2]\\
&+\frac{B_R}{2m^2}(f_{LL}+f_{LR})f_{LL}\mathrm{Tr}[q(t-\bar{t})\bar{q}\bar{t}_1(t_1-\bar{t}_2)t_2]\\
&+\frac{B_R}{2m^2}(f_{LL}+f_{LR})f_{LR}\mathrm{Tr}[q(t-\bar{t})\bar{q}t_1(t_2-\bar{t}_1)\bar{t}_2]\Big] \ , \qquad (4.17)
\end{aligned}
$$

The squared amplitudes for $e^-_Re^+_L$ scattering process are obtained by interchanging suffices $L,\ R$ as well as $\uparrow,\ \downarrow$ in Eqns.(4.14)$\sim$(4.17).

The differential cross-section at the one-loop level in the CM frame as shown in Fig.3.2 is given by

$$
\begin{aligned}
&\frac{d\sigma}{d\cos\theta}\left(e^-_Le^+_R\to t_\uparrow\bar{t}_\uparrow\right)=\frac{d\sigma}{d\cos\theta}\left(e^-_Le^+_R\to t_\downarrow\bar{t}_\downarrow\right)\\
&=\left(\frac{3\pi\alpha^2}{2s}\beta\right)(A_{LR}\cos\xi-B_{LR}\sin\xi) \qquad (4.18)\\
&\qquad\times\Big[(A_{LR}\cos\xi-B_{LR}\sin\xi)(1+2A_R+2B_R)\\
&\qquad\qquad-2\left(\gamma^2A_{LR}\cos\xi-\bar{B}_{LR}\sin\xi\right)B_R\Big] \ ,\\
&\frac{d\sigma}{d\cos\theta}\left(e^-_Le^+_R\to t_\uparrow\bar{t}_\downarrow \text{ or } t_\downarrow\bar{t}_\uparrow\right)\\
&=\left(\frac{3\pi\alpha^2}{2s}\beta\right)(A_{LR}\sin\xi+B_{LR}\cos\xi\pm D_{LR}) \qquad (4.19)\\
&\qquad\times\Big[(A_{LR}\sin\xi+B_{LR}\cos\xi\pm D_{LR})(1+2A_R+2B_R)\\
&\qquad\qquad-2\left(\gamma^2A_{LR}\sin\xi+\bar{B}_{LR}\cos\xi\pm\bar{D}_{LR}\right)B_R\Big].
\end{aligned}
$$

Here, the angle θ is the scattering angle of the top quark with respect to the incident electron, α is the QED fine structure constant and $\gamma=1/\sqrt{1-\beta^2}$. The quantities $A_{LR}, B_{LR}, \bar{B}_{LR}, D_{LR}$ and $\bar{D}_{LR}$ are defined by

$$
\begin{aligned}
A_{LR} &= \Big[(f_{LL}+f_{LR})\sqrt{1-\beta^2}\,\sin\theta\Big]/\,2 \ ,\\
B_{LR} &= \Big[f_{LL}(\cos\theta+\beta)+f_{LR}(\cos\theta-\beta)\Big]/\,2=\bar{B}_{LR}(-\beta) \ , \qquad (4.20)\\
D_{LR} &= \Big[f_{LL}(1+\beta\cos\theta)+f_{LR}(1-\beta\cos\theta)\Big]/\,2=\bar{D}_{LR}(-\beta) \ .
\end{aligned}
$$

The cross-sections Eqns.(4.18) and (4.19) contain an infrared singularities (in the form factor A_R) that will be canceled by the contributions from the real gluon emission.

4.1.2 Spin Correlations in the Soft Gluon Approximation

Now we consider the cross-sections for the real gluon emission. We isolate the soft gluon singularity by splitting the $t\bar{t}g$ phase space into a soft and a hard region. Since the hard gluon with high momentum make the momenta of the top and anti-top quarks change, the top and the anti-top quarks are not produced back to back. Hence, in the hard gluon region, it is difficult to investigate the $\gamma/Z - t - \bar{t}$ vertex. Then, we concentrate on only the soft gluon region to study the vertex structure induced by the QCD corrections [41, 42].

In the soft gluon approximation, it is very easy to calculate the real gluon contribution. As is well known, the amplitude for the soft gluon emissions can be written in the factorized form proportional to the tree amplitude. This means that the soft gluon emission does not change the spin configurations or momentum of the produced heavy quark pairs from the tree level values. Therefore, the QCD radiative corrections enter mainly through the modifications of the vertex parts Eqns.(4.1) and (4.2). The cross-section for the soft gluon emissions can be written as

$$\frac{d\sigma}{d\cos\theta} = J_{\rm IR}\ \frac{d\sigma_0}{d\cos\theta}\ , \tag{4.21}$$

where the subscript 0 denotes the tree level cross-section. The soft gluon contribution $J_{\rm IR}$ is defined by

$$J_{\rm IR} \equiv -4\pi C_2(R)\alpha_s \int^{k^0=\omega_{\rm max}} \frac{d^3\vec{k}}{(2\pi)^3 2k^0} \left(\frac{t_\mu}{t\cdot k} - \frac{\bar{t}_\mu}{\bar{t}\cdot k}\right)^2\ ,$$

where $\omega_{\rm max}$ is the cut-off of the soft gluon energy, and

$$\omega_{\rm max}\ \leq\ \sqrt{s} - 2m\ ,$$

where the maximum value of $\omega_{\rm max}$ is constrained by the momentum conservation. At large $\omega_{\rm max}$, the soft-gluon approximation is spoiled, because it is the leading order of the amplitude in the expansion of $\omega_{\rm max}$. Therefore $\omega_{\rm max}$ should be

$$\omega_{\rm max}\ =\ x_{\rm min}(\sqrt{s} - 2m)\ , \tag{4.22}$$

where $x_{\rm min}$ is a sufficiently small number. The integral of $J_{\rm IR}$ can be easily performed and we obtain

$$\begin{aligned} J_{\rm IR}\ =\ & 2\hat{\alpha}_s \left[\left(\frac{1+\beta^2}{\beta}\ln\frac{1+\beta}{1-\beta} - 2\right)\ln\frac{4\omega_{\rm max}^2}{\lambda^2}\right. \\ & \left. + \frac{2}{\beta}\ln\frac{1+\beta}{1-\beta} - \frac{1+\beta^2}{\beta}\left[2{\rm Li}_2\left(\frac{2\beta}{1+\beta}\right) + \frac{1}{2}\ln^2\frac{1+\beta}{1-\beta}\right]\right]\ . \end{aligned}$$

By adding the one-loop contributions Eqns.(4.18) and (4.19) and the soft gluon ones Eqn.(4.21), one can see that the infrared singularities, $\ln\lambda$, are canceled out and the finite results are obtained by replacing $2A_R$ by

$$\begin{aligned} & 2A_R + J_{\rm IR} \\ &= 2\hat{\alpha}_s \left[\left(\frac{1+\beta^2}{\beta} \ln\frac{1+\beta}{1-\beta} - 2 \right) \ln\frac{4\omega_{\rm max}^2}{m^2} - 4 + \frac{2+3\beta^2}{\beta} \ln\frac{1+\beta}{1-\beta} \right. \\ &+ \left. \frac{1+\beta^2}{\beta} \left\{ \ln\frac{1-\beta}{1+\beta} \left(3\ln\frac{2\beta}{1+\beta} + \ln\frac{2\beta}{1-\beta} \right) + 4{\rm Li}_2\left(\frac{1-\beta}{1+\beta}\right) + \frac{1}{3}\pi^2 \right\} \right] , \end{aligned}$$

in Eqns.(4.18) and (4.19).

Thus we obtain the $\mathcal{O}(\alpha_s)$ polarized cross-sections in the soft-gluon approximation using the generic spin basis:

$$\begin{aligned} & \frac{d\sigma}{d\cos\theta}\left(e_L^- e_R^+ \to t_\uparrow \bar{t}_\uparrow\right) = \frac{d\sigma}{d\cos\theta}\left(e_L^- e_R^+ \to t_\downarrow \bar{t}_\downarrow\right) \\ &= \left(\frac{3\pi\alpha^2}{2s}\beta\right)(A_{LR}\cos\xi - B_{LR}\sin\xi) \\ &\quad \times\Big[(A_{LR}\cos\xi - B_{LR}\sin\xi)(1+S_I) \\ &\qquad - 2\left(\gamma^2 A_{LR}\cos\xi - \bar{B}_{LR}\sin\xi\right) S_{II} \Big] , \end{aligned} \tag{4.23}$$

$$\begin{aligned} & \frac{d\sigma}{d\cos\theta}\left(e_L^- e_R^+ \to t_\uparrow \bar{t}_\downarrow \text{ or } t_\downarrow \bar{t}_\uparrow\right) \\ &= \left(\frac{3\pi\alpha^2}{2s}\beta\right)(A_{LR}\sin\xi + B_{LR}\cos\xi \pm D_{LR}) \\ &\quad \times\Big[(A_{LR}\sin\xi + B_{LR}\cos\xi \pm D_{LR})(1+S_I) \\ &\qquad - 2\left(\gamma^2 A_{LR}\sin\xi + \bar{B}_{LR}\cos\xi \pm \bar{D}_{LR}\right) S_{II} \Big], \end{aligned} \tag{4.24}$$

where

$$\begin{aligned} S_I &= 2\hat{\alpha}_s \left[\left(\frac{1+\beta^2}{\beta} \ln\frac{1+\beta}{1-\beta} - 2 \right) \ln\frac{4\omega_{\rm max}^2}{m^2} - 4 + \frac{3+2\beta^2}{\beta} \ln\frac{1+\beta}{1-\beta} \right. \\ &+ \left. \frac{1+\beta^2}{\beta} \left\{ \ln\frac{1-\beta}{1+\beta} \left(3\ln\frac{2\beta}{1+\beta} + \ln\frac{2\beta}{1-\beta} \right) + 4{\rm Li}_2\left(\frac{1-\beta}{1+\beta}\right) + \frac{1}{3}\pi^2 \right\} \right] , \end{aligned} \tag{4.25}$$

$$S_{II} = \hat{\alpha}_s \frac{1-\beta^2}{\beta} \ln\frac{1+\beta}{1-\beta} . \tag{4.26}$$

Since we are interested in maximizing the spin correlations of the top quark pairs, we vary the spin angle, ξ, to find the appropriate spin basis. As shown in the previous chapter, we analyze the polarized cross-section in "helicity", "beamline" and "off-diagonal" bases at one-loop level in the soft-gluon approximation.

1. Helicity basis:

   The helicity basis is given by

$$\cos\xi \;=\; \pm 1.$$

   Above condition leads to the following differential cross-sections;

$$\begin{aligned}
&\frac{d\sigma}{d\cos\theta}(e^-_L e^+_R \to t_L\bar{t}_L) \;=\; \frac{d\sigma}{d\cos\theta}(e^-_L e^+_R \to t_R\bar{t}_R)\\
&= \frac{3\pi\alpha^2}{8s}(f_{LL}+f_{LR})^2\sin^2\theta\left[(1-\beta^2)(1+S_I)-2S_{II}\right]\,, \qquad (4.27)\\
&\frac{d\sigma}{d\cos\theta}(e^-_L e^+_R \to t_R\bar{t}_L \text{ or } t_L\bar{t}_R)\\
&= \frac{3\pi\alpha^2}{8s}(1\mp\cos\theta)\left[f_{LL}(1\mp\beta)+f_{LR}(1\pm\beta)\right] \qquad (4.28)\\
&\times\left[\{f_{LL}(1\mp\beta)+f_{LR}(1\pm\beta)\}(1+S_I)-2\{f_{LL}(1\pm\beta)+f_{LR}(1\mp\beta)\}S_{II}\right].
\end{aligned}$$

2. Beamline basis:

   In the beamline basis, the top (anti-top) quark spin is defined in the positron (electron) direction in its rest frame. The spin angle ξ is obtained by

$$\cos\xi \;=\; \frac{\cos\theta+\beta}{1+\beta\cos\theta}. \qquad (4.29)$$

   The differential polarized cross-sections in the beamline basis are obtained by Eqns.(4.23), (4.24) and (4.29).

$$\begin{aligned}
&\frac{d\sigma}{d\cos\theta}(e^-_L e^+_R \to t_\uparrow\bar{t}_\uparrow) \;=\; \frac{d\sigma}{d\cos\theta}(e^-_L e^+_R \to t_\downarrow\bar{t}_\downarrow)\\
&= \left(\frac{3\pi\alpha^2}{2s}\beta\right)\frac{\beta^2\sin^2\theta}{(1+\beta\cos\theta)^2}\Bigg[f^2_{LR}(1-\beta^2)(1+S_I)\\
&\qquad -\Big[\{2-\beta(\beta-\cos\theta)\}f_{LL}f_{LR}+\beta(\beta+\cos\theta)f^2_{LR}\Big]S_{II}\Bigg], \qquad (4.30)\\
&\frac{d\sigma}{d\cos\theta}(e^-_L e^+_R \to t_\downarrow\bar{t}_\uparrow)\\
&= \left(\frac{3\pi\alpha^2}{2s}\beta\right)\frac{\beta^4\sin^4\theta}{(1+\beta\cos\theta)^2}\left[f^2_{LR}(1+S_I+S_{II})-f_{LL}f_{LR}S_{II}\right], \qquad (4.31)\\
&\frac{d\sigma}{d\cos\theta}(e^-_L e^+_R \to t_\uparrow\bar{t}_\downarrow)\\
&= \left(\frac{3\pi\alpha^2}{2s}\beta\right)\left[f_{LL}(1+\beta\cos\theta)+f_{LR}\frac{(1-\beta)^2}{(1+\beta\cos\theta)}\right]\\
&\times\Bigg[\left\{f_{LL}(1+\beta\cos\theta)+f_{LR}\frac{(1-\beta)^2}{(1+\beta\cos\theta)}\right\}(1+S_I) \qquad (4.32)\\
&+\left(\frac{1}{1+\beta\cos\theta}\right)\Big\{(f_{LL}-f_{LR})(\beta^2(1+\cos^2\theta)-2)-4f_{LR}(1+\beta\cos\theta)\Big\}S_{II}\Bigg].
\end{aligned}$$

3. Off-diagonal basis:

   At the tree level, we have shown that the "off-diagonal" basis makes the contributions from the like-spin configuration vanish [16, 34]. At order $\mathcal{O}(\alpha_s)$, we can find two off-diagonal bases for the $e_L^- e_R^+$ scattering. The first basis is given by

$$A_{LR}\cos\xi - B_{LR}\sin\xi \;=\; 0\ .$$

   This equation leads to the relation between the spin angle ξ and the scattering angle θ,

$$\tan\xi = \frac{A_{LR}}{B_{LR}} = \frac{(f_{LL}+f_{LR})\sqrt{1-\beta^2}\,\sin\theta}{f_{LL}(\cos\theta+\beta)+f_{LR}(\cos\theta-\beta)}\ . \tag{4.33}$$

   This basis is equivalent to Eqn.(3.38) in the leading order analysis, and not modified by the QCD corrections. The first order QCD corrected cross-sections in this basis are

$$\frac{d\sigma}{d\cos\theta}\left(e_L^- e_R^+ \to t_\uparrow\bar{t}_\uparrow \text{ and } t_\downarrow\bar{t}_\downarrow\right) = 0\ , \tag{4.34}$$

$$\frac{d\sigma}{d\cos\theta}\left(e_L^- e_R^+ \to t_\uparrow\bar{t}_\downarrow \text{ or } t_\downarrow\bar{t}_\uparrow\right) = \left(\frac{3\pi\alpha^2}{2s}\beta\right)\left(\sqrt{A_{LR}^2+B_{LR}^2}\mp D_{LR}\right) \tag{4.35}$$

$$\times\left[\left(\sqrt{A_{LR}^2+B_{LR}^2}\mp D_{LR}\right)\left(1+S_I\right) - 2\left(\frac{\gamma^2A_{LR}^2+B_{LR}\bar{B}_{LR}}{\sqrt{A_{LR}^2+B_{LR}^2}}\mp\bar{D}_{LR}\right)S_{II}\right].$$

   The second basis is defined by,

$$(A_{LR}\cos\xi - B_{LR}\sin\xi)(1+S_I) - 2(\gamma^2A_{LR}\cos\xi - \bar{B}_{LR}\sin\xi)S_{II} \;=\; 0\ . \tag{4.36}$$

   Therefore the spin angle, ξ, satisfies the following relation,

$$\tan\xi \;=\; \frac{(1+S_I)-2\gamma^2S_{II}}{B_{LR}(1+S_I)-2\bar{B}_{LR}S_{II}}A_{LR}\ . \tag{4.37}$$

   Since S_I and S_{II} are $\mathcal{O}(\alpha_s)$, there is only difference of $\mathcal{O}(\alpha_s)$ between the Eqn.(4.33) and (4.37). Hence, we use the off-diagonal basis defined by Eqn.(4.33). A similar result holds for $e_R^- e_L^+$ scattering.

In the soft-gluon approximation, the polarized cross-sections depend on the unknown value of $\omega_{\max}$ for the soft gluon. Before discussing the spin correlations in the soft-gluon approximation, we will examine the the $\omega_{\max}$ dependence of the cross section. Since we are interested in the cross-section mainly in the off-diagonal basis, we present the $\omega_{\max}$ dependence of the differential cross-section in the off-diagonal basis. Fig.4.2 shows the $\omega_{\max}$ dependence of the differential cross-section, where the numerical values of parameters are taken from Table.3.1

in Chapter 3. The running strong coupling constant is obtained by evolving $\alpha_s(M_Z^2) = 0.118$ with 5 flavor to $\alpha_s(s)$ with 6 flavor. Here we use the renormalization equation for the running coupling constant up to QCD two-loop level. We plot the cross-section at values for the $\omega_{\max}$;

$$\omega_{\max} \;=\; x_{\min}(\sqrt{s} - 2m) \;, \quad \left(x_{\min} = \frac{1}{50},\ \frac{1}{10},\ \frac{1}{5}\right).$$

The cross-sections behaves quite uniformly as the value of $\omega_{\max}$ is changed. This tells us that the behavior are qualitatively the same for any reasonable value of $\omega_{\max}$.

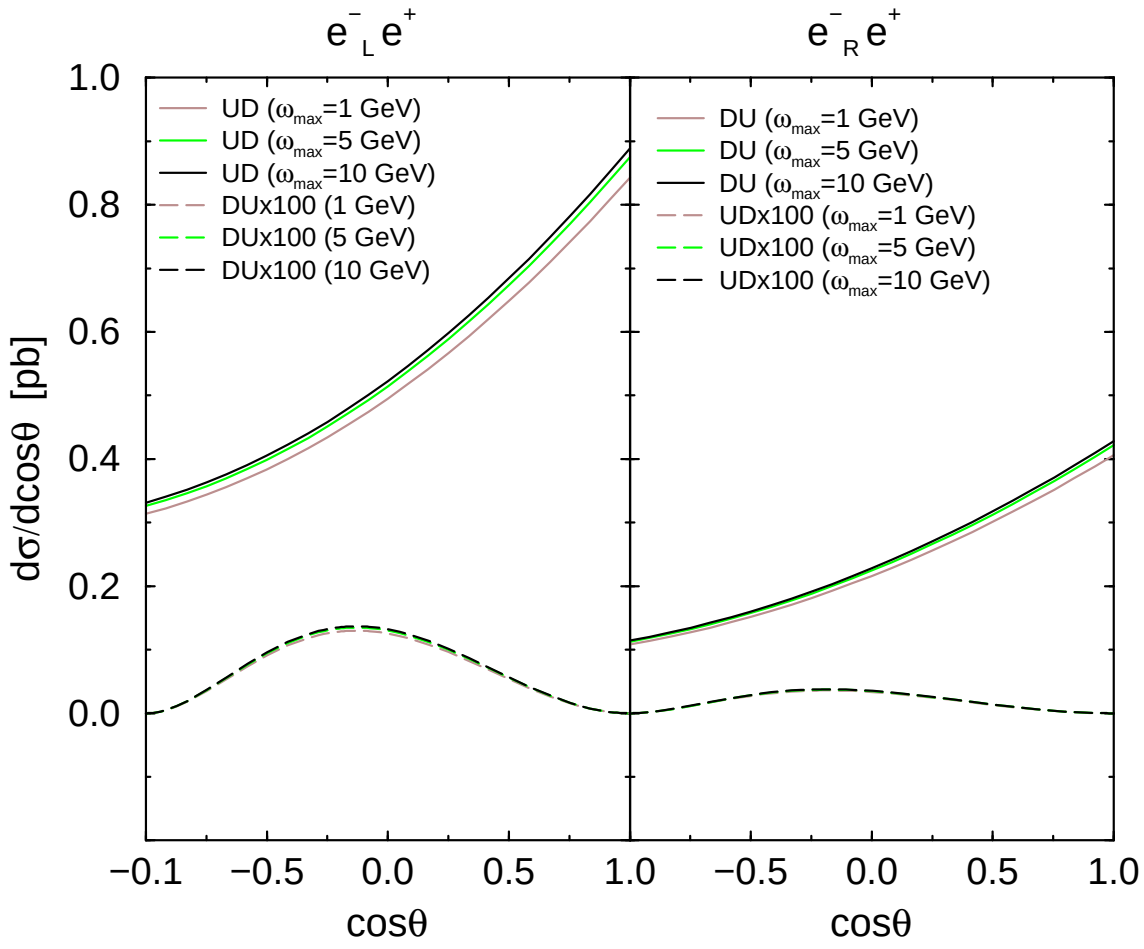

Figure 4.2: The $\omega_{\max}$ dependence of the cross-sections in the off-diagonal basis at $\sqrt{s} = 400\,\text{GeV}$. The DU (UD) component for the $e_L^- e^+$ ($e_R^- e^+$) process at $\sqrt{s} = 400\,\text{GeV}$ is multiplied by 100.

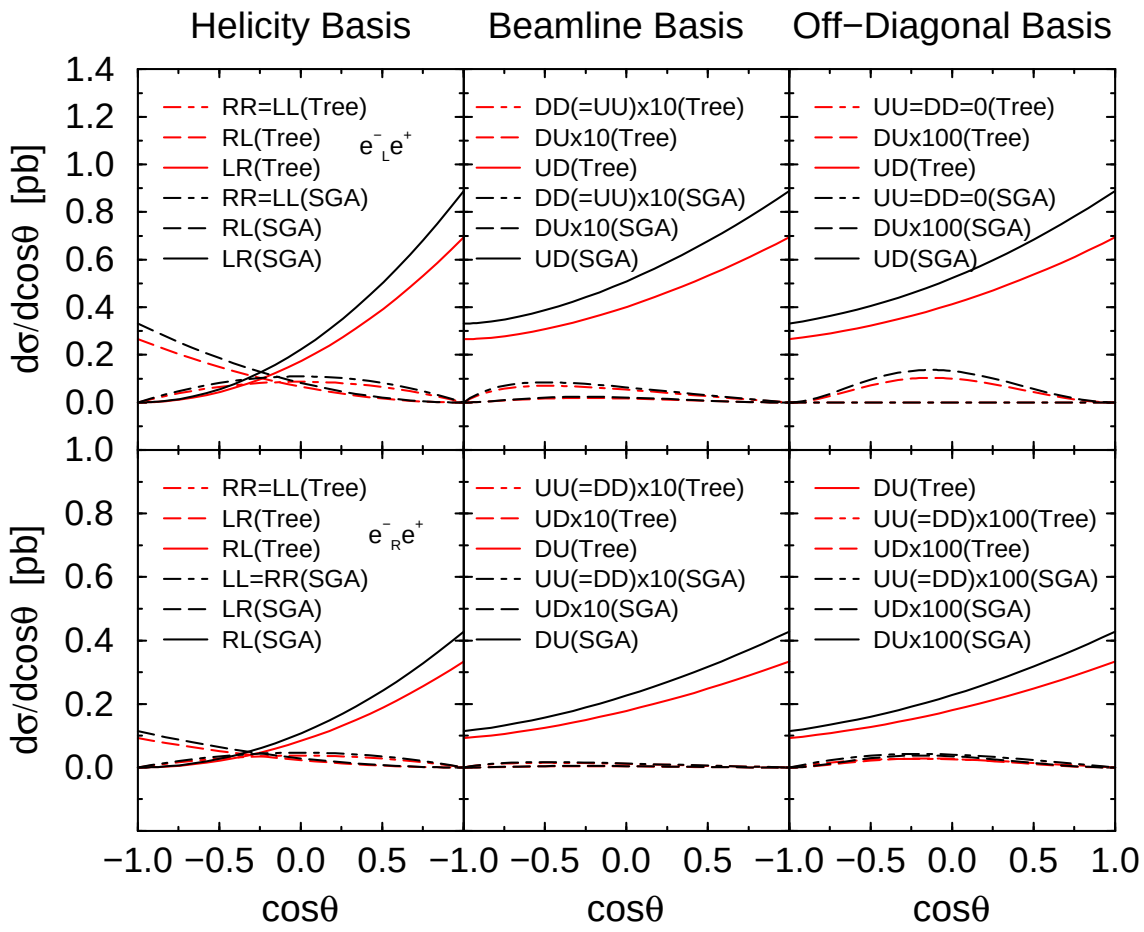

Figure 4.3: The cross-sections in the helicity, beamline and off-diagonal bases at $\sqrt{s} = 400\,\mathrm{GeV}, \omega_{\max} = 10\,\mathrm{GeV}$ for the $e^-e^+ \to t\bar{t}$ process: $t_L\bar{t}_R$ (LR), $t_R\bar{t}_L$ (RL), $t_L\bar{t}_L$ (LL) and $t_R\bar{t}_R$ (RR) in the helicity, $t_\uparrow\bar{t}_\downarrow$ (UD), $t_\downarrow\bar{t}_\uparrow$ (DU), $t_\uparrow\bar{t}_\uparrow$ (UU) and $t_\downarrow\bar{t}_\downarrow$ (DD) in the beamline and off-diagonal bases. The suffices "Tree" and "SGA" mean the differential cross-section at the tree level and at the one-loop level in the soft gluon approximation. It should be noted that DU (UD,UU,DD) component for the $e^-_L e^+$ ($e^-_R e^+$) process in off-diagonal basis is multiplied by 100, and that DU, UU, DD (UD,UU,DD) components for the $e^-_L e^+$ ($e^-_R e^+$) process in beamline basis is multiplied by 10

$e^-_L e^+$	Helicity	Beamline	Off-Diagonal
Dominant Frac.	0.53610 (LR)	0.97964 (UD)	0.99871 (UD)
Sub-Dominant Frac.	0.19992 (RL)	0.00905 (UU,DD)	0.00129 (DU)
$e^-_R e^+$	Helicity	Beamline	Off-Diagonal
Dominant Frac.	0.58709 (RL)	0.99084 (DU)	0.99699 (DU)
Sub-Dominant Frac.	0.15662 (LR)	0.00406 (UU,DD)	0.00110 (UU,DD)

Table 4.1: The fraction of $e^-_{L/R}e^+$ cross-sections for the dominant and the sub-dominant spin configurations in the helicity, beamline and off-diagonal bases at $O(\alpha_s)$ in soft-gluon approximation. Where $\sqrt{s} = 400$ GeV and $\omega_{\max} = 10$ GeV.

In Fig.4.3, we show the differential cross-sections in three bases, at $\sqrt{s} = 400\,\text{GeV}$ and $\omega_{\max} = 10\ GeV$. Table 4.1 shows the fraction of the $e^-_{L/R} \to t\bar{t}$ cross-section for the dominant and the sub-dominant spin configurations. The dominant components in the helicity basis are $t_L\bar{t}_R$ (LR) for $e^-_L e^+$ scattering and $t_R\bar{t}_L$ (RL) for $e^-_R e^+$ scattering at $\sqrt{s} = 400$ GeV. This component occupies 53% of total cross-section for $e^-_L e^+$ and 58% of total cross-section for $e^-_R e^+$ scattering. In the beamline basis, only UD ($t_\uparrow \bar{t}_\downarrow$) component is dominant for $e^-_L e^+_R$ cross-section, which makes up more than 97%. On the other hand, DU ($t_\downarrow \bar{t}_\uparrow$) component is dominant for $e^-_R e^+_L$ cross-section, which makes up more than 99%. For $e^-_L e^+_R$ cross-section in the off-diagonal basis, the UU ($t_\uparrow \bar{t}_\uparrow$) and the DD ($t_\downarrow \bar{t}_\downarrow$) components are identically zero. The total cross-section is dominated by the UD ($t_\uparrow \bar{t}_\downarrow$) component which amount to more than 99% and DU ($t_\downarrow \bar{t}_\uparrow$) component contributes less than 1 %. For $e^-_R e^+_L$ scattering the UU ($t_\uparrow \bar{t}_\uparrow$) and the DD ($t_\downarrow \bar{t}_\downarrow$) components are non-zero because we have used the off-diagonal basis for $e^-_L e^+_R$ scattering. However the DU ($t_\downarrow \bar{t}_\uparrow$) component is still more than 99% of the total cross-section. Although there exist a magnetic moment modification to the $\gamma/Z - t - \bar{t}$ vertex from QCD corrections, this does not change the behavior of the spin dependent cross-sections in the helicity, beamline and off-diagonal bases. The QCD corrections, however, make the differential cross-sections larger by $\sim 30\%$ compared to the tree level ones at this $\sqrt{s}$. Thus the off-diagonal and the beamline bases continue to display very strong spin correlations for the top quark pairs even after taking the QCD corrections into account, at least in the soft gluon approximation.

4.2 Single Spin Correlations in e^+e^- Process

The result in the soft gluon approximation imply that the QCD corrections do not change the behavior of the spin dependent cross-sections in any basis. However, the following two points are shortcomings of this approximation. First, soft gluon emission cannot change the spin of the heavy quarks. Second, the heavy quark pairs are produced always back to back. These points are invalid for the hard gluon, and it is possible that the full $\mathcal{O}(\alpha_s)$ QCD corrections might completely change the conclusions of the previous section. In this section, we investigate the full $\mathcal{O}(\alpha_s)$ QCD corrections [34, 41]. Since, in the presence of a hard gluon, the top and anti-top quarks are not generally produced back-to-back, it is instructive to consider the single heavy quark spin correlations. Namely, we investigate the inclusive cross-section for the production of the top (or anti-top) quark in a particular spin configuration. We have organized this section as follows. After defining the kinematics and our conventions, we give the polarized cross-section for the top quark using a generic spin basis closely related to the spin basis of the previous section. The numerical analysis will be relegated to the next section.

4.2.1 Amplitudes and Kinematics

The principle result of this section will be the inclusive cross-section for the polarized top quark production, $e^+e^- \to t_\uparrow$ or $t_\downarrow + X$, where $X = \bar{t}$ or $\bar{t}g$ (The cross-section for the anti-top quark inclusive production can be easily obtained from the results in this section.).

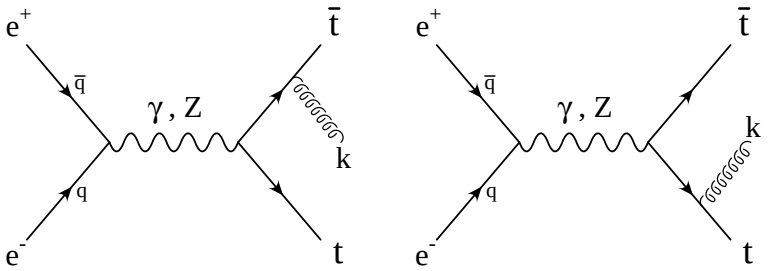

Figure 4.4: The real gluon emission contributions to top quark pair production.

Since the vertex corrections are the same as in the previous section, all that is required is the full real gluon emission contributions. The real gluon emission diagrams to leading order in α_s are given in Fig.4.4. Figure 4.4 also defines the momenta of particles. We also use the

spinor helicity method for massive fermions to calculate the squares of these amplitudes for a polarized top quark (see Chapter 2).

The top quark momentum t is decomposed into a sum of two massless momenta t_1 , t_2 such that in the rest frame of the top quark the spatial momentum of t_1 defines the spin axis for the top quark.

$$t = t_1 + t_2 \quad , \quad m s_t = t_1 - t_2 \ ,$$

where s_t is the spin four vector of the top quark. The amplitude for Fig.4.4 is given by

$$\begin{aligned} M(e_L^- e_R^+ \to t_{s_t} \bar{t}_{s_{\bar{t}}} g) &= \langle \bar{q} - | (\gamma_L)_\mu | q - \rangle \\ \times \quad \bar{u}(t, s_t) \Big[\frac{1}{2\bar{t}\cdot k} \left(\frac{a_{LL}}{2} \gamma_L^\mu + \frac{a_{LR}}{2} \gamma_R^\mu \right) (-\hat{\bar{t}} - \hat{k} + m) \gamma_\nu \\ + \frac{1}{2t\cdot k} \gamma_\nu (\hat{t} + \hat{k} + m) \left(\frac{a_{LL}}{2} \gamma_L^\mu + \frac{a_{LR}}{2} \gamma_R^\mu \right) \Big] T^a v(\bar{t}, s_{\bar{t}}) \varepsilon_a^\nu(k) \ , \end{aligned} \tag{4.38}$$

where ε is the polarization vector of the gluon. T^a is the color matrix, and $\hat{p} = p^\mu \gamma_\mu$. The coupling constants a_{LI} are defined as follows:

$$\frac{a_{LI}}{2} = \frac{e^2 g}{s} f_{LI} \ .$$

The expressions for the squares of the amplitudes given below have been summed over the spins of the unobserved particles (the anti-top quark and gluon) as well as the colors of the final state particles. Let us write the square of the amplitude for the top quark with spin "up" as

$$\begin{aligned} & |M(e_L^- e_R^+ \to t_\uparrow \bar{t} g)|^2 \\ &= \quad N_c C_2(R) \left[\frac{1}{(\bar{t}\cdot k)^2} T_1 + \frac{1}{(\bar{t}\cdot k)(t\cdot k)} T_2 + \frac{1}{(t\cdot k)^2} T_3 \right] \ . \end{aligned} \tag{4.39}$$

After some calculation, we find

$$\begin{aligned} T_1 &= 4\,|a_{LL}|^2 \left[(\bar{t}\cdot k)(q\cdot k) - m^2 q\cdot(\bar{t}+k) \right] (t_2\cdot\bar{q}) \\ &+ 4\,|a_{LR}|^2 \left[(\bar{t}\cdot k)(\bar{q}\cdot k) - m^2 \bar{q}\cdot(\bar{t}+k) \right] (t_1\cdot q) \\ &- \left[a_{LL} a_{LR}^* ((\bar{t}\cdot k) + m^2) \mathrm{Tr}(\gamma_R\, t_1\, t_2\, \bar{q}\, q) + c.c. \right] \ , \\ T_2 &= |a_{LL}|^2 \left[4(t\cdot\bar{t})(\bar{t}\cdot q)(t_2\cdot\bar{q}) + (t_2\cdot\bar{q})\mathrm{Tr}(\gamma_R\, q\, k\, t\, \bar{t}) + (\bar{t}\cdot q)\mathrm{Tr}(\gamma_L\, t_2\, \bar{q}\, k\, \bar{t}) \right] \\ &+ |a_{LR}|^2 \left[4\,(t\cdot\bar{t})(\bar{t}\cdot\bar{q})(t_1\cdot q) + (t_1\cdot q)\mathrm{Tr}(\gamma_L\, \bar{q}\, k\, t\, \bar{t}) + (\bar{t}\cdot\bar{q})\mathrm{Tr}(\gamma_R\, t_1\, q\, k\, \bar{t}) \right] \\ &+ a_{LL} a_{LR}^* \Big[(t\cdot\bar{t})\mathrm{Tr}(\gamma_R\, t_1\, t_2\, \bar{q}\, q) - (k\cdot q)\mathrm{Tr}(\gamma_R\, t_1\, t_2\, \bar{q}\, k) \\ &\qquad + \frac{1}{2}\mathrm{Tr}(\gamma_R\, t_2\, t_1\, q\, k\, t\, \bar{q}) + \frac{1}{2}\mathrm{Tr}(\gamma_R\, t_1\, t_2\, \bar{q}\, q\, k\, \bar{t}) \Big] \end{aligned}$$

$$
\begin{aligned}
&+ \quad a^*_{LL}a_{LR}\Big[(t\cdot\bar{t})\mathrm{Tr}(\gamma_L\, t_2\, t_1\, q\, \bar{q}) - (k\cdot\bar{q})\mathrm{Tr}(\gamma_L\, t_2\, t_1\, q\, k) \\
&\qquad\qquad +\frac{1}{2}\mathrm{Tr}(\gamma_L\, t_1\, t_2\, \bar{q}\, k\, t\, q) + \frac{1}{2}\mathrm{Tr}(\gamma_L\, t_2\, t_1\, q\, \bar{q}\, k\, \bar{t})\Big] \\
&+ \quad c.c.\ , \\
T_3 \;&= \; 2\,|a_{LL}|^2\left[-m^2(k\cdot\bar{q}) - 2(m^2+(t\cdot k))(t_2\cdot\bar{q}) + 2((t+k)\cdot\bar{q})(t_2\cdot k)\right](\bar{t}\cdot q) \\
&+ \quad 2\,|a_{LR}|^2\left[-m^2(k\cdot q) - 2(m^2+(t\cdot k))(t_1\cdot q) + 2((t+k)\cdot q)(t_1\cdot k)\right](\bar{t}\cdot\bar{q}) \\
&- \quad \frac{m^2}{2}\left[a_{LL}a^*_{LR}\{2\mathrm{Tr}(\gamma_R\, t_1\, t_2\, \bar{q}\, q) + \mathrm{Tr}(\gamma_R\, k\, t_2\, \bar{q}\, q) + \mathrm{Tr}(\gamma_R\, t_1\, k\, \bar{q}\, q)\} + c.c.\right]\ ,
\end{aligned}
$$

where $\gamma_{R/L} \equiv \frac{1\pm\gamma_5}{2}$ and that all momentum, p, under the "Tr" operator are understood to be $\hat{p}$. By interchanging the t_1 and t_2 vectors in the above expressions, we can get the amplitude square for the top quark with spin "down". Since we neglect the Z width, all the coupling constants a_{LI} are real.

To define the spin basis for the top quark, we naturally extend the spin definition of the previous section to the present case. The top quark spin is decomposed along the direction $\mathbf{s}_t$ in the rest frame of the top quark which makes an angle ξ with the sum of the anti-top quark and the gluon momenta in the clockwise direction, see Fig.4.5.

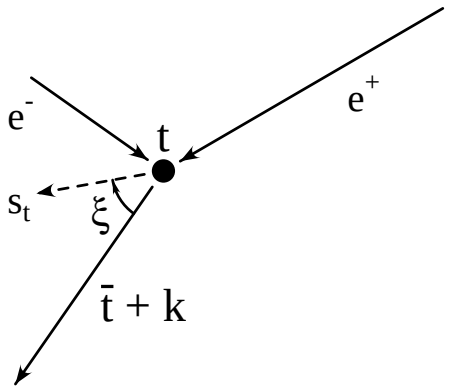

Figure 4.5: The spin basis for the top quark in the process $e^-e^+ \to t\bar{t}g$.

(We consider the case in which there is no transverse polarization.) To calculate the cross-section from Eqn.(4.39), we take the CM frame in which the e^+e^- beam line coincides with the z-axis,

$$q = \frac{\sqrt{s}}{2}(1\,,\,0\,,\,0\,,\,1) \quad , \quad \bar{q} = \frac{\sqrt{s}}{2}(1\,,\,0\,,\,0\,,\,-1)\ .$$

We define the variables x, y and z which are related to CM energies of the gluon, top and

anti-top quarks by

$$x \equiv 1 - \frac{2\,k\cdot(q+\bar{q})}{s}\ ,\ y \equiv 1 - \frac{2\,t\cdot(q+\bar{q})}{s}\ ,\ z \equiv 1 - \frac{2\,\bar{t}\cdot(q+\bar{q})}{s}\ .$$

The momenta of the final state particles, in terms of these variables, are

$$k = \frac{\sqrt{s}}{2}(1-x\,,\,(1-x)\,\boldsymbol{k})\ ,\ t = \frac{\sqrt{s}}{2}(1-y\,,\,a(y)\,\boldsymbol{t})\ ,\ \bar{t} = \frac{\sqrt{s}}{2}(1-z\,,\,a(z)\,\bar{\boldsymbol{t}})\ \ ,$$

where $\boldsymbol{k}$, $\boldsymbol{t}$ and $\bar{\boldsymbol{t}}$ mean the unit space vectors respectively and

$$a(y) \equiv \sqrt{(1-y)^2 - a}\quad ,\quad a(z) \equiv \sqrt{(1-z)^2 - a}\ ,$$

with $a \equiv 4m^2/s$. Fig.4.6 defines the orientation of the top and anti-top momenta and by energy-momentum conservation the momentum of the gluon is also determined.

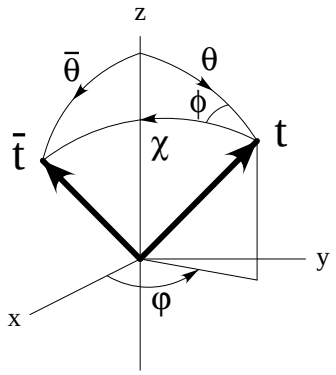

Figure 4.6: The momentum (unit vectors) configuration of the top and anti-top quarks in the CM frame. The momentum of e^- (e^+) is in the $+z$ ($-z$) direction.

One can easily obtain the spin four vector of the top quark in the CM frame by boosting the spin vector characterized by ξ in the top quark rest frame in the direction of top quark momentum by $\beta(y)$ (the speed of the top quark in the CM frame). The explicit form for t_1 ($t_2 = t - t_1$) is given by

$$\begin{aligned}
t_1^0 &= \frac{m}{2}\left[\,\gamma(y)\,(1-\beta(y)\cos\xi)\,\right]\ ,\\
t_1^1 &= \frac{m}{2}\left[\,\gamma(y)\,(\beta(y)-\cos\xi)\sin\theta\cos\varphi + \sin\xi\cos\theta\cos\varphi\,\right]\ ,\\
t_1^2 &= \frac{m}{2}\left[\,\gamma(y)\,(\beta(y)-\cos\xi)\sin\theta\sin\varphi + \sin\xi\cos\theta\sin\varphi\,\right]\ ,\\
t_1^3 &= \frac{m}{2}\left[\,\gamma(y)\,(\beta(y)-\cos\xi)\cos\theta - \sin\xi\sin\theta\,\right]\ ,
\end{aligned} \tag{4.40}$$

where

$$\sqrt{a}\,\gamma(y) = 1 - y \quad , \quad \sqrt{a}\,\gamma(y)\,\beta(y) = a(y) \ .$$

If we eliminate the gluon momentum k using the energy momentum conservation and use the angular variables χ , ϕ in Fig.4.6 to specify the orientation of the anti-top quark (if one eliminates the anti-top momentum, one can proceed in the similar way by introducing other angular variables), the square of the amplitude Eqn.(4.39) can be written as

$$|M(e_L^- e_R^+ \to t_\uparrow \bar{t} g)|^2 = \frac{s}{8}\, N_c C_2(R) \left[a_{LL}^2 M_1 + a_{LR}^2 M_2 + a_{LL} a_{LR} M_3 \right] \ , \tag{4.41}$$

where M_i are the functions of y , z, angles defined above and the spin orientation ξ.

$$\begin{aligned}
M_1 &= \frac{8}{s}\Big[\frac{m^2}{(\bar{t}\cdot k)^2}(2t\cdot q - s)(t\cdot\bar{q} - \delta t\cdot\bar{t}) \\
&\quad + \frac{1}{(t\cdot k)^2}\Big[m^2(2\bar{t}\cdot\bar{q} - s)(\bar{t}\cdot q) + s(z + \frac{a}{2})(\bar{t}\cdot q)(\delta t\cdot\bar{q}) + (2\bar{t}\cdot\bar{q} - s)(\bar{t}\cdot q)(\delta t\cdot k)\Big] \\
&\quad + \frac{1}{(t\cdot k)(\bar{t}\cdot k)}\Big[s\Big\{\frac{s}{2}(1 - y\frac{a}{2}) - (1 - \frac{a}{2}(t\cdot q)\Big\}(t\cdot\bar{q}) \\
&\qquad\qquad + s\Big\{\frac{s}{2}(1 - z\frac{a}{2}) - (1 - \frac{a}{2}(\bar{t}\cdot\bar{q})\Big\}(\bar{t}\cdot q) \\
&\qquad\qquad - s\Big\{\frac{s}{2}(1 - y - \frac{a}{2}) - (1 - \frac{a}{2})(t\cdot q)\Big\}(t\cdot\bar{q}) \\
&\qquad\qquad + s\Big\{\frac{s}{2}(1 - z - \frac{a}{2}) - 2(\bar{t}\cdot\bar{q})\Big\}(\bar{t}\cdot q)(\delta t\cdot\bar{q}) \\
&\qquad\qquad + 2(\bar{t}\cdot\bar{q})(\bar{t}\cdot q)(\delta t\cdot q) + (2t\cdot\bar{q} - s)(\bar{t}\cdot q)(\delta t\cdot\bar{t})\Big]\Big] \ , \\
M_2 &= M_1(q \leftrightarrow \bar{q}\ \delta t \to -\delta t) \ , \\
M_3 &= \frac{8}{s}\Big[\frac{1}{(\bar{t}\cdot k)^2}\frac{s}{2}(y + \frac{a}{2})(-m^2 s - 2(t\cdot\bar{q})(\delta t\cdot q) + 2(t\cdot q)(\delta t\cdot\bar{q})) \\
&\quad + \frac{m^2}{(t\cdot k)^2}\Big[-\frac{s^2}{2}(z + \frac{a}{2}) - (s - 2\bar{t}\cdot\bar{q})(\delta t\cdot q) + (s - 2\bar{t}\cdot q)(\delta t\cdot\bar{q})\Big] \\
&\quad + \frac{1}{(t\cdot k)(\bar{t}\cdot k)}\Big[m^2\Big\{\frac{s}{2}(2 - a - y - z) - 4(k\cdot q)(k\cdot\bar{q})\Big\} \\
&\qquad\qquad + \left(-\frac{s^2}{2}z + s(2 - a + z)(t\cdot\bar{q}) - s(z + \frac{a}{2})(k\cdot\bar{q}) \right)(\delta t\cdot q) \\
&\qquad\qquad - \left(-\frac{s^2}{2}z + s(2 - a + z)(t\cdot q) - s(z + \frac{a}{2})(k\cdot\bar{q}) \right)(\delta t\cdot q) \\
&\qquad\qquad + \Big(s(1 - y)\Big\{ s - (\bar{t}\cdot\bar{q})\Big\} - s(3 + z)(t\cdot\bar{q})\Big)(\delta t\cdot k)\Big]\Big],
\end{aligned}$$

where δt is defined as

$$\delta t \equiv \frac{4}{s}(t_1 - t_2) \ .$$

We transform the scalar product of the momenta to the kinematical variables in the CM frame. The functions M_i's are rewritten as

$$\begin{aligned}
M_1 &= \frac{2}{yz}\left[(1-y)^2+a^2(y)\cos^2\theta+(1-z)^2+a^2(z)\cos^2\bar{\theta}\right] \\
&- a\left(\frac{1}{yz}+\frac{1}{y^2}\right)(1-y^2+a^2(y)\cos^2\theta) - a\left(\frac{1}{yz}+\frac{1}{z^2}\right)(1-z^2+a^2(z)\cos^2\bar{\theta}) \\
&+ 2\left(\frac{2-2y-a}{yz}-\frac{a}{y^2}\right)a(y)\cos\theta - 2\left(\frac{2-2z-a}{yz}-\frac{a}{z^2}\right)a(z)\cos\bar{\theta} \\
&+ \frac{1}{yz^2}(1-z-a(z)\cos\bar{\theta})\left[y(1-a(z)\cos\bar{\theta})-z(1-a(y)\cos\theta)\right](\delta t\cdot\bar{t}) \\
&- \frac{1}{yz^2}(1-z-a(z)\cos\bar{\theta})\left[y-z+(y+z)(z-a(z)\cos\bar{\theta})\right](\delta t\cdot(\bar{q}+q)) \\
&+ \frac{a}{yz}\left(\frac{1}{y}+\frac{1}{z}\right)\left[y(1-a(z)\cos\bar{\theta})+z(1+a(y)\cos\theta)\right](\delta t\cdot\bar{q}) \\
&- \frac{2}{yz}\left[(1-y+a(y)\cos\theta)+(1-y-z)(1-z-a(z)\cos\bar{\theta})\right](\delta t\cdot\bar{q}) \ , \\
M_2 &= M_1(\cos\theta\to-\cos\theta\,,\,\cos\bar{\theta}\to-\cos\bar{\theta}\,,\,\delta t\to-\delta t) \ , \\
M_3 &= 2a\left\{\frac{4}{yz}-\frac{4}{y}-\frac{4}{z}-\frac{(y+z)^2}{yz}+\frac{(y+z)^2}{yz}\cos^2\theta_k\right\}-2a^2\left(\frac{1}{y}+\frac{1}{z}\right)^2 \\
&+ \frac{a}{yz}\left(\frac{1}{y}+\frac{1}{z}\right)(ya(z)\cos\bar{\theta}-za(y)\cos\theta)(\delta t\cdot(\bar{q}+q)) \\
&- \frac{2}{yz}\left[a(y)\cos\theta+(1-y-z)a(z)\cos\bar{\theta}\right](\delta t\cdot(\bar{q}+q)) \\
&+ a\left(\frac{1}{y}+\frac{1}{z}\right)^2(\delta t\cdot(\bar{q}-q))+\frac{2}{yz}\left[z(y+z)-2(1-y-z)\right](\delta t\cdot(\bar{q}-q)) \\
&+ \frac{2}{yz}\left[(1-y)a(z)\cos\bar{\theta}+(3+z)a(y)\cos\theta\right](\delta t\cdot\bar{t}) \ .
\end{aligned}$$

In the above equations, θ_k is the angle between the z axis and the gluon momentum

$$(y+z)\cos\theta_k = -a(y)\cos\theta - a(z)\cos\bar{\theta} \ .$$

Using Eqn.(4.40) we find that the products of δt with momenta q , $\bar{q}$ and $\bar{t}$ are

$$\begin{aligned}
\delta t\cdot q &= \{(1-y)\cos\theta-a(y)\}\cos\xi+\sqrt{a}\sin\theta\sin\xi \ , \\
\delta t\cdot\bar{q} &= \{-(1-y)\cos\theta-a(y)\}\cos\xi-\sqrt{a}\sin\theta\sin\xi \ , \\
\delta t\cdot\bar{t} &= \{-(1-z)a(y)+(1-y)a(z)\cos\chi\}\cos\xi \\
&\qquad +\sqrt{a}a(z)\sin\xi\sin\chi\cos\phi \ .
\end{aligned}$$

The unpolarized top quark production process is given by dropping the spin dependent parts (terms proportional to δt) in Eqn.(4.41). As a check we have reproduced the results of Ref. [17] by putting $a_{LL} = a_{LR} = -\frac{2e^2 g}{s} Q_q$.

The cross-section is given by

$$d\sigma(e_L^- e_R^+ \to t_\uparrow \bar{t} g) = \frac{1}{2s} |M(e_L^- e_R^+ \to t_\uparrow \bar{t} g)|^2 (PS)_3 \ , \tag{4.42}$$

where $(PS)_3$ is the three particle phase space.

$$(PS)_3 = \frac{d^3 t}{(2\pi)^3 2t^0} \frac{d^3 \bar{t}}{(2\pi)^3 2\bar{t}^0} \frac{d^3 k}{(2\pi)^3 2k^0} (2\pi)^4 \delta^4 (t + \bar{t} + k - q - \bar{q}) \ .$$

We introduce a small mass λ for the gluon to regularize the infrared singularities. It is easy to rewrite the above phase space integral as,

$$\begin{aligned} \int (PS)_3 &= \frac{s}{(4\pi)^5} \int_{y_-}^{y_+} dy \int_{z_-(y)}^{z_+(y)} dz \\ &\qquad \times \int d\Omega d\cos\chi d\phi \, \delta \left(\cos\chi - \frac{y + z + yz + a - 1 - 2a_\lambda}{a(y) a(z)} \right) \ , \end{aligned}$$

where $d\Omega = d\cos\theta d\varphi$ is the solid angle for the top quark and $a_\lambda \equiv \lambda^2/s$. The integration regions over y and z are determined by the condition $|\cos\chi| \leq 1$,

$$\begin{aligned} y_+ &= 1 - \sqrt{a} \quad , \quad y_- = \sqrt{a a_\lambda} + a_\lambda \ , \\ z_\pm(y) &= \frac{2}{4y + a} \left[y \left(1 - y - \frac{a}{2} + a_\lambda \right) + a_\lambda \pm a(y) \sqrt{(y - a_\lambda)^2 - a a_\lambda} \right] \ . \end{aligned}$$

The integration over the angle ϕ is not difficult if one uses the relation

$$\cos\bar{\theta} = \cos\theta \cos\chi + \sin\theta \sin\chi \cos\phi \ .$$

The integrals we need are the followings:

$$\begin{aligned} \int \cos\bar{\theta} \ d\phi &= 2\pi \cos\theta \cos\chi \ , \\ \int \cos^2\bar{\theta} \ d\phi &= 2\pi \left[\cos^2\theta + \frac{1}{2}(1 - 3\cos^2\theta) \sin^2\chi \right] \ , \\ \int \cos^2\theta_k \ d\phi &= 2\pi \left[\cos^2\theta + \frac{1}{2}(1 - 3\cos^2\theta) \ \frac{a^2(z)}{(y+z)^2} \ \sin^2\chi \right] \ , \\ \int \cos\bar{\theta} \cos\phi \ d\phi &= \pi \sin\theta \sin\chi \ , \\ \int \cos^2\bar{\theta} \cos\phi \ d\phi &= 2\pi \sin\theta \cos\theta \sin\chi \cos\chi \ . \end{aligned}$$

Due to the δ function in the phase space integral, the angle χ is a function of y and z:

$$\begin{aligned}\cos\chi &= \frac{y+z+yz+a-1}{a(y)a(z)} \ , \\ \sin^2\chi &= \frac{4yz(1-z-y)-a(y+z)^2}{a^2(y)a^2(z)} \ ,\end{aligned}$$

where we have put a_λ to be zero since the $\lambda \to 0$ limit does not produce any singularities in the (squared) amplitude. The remaining integrals to get the cross-section are over the variables y and z. According to the type of integrand, we group the phase space integrals (after the integrations over the angular variables) into four distinct classes $\{J_i\}$, $\{N_i\}$, $\{L_i\}$ and $\{K_i\}$ [20]. The individual integrals of these classes are summarized in Appendix.

4.2.2 Cross-Section in the Generic Spin Basis

We write the inclusive cross-section for the top quark in the following form.

$$\frac{d\sigma}{d\cos\theta}(e^-_L e^+_R \to t_\uparrow X) = \frac{3\pi\alpha^2}{4s}\sum_{klmn}(D_{klmn}+\hat{\alpha}_s C_{klmn})\cos^k\theta\sin^l\theta\cos^m\xi\sin^n\xi \ , \qquad (4.43)$$

where D_{klmn} are the contributions from the tree and the one-loop diagrams and C_{klmn} are from the real emission diagrams. Let us first write down the D_{klmn},

$$\begin{aligned}
D_{0000} &= \beta[f_{LL}^2+f_{LR}^2+2af_{LL}f_{LR}](1+\hat{\alpha}_s V_I) \\
&\qquad -\beta[2(f_{LL}+f_{LR})^2-\beta^2(f_{LL}-f_{LR})^2]\hat{\alpha}_s V_{II} \ , \\
D_{2000} &= \beta^3(f_{LL}^2+f_{LR}^2)(1+\hat{\alpha}_s V_I)+\beta^3(f_{LL}-f_{LR})^2\hat{\alpha}_s V_{II} \ , \\
D_{1000} &= 2\beta^2(f_{LL}^2-f_{LR}^2)(1+\hat{\alpha}_s V_I) \ , \\
D_{0010} &= \beta^2(f_{LL}^2-f_{LR}^2)(1+\hat{\alpha}_s V_I) \ , \\
D_{2010} &= \beta^2(f_{LL}^2-f_{LR}^2)(1+\hat{\alpha}_s V_I) \ , \\
D_{1010} &= \beta[(f_{LL}+f_{LR})^2+\beta^2(f_{LL}-f_{LR})^2](1+\hat{\alpha}_s V_I) \\
&\qquad -2\beta[(f_{LL}+f_{LR})^2-\beta^2(f_{LL}-f_{LR})^2]\hat{\alpha}_s V_{II} \ , \\
D_{0101} &= \frac{\beta}{\sqrt{a}}(f_{LL}+f_{LR})^2[a(1+\hat{\alpha}_s V_I)-(1+a)\hat{\alpha}_s V_{II}] \ , \\
D_{1101} &= \frac{\beta^2}{\sqrt{a}}(f_{LL}^2-f_{LR}^2)[a(1+\hat{\alpha}_s V_I)-(1-a)\hat{\alpha}_s V_{II}] \ ,
\end{aligned}$$

with

$$\beta=\beta(0)=\sqrt{1-a} \quad , \quad \hat{\alpha}_s V_I = 2A+2B_R \quad , \quad \hat{\alpha}_s V_{II} = B_R \ .$$

A_R, B_R are defined in Eqns.(4.9) and (4.10).

For the C_{klmn} we find,

$$
\begin{aligned}
C_{0000} &= 2\,(f_{LL}^2+f_{LR}^2)\,\Big[\,J_{\rm IR}^1-(4-a)J_3+(2+a)J_2+aJ_1+\frac{1}{4}R_1\Big] \\
&\quad +4a\,f_{LL}f_{LR}\,\Big[\,J_{\rm IR}^1-4J_3-J_2-J_1+\frac{1}{4}R_2\Big]\,, \\
C_{2000} &= 2\,(f_{LL}^2+f_{LR}^2)\,\Big[\,(1-a)J_{\rm IR}^1-(4-a)J_3+(2-a)J_2-aJ_1-\frac{3}{4}R_1\Big] \\
&\quad +4a\,f_{LL}f_{LR}\,\Big[\,J_2+J_1-\frac{3}{4}R_2\Big]\,, \\
C_{1000} &= 2\,(f_{LL}^2-f_{LR}^2)\,\Big[\,(1-a)J_{\rm IR}^2+\,aN_{10}-2(4-3a)N_9 \\
&\qquad\qquad -(4-5a)N_8-2N_7+2N_6+6N_3+2N_2\Big]\,, \\
C_{0010} &= \frac{1}{2}\,C_{1000} \\
&\quad +(f_{LL}^2-f_{LR}^2)\,\Big[\,-4N_6-aN_4-aN_3-aN_2+(4-a)N_1+\frac{1}{2}R_3\Big]\,, \\
C_{2010} &= C_{0010}-2(f_{LL}^2-f_{LR}^2)R_3\,, \\
C_{1010} &= (f_{LL}^2+f_{LR}^2)\,\Big[\,2(2-a)J_{\rm IR}^1+2aJ_4-2(8-5a)J_3 \\
&\qquad -2a(1-a)L_8-2a(1-a)L_7-2(4+3a)L_6+2(4-3a)L_5 \\
&\qquad +2aL_4+a(10-a)L_3+(8-6a-a^2)L_2-2(4-3a+a^2)L_1\Big] \\
&\quad +2a\,f_{LL}f_{LR}\,\Big[\,2J_{\rm IR}^1-8J_3+4L_6+4L_5+aL_3+aL_2-2(2-a)L_1\Big]\,, \\
C_{0101} &= \frac{\sqrt{a}}{2}\,(f_{LL}^2+f_{LR}^2)\,\Big[\,4J_{\rm IR}^1-(8+a)J_3-(8-a)(1-a)L_7-(12+a)L_6 \\
&\qquad -2aL_5+2aL_4+(8+a)L_3+(4-5a)L_2+4(2-a)L_1\Big] \\
&\quad +\sqrt{a}\,f_{LL}f_{LR}\,\Big[\,4J_{\rm IR}^1-(16-a)J_3-a(1-a)L_7+(4+a)L_6 \\
&\qquad\qquad +2aL_5+aL_3-(4-3a)L_2+2aL_1\Big]\,, \\
C_{1101} &= \frac{\sqrt{a}}{2}\,C_{1000}+\sqrt{a}\,(f_{LL}^2-f_{LR}^2) \\
&\quad \times\Bigg[\,-aN_{10}-9aN_9+2N_7-2N_6-\frac{1}{2}(12+a)N_3+\frac{a}{2}N_2-(12+a)N_1 \\
&\qquad -a(1+a)K_8+a(1-a)K_7+9a(1-a)K_6-3a(5+a)K_5 \\
&\qquad -(12+a)K_4+(4-5a)K_3-3(4+5a)K_2+3(4+a)(1-a)K_1\Bigg]\,,
\end{aligned}
$$

where we have defined

$$
\begin{aligned}
J_{\rm IR}^1 &= (2-a)J_6-aJ_5\,, \\
J_{\rm IR}^2 &= 2(2-a)N_{13}-aN_{12}-aN_{11}\,, \\
R_1 &= -4a(1-a)L_7-4(2-a)L_6-8(1-a)L_5
\end{aligned}
$$

$$
\begin{aligned}
& + a^2 L_4 + a(2+3a)L_3 - a(2-a)L_2 + (8 - 8a + 3a^2)L_1 \ , \\
R_2 &= -4L_6 - 4L_5 - aL_3 - aL_2 + 2(2-a)L_1 \ , \\
R_3 &= a^2 N_{10} + 3a(2+a)N_9 + 4aN_3 - 2aN_2 + 8(1+a)N_1 \\
& + 2a^2 K_8 - a^2(1-a)K_7 - 3a(1-a)(2+a)K_6 + 6a(1+2a)K_5 \\
& + 2(4+3a)K_4 + (a^2 + 6a - 8)K_3 + 3a(8+a)K_2 - 12a(1-a)K_1 \ .
\end{aligned}
$$

Note that the integrals $J^1_{\rm IR}$, $J^2_{\rm IR}$ namely J_5 , J_6 , N_{11} , N_{12} and N_{13} contain the infrared singularity. This singularity is exactly canceled out in the sum Eqn.(4.43) by the contributions from D_{klmn}.The numerical value of the coefficients C_{klmn} and D_{klmn} are show in Appendix. We are now ready to discuss our numerical results.

4.3 Numerical Results

We are now in the position to give the cross-section for polarized top quark production for any e^+e^- collider. Since we did not specify the spin angle ξ for the top quark, we can predict the polarized cross-section for any top quark spin. The spin configurations we will display are the helicity, the beamline and the off-diagonal bases for center of mass energies $\sqrt{s} = 400\,\text{GeV}$, $500\,\text{GeV}$, $800\,\text{GeV}$, $1000\,\text{GeV}$, $1500\,\text{GeV}$ and $4000\,\text{GeV}$.

$\sqrt{s}$	400 GeV	500 GeV	800 GeV	1000 GeV	1500 GeV	4000 GeV
β	0.4841	0.7141	0.8992	0.9368	0.9723	0.9962
α_s	0.09804	0.09564	0.09096	0.08890	0.08539	0.07794
$\sigma^0_{T,L}$ [pb]	0.8707	0.7728	0.3531	0.2312	0.1047	0.0149
$\sigma^{SGA}_{T,L}$ [pb]	1.105	0.8578	0.3643	0.2358	0.1058	0.0150
$\sigma^1_{T,L}$ [pb]	1.113	0.8719	0.3734	0.2418	0.1084	0.0153
$\sigma^0_{T,R}$ [Pb]	0.3827	0.3562	0.1710	0.1132	0.0519	0.0074
$\sigma^{SGA}_{T,R}$ [pb]	0.4865	0.3964	0.1768	0.1157	0.0525	0.0075
$\sigma^1_{T,R}$ [pb]	0.4898	0.4031	0.1813	0.1187	0.0537	0.0076
κ_L	0.2778	0.1283	0.0575	0.0457	0.0347	0.0259
κ_R	0.2799	0.1316	0.0602	0.0461	0.0360	0.0262

Table 4.2: The values of β, α_s, tree level cross-section, one-loop cross-section in soft-gluon approximation and full one-loop cross-section and $\kappa_{L/R}$ for $e^-_{L/R}e^+$ scattering. The superscript $0, 1$ and SGA stand for tree level, full one-loop, soft-gluon approximation with $\omega_{\max} = (\sqrt{s} - 2m)/5 = 10$ GeV.

Table 4.2 contains the values of the maximum center of mass speed β, the running α_s, and the tree level cross-section $\sigma^0_{T,L/R}$, the one-loop total cross-section $\sigma^{SGA}_{T,L/R}$, the full one-loop total cross-section $\sigma^1_{T,L/R}$ for $e^-_{L/R}e^+$ scattering. $\kappa_{L/R}$ stands for the fractional $\mathcal{O}(\alpha_s)$ enhancement of the tree level cross-section for top quark pair production in $e^-_{L/R}e^+$ scattering.

$$\kappa_{L/R} \;=\; \frac{\sigma^1_{T,L/R} - \sigma^0_{T,L/R}}{\sigma^0_{T,L/R}} \;.$$

At $\sqrt{s} = 400$ GeV, the QCD corrections enhance the total cross-section by $\sim 30\%$ compared to the tree level results. At higher energies, $800 \sim 4000$ GeV, the enhancements are at the $2 \sim 6\%$ level.

Next we present the numerical values for the coefficients $(D_{klmn} + \hat{\alpha}_s C_{klmn})$ in Eqn.(4.43). Since the dominant effect of the $\mathcal{O}(\alpha_s)$ corrections is a multiplicative enhancement of the tree

level result, we have chosen to write

$$D_{klmn} + \hat{\alpha}_s C_{klmn} \equiv (1 + \kappa_{L/R}) D^0_{klmn} + S_{klmn}.$$

The $(1+\kappa_{L/R})D^0_{klmn}$ terms are the multiplicative enhancement of the tree level result whereas the S_{klmn} give the α_s deviations to the spin correlations. The coefficients D^0_{klmn} are given by the D_{klmn} with limit, $\alpha_s \to 0$. The numerical value of these coefficients are given in Table 4.3 and 4.4.

	400 GeV	500 GeV	800 GeV	1000 GeV	1500 GeV	4000GeV
$(1+\kappa_L)D^0_{0000}$	1.511	1.724	1.722	1.700	1.671	1.644
$(1+\kappa_L)D^0_{2000}$	0.2404	0.6724	1.241	1.383	1.526	1.624
$(1+\kappa_L)D^0_{1000}$	0.7809	1.466	2.126	2.269	2.406	2.494
$(1+\kappa_L)D^0_{0010}$	0.3905	0.7330	1.063	1.134	1.203	1.247
$(1+\kappa_L)D^0_{2010}$	0.3905	0.7330	1.063	1.134	1.203	1.247
$(1+\kappa_L)D^0_{1010}$	1.751	2.396	2.963	3.083	3.197	3.268
$(1+\kappa_L)D^0_{0101}$	1.452	1.502	1.100	0.9048	0.6186	0.2353
$(1+\kappa_L)D^0_{1101}$	0.3416	0.5131	0.4650	0.3970	0.2807	0.1091
S_{0000}	−0.002552	−0.005000	0.0005645	0.004836	0.01172	0.02039
S_{2000}	0.007655	0.01500	−0.001682	−0.01450	−0.03516	−0.06116
S_{1000}	0.02154	0.03170	0.01224	−0.0008102	−0.02085	−0.04516
S_{0010}	0.01094	0.01785	0.01586	0.01304	0.008357	0.002274
S_{2010}	0.01059	0.01356	−0.006158	−0.01791	−0.03614	−0.05987
S_{1010}	0.004433	0.005069	−0.02030	−0.03590	−0.06134	−0.09742
S_{0101}	−0.006564	−0.02193	−0.04413	−0.04852	−0.04952	−0.03639
S_{1101}	0.007920	0.004308	−0.01270	−0.01734	−0.02047	−0.01642

Table 4.3: The values of $(1+\kappa_L)D^0_{klmn}$ and S_{klmn} for $e^-_L e^+$ scattering.

$\sqrt{s}$	400 GeV	500 GeV	800 GeV	1000 GeV	1500 GeV	4000 GeV
$(1+\kappa_R)D^0_{0000}$	0.6613	0.7901	0.8313	0.8307	0.8266	0.8204
$(1+\kappa_R)D^0_{2000}$	0.1174	0.3318	0.6180	0.6899	0.7622	0.8112
$(1+\kappa_R)D^0_{1000}$	0.4408	0.8357	1.222	1.306	1.386	1.437
$(1+\kappa_R)D^0_{0010}$	0.2204	0.4178	0.6109	0.6529	0.6931	0.7187
$(1+\kappa_R)D^0_{2010}$	0.2204	0.4178	0.6109	0.6529	0.6931	0.7187
$(1+\kappa_R)D^0_{1010}$	0.7787	1.122	1.449	1.521	1.589	1.632
$(1+\kappa_R)D^0_{0101}$	0.6216	0.6547	0.4875	0.4024	0.2759	0.1052
$(1+\kappa_R)D^0_{1101}$	0.1929	0.2925	0.2673	0.2285	0.1617	0.06289
S_{0000}	-0.001287	-0.002358	0.0006297	0.002742	0.006079	0.01024
S_{2000}	0.003862	0.007074	-0.001884	-0.008222	-0.01824	-0.03072
S_{1000}	0.01143	0.01556	0.003835	-0.003159	-0.01367	-0.02639
S_{0010}	0.005814	0.008914	0.007500	0.006143	0.003972	0.001128
S_{2010}	0.005612	0.006475	-0.005121	-0.01164	-0.02164	-0.03468
S_{1010}	0.002248	0.002290	-0.01078	-0.01854	-0.03107	-0.04878
S_{0101}	-0.003764	-0.01122	-0.02028	-0.02189	-0.02208	-0.01640
S_{1101}	0.004154	0.001587	-0.007977	-0.01043	-0.01198	-0.009478

Table 4.4: The values of $(1+\kappa_R)D^0_{klmn}$ and S_{klmn} for $e^-_R e^+$ scattering.

$e_L^- e^+$	400 GeV	500 GeV	800 GeV	1000 GeV	1500 GeV	4000 GeV
R_{0000}	−0.001689	−0.002900	0.0003278	0.002845	0.007014	0.01240
R_{2000}	0.03184	0.02231	−0.001356	−0.01048	−0.02304	−0.03767
R_{1000}	0.02758	0.02163	0.005757	−0.0003571	−0.008667	−0.01811
R_{0010}	0.02803	0.02435	0.01492	0.01150	0.006948	0.001823
R_{2010}	0.02711	0.01849	−0.005793	−0.01579	−0.03004	−0.04802
R_{1010}	0.0025310	0.002115	−0.006849	−0.01165	−0.01919	−0.02981
R_{0101}	−0.004520	−0.01460	−0.04013	−0.05362	−0.08005	−0.15465
R_{1101}	0.02318	0.008395	−0.02731	−0.04369	−0.07294	−0.15050
$e_R^- e^+$	400 GeV	500 GeV	800 GeV	1000 GeV	1500 GeV	4000 GeV
R_{0000}	−0.001947	−0.002985	0.0007576	0.003301	0.007354	0.01248
R_{2000}	0.03289	0.02132	−0.003048	−0.01192	−0.02393	−0.03787
R_{1000}	0.02593	0.01862	0.003139	−0.002419	−0.009864	−0.01836
R_{0010}	0.02638	0.02133	0.01228	0.009409	0.005731	0.001570
R_{2010}	0.02546	0.01550	−0.008382	−0.01782	−0.03122	−0.04826
R_{1010}	0.002886	0.002041	−0.007438	−0.01219	−0.01955	−0.02989
R_{0101}	−0.006056	−0.01714	−0.04161	−0.05439	−0.08003	−0.1559
R_{1101}	0.02154	0.005427	−0.02984	−0.04566	−0.07406	−0.1507

Table 4.5: The ratios, $R_{klmn} = S_{klmn}/(1+\kappa)D^0_{klmn}$, for $e^-_{L/R}e^+$ scattering.

Table 4.5 shows the ratios,

$$R_{klmn} \;=\; S_{klmn}/(1+\kappa)D^0_{klmn}.$$

The ratios are never larger than 10% and are typically of order a few percent. Hence the $\mathcal{O}(\alpha_s)$ corrections make only small changes to the spin orientation of the top quark.

To illustrate the cross-sections in different spin bases, we present the top quark production cross-section in the three different spin bases discussed in the previous Section. One is the usual helicity basis which corresponds to $\cos\xi = +1$. The second is the beamline basis, in which the top quark spin is aligned with the positron momentum in the top quark rest frame. In this basis, ξ is obtained by Eqn.(4.29). The third corresponds to the off-diagonal basis which has been defined in Eqn.(4.33). Note that as $\beta \to 1$, the helicity and off-diagonal bases coincide. Therefore, at an extremely high energy collider, there will be no significant difference between these bases. But a remarkable differences among these bases exists at moderate energies. Now let us show the polarized differential cross-sections at $\sqrt{s} = 400$ and 500 GeV.

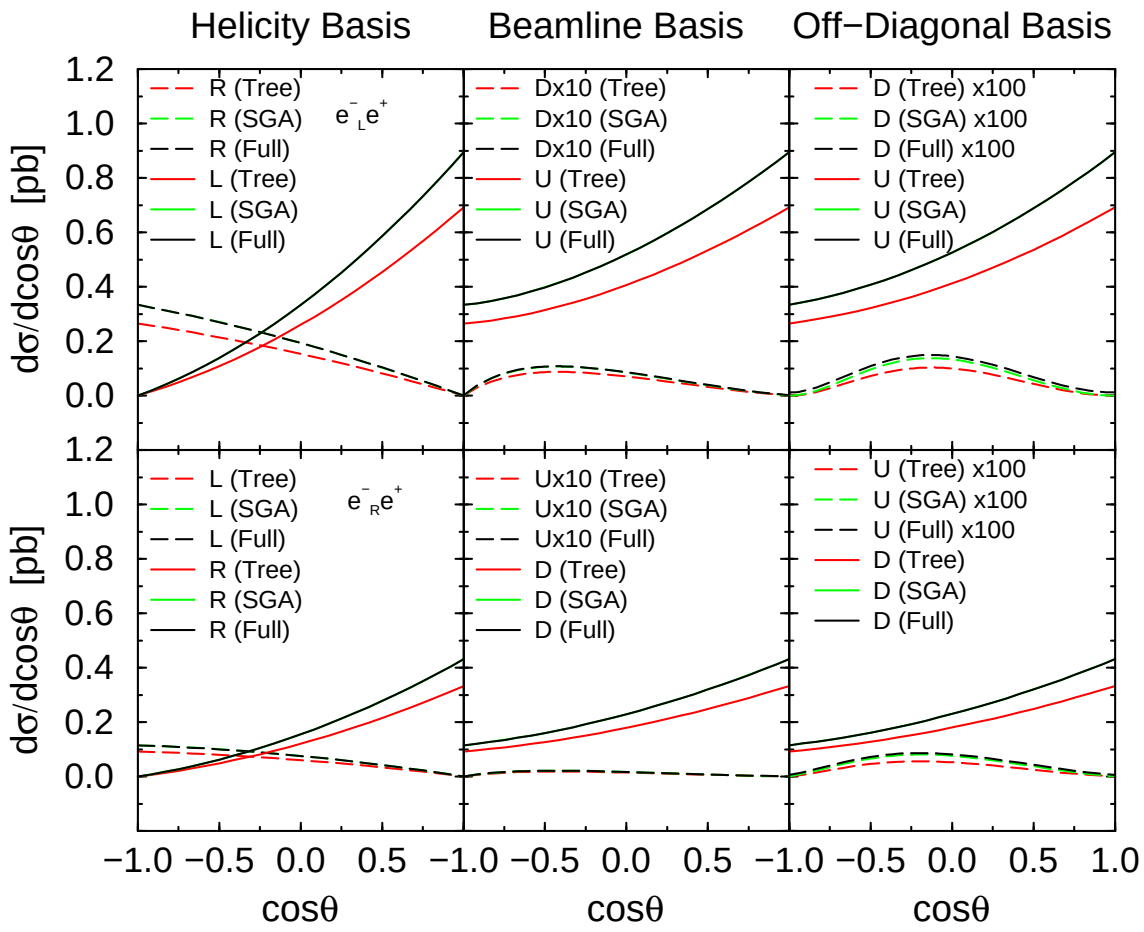

Figure 4.7: The cross-sections in the helicity, beamline and off-diagonal bases at $\sqrt{s} = 400\,\text{GeV}$. Here we use a "beamline basis", in which the top quark axis is the positron direction in the top rest frame, for each $e_L^- e^+$ and $e_R^- e^+$ scattering. For the soft gluon approximation (SGA) $\omega_{\max} = (\sqrt{s} - 2m)/5 = 10$ GeV.

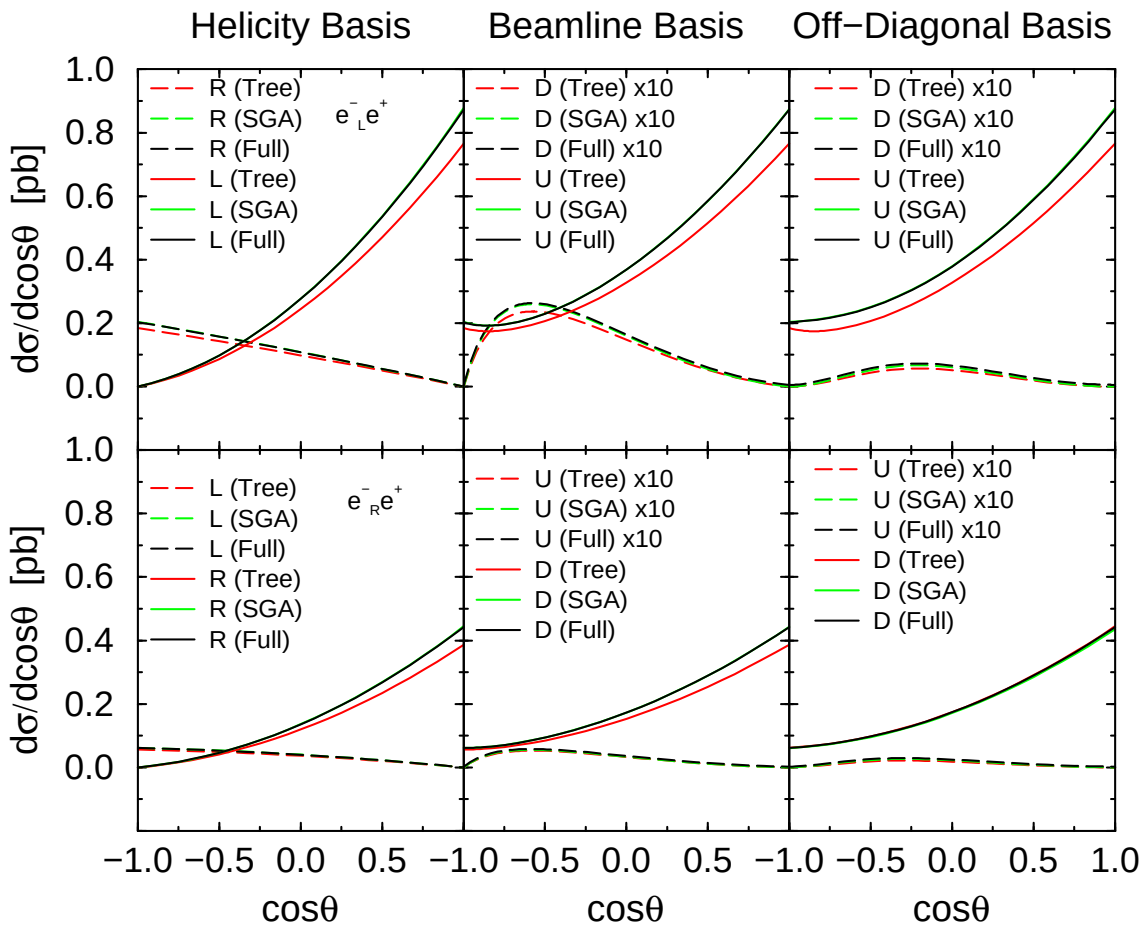

Figure 4.8: The cross-sections in the helicity, beamline and off-diagonal bases at $\sqrt{s} = 500\,\text{GeV}$. Here we use a "beamline basis", in which the top quark axis is the positron direction in the top rest frame, for each $e^-_L e^+$ and $e^-_R e^+$ scattering. For the soft gluon approximation (SGA) $\omega_{\max} = (\sqrt{s} - 2m)/5 = 30$ GeV.

In Fig.4.7 and Fig.4.8, we give the results for $\sqrt{s} = 400$ and 500 GeV for both $e^-_L e^+$ and $e^-_R e^+$ scattering using the helicity, beamline and off-diagonal spin bases. These figures show the tree level, the SGA and the full QCD results for all three spin bases. Since the SGA results almost coincide with the full QCD results, the probability that hard gluon emission flips the spin of the top quark is very small. Clearly, the qualitative features of the cross-sections remain the same as those in the leading order analysis. That is the top quarks are produced with very high polarization in polarized e^+e^- scattering. In Table 4.6 and 4.7, we give the fraction of the top quarks in the sub-dominant spin configuration for $e^-_{L/R} e^+$ scattering,

$$\sigma\left(e^-_L e^+ \to t_\uparrow X(\bar{t} \text{ or } \bar{t}g)\right)/\sigma^1_{T,L}$$

for the three bases. Similar results also hold for $e^-_R e^+$ scattering.

$e^-_L e^+$	Helicity	Beamline	Off-Diagonal
Tree	0.336	0.0119	0.00124
SGA	0.332	0.0113	0.00129
$\mathcal{O}(\alpha_s)$	0.332	0.0115	0.00150
$e^-_R e^+$	Helicity	Beamline	Off-Diagonal
Tree	0.290	0.00564	0.00167
SGA	0.285	0.00510	0.00191
$\mathcal{O}(\alpha_s)$	0.285	0.00530	0.00214

Table 4.6: The fraction of the $e^-_{L/R} e^+$ cross-section in the sub-dominant spin at $\sqrt{s} = 400$ GeV for the helicity, beamline and off-diagonal bases. For the soft gluon approximation (SGA) $\omega_{\max} = (\sqrt{s} - 2m)/5 =$ 10 GeV.

$e^-_L e^+$	Helicity	Beamline	Off-Diagonal
Tree	0.249	0.0323	0.00745
SGA	0.243	0.0321	0.00775
$\mathcal{O}(\alpha_s)$	0.243	0.0311	0.00907
$e^-_R e^+$	Helicity	Beamline	Off-Diagonal
Tree	0.191	0.0157	0.00629
SGA	0.185	0.0145	0.00682
$\mathcal{O}(\alpha_s)$	0.185	0.0156	0.00816

Table 4.7: The fraction of the $e^-_{L/R} e^+$ cross-section in the sub-dominant spin at $\sqrt{s} = 500$ GeV for the helicity, beamline and off-diagonal bases. For the soft gluon approximation (SGA) $\omega_{\max} = (\sqrt{s} - 2m)/5 =$ 30 GeV.

In Fig.4.9 $\sim$ 4.12, we have plotted the similar results for 800,1000,1500 and 4000 GeV colliders. The fraction of top quarks in the sub-dominant spin component for $e^-_L e^+$ is given in Tables 4.8 and 4.11. Our numerical studies demonstrate that the QCD corrections have a small effect on the spin configuration of the produced top (or anti-top) quark for any spin basis. The off-diagonal and beamline bases are clearly more sensitive to the radiative corrections than the helicity basis. However, in the off-diagonal basis, the top (and/or anti-top) quarks are produced in an essentially unique spin configuration even after including the lowest order QCD corrections.

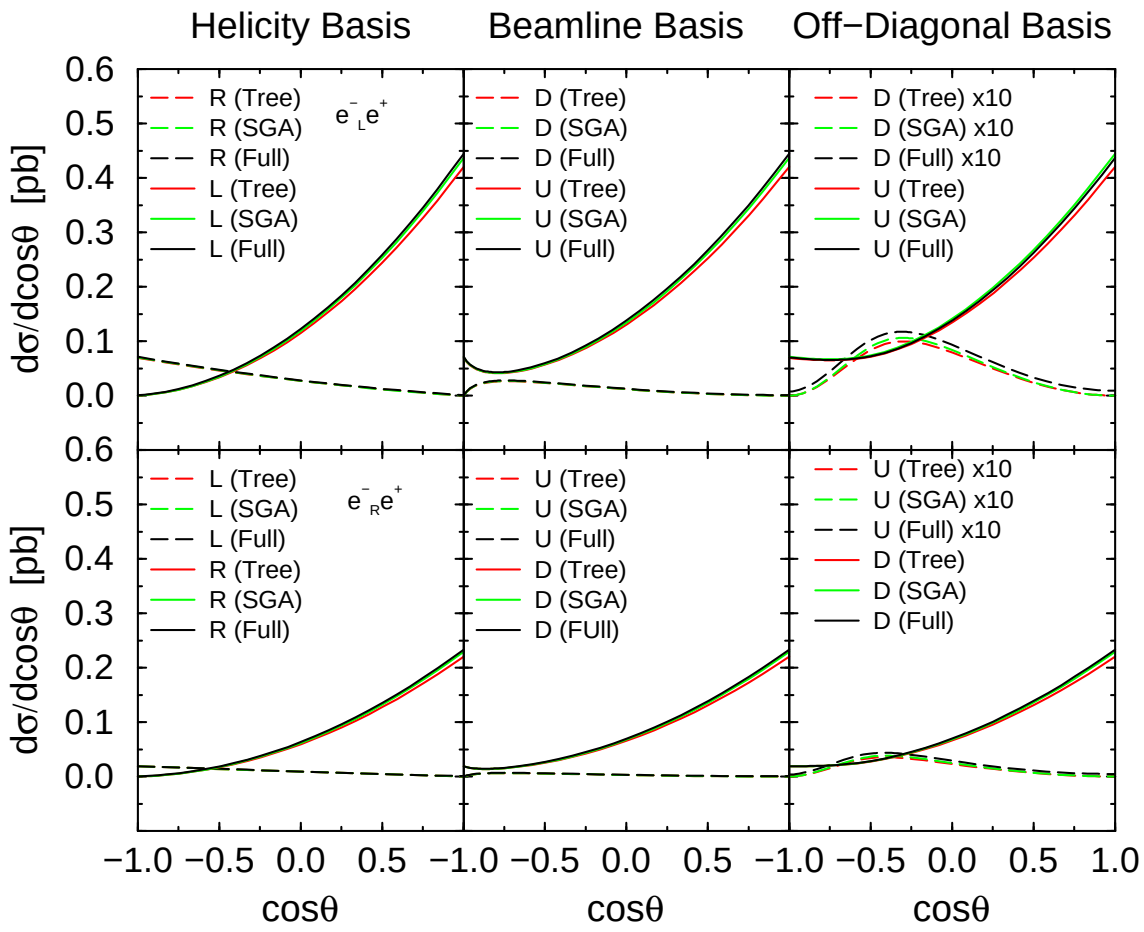

Figure 4.9: The cross-sections in the helicity, beamline and off-diagonal bases at $\sqrt{s} = 800\,\text{GeV}$. Here we use a "beamline basis", in which the top quark axis is the positron direction in the top rest frame, for each $e_L^- e^+$ and $e_R^- e^+$ scattering. For the soft gluon approximation (SGA) $\omega_{\max} = (\sqrt{s} - 2m)/5 = 90$ GeV.

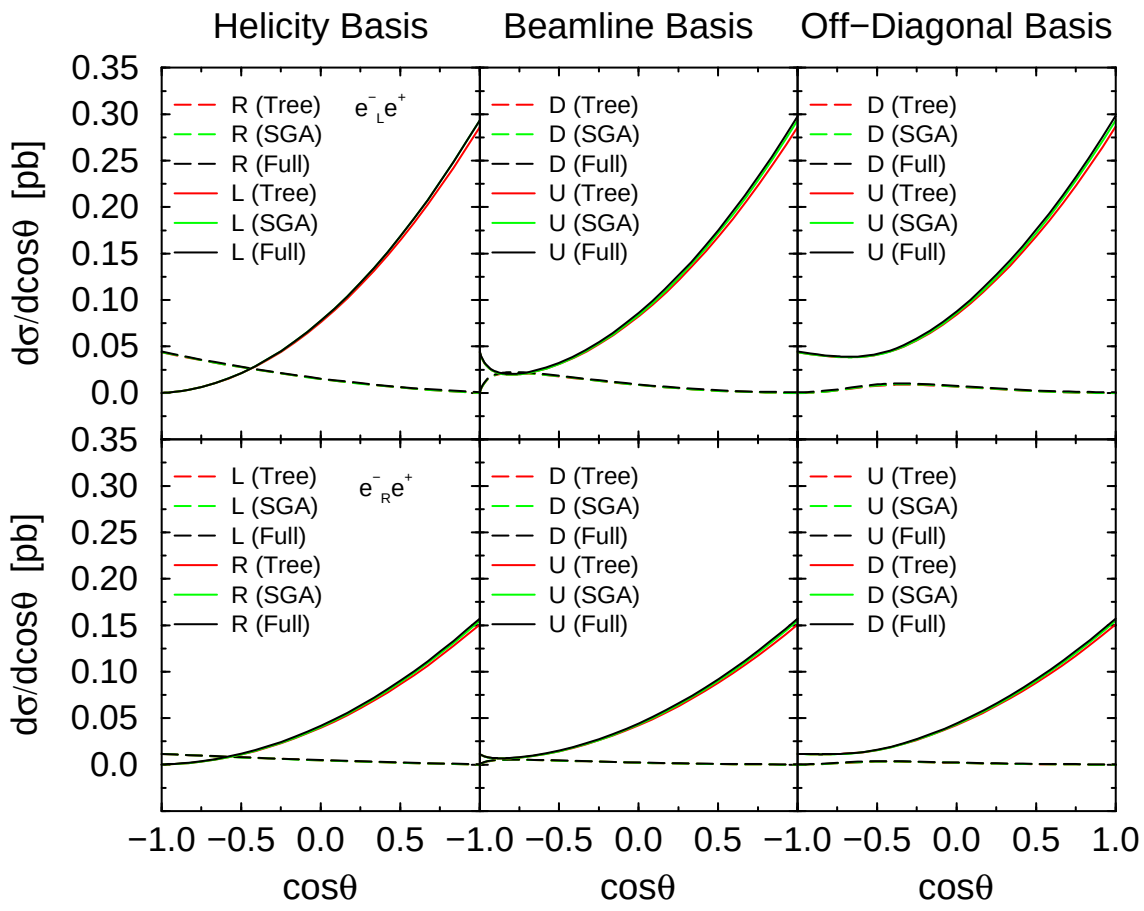

Figure 4.10: The cross-sections in the helicity, beamline and off-diagonal bases at $\sqrt{s} = 1000\,\text{GeV}$. Here we use a "beamline basis", in which the top quark axis is the positron direction in the top rest frame, for each $e_L^- e^+$ and $e_R^- e^+$ scattering. For the soft gluon approximation (SGA) $\omega_{\max} = (\sqrt{s} - 2m)/5 = 130$ GeV.

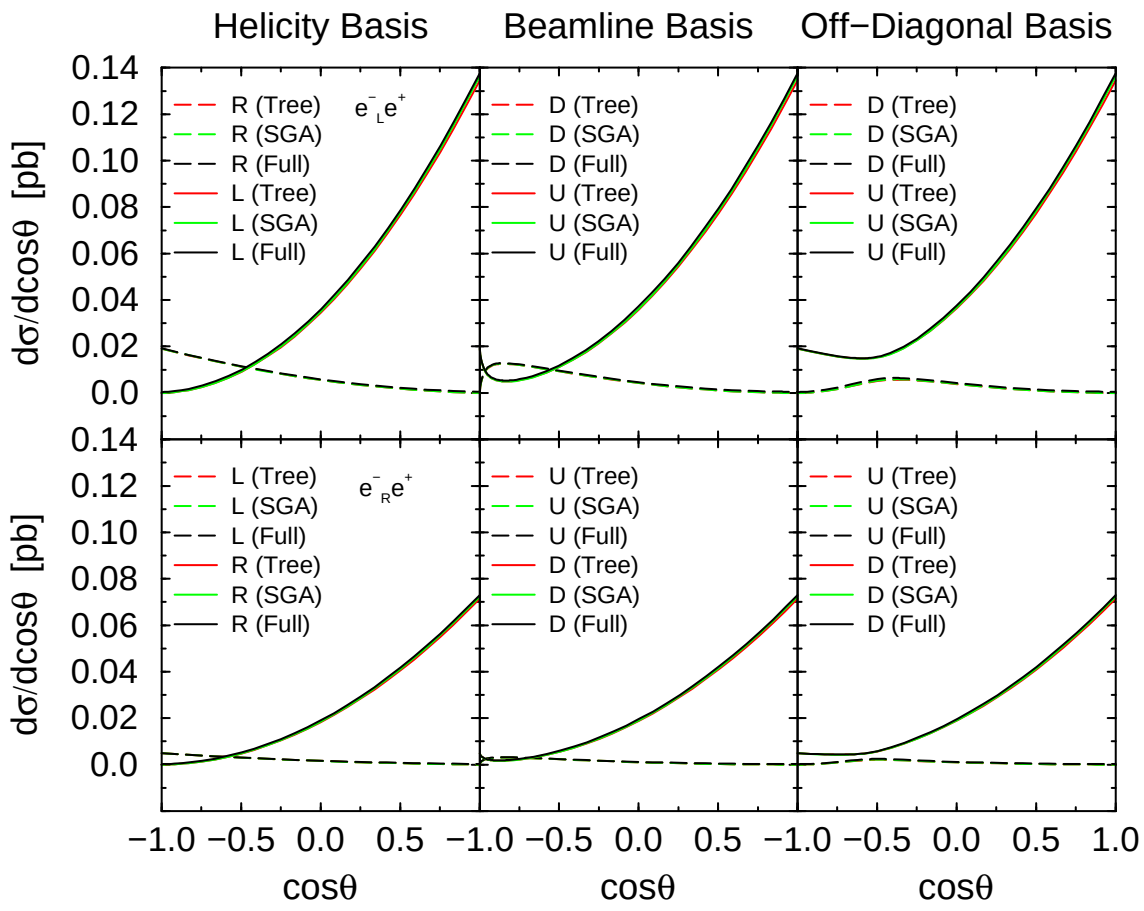

Figure 4.11: The cross-sections in the helicity, beamline and off-diagonal bases at $\sqrt{s} = 1500\,\mathrm{GeV}$. Here we use a "beamline basis", in which the top quark axis is the positron direction in the top rest frame, for each $e^-_L e^+$ and $e^-_R e^+$ scattering. For the soft gluon approximation (SGA) $\omega_{\max} = (\sqrt{s} - 2m)/5 = 230$ GeV.

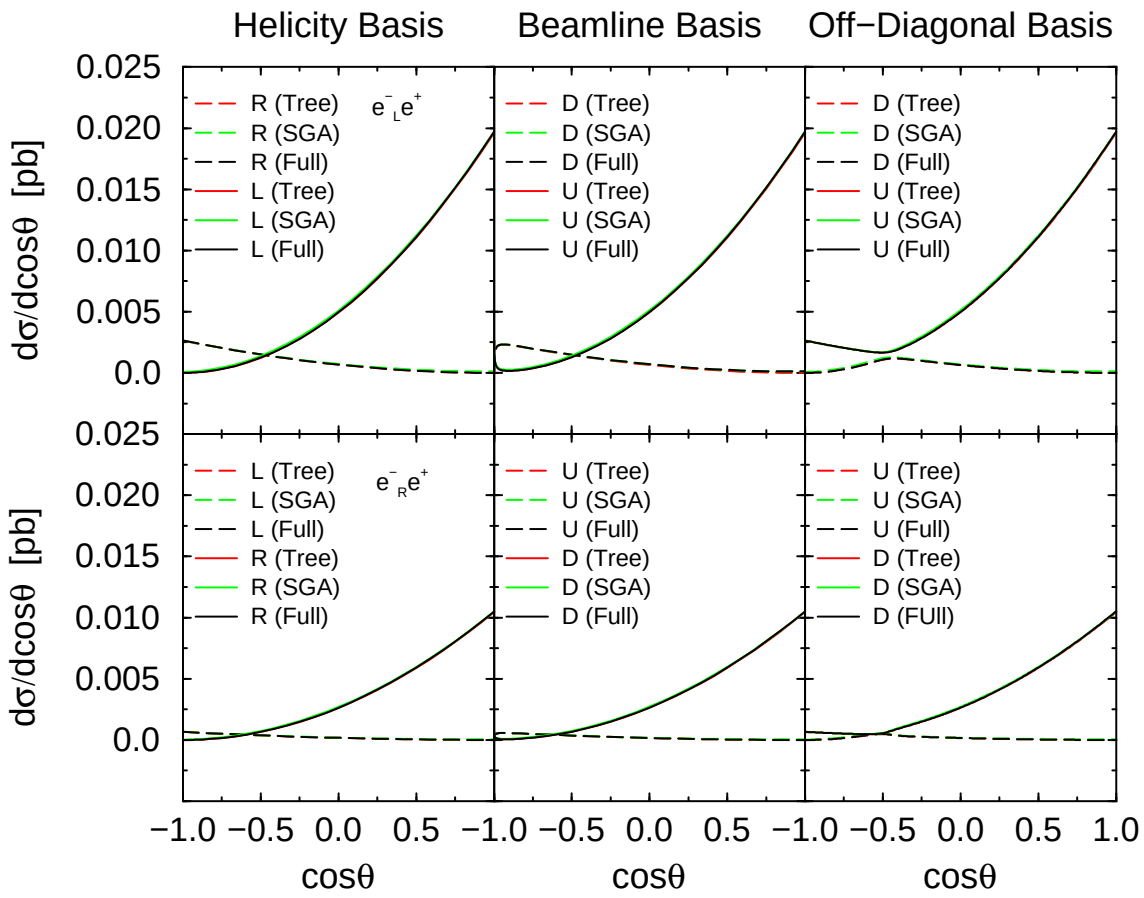

Figure 4.12: The cross-sections in the helicity, beamline and off-diagonal bases at $\sqrt{s} = 4000\,\text{GeV}$. Here we use a "beamline basis", in which the top quark axis is the positron direction in the top rest frame, for each $e^-_L e^+$ and $e^-_R e^+$ scattering. For the soft gluon approximation (SGA) $\omega_{\max} = (\sqrt{s} - 2m)/5 = 730$ GeV.

$e_L^- e^+$	Helicity	Beamline	Off-Diagonal
Tree	0.168	0.0690	0.0265
SGA	0.164	0.0679	0.0272
$\mathcal{O}(\alpha_s)$	0.165	0.0708	0.0319
$e_R^- e^+$	Helicity	Beamline	Off-Diagonal
Tree	0.107	0.0342	0.0186
SGA	0.103	0.0331	0.0194
$\mathcal{O}(\alpha_s)$	0.105	0.0360	0.0239

Table 4.8: The fraction of the $e_{L/R}^- e^+$ cross-section in the sub-dominant spin at $\sqrt{s} = 800$ GeV for the helicity, beamline and off-diagonal bases. For the soft gluon approximation (SGA) $\omega_{\max} = (\sqrt{s} - 2m)/5 = 90$ GeV.

$e_L^- e^+$	Helicity	Beamline	Off-Diagonal
Tree	0.150	0.0818	0.0349
SGA	0.147	0.0809	0.0357
$\mathcal{O}(\alpha_s)$	0.148	0.0844	0.0417
$e_R^- e^+$	Helicity	Beamline	Off-Diagonal
Tree	0.0896	0.0407	0.0238
SGA	0.0867	0.0398	0.0246
$\mathcal{O}(\alpha_s)$	0.0886	0.0433	0.0304

Table 4.9: The fraction of the $e_{L/R}^- e^+$ cross-section in the sub-dominant spin at $\sqrt{s} = 1000$ GeV for the helicity, beamline and off-diagonal bases. For the soft gluon approximation (SGA) $\omega_{\max} = (\sqrt{s} - 2m)/5 = 130$ GeV.

$e_L^- e^+$	Helicity	Beamline	Off-Diagonal
Tree	0.132	0.0978	0.0466
SGA	0.130	0.0973	0.0472
$\mathcal{O}(\alpha_s)$	0.133	0.101	0.0552
$e_R^- e^+$	Helicity	Beamline	Off-Diagonal
Tree	0.0724	0.0488	0.0310
SGA	0.0709	0.0483	0.0316
$\mathcal{O}(\alpha_s)$	0.0739	0.0527	0.0394

Table 4.10: The fraction of the $e_{L/R}^- e^+$ cross section in the sub-dominant spin at $\sqrt{s} = 1500$ GeV for the helicity, beamline and off-diagonal bases. For the soft gluon approximation (SGA) $\omega_{\max} = (\sqrt{s} - 2m)/5 =$ 230 GeV.

$e_L^- e^+$	Helicity	Beamline	Off-Diagonal
Tree	0.120	0.113	0.0594
SGA	0.119	0.113	0.0596
$\mathcal{O}(\alpha_s)$	0.124	0.118	0.0698
$e_R^- e^+$	Helicity	Beamline	Off-Diagonal
Tree	0.0607	0.0568	0.0388
SGA	0.0604	0.0566	0.0391
$\mathcal{O}(\alpha_s)$	0.0655	0.0622	0.0492

Table 4.11: The fraction of the $e_{L/R}^- e^+$ cross-section in the sub-dominant spin at $\sqrt{s} = 4000$ GeV for the helicity, beamline and off-diagonal bases. For the soft gluon approximation (SGA) $\omega_{\max} = (\sqrt{s} - 2m)/5 =$ 730 GeV.

4.4 $f_{LR} = f_{RL} = 0$ Limit

In the previous chapter, we investigated why the polarized cross-sections for the beamline and off-diagonal bases give similar behaviors. At the leading order, the polarized cross-sections under the approximation $f_{LR} = f_{RL} = 0$ in the beamline and off-diagonal bases coincide, the top spin-down configuration for the $e^-_L e^+$ scattering process is identically zero, alternatively, the top spin-up configuration for the $e^-_R e^+$ scattering process is identically zero. The smallness of the parameters $f_{LR} \sim f_{RL} \sim 0$ is a key point to understand the relation between the beamline and the off-diagonal bases.

Since these analyses were useful to get further understanding on the off-diagonal and the beamline bases, we examine the polarized cross-sections at the one-loop level by setting $f_{LR} = f_{RL} = 0$.

$\sqrt{s}$	400 GeV	500 GeV	800 GeV	1000 GeV	1500 GeV
Tree	1	1	1	1	1
$\mathcal{O}(\alpha_s)$	0.9998	0.9988	0.9969	0.9962	0.9952

Table 4.12: The fraction of the $e^-_{L/R} e^+ \to t_{\uparrow/\downarrow}\bar{t}$ cross-section with $f_{LR} = f_{RL} = 0$ in the dominant spin at $\sqrt{s} = 400,\ 500,\ 800,\ 1000$ and 1500 GeV for the beamline and off-diagonal bases. Note that cross-section in the beamline basis coincides with that in the off-diagonal basis with $f_{LR} = 0$.

Table 4.12 shows the fraction of the $e^-_{L/R} e^+$ cross-section with $f_{LR} = f_{RL} = 0$ in the dominant spin at the energy region 400 $\sim$ 1500 GeV. The QCD corrections to these processes slightly change the tree level result. Although the top spin-up configuration for the $e^-_L e^+$ scattering process is 100% at the tree level, its configuration at the QCD one-loop level is less than 100%. However this change is of order 0.002 $\sim$ 0.05% at energy region 400 $\sim$ 1500 GeV and the QCD corrections are almost negligible. We plot the differential cross-sections with $f_{LR} = f_{RL} = 0$ in the helicity, beamline and off-diagonal bases in Fig.4.13 $\sim$ Fig.4.17. The characteristic features of the polarized cross-sections in the beamline and off-diagonal bases do not change even after including the lowest order QCD corrections.

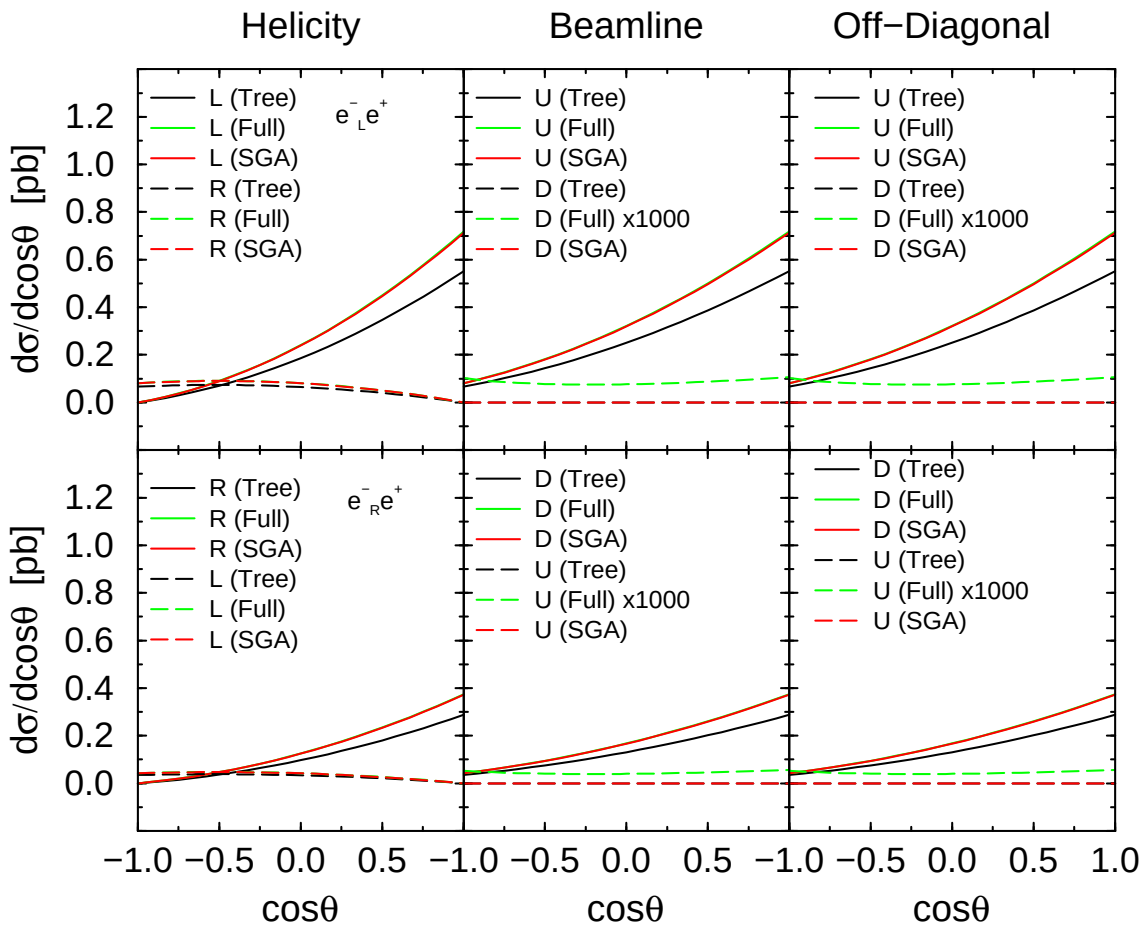

Figure 4.13: The cross-sections for $f_{LR} = f_{RL} = 0$ in the helicity, beamline and off-diagonal bases at $\sqrt{s} = 400\,\text{GeV}$.

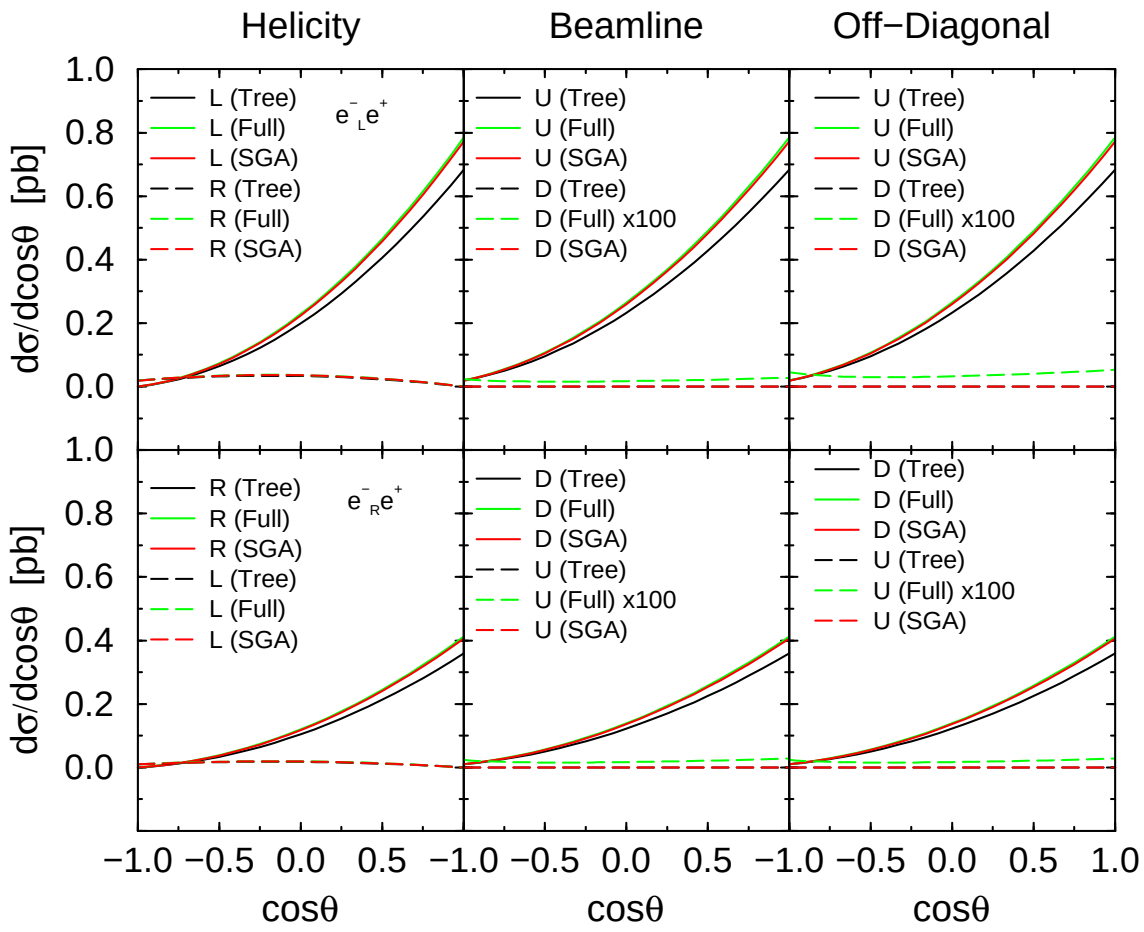

Figure 4.14: The cross-sections for $f_{LR} = f_{RL} = 0$ in the helicity, beamline and off-diagonal bases at $\sqrt{s} = 500\,\mathrm{GeV}$.

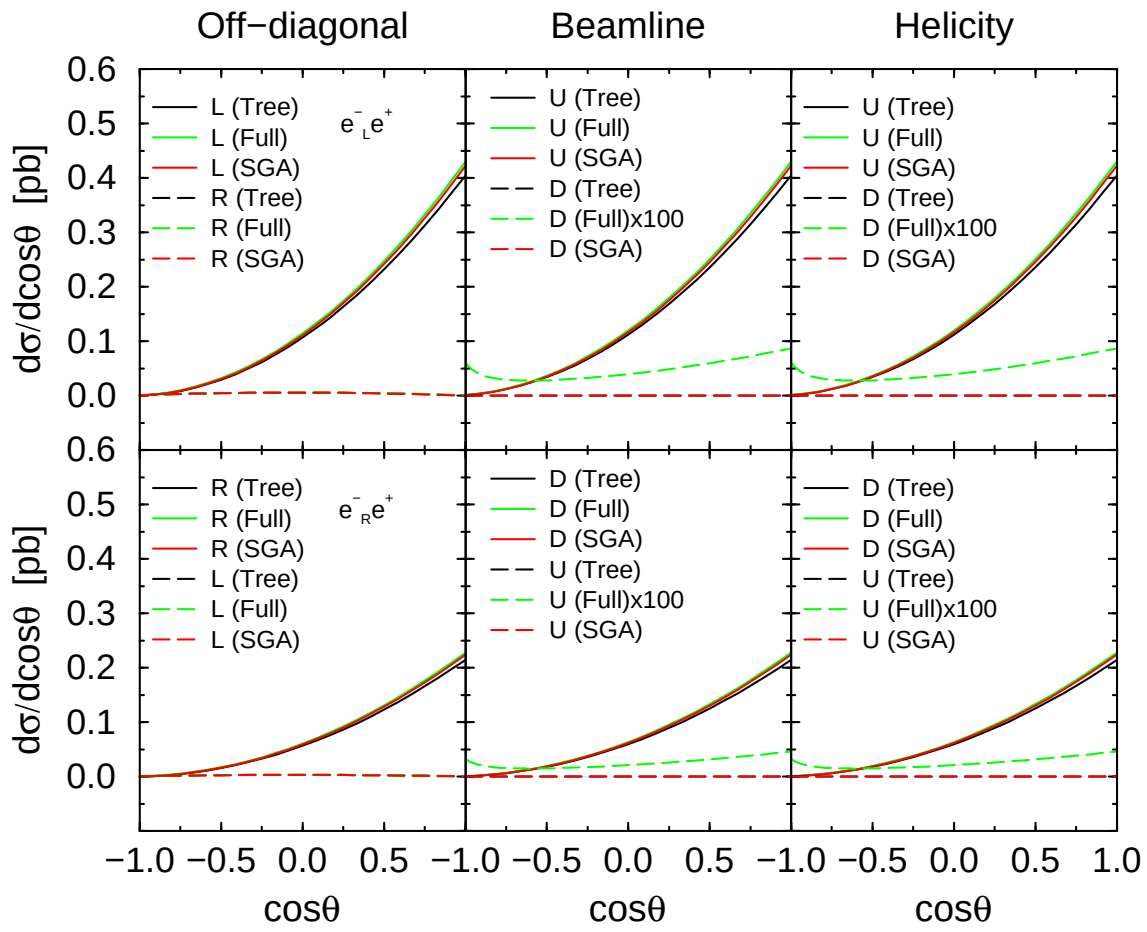

Figure 4.15: The cross-sections for $f_{LR} = f_{RL} = 0$ in the helicity, beamline and off-diagonal bases at $\sqrt{s} = 800\,\mathrm{GeV}$.

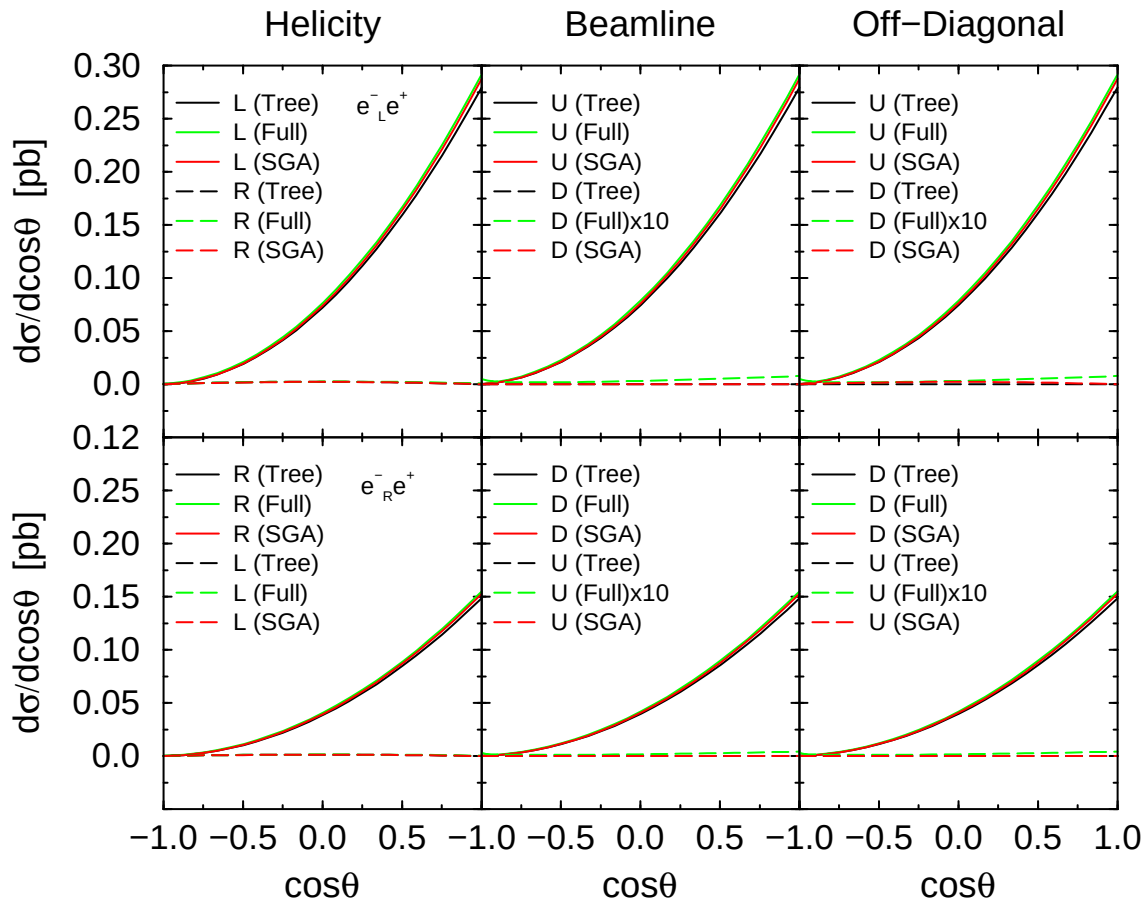

Figure 4.16: The cross-sections for $f_{LR} = f_{RL} = 0$ in the helicity, beamline and off-diagonal bases at $\sqrt{s} = 1000\,\mathrm{GeV}$.

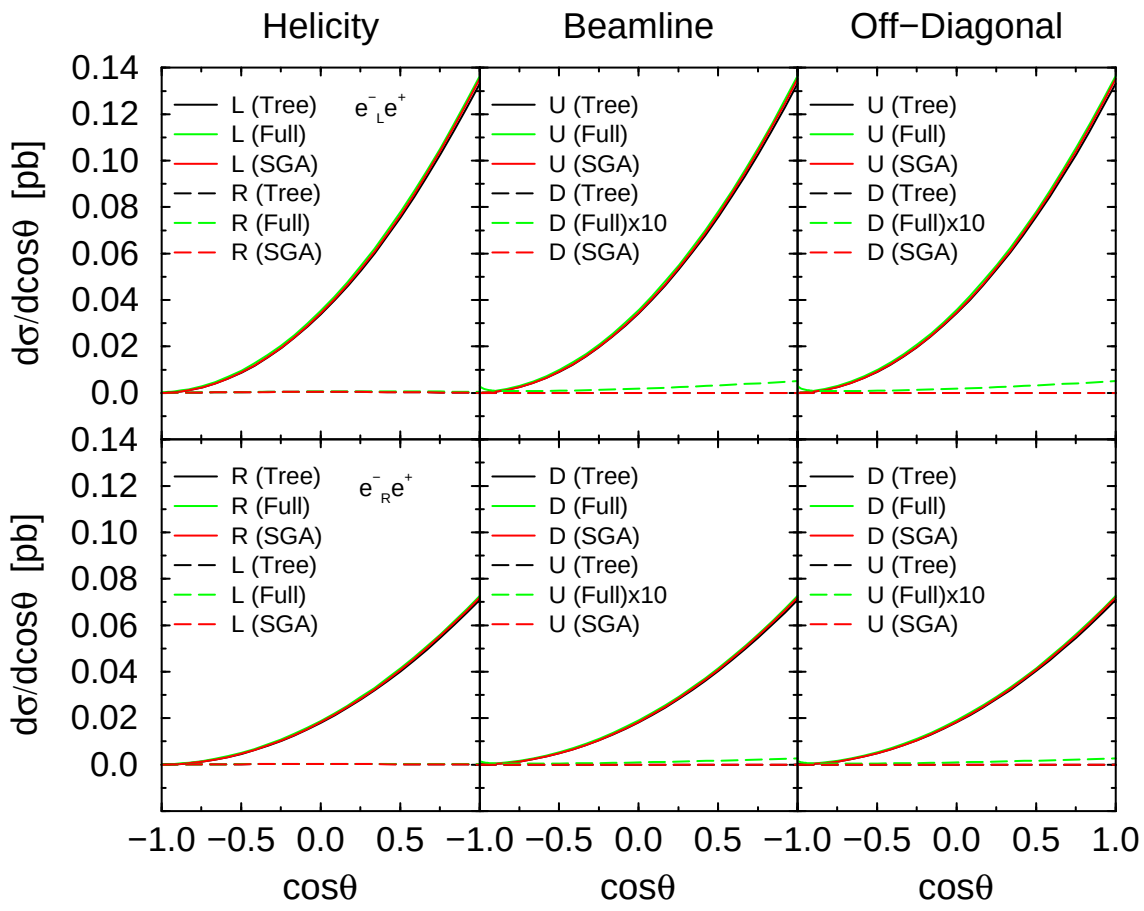

Figure 4.17: The cross-sections for $f_{LR} = f_{RL} = 0$ in the helicity, beamline and off-diagonal bases at $\sqrt{s} = 1500\,\text{GeV}$.

4.5 Validity of Soft Gluon Approximation

In the previous section, we have arrived at the following results. The spin-flip effects caused by the hard gluon are quit small, and the QCD corrections produce only the multiplicative enhancement to the leading order results. Moreover, this enhancement is almost attributed to the soft-gluon effects. In this Section, we consider the possibility that the full QCD corrections are reproduced by the soft-gluon approximation with effective cut-off $\omega_{\max}$. We repeat the same procedure as in the previous analyses in the soft-gluon approximation. At first, let us rewrite the spin dependent cross-sections in the generic spin basis as follows,

$$\frac{d\sigma^{\rm SGA}}{d\cos\theta}(e^-_L e^+_R \to t_\uparrow X(\bar{t}g)) = \frac{3\pi\alpha^2}{4s}\sum_{klmn}\left(D^0_{klmn}+B^1_{klmn}\right)\cos^k\theta\sin^l\theta\cos^m\xi\sin^n\xi \ , \quad (4.44)$$

with

$$\begin{aligned}
B^1_{0000} &= \beta[f^2_{LL}+f^2_{LR}+2af_{LL}f_{LR}]S_I \\
&\qquad -\beta[2(f_{LL}+f_{LR})^2-\beta^2(f_{LL}-f_{LR})^2]S_{II} \ , \\
B^1_{2000} &= \beta^3(f^2_{LL}+f^2_{LR})S_I+\beta^3(f_{LL}-f_{LR})^2S_{II} \ , \\
B^1_{1000} &= 2\beta^2(f^2_{LL}-f^2_{LR})S_I \ , \\
B^1_{0010} &= \beta^2(f^2_{LL}-f^2_{LR})S_I \ , \\
B^1_{2010} &= \beta^2(f^2_{LL}-f^2_{LR})S_I \ , \\
B^1_{1010} &= \beta[(f_{LL}+f_{LR})^2+\beta^2(f_{LL}-f_{LR})^2]S_I \\
&\qquad -2\beta[(f_{LL}+f_{LR})^2-\beta^2(f_{LL}-f_{LR})^2]S_{II} \ , \\
B^1_{0101} &= \frac{\beta}{\sqrt{a}}(f_{LL}+f_{LR})^2[aS_I-(1+a)S_{II}] \ , \\
B^1_{1101} &= \frac{\beta^2}{\sqrt{a}}(f^2_{LL}-f^2_{LR})[aS_I-(1-a)S_{II}] \ .
\end{aligned}$$

Now we separate the multiplicative enhancement factor from the coefficients, $D^0_{klmn}+B^1_{klmn}$.

$$D^0_{klmn}+B^1_{klmn} \equiv (1+\kappa)D^0_{klmn}+S^{\rm SGA}_{klmn} \ .$$

The deviations $S^{\rm SGA}_{klmn}$ from the multiplicative enhancement and the ratio $R^{\rm SGA}_{klmn}$ are defined by

$$\begin{aligned}
S^{\rm SGA}_{klmn} &= B^1_{klmn}-\kappa D^0_{klmn} \ . \\
R^{\rm SGA}_{klmn} &= \frac{S^{\rm SGA}_{klmn}}{(1+\kappa)D^0_{klmn}} \ .
\end{aligned}$$

At first we determine the effective energy cut-off $\omega_{\max}$ of gluon such that the total cross-section in the soft-gluon approximation reproduces the full $\mathcal{O}(\alpha_s)$ total cross-section.

$$\begin{aligned} & \int_{-1}^{1} d\cos\theta \sum_{s=\uparrow,\downarrow} \frac{d\sigma_{T,L/R}}{d\cos\theta}(e^-_{L/R}e^+ \to t_s X(\bar{t} \text{ or } \bar{t}g)) \\ = & \int_{-1}^{1} d\cos\theta \sum_{s=\uparrow,\downarrow} \frac{d\sigma_{SGA,L/R}}{d\cos\theta}(e^-_{L/R}e^+ \to t_s\bar{t}). \end{aligned}$$

Next using this cut-off $\omega_{\max}$, we compare the above deviation R^{SGA}_{klmn} with R_{klmn} in the full calculation.

We show the effective $\omega_{\max}$ and the numerical results of B^1_{klmn}, $S^{\rm SGA}_{klmn}$ and $R^{\rm SGA}_{klmn}$ in Table.4.13 and 4.14. Compared to Table 4.3$\sim$4.5 in the previous Section, we find that all values are in good agreement with the full calculation results at $\sqrt{s} = 400$ and 500 GeV. As the total energy get larger, the difference of results between the soft-gluon approximation and in the full $\mathcal{O}(\alpha_s)$ calculation become more remarkable. However the spin-flip effects, S^{SGA}_{klmn}, are still small. These become smaller and negligible, as the total energy get larger. Therefore we conclude that the soft-gluon approximation can be an effective tool to represent the spin dependent cross-section at $\mathcal{O}(\alpha_s)$. We also present the polarized cross-sections in the helicity, beamline and off-diagonal bases.

$e_L^- e^+$	400 GeV	500 GeV	800 GeV	1000 GeV	1500 GeV	4000 GeV
ω_{max}	13.49	38.60	106.7	149.7	254.8	775.9
B^1_{0000}	0.3259	0.1900	0.08785	0.06979	0.05347	0.04103
B^1_{2000}	0.06009	0.09431	0.08469	0.07414	0.05908	0.04258
B^1_{1000}	0.1911	0.1996	0.1407	0.1183	0.09133	0.06506
B^1_{0010}	0.09556	0.09979	0.07034	0.05916	0.04567	0.03253
B^1_{2010}	0.09556	0.09979	0.07034	0.05916	0.04567	0.03253
B^1_{1010}	0.3860	0.2843	0.1725	0.1439	0.1126	0.08361
B^1_{0101}	0.3099	0.1540	0.03373	0.01373	−0.001588	−0.005863
B^1_{1101}	0.08219	0.06395	0.01957	0.009227	0.0004544	−0.002634
$S^{\rm SGA}_{0000}$	−0.002607	−0.005957	−0.005747	−0.004551	−0.002615	−0.0005169
$S^{\rm SGA}_{2000}$	0.007821	0.01787	0.01724	0.01365	0.007846	0.001551
$S^{\rm SGA}_{1000}$	0.02134	0.03293	0.02514	0.01910	0.01057	0.002038
$S^{\rm SGA}_{0010}$	0.01067	0.01646	0.01257	0.009549	0.005284	0.001019
$S^{\rm SGA}_{2010}$	0.01067	0.01646	0.01257	0.009549	0.005284	0.001019
$S^{\rm SGA}_{1010}$	0.005214	0.01191	0.01149	0.009101	0.005231	0.001034
$S^{\rm SGA}_{0101}$	−0.005870	−0.01676	−0.02604	−0.02585	−0.02235	−0.01181
$S^{\rm SGA}_{1101}$	0.007915	0.005621	−0.005706	−0.008136	−0.008968	−0.005391
R^{SGA}_{0000}	−0.001725	−0.003455	−0.003337	−0.002677	−0.001566	−0.0003144
R^{SGA}_{2000}	0.03253	0.02658	0.01389	0.009870	0.005141	0.0009552
R^{SGA}_{1000}	0.02733	0.02246	0.01183	0.008418	0.004393	0.0008172
R^{SGA}_{0010}	0.02733	0.02246	0.01183	0.008418	0.004393	0.0008172
R^{SGA}_{2010}	0.02733	0.02246	0.01183	0.008418	0.004393	0.0008172
R^{SGA}_{1010}	0.002977	0.004972	0.003879	0.002952	0.001636	0.0003164
R^{SGA}_{0101}	−0.004042	−0.01115	−0.02368	−0.02857	−0.03614	−0.05018
R^{SGA}_{1101}	0.02317	0.01096	−0.01227	−0.02049	−0.03195	−0.04941

Table 4.13: The values of B^1_{klmn}, S_{klmn} and $R^{\rm SGA}_{klmn}$ for $e_L^- e^+$ scattering

	400 GeV	500 GeV	800 GeV	1000 GeV	1500 GeV	4000 GeV
ω_{max}	13.55	38.84	107.2	150.2	255.2	776.1
B^1_{0000}	0.1433	0.1907	0.08886	0.07067	0.05405	0.04117
B^1_{2000}	0.02964	0.09457	0.08541	0.07486	0.05962	0.04272
B^1_{1000}	0.1078	0.2002	0.1419	0.1195	0.09217	0.06527
B^1_{0010}	0.05388	0.1001	0.07096	0.05975	0.04609	0.03264
B^1_{2010}	0.05388	0.1001	0.07096	0.05975	0.04609	0.03264
B^1_{1010}	0.1729	0.2853	0.1743	0.1455	0.1137	0.08389
B^1_{0101}	0.1325	0.1546	0.03437	0.01420	−0.001372	−0.005843
B^1_{1101}	0.04635	0.06415	0.01984	0.009433	0.0005521	−0.002624
S^{SGA}_{0000}	−0.001319	−0.0103680	−0.009239	−0.007183	−0.002033	−0.0003753
S^{SGA}_{2000}	0.003957	0.01615	0.01473	0.01151	0.008378	0.001691
S^{SGA}_{1000}	0.01137	0.02918	0.02083	0.01558	0.01141	0.002253
S^{SGA}_{0010}	0.005683	0.01459	0.01042	0.007792	0.005703	0.001126
S^{SGA}_{2010}	0.005683	0.01459	0.01042	0.007792	0.005703	0.001126
S^{SGA}_{1010}	0.002638	0.005783	0.005487	0.004327	0.006345	0.001315
S^{SGA}_{0101}	−0.003445	−0.02060	−0.02827	−0.02725	−0.02214	−0.011790
S^{SGA}_{1101}	0.004170	0.004308	−0.006649	−0.008751	−0.008870	−0.005381
R^{SGA}_{0000}	−0.001994	−0.005996	−0.005351	−0.004217	−0.001217	−0.0002282
R^{SGA}_{2000}	0.03369	0.02395	0.01183	0.008305	0.005490	0.001041
R^{SGA}_{1000}	0.02578	0.01984	0.009774	0.006855	0.004741	0.0009033
R^{SGA}_{0010}	0.02578	0.01984	0.009774	0.006855	0.004741	0.0009033
R^{SGA}_{2010}	0.02578	0.01984	0.009774	0.006855	0.004741	0.0009033
R^{SGA}_{1010}	0.003387	0.002406	0.001847	0.001401	0.001985	0.0004025
R^{SGA}_{0101}	−0.005543	−0.01367	−0.02564	−0.03005	−0.03579	−0.05010
R^{SGA}_{1101}	0.02162	0.008372	−0.01426	−0.02200	−0.03161	−0.04932

Table 4.14: The values of B^1_{klmn}, S_{klmn} and R^{SGA}_{klmn} for $e^-_R e^+$ scattering

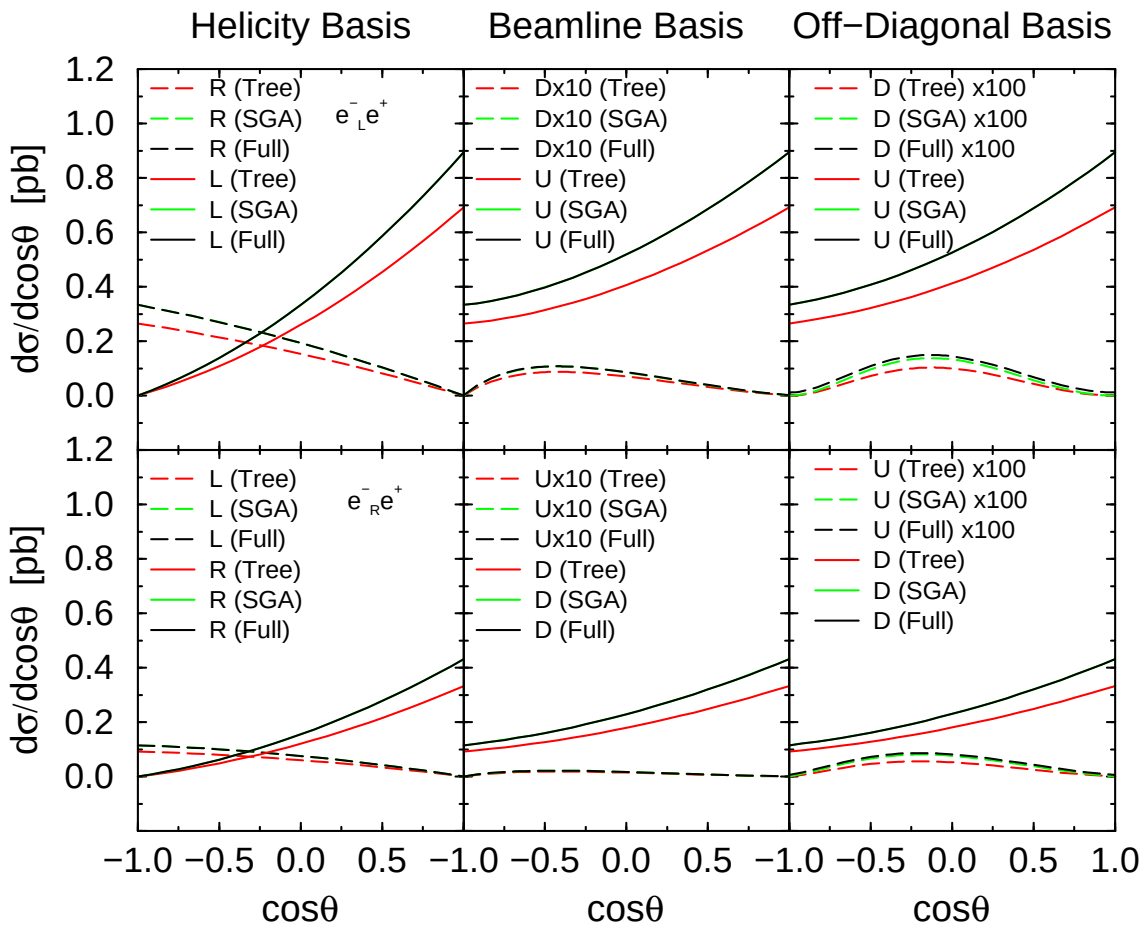

Figure 4.18: The cross-sections in the helicity, beamline and off-diagonal bases at $\sqrt{s} = 400$ GeV. Here we use a "beamline basis", in which the top quark axis is the positron direction in the top rest frame, for each $e_L^- e^+$ and $e_R^- e^+$ scattering. For the soft gluon approximation (SGA) $\omega_{\max} = 13.49$ GeV.

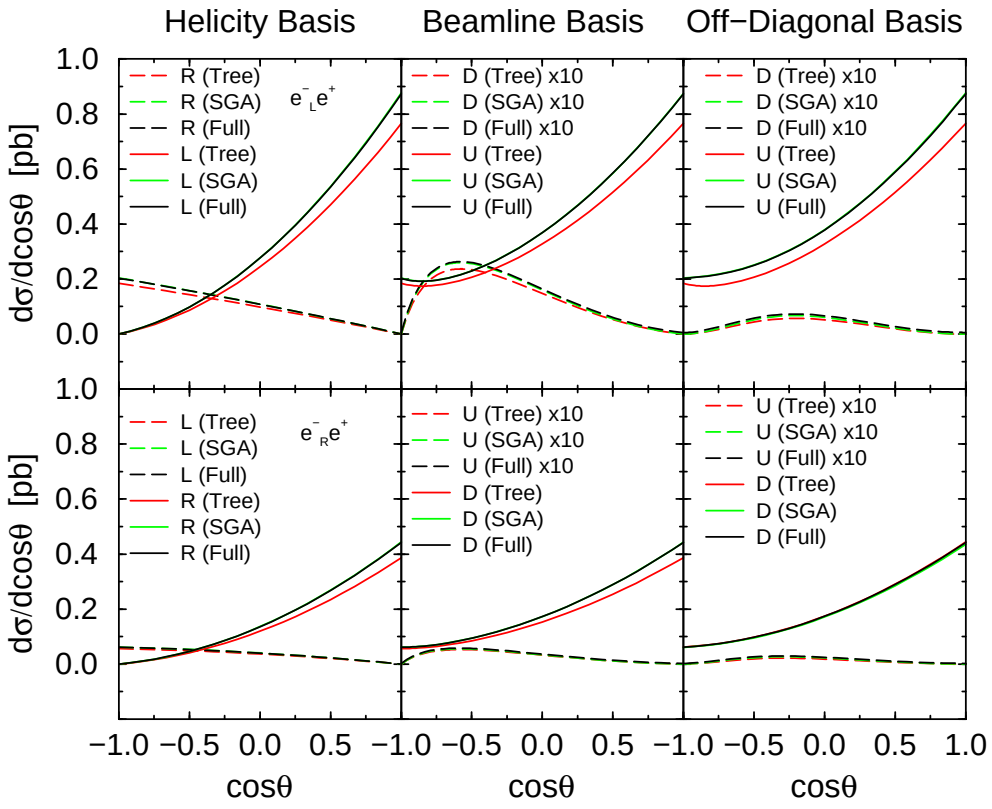

Figure 4.19: The cross-sections in the helicity, beamline and off-diagonal bases at $\sqrt{s} = 500\,\text{GeV}$. Here we use a "beamline basis", in which the top quark axis is the positron direction in the top rest frame, for each $e^-_L e^+$ and $e^-_R e^+$ scattering. For the soft gluon approximation (SGA) $\omega_{\max} = 38.60$ GeV.

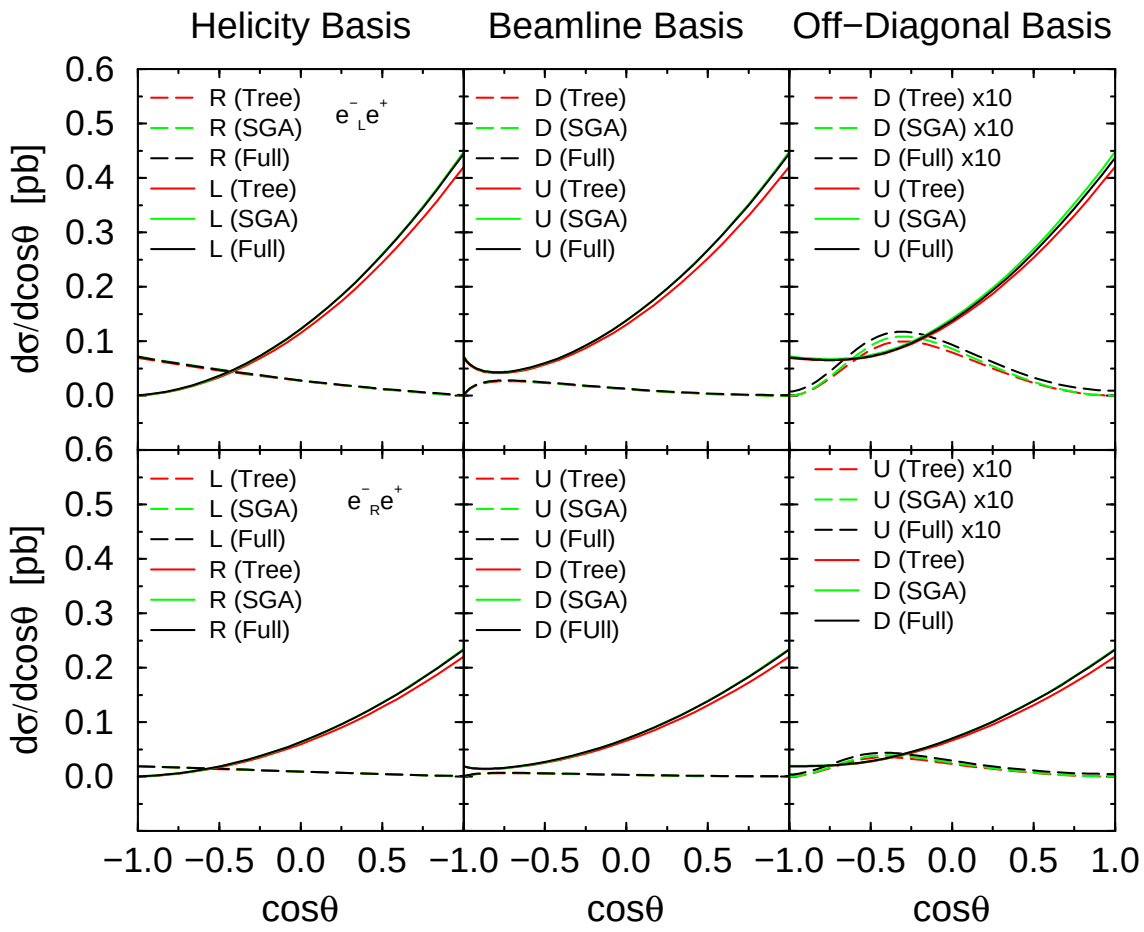

Figure 4.20: The cross-sections in the helicity, beamline and off-diagonal bases at $\sqrt{s} = 800$ GeV. Here we use a "beamline basis", in which the top quark axis is the positron direction in the top rest frame, for each $e^-_L e^+$ and $e^-_R e^+$ scattering. For the soft gluon approximation (SGA) $\omega_{\max} = 106.7$ GeV.

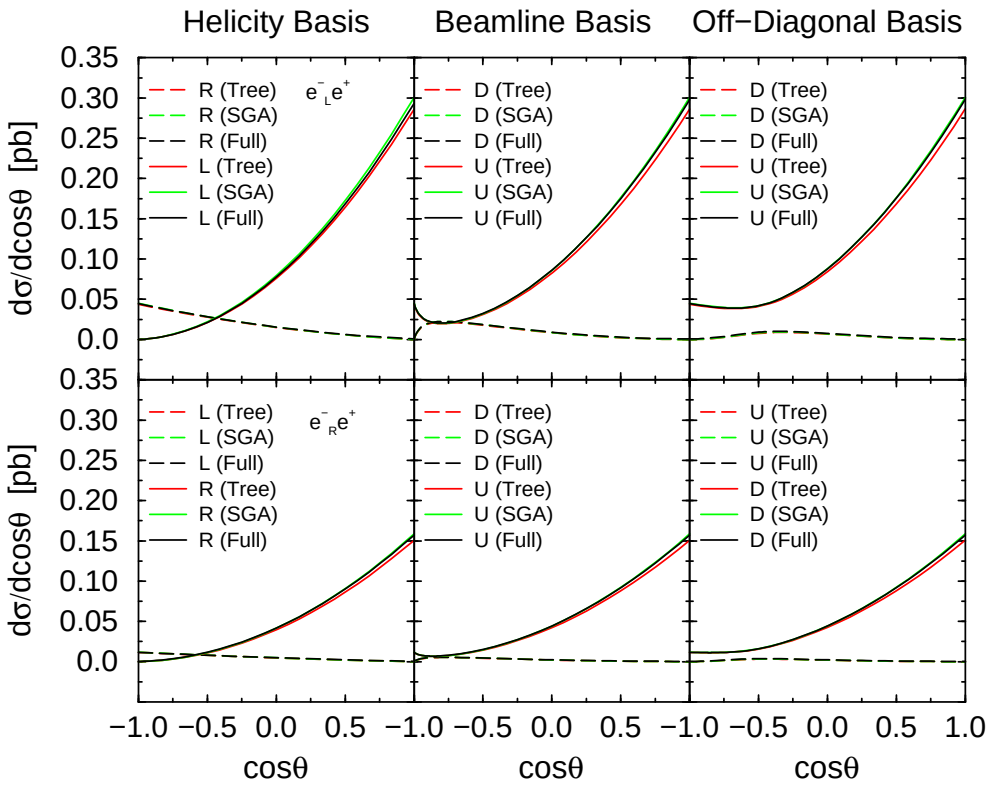

Figure 4.21: The cross-sections in the helicity, beamline and off-diagonal bases at $\sqrt{s} = 1000\,\text{GeV}$. Here we use a "beamline basis", in which the top quark axis is the positron direction in the top rest frame, for each $e^-_L e^+$ and $e^-_R e^+$ scattering. For the soft gluon approximation (SGA) $\omega_{\text{max}} = 149.7$ GeV.

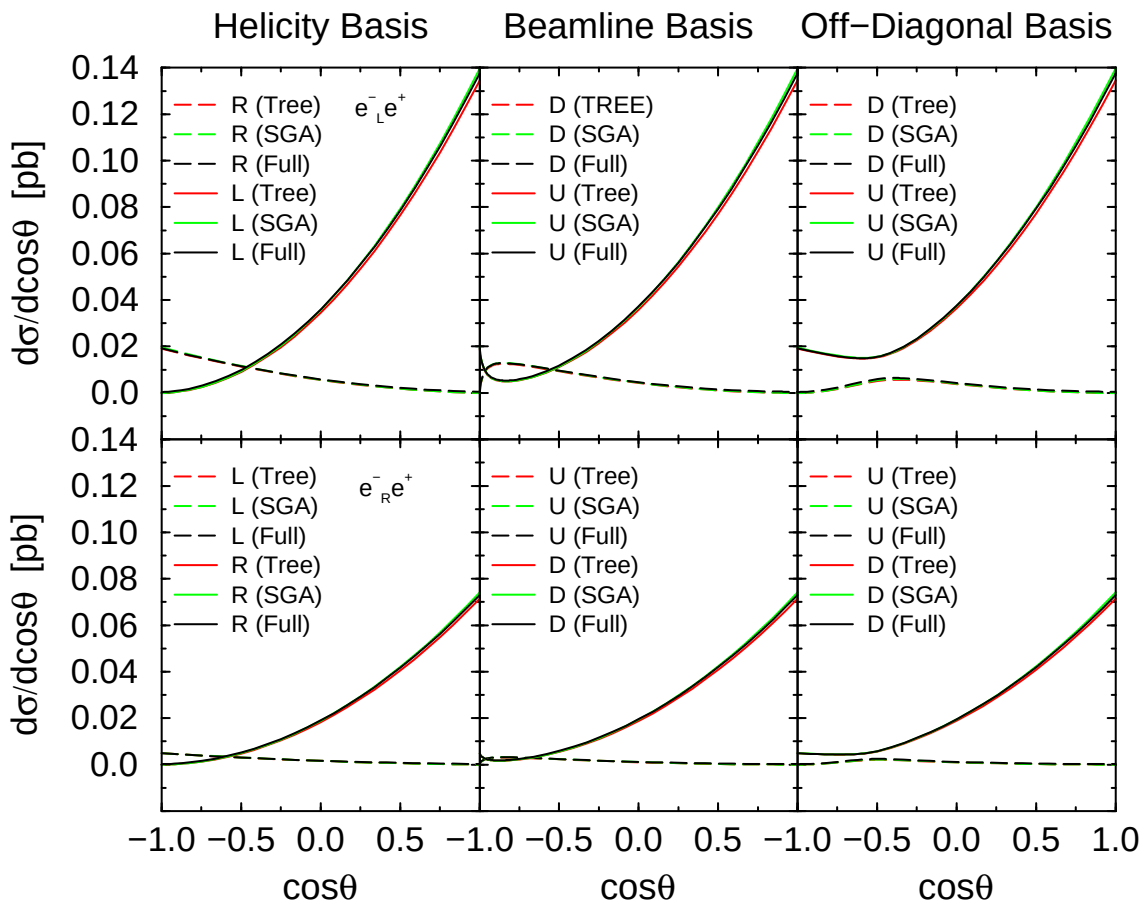

Figure 4.22: The cross-sections in the helicity, beamline and off-diagonal bases at $\sqrt{s} = 1500\,\text{GeV}$. Here we use a "beamline basis", in which the top quark axis is the positron direction in the top rest frame, for each $e^-_L e^+$ and $e^-_R e^+$ scattering. For the soft gluon approximation (SGA) $\omega_{\text{max}} = 254.8$ GeV.

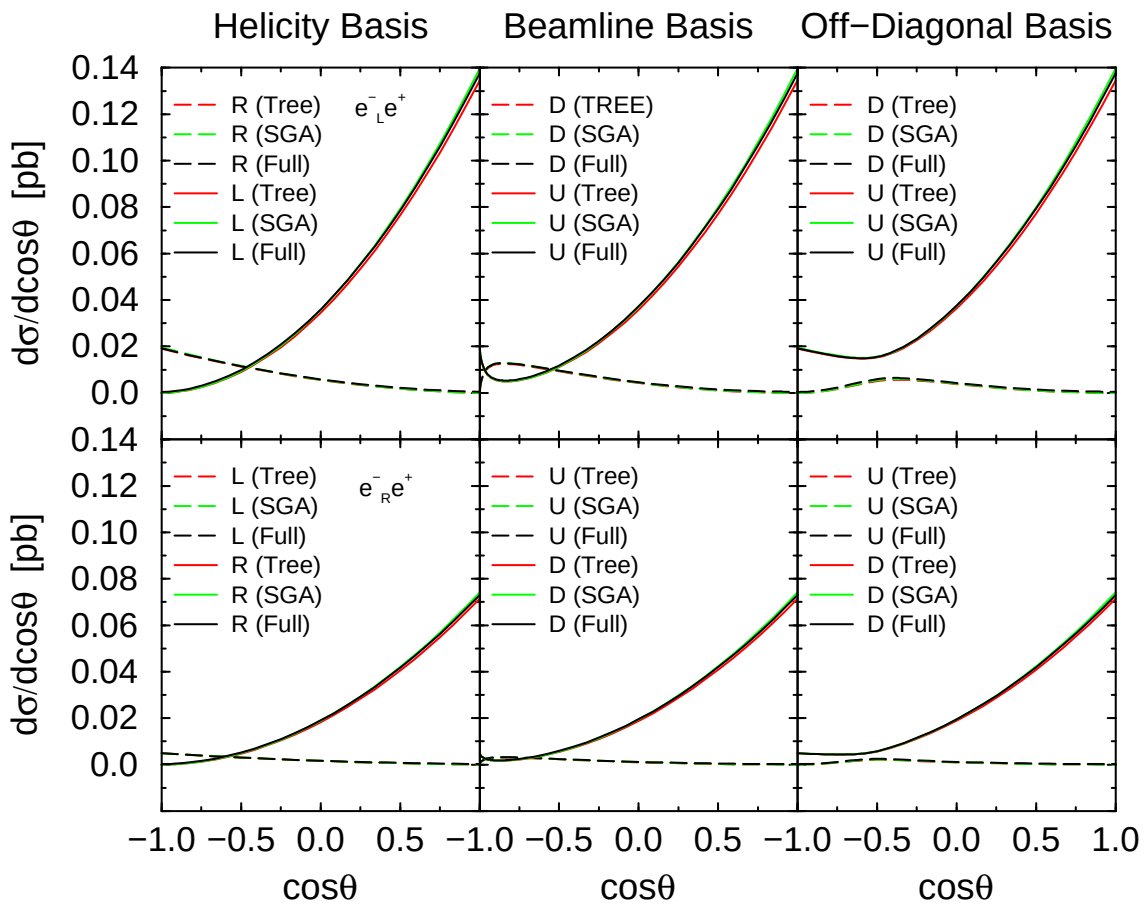

Figure 4.23: The cross-sections in the helicity, beamline and off-diagonal bases at $\sqrt{s} = 4000\,\text{GeV}$. Here we use a "beamline basis", in which the top quark axis is the positron direction in the top rest frame, for each $e^-_L e^+$ and $e^-_R e^+$ scattering. For the soft gluon approximation (SGA) $\omega_{\max} = 775.9$ GeV.

4.6 Fourth Generations Quarks

The existence of three generations of quarks and leptons is well established in the Standard Model. Although there is no strong expectation of additional quarks and leptons, there is no reason that additional generations are ruled out. Several models with new generations or arguments flavoring new generations have been proposed [43].

We have shown the efficiency and the usefulness of the study of spin correlations in the previous Sections and Chapters. Therefore, we consider the pair production of a fourth generation quark (b') with charge $-1/3$. and investigate the polarized cross-sections at polarized e^+e^- linear colliders. Here we assume that the b' mass is between 150 GeV and 300 GeV, and take the CM energy at 500 and 1000 GeV. In this analyses, we use three bases as shown in the previous Sections. One is the usual helicity basis which corresponds to $\cos\xi = +1$. The second is the beamline basis, in which the top quark spin is aligned with the positron momentum in the top quark rest frame. The third is the off-diagonal basis which makes like-spin configuration vanish in the $e^-_L e^+$ scattering process.

To present the differential cross-section, we investigate the b' quark speed, β, dependence of couplings f_{IJ}'s. These couplings are given by,

$$0.97 \leq f_{LL} \leq 1.02 \quad , \quad 0.208 \leq f_{LR} \leq 0.218 \ ,$$
$$0.433 \leq f_{RR} \leq 0.442 \quad , \quad -0.260 \leq f_{RL} \leq -0.215 \ .$$

The couplings f_{IJ}'s have weak β dependence. Without Z boson couplings, the couplings become $f_{LL} = f_{LR} = 1/3$. So the contribution from the Z boson is constructive to the f_{LL} and f_{RR}, and destructive to the f_{LR} and f_{RL}.

Next, we plot the β dependence of the ratios, f_{LR}/f_{LL} and f_{RL}/f_{RR}, in Fig.4.24. The ratio f_{LR}/f_{LL} has a weak β dependence, and it shows the similar behavior as the ratios of the top quark couplings, f_{LR}/f_{LL} and f_{RL}/f_{RR}. However, the ratio f_{RL}/f_{RR} for b' productions gives the large contribution ~ 0.5 compared to the top quark case. As discussed previously, the parameters f_{LL} and f_{RR} control the behavior of the dominant configurations in the beamline and off-diagonal bases, and the parameters f_{LR}/f_{LL} and f_{RL}/f_{RR} decide the behavior of the subdominant configuration. Therefore, in the $e^-_R e^+ \to b'X(\bar{b}'$ or $\bar{b}'g)$ process, the subdominant configuration gives larger contribution to the total cross-section than $e^-_L e^+ \to b'X(\bar{b}'$ or $\bar{b}'g)$ process.

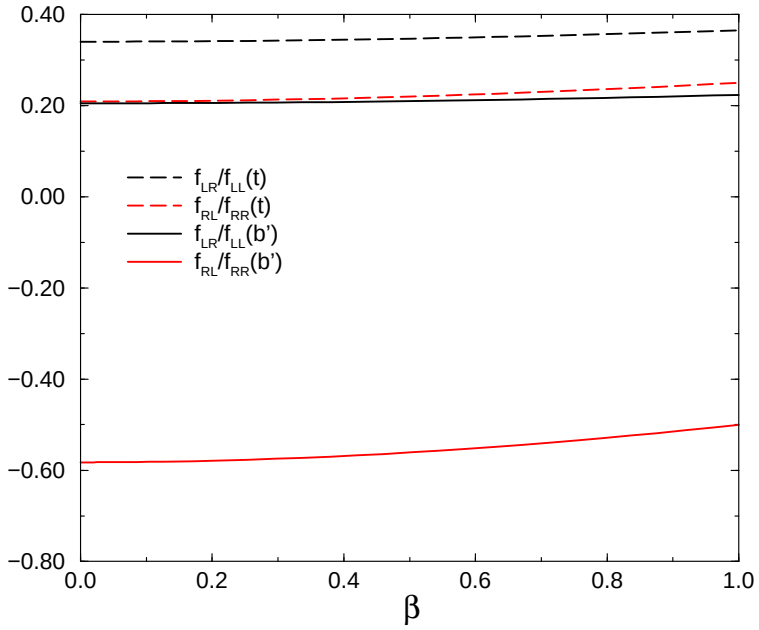

Figure 4.24: b' quark speed, β, dependence of ratios, f_{LR}/f_{LL} and f_{RL}/f_{RR}.

The differential cross-sections in three bases are shown in Fig.4.25 $\sim$ Fig.4.29, and these figures contain the results of the tree level and the full QCD. For the $e^-_L e^+ \to b'X(\bar{b}'$ or $\bar{b}'g)$ process, the dominant component is top quark spin-up configuration. In the beamline and off-diagonal bases, this configuration makes up more than 96% of total cross-section in Fig.4.25 $\sim$ Fig.4.29. While, in the helicity basis, the dominant configuration occupies 77% of the total cross-section with b' mass $m = 200$ GeV at $\sqrt{s} = 500$ GeV, and is less than 92% of the total cross-section in Fig.4.25 $\sim$ Fig.4.29. The off-diagonal and the beamline bases represent very strong spin correlations. Thus, b' quark is produced in an essentially unique spin configuration even after including the lowest order QCD corrections. This result is the same as the top quark case.

For the $e^-_R e^+ \to b'X(\bar{b}'$ or $\bar{b}'g)$ process, the dominant component is top quark spin-down configuration. In the helicity basis, the dominant configuration contributes to 80 $\sim$ 87% of the total cross-section. In the beamline and off-diagonal bases, this configuration contributes to the 83 $\sim$ 88% of total cross-section. This results show that the dominant configuration gives the same amount of contribution to the total cross-section in these three basis.

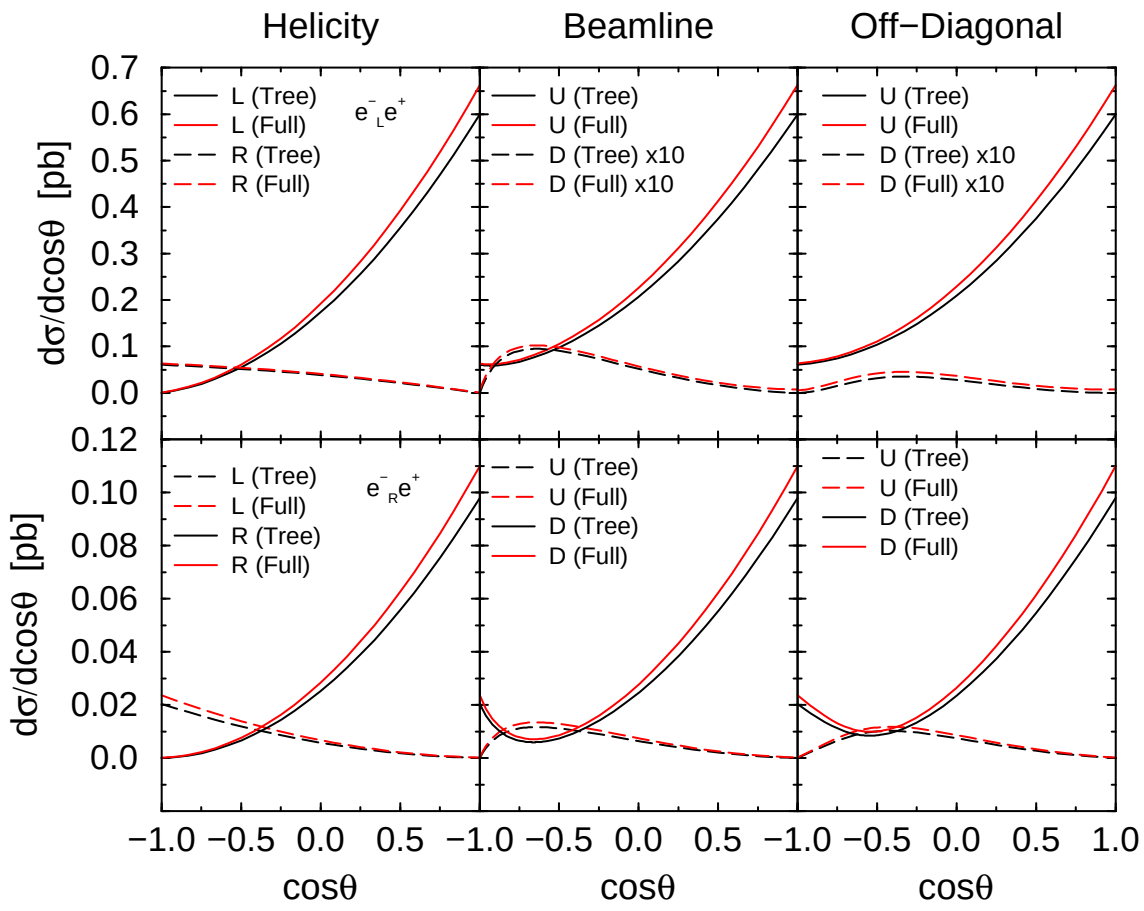

Figure 4.25: The cross-sections for the process $e^+e^- \to b'X(\bar{b}'$ or $\bar{b}'g)$ in the helicity, beamline and off-diagonal bases at $\sqrt{s} = 500\,\text{GeV}$. The value of b' mass is 150GeV.

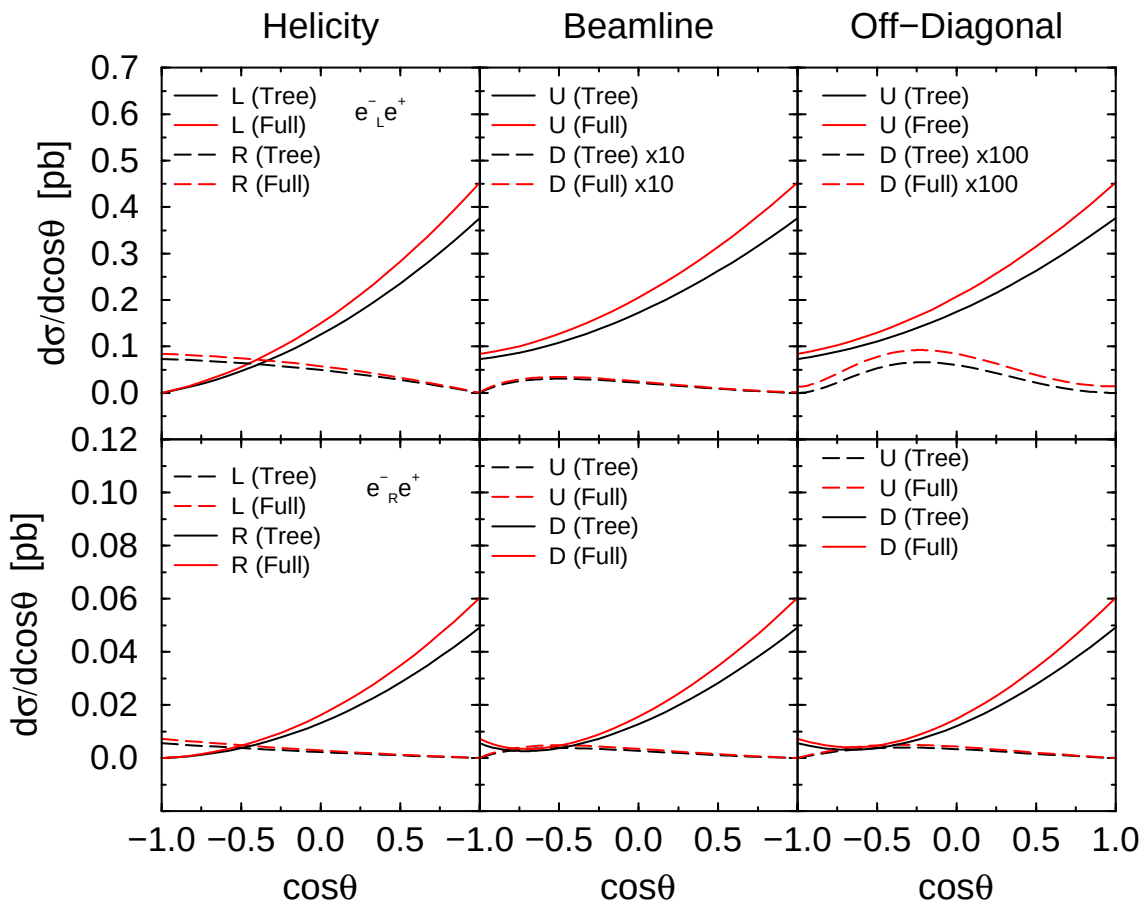

Figure 4.26: The cross-sections for the process $e^+e^- \to b'X(\bar{b}'$ or $\bar{b}'g)$ in the helicity, beamline and off-diagonal bases at $\sqrt{s} = 500\,\text{GeV}$. The value of b' mass is 200 GeV.

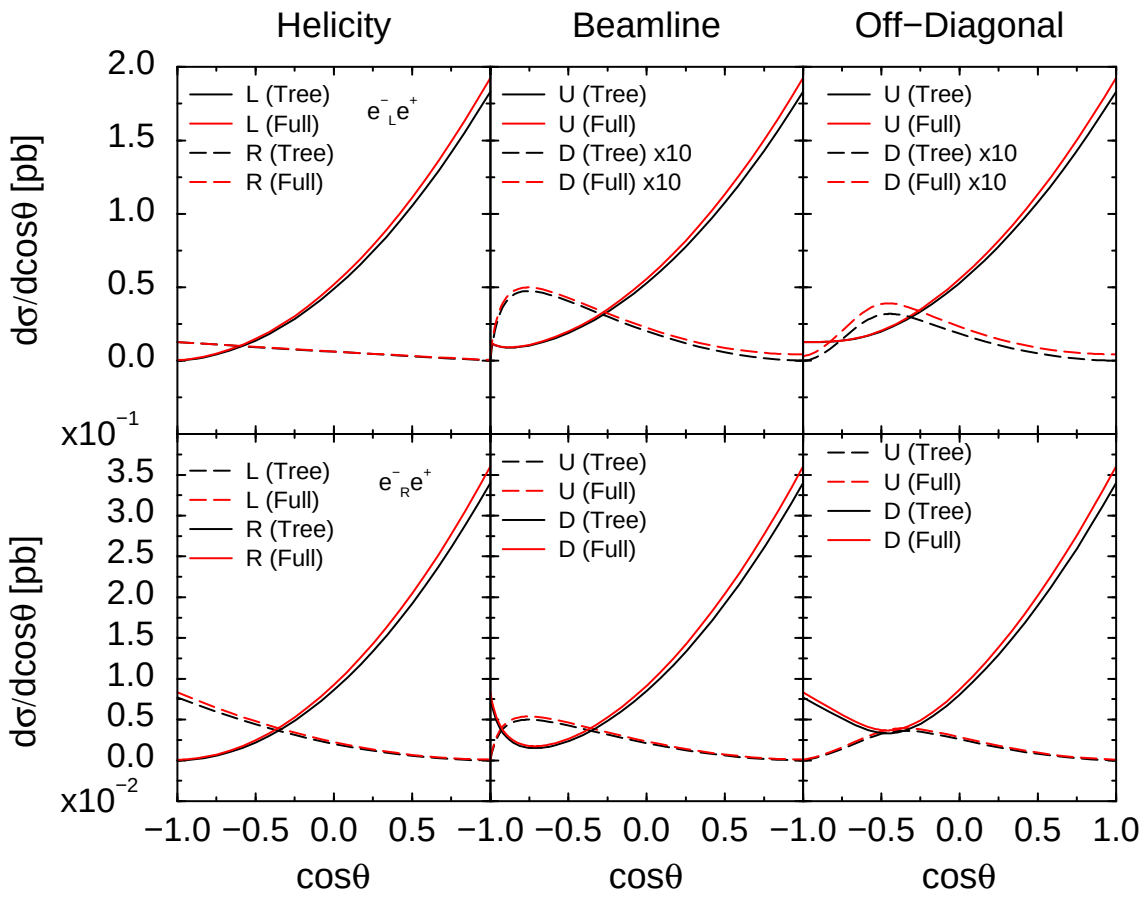

Figure 4.27: The cross-sections for the process $e^+e^- \to b'X(\bar{b}'$ or $\bar{b}'g)$ in the helicity, beamline and off-diagonal bases at $\sqrt{s} = 1000$GeV. The value of b' mass is 200 GeV.

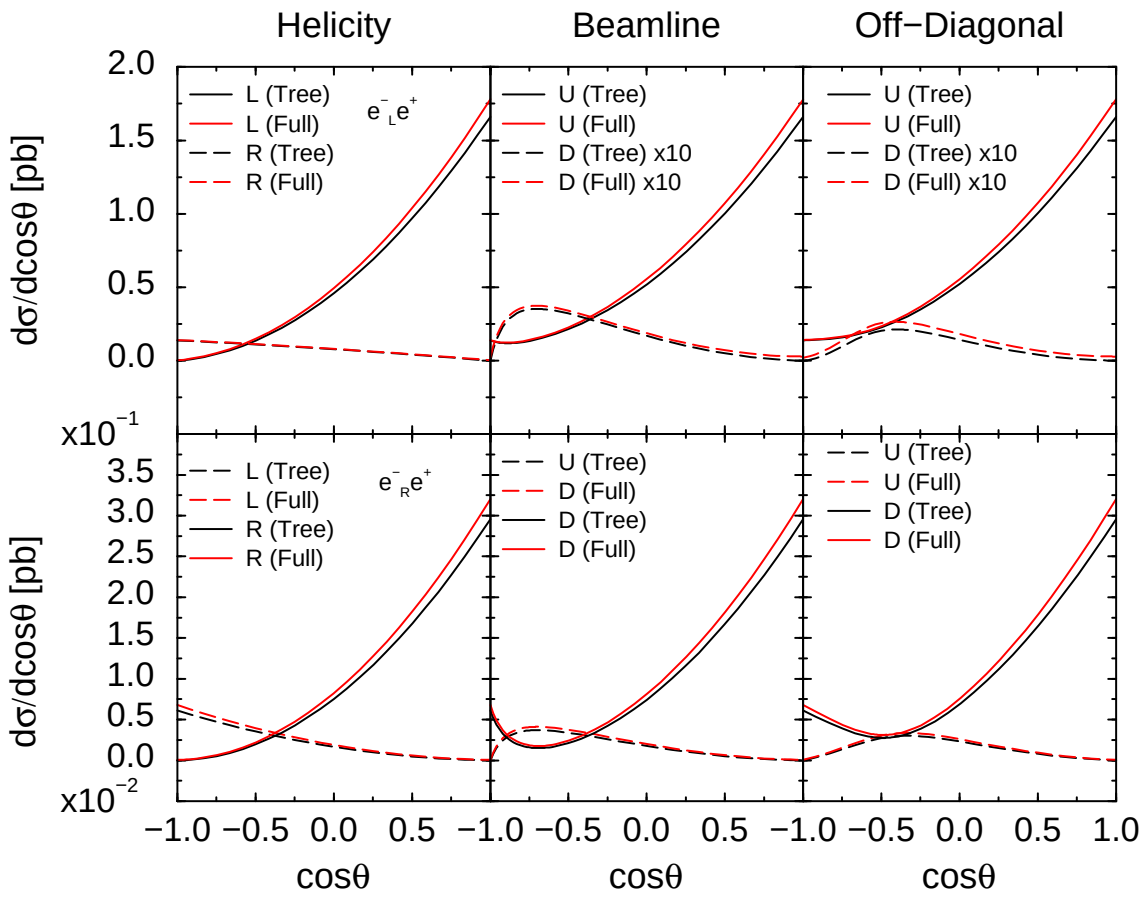

Figure 4.28: The cross-sections for the process $e^+e^- \to b'X(\bar{b}' \text{ or } \bar{b}'g)$ in the helicity, beamline and off-diagonal bases at $\sqrt{s} = 1000$GeV. The value of b' mass is 250 GeV.

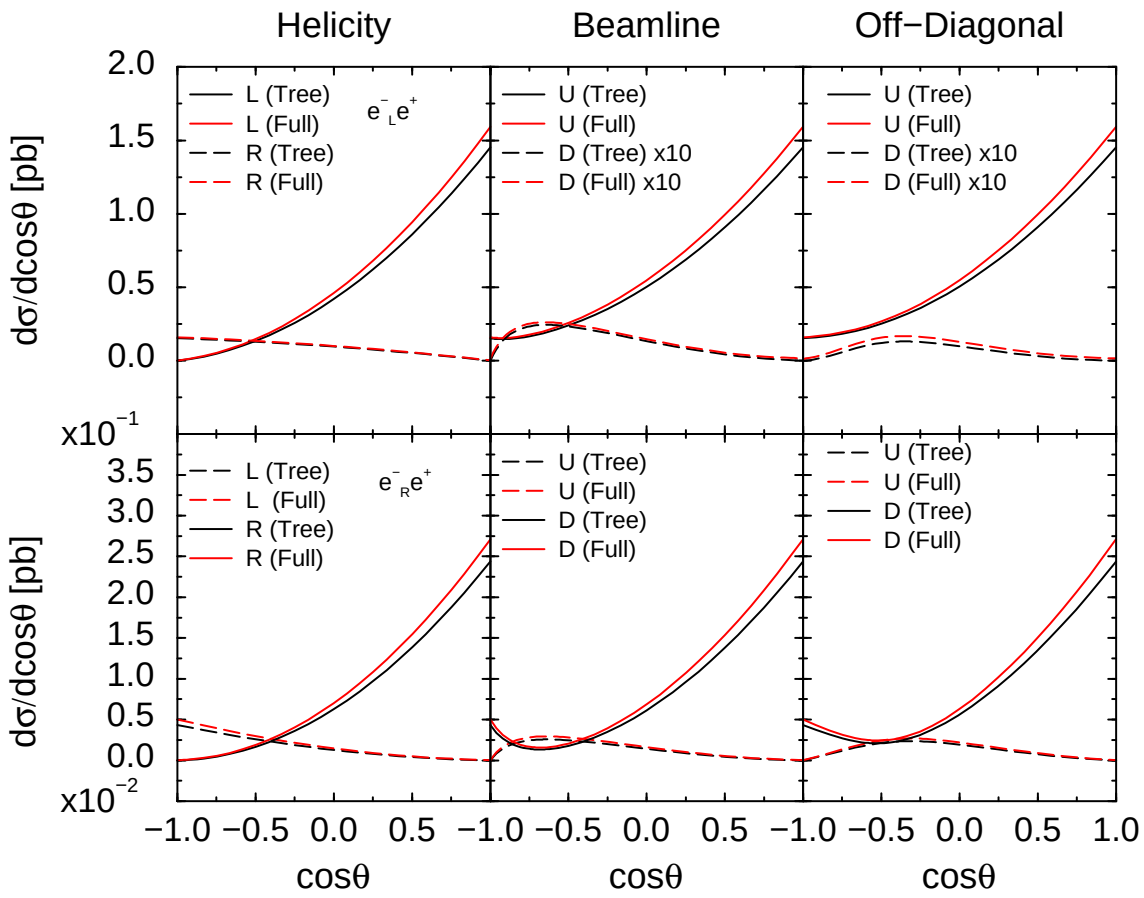

Figure 4.29: The cross-sections for the process $e^+e^- \to b'X(\bar{b}'$ or $\bar{b}'g)$ in the helicity, beamline and off-diagonal bases at $\sqrt{s} = 1000$GeV. The value of b' mass is 300 GeV.

Chapter 5

Summary and Outlook

We have studied in detail the spin-spin correlations for top quark productions and spin-angular correlations for its decay at polarized e^+e^- linear colliders as well as an brief introduction to the spinor helicity method which is a powerful calculational technique to obtain analytically compact expression for the complicated process.

For the top quark productions, we presented the polarized cross-sections using a "generic" spin basis. We introduced three characteristic bases; "helicity", "beamline" and "off-diagonal" bases, and discussed the differences among these bases. At threshold energy, the beamline basis is equivalent to the off-diagonal basis. In the high energy limit, the beamline and the helicity bases coincide. However, at moderate energies, there are remarkable differences among these bases. We first analyzed the polarized cross-sections in these bases at the center of mass energy far above the threshold at the leading order of perturbation theory. We have shown that the most optimal spin basis is the off-diagonal basis. In this basis, the like spin configurations, UU ($t_\uparrow,\ \bar{t}_\uparrow$) and DD ($t_\downarrow,\ \bar{t}_\downarrow$), vanish, and UD ($t_\uparrow,\ \bar{t}_\downarrow$) configuration dominates to total cross-section, for instance, occupies 99.88% at the 400 GeV e^+e^- collider. This result show that the top (anti-top) quark spin is strongly correlated with the positron (electron) spin and top quark pairs are produced in a unique spin configuration in the off-diagonal basis. We have also discussed why the top (anti-top) quark spin is associated with the positron (electron) spin and the relation between the beamline and off-diagonal bases. We have clarified that the smallness of parameters $f_{LR} \sim f_{RL} \sim 0$ is a key point to answer these questions.

For the top quark decay, we investigated the correlation between the direction of top quark spin and the direction of motion of the decay products. The consequence was that the anti-lepton and d-type quark are maximally correlated with the top quark spin. The longitudinal and the transverse W boson contribution to the top quark decay was also explained. The

interference effect between the longitudinal and the transverse W boson produces significant contributions to the angular distribution of the decay products. Thus the topology of the top quark decay provides us important information to obtain a constraint to the Standard Model. We also suggested that the spin correlations can be measured by analyzing the decay products of the top and ant-top quark.

We have extended the analyses of top quark productions at the leading order to the next to leading order of QCD, and studied the $\mathcal{O}(\alpha_s)$ QCD corrections to top quark productions in a generic spin basis. The QCD corrections introduce two effects not included in the tree level approximation. One is the modification of the coupling of the top and anti-top quarks to γ and Z bosons due to the virtual corrections. The other is the presence of the real gluon emission process. First, we consider the QCD corrections in the soft gluon approximation to see the effects of the modified $\gamma/Z - t - \bar{t}$ vertex. Using this approximation, we found that the tree level off-diagonal basis continues to make the like spin components vanish and that the effects of the induced anomalous magnetic moment are small. Next we analyzed the full QCD corrections at the one-loop level. When we consider the three particle final state, the top and anti-top quarks are not necessarily produced back to back. So we have calculated the inclusive top (anti-top) quark production. We have given an exact analytic form for the differential cross-section with an arbitrary orientation of the top quark spin. Our numerical studies show that the $\mathcal{O}(\alpha_s)$ QCD corrections enhance the tree level results and modify only slightly the spin orientation of the produced top quark. In the kinematical region where the emitted gluon has small energy, it is natural to expect that the real gluon emission effects introduce only a multiplicative correction to the tree level result. Therefore only "hard" gluon emission could possibly modify the top quark spin orientation. What we have found, by explicit calculation, is that this effect is numerically very small. The size of the QCD corrections to the total cross-section is summarized in Table 4.2 of Chapter 4. At $\sqrt{s} = 400\,\text{GeV}$, the enhancement from the tree level result is $\sim 30\%$ whereas at higher energies, $800 \sim 4000$ GeV, it is at the $2 \sim 6\%$ level. Near the threshold, the QCD corrections have a singular behavior in β, the speed of the produced quark. This factor enhances the value of the correction at smaller energies. The size of these corrections is reasonable for QCD. On the other hand, the change of the orientation of top quark spin is quite small. The deviation from the enhanced tree level result is less than a few percent. Actually, the fraction of the top quarks in the dominant (up) spin configuration for $e^-_L e^+$ scattering in the off-diagonal basis is more than 93% at all energies we have considered. We can, therefore, conclude that the results of the

tree level analysis are not altered even after including QCD radiative corrections except for a multiplicative enhancement. Since the the dominant enhancement can be described by the soft-gluon approximation, we have also analyzed the validity of the soft-gluon approximation and shown the efficiency of this approximation.

Finally two additional discussions regarding the spin correlations have been presented. One is the analysis of the polarized cross-sections under the approximation $f_{LR}/f_{LL} = f_{RL}/f_{RR} = 0$ at the QCD one-loop level. The other is the pair production of the "fourth" generation quark b' with the charge $-1/3$. We have estimated the polarized cross-sections for the b' quark productions with b' mass between 150 GeV and 300 GeV, at the center of mass energy 500 and 1000 GeV. For the $e_L^- e^+$ scattering process, the differential cross-sections in three bases show the same behavior as the top quark productions except for magnitude of total cross-section. The dominant configuration is the spin-up b' quark, which is strongly correlated with the positron spin. However, for the $e_R^- e^+$ scattering process, the dominant configuration in three bases almost give the same contribution to the total cross-section. This fact is caused by the ratio of the coupling, $|f_{RL}/f_{RR}| \sim 0.5$. This situation is the characteristic feature of b' quark productions.

As has been discussed in this thesis and many articles, there are strong correlations between the orientation of the spin of produced top (anti-top) quark and the angular distribution of its decay products. And the radiative corrections to these correlation seem to be very small as we have explicitly shown for the production process. Therefore, measuring the top quark spin orientation will give us important information on the top quark sector of the Standard Model as well as possible physics beyond the Standard Model.

Appendix A

Notation and Conventions

A.1 Natural Unit and Convention

- Natural Unit:

$$\hbar \;=\; c \;=\; 1, \;\; (\hbar \;=\; \frac{h}{2\pi}) \; .$$

- Transform rules of Unit:

$$\begin{aligned}
1 \text{ kg} &= 5.61 \times 10^{26} \text{ GeV} : \left(\frac{\text{GeV}}{\text{c}^2}\right), \\
1 \; m &= 5.07 \times 10^{15} \text{ GeV}^{-1} : \left(\frac{\hbar c}{\text{GeV}}\right), \\
1 \text{ sec} &= 1.52 \times 10^{24} \text{ GeV}^{-1} : \left(\frac{\hbar}{\text{GeV}}\right), \\
1 \text{ TeV} &= 10^3 \text{ GeV} \;=\; 10^6 \text{ MeV} \;=\; 10^9 \text{ KeV} \;=\; 10^{12} \text{ eV}, \\
1 \text{ fermi} &= 1 \text{ fm} \;=\; 10^{-13} \text{ cm} \;=\; 10^{-15} \text{ m} \;=\; 5.07 \text{ GeV}^{-1}, \\
(1 \text{ fermi})^2 &= 10 \text{ mb} \;=\; 10^4 \; \mu\text{b} \;=\; 10^7 \text{ nb} \;=\; 10^{10} \text{ pb} \;=\; 10^{13} \text{ fb}, \\
1 \; b &= 10^2 \text{ fm}^2 \;=\; 10^{-24} \text{ cm}^2 \;=\; 10^{-28} \text{ m}^2, \\
(1 \text{ GeV})^{-2} &= 0.389 \text{ mb} \;=\; 3.89 \;\times\; 10^8 \text{ pb} \; .
\end{aligned}$$

A.2 Metric Tensor

Our Metric Tensor $g_{\mu\nu}$ in Minkowski Space $\{x^\mu \; : (\; \mu \;=\; 0, 1, 2, 3 \;)\}$,

$$g_{\mu\nu} \;=\; g^{\mu\nu} \;=\; \begin{pmatrix} +1 & 0 & 0 & 0 \\ 0 & -1 & 0 & 0 \\ 0 & 0 & -1 & 0 \\ 0 & 0 & 0 & -1 \end{pmatrix} \; .$$

A.3 Coordinates and Momenta

The space-time coordinates $(t, x, y, z) \equiv (t, \boldsymbol{x})$ are denoted by the covariant four-vector:

$$\begin{aligned} x^\mu &\equiv (x^0, x^1, x^2, x^3) \\ &\equiv (t, x, y, z) \ . \end{aligned}$$

The covariant four-vector x^μ is obtained by the sign of the space components:

$$\begin{aligned} x_\mu &\equiv (x_0, x_1, x_2, x_3) \\ &\equiv (t, -x, -y, -z) \\ &= g_{\mu\nu} x^\nu \ . \end{aligned}$$

The inner product is given by

$$\begin{aligned} x \cdot x &\equiv x^\mu x_\mu \\ &= t^2 - \boldsymbol{x}^2 \ . \end{aligned}$$

Momentum vectors are similarly defined by

$$\begin{aligned} p^\mu &\equiv (p^0, p^1, p^2, p^3) \\ &\equiv (E, p_x, p_y, p_z) \\ &= g^{\mu\nu} p_\nu \ . \end{aligned}$$

The inner product is given by

$$\begin{aligned} p_1 \cdot p_2 &\equiv p_1^\mu p_{2\mu} \\ &= E_1 E_2 - \boldsymbol{p}_1 \cdot \boldsymbol{p}_2 \ . \end{aligned}$$

A.4 Pauli Matrices

- Pauli σ Matrices:

$$\sigma_1 = \begin{pmatrix} 0 & 1 \\ 1 & 0 \end{pmatrix} \ , \ \sigma_2 = \begin{pmatrix} 0 & -i \\ i & 0 \end{pmatrix} \ , \ \sigma_3 = \begin{pmatrix} 1 & 0 \\ 0 & -1 \end{pmatrix} \ .$$

- The Relations of Pauli Matrices:

$$\begin{aligned} \{\sigma_i, \sigma_j\} &= 2\delta_{ij}, \\ [\sigma_i, \sigma_j] &= 2i\varepsilon_{ijk}\sigma_k \ . \end{aligned}$$

- The Properties of Pauli Matrices:

$$\sigma_i^\dagger \;=\; \sigma_i,\; \det(\sigma_i) \;=\; -1,\; \mathrm{Tr}[\sigma_i] \;=\; 0\;.$$

- Useful Relation:

$$(\;\boldsymbol{\sigma}\;\cdot\;\boldsymbol{a}\;)(\;\boldsymbol{\sigma}\;\cdot\;\boldsymbol{b}\;) \;=\; (\;\boldsymbol{a}\;\cdot\;\boldsymbol{b}\;) + i\;\boldsymbol{\sigma}\;\cdot(\;\boldsymbol{a}\;\times\;\boldsymbol{b}\;)\;.$$

A.5 γ Matrices

- Dirac γ Matrices, $\gamma^\mu \;=\; (\gamma^0,\;\boldsymbol{\gamma}\;)$:

$$\begin{aligned}
\{\gamma^\mu,\gamma^\nu\} \;&=\; \gamma^\mu\gamma^\nu \;+\; \gamma^\nu\gamma^\mu \;=\; 2\;g^{\mu\nu},\\
[\gamma^\mu,\gamma^\nu] \;&=\; \gamma^\mu\gamma^\nu \;-\; \gamma^\nu\gamma^\mu \;=\; -2i\;\sigma^{\mu\nu},\\
\gamma_\mu \;&=\; g_{\mu\nu}\gamma^\nu \;=\; (\gamma^0,-\boldsymbol{\gamma}\;)\;.
\end{aligned}$$

- γ_5 Matrix:

$$\begin{aligned}
\gamma_5 \equiv\; \gamma^5 \;&=\; i\gamma^0\gamma^1\gamma^2\gamma^3 \;=\; -\frac{i}{4!}\varepsilon_{\mu\nu\lambda\sigma}\gamma^\mu\gamma^\nu\gamma^\lambda\gamma^\sigma\;,\\
\varepsilon^{0123} \;&=\; -\varepsilon_{0123} \;=\; +1\;.
\end{aligned}$$

- The Relation of γ_5 Matrix:

$$\begin{aligned}
\gamma_5^2 \;&=\; 1,\\
\{\gamma_5,\gamma^\mu\} \;&=\; 0\;.
\end{aligned}$$

- Familiar Presentation of γ:

$$\gamma^0 \;=\; \begin{pmatrix} 1 & 0\\ 0 & -1\end{pmatrix}\;,\;\boldsymbol{\gamma} \;=\; \begin{pmatrix} 0 & \boldsymbol{\sigma}\\ -\boldsymbol{\sigma} & 0\end{pmatrix}\;,\;\gamma_5 \;=\; \begin{pmatrix} 0 & 1\\ 1 & 0\end{pmatrix}\;,$$

  where $\boldsymbol{\sigma}$ is given by

$$\boldsymbol{\sigma} \;=\; (\sigma_1,\sigma_2,\sigma_3).$$

A.6 Dirac Spinors

Dirac spinors for fermion with momentum p, $u_\lambda(p)$ and for anti-fermion with momentum p $v_\lambda(p)$ satisfy following equations. (p: momentum , λ: spin components , m: fermion mass.)

- Equations of Motion:

$$\begin{aligned}(\not{p} - m)u_\lambda(p) &= 0,\\ (\not{p} + m)v_\lambda(p) &= 0\ .\end{aligned}$$

- Normalization:

$$\begin{aligned}\bar{u}_\lambda(p)u_{\lambda'}(p) &= 2m\ \delta_{\lambda\lambda'},\\ \bar{v}_\lambda(p)v_{\lambda'}(p) &= -2m\ \delta_{\lambda\lambda'}\ .\end{aligned}$$

- Projection Operators (In the case of Spin Sum):

$$\begin{aligned}\sum_\lambda u_\lambda(p)\bar{u}_\lambda(p) &= \not{p} + m,\\ \sum_\lambda v_\lambda(p)\bar{v}_\lambda(p) &= \not{p} - m\ .\end{aligned}$$

A.7 Spin Vector

spin vector s^μ for fermions is taken to be,

$$s^\mu \equiv \left(\frac{\vec{p}\cdot\vec{s}}{m},\ \vec{s} + \frac{\vec{p}(\vec{p}\cdot\vec{s})}{m(p^0+m)}\right)\ .$$

where

$$(\vec{s})^2 = 1,\ \ s^2 = s^\mu s_\mu = -1,\ s^\mu\, p_\mu = s\cdot p = 0\ .$$

- The Relations between Spin Vector and Spinor:

$$\bar{u}(p,s)\gamma^\mu\gamma_5 u(p,s) = 2m\ s^\mu\ .$$

- Projection Operators:

$$\begin{aligned}u(p,s)\bar{u}(p,s) &= (\not{p} + m)\frac{1+\gamma_5\not{s}}{2},\\ v(p,s)\bar{v}(p,s) &= (\not{p} - m)\frac{1+\gamma_5\not{s}}{2}\ .\end{aligned}$$

Appendix B

Useful Formulae

B.1 Dirac γ Matrices

- $\gamma^\dagger$ and $\overline{\gamma}$:

$$\begin{aligned}
\gamma^{\mu\dagger} &= \gamma^0\gamma^\mu\gamma^0 \ , \\
\gamma^{0\dagger} &= \gamma^0 \ , \ \gamma^{k\dagger} = -\gamma^k \ \ (\text{where } k = 1,\ 2,\ 3) \ , \\
\gamma^{5\dagger} &= \gamma^5 \ , \ \sigma^\dagger_{\mu\nu} = \sigma_{\mu\nu} \ , \\
\overline{\Gamma} &\equiv \gamma^0\Gamma^\dagger\gamma^0 \ , \\
\overline{\gamma^\mu} &= \gamma^0\gamma^{\mu\dagger}\gamma^0 = \gamma^\mu \ , \ \overline{\gamma^\mu\gamma^5} = \gamma^\mu\gamma^5 \ , \\
\overline{\sigma}^{\mu\nu} &= \gamma^0\sigma^{\mu\nu\dagger}\gamma^0 = \sigma^{\mu\nu} \ , \\
\overline{i\gamma_5} &= \gamma^0\left(i\gamma_5\right)\gamma^0 = i\gamma_5 \ , \\
\overline{\not{a}\ \not{b}\ \not{c}\ \not{d}\cdots\not{p}} &= \not{p}\cdots\not{c}\ \not{b}\ \not{a} \ .
\end{aligned}$$

- Matrix Element:

$$\left[\bar{u}(p',s')\ \Gamma\ u(p,s)\right]^\dagger = \bar{u}(p,s)\ \overline{\Gamma}\ u(p',s') \ ,$$

- Trace Theorems:

$$\begin{aligned}
\mathrm{Tr}\left[\gamma^{\mu_1}\gamma^{\mu_2}\cdots\gamma^{\mu_n}\right] &= 0 \ \ (\text{ for } n = \text{odd }) \ , \\
\mathrm{Tr}\ 1 &= 4 \ , \\
\mathrm{Tr}\left[\gamma^\mu\gamma^\nu\right] &= 4g^{\mu\nu} \ , \\
\mathrm{Tr}\left[\gamma^\mu\gamma^\nu\gamma^\lambda\gamma^\sigma\right] &= 4\left(g^{\mu\nu}g^{\lambda\sigma} - g^{\mu\lambda}g^{\nu\sigma} + g^{\mu\sigma}g^{\nu\lambda}\right) \ , \\
\mathrm{Tr}\left[\gamma^\lambda\gamma^\mu\gamma^\nu\gamma^\rho\gamma^\sigma\gamma^\tau\right] &= g^{\lambda\mu}\mathrm{Tr}\left[\gamma^\nu\gamma^\rho\gamma^\sigma\gamma^\tau\right] - g^{\lambda\nu}\mathrm{Tr}\left[\gamma^\mu\gamma^\rho\gamma^\sigma\gamma^\tau\right] + g^{\lambda\rho}\mathrm{Tr}\left[\gamma^\mu\gamma^\nu\gamma^\sigma\gamma^\tau\right]
\end{aligned}$$

$$
\begin{aligned}
& -g^{\lambda\sigma}\mathrm{Tr}\left[\gamma^{\mu}\gamma^{\nu}\gamma^{\rho}\gamma^{\tau}\right] + g^{\lambda\tau}\mathrm{Tr}\left[\gamma^{\mu}\gamma^{\nu}\gamma^{\rho}\gamma^{\sigma}\right] \ , \\
\mathrm{Tr}\left[\gamma^{\mu_1}\gamma^{\mu_2}\cdots\gamma^{\mu_n}\right] &= g^{\mu_1\mu_2}\mathrm{Tr}\left[\gamma^{\mu_3}\gamma^{\mu_4}\cdots\gamma^{\mu_n}\right] \ - \ g^{\mu_1\mu_3}\mathrm{Tr}\left[\gamma^{\mu_2}\gamma^{\mu_4}\cdots\gamma^{\mu_n}\right] \\
& + \cdots \ + \ g^{\mu_1\mu_n}\mathrm{Tr}\left[\gamma^{\mu_1}\gamma^{\mu_2}\cdots\gamma^{\mu_{n-1}}\right] \ \ (\text{ for } n = \text{even }) \ , \\
\mathrm{Tr}\left[\gamma_5\gamma^{\mu_1}\gamma^{\mu_2}\cdots\gamma^{\mu_n}\right] &= 0 \ \ (\text{ for } n \leq 3 \ ) \\
\mathrm{Tr}\left[\gamma_5\gamma^{\mu}\gamma^{\nu}\gamma^{\lambda}\gamma^{\sigma}\right] &= -4i\varepsilon^{\mu\nu\lambda\sigma} \ , \\
\mathrm{Tr}\left[\gamma_5\gamma^{\lambda}\gamma^{\mu}\gamma^{\nu}\gamma^{\rho}\gamma^{\sigma}\gamma^{\tau}\right] &= \ -4i(\varepsilon^{\lambda\mu\nu\rho}g^{\sigma\tau} \ - \ \varepsilon^{\lambda\mu\nu\sigma}g^{\rho\tau} \ + \ \varepsilon^{\lambda\mu\nu\tau}g^{\rho\sigma} \\
& \qquad - \ \varepsilon^{\nu\tau\sigma\rho}g^{\lambda\mu} \ + \ \varepsilon^{\mu\tau\sigma\rho}g^{\lambda\nu} \ - \ \varepsilon^{\lambda\tau\sigma\rho}g^{\mu\nu}) \ .
\end{aligned}
$$

- γ Identities:

$$
\begin{aligned}
\gamma_{\mu}\gamma^{\mu} &= 4 \ , \\
\gamma_{\mu}\gamma^{\nu}\gamma^{\mu} &= -2\gamma^{\nu} \ , \\
\gamma_{\mu}\gamma^{\lambda}\gamma^{\nu}\gamma^{\mu} &= 4g_{\lambda\nu} \ , \\
\gamma_{\mu}\gamma^{\lambda}\gamma^{\nu}\gamma^{\sigma}\gamma^{\mu} &= -2\gamma^{\sigma}\gamma^{\nu}\gamma^{\lambda} \ , \\
\gamma_{\mu}\gamma^{\lambda}\gamma^{\nu}\gamma^{\sigma}\gamma^{\rho}\gamma^{\mu} &= 2(\gamma^{\rho}\gamma^{\lambda}\gamma^{\nu}\gamma^{\sigma} + \gamma^{\sigma}\gamma^{\nu}\gamma^{\lambda}\gamma^{\rho}) \ ,
\end{aligned}
$$

- Version:

$$
\begin{aligned}
\gamma_{\mu} \not{a}\gamma^{\mu} &= -2 \not{a} \ , \\
\gamma_{\mu} \not{a} \not{b}\gamma^{\mu} &= 4a \cdot b \ , \\
\gamma_{\mu} \not{a} \not{b} \not{c}\gamma^{\mu} &= -2 \not{c} \not{b} \not{a} \ , \\
\gamma_{\mu} \not{a} \not{b} \not{c} \not{d}\gamma^{\mu} &= 2 \left(\not{d} \not{a} \not{b} \not{c} + \not{c} \not{b} \not{a} \not{d} \right)
\end{aligned}
$$

- Other Relations:

$$
\begin{aligned}
g^{\mu\nu}\varepsilon^{\lambda\sigma\tau\rho} - g^{\mu\lambda}\varepsilon^{\nu\sigma\tau\rho} + g^{\mu\sigma}\varepsilon^{\nu\lambda\tau\rho} - g^{\mu\tau}\varepsilon^{\nu\lambda\sigma\rho} + g^{\mu\rho}\varepsilon^{\nu\lambda\sigma\tau} &= 0 \ , \\
(g^{\mu\nu}\varepsilon^{\lambda\sigma\tau\rho} &= g^{\mu\lambda}\varepsilon^{\nu\sigma\tau\rho} + g^{\mu\sigma}\varepsilon^{\lambda\nu\tau\rho} + g^{\mu\tau}\varepsilon^{\lambda\sigma\nu\rho} + g^{\mu\rho}\varepsilon^{\lambda\sigma\tau\nu}) \ .
\end{aligned}
$$

B.2 Conventions for Dimensional Regularization

- γ Identities (D-dimension):

$$
\begin{aligned}
\gamma_{\mu}\gamma^{\mu} &= D \ , \\
\gamma_{\mu}\gamma^{\nu}\gamma^{\mu} &= (2 - D)\gamma^{\nu} \ ,
\end{aligned}
$$

$$
\begin{aligned}
\gamma_\mu\gamma^\lambda\gamma^\nu\gamma^\mu &= 4g_{\lambda\nu} + (D-4)\gamma^\lambda\gamma^\nu \ , \\
\gamma_\mu\gamma^\lambda\gamma^\nu\gamma^\sigma\gamma^\mu &= -2\gamma^\sigma\gamma^\nu\gamma^\lambda - (D-4)\gamma^\lambda\gamma^\nu\gamma^\sigma \ , \\
\gamma_\mu\gamma^\lambda\gamma^\nu\gamma^\sigma\gamma^\rho\gamma^\mu &= 2(\gamma^\rho\gamma^\lambda\gamma^\nu\gamma^\sigma + \gamma^\sigma\gamma^\nu\gamma^\lambda\gamma^\rho) + (D-4)\gamma^\lambda\gamma^\nu\gamma^\sigma\gamma^\rho \ ,
\end{aligned}
$$

- Version:

$$
\begin{aligned}
\gamma_\mu \not{a}\gamma^\mu &= (2-D)\ \not{a} \ , \\
\gamma_\mu \not{a}\not{b}\gamma^\mu &= 4a\cdot b \ + \ (D-4)\ \not{a}\not{b} \ , \\
\gamma_\mu \not{a}\not{b}\not{c}\gamma^\mu &= -2\ \not{c}\not{b}\not{a} - (D-4)\ \not{a}\not{b}\not{c} \ , \\
\gamma_\mu \not{a}\not{b}\not{c}\not{d}\gamma^\mu &= 2\,(\not{d}\not{a}\not{b}\not{c} + \not{c}\not{b}\not{a}\not{d}) + (D-4)\ \not{a}\not{b}\not{c}\not{d} \ .
\end{aligned}
$$

- Expansion in ε:

$$
\begin{aligned}
a^\varepsilon &= e^{\varepsilon \ln a} \ = \ 1 + \varepsilon \ln a + \frac{\varepsilon^2}{2!}(\ln a)^2 + \frac{\varepsilon^3}{3!}(\ln a)^3 + \mathcal{O}(\varepsilon^4) \ , \\
\Gamma(\varepsilon) &= \frac{1}{\varepsilon} - \gamma_E + \frac{\varepsilon}{2}(\gamma_E^2 + \frac{\pi^2}{6}) + \mathcal{O}(\varepsilon^2) \ , \\
\Gamma(\varepsilon-1) &= -\frac{1}{\varepsilon} - (\gamma_E - 1) - \frac{\varepsilon}{2}(\gamma_E^2 - 2\gamma_E + \frac{\pi^2}{6}) + \mathcal{O}(\varepsilon^2) \ , \\
\Gamma(\varepsilon-n) &= \frac{(-1)^n}{n!}\left[\frac{1}{\varepsilon} + (\sum_{k=1}^{n}\frac{1}{k}) - \gamma_E\right] + \mathcal{O}(\varepsilon) \ .
\end{aligned}
$$

- Γ - Function:

$$
\begin{aligned}
z\Gamma(z) &= \Gamma(z+1) \ , \\
\Gamma(z)\Gamma(1-z) &= \frac{\pi}{\sin\pi z} \ , \\
\Gamma\left(z+\frac{1}{2}\right)\Gamma\left(-z+\frac{1}{2}\right) &= \frac{\pi}{\cos\pi z} \ , \\
\Gamma(2z) &= \frac{2^{2z-1}}{\sqrt{\pi}}\Gamma(z)\,\Gamma\left(z+\frac{1}{2}\right) \ , \\
\Gamma(1) \ = \ \Gamma(2) \ = \ 1, \Gamma(3) &= 2, \ \Gamma(n+1) \ = \ n!, \\
\Gamma\left(\frac{1}{2}\right) \ = \ \sqrt{\pi}\,, \Gamma\left(\frac{3}{2}\right) &= \frac{\sqrt{\pi}}{2}\,, \Gamma\left(\frac{5}{2}\right) \ = \ \frac{3\sqrt{\pi}}{4} \ , \\
\Gamma\left(n+\frac{1}{2}\right) &= \frac{(2n-1)!!}{2^n}\sqrt{\pi} \ = \ \frac{(2n)!}{4^n n!}\sqrt{\pi}, \\
\Gamma\left(-n \ + \ \frac{1}{2}\right) &= \frac{(-)^n 2^n}{(2n-1)!!}\sqrt{\pi} \ = \ \frac{(^4)^n n!}{(2n)!}\sqrt{\pi} \ .
\end{aligned}
$$

- ψ - Function:

$$\begin{aligned}
\psi(1) &= -\gamma\ ,\ \psi(2) = 1 - \gamma\ , \psi(n) = \sum_{i=1}^{n-1}\frac{1}{i} - \gamma\ , \\
\psi\left(\frac{1}{2}\right) &= -\ln 4 - \gamma\ , \psi\left(\pm n + \frac{1}{2}\right) = 2\sum_{i=1}^{n}\frac{1}{2i-1} - \ln 4 - \gamma\ .
\end{aligned}$$

- β - function:

$$\begin{aligned}
B(x,y) &\equiv \int_0^1 \xi^{x-1}(1-\xi)^{y-1} \qquad (x,y > 0)\ , \\
B(x,y) &= B(y,x)\ , \\
B(x,y) &= 2\int_0^{\pi/2} d\theta \cos^{2x-1}\theta\ \sin^{2y-1}\theta\ , \\
B(x,x) &= 2^{1-2x}B(x,\frac{1}{2})\ , \\
B(x,y) &= \frac{\Gamma(x)\Gamma(y)}{\Gamma(x+y)}\ .
\end{aligned}$$

- Feynman Parametrization:

$$\begin{aligned}
\frac{1}{a_1 a_2\cdots a_n} &= (n-1)!\int d\alpha_1 d\alpha_2\cdots d\alpha_n \frac{\delta(1-\alpha_1-\alpha_2-\cdots-\alpha_n)}{(\alpha_1 a_1+\alpha_2 a_2+\cdots+\alpha_n a_n)^n}\ , \\
\frac{1}{AB} &= \int_0^1 dx \frac{1}{[xA+(1-x)B]^2}\ , \\
\frac{1}{A^\alpha B^\beta} &= \frac{\Gamma(\alpha+\beta)}{\Gamma(\alpha)\Gamma(\beta)}\int_0^1 dx \frac{x^{\alpha-1}(1-x)^{\beta-1}}{[xA+(1-x)B]^{\alpha+\beta}}\ , \\
\frac{1}{ABC} &= \int_0^1 dx\int_0^{1-x} dy \frac{2}{[xA+yB+(1-x-y)C]^3}\ .
\end{aligned}$$

- D-Dimension Integral:

$$\begin{aligned}
\int \frac{d^Dk}{(2\pi)^D}\frac{1}{[k^2-L]^n} &= \frac{i}{(4\pi)^{\frac{D}{2}}}(-)^n\frac{\Gamma\left(n-\frac{D}{2}\right)}{\Gamma(n)}L^{\frac{D}{2}-n}\ , \\
\int \frac{d^Dk}{(2\pi)^D}\frac{k^2}{[k^2-L]^n} &= \frac{i}{(4\pi)^{\frac{D}{2}}}(-)^{n+1}\frac{\Gamma\left(n-1-\frac{D}{2}\right)}{\Gamma(n)}\frac{D}{2}L^{\frac{D}{2}+1-n}\ , \\
\int \frac{d^Dk}{(2\pi)^D}\frac{k^\mu k^\nu}{[k^2-L]^n} &= \frac{i}{(4\pi)^{\frac{D}{2}}}(-)^{n+1}\frac{\Gamma\left(n-1-\frac{D}{2}\right)}{\Gamma(n)}\frac{g^{\mu\nu}}{2}L^{\frac{D}{2}+1-n}\ , \\
\int \frac{d^Dk}{(2\pi)^D}\frac{k^\mu k^\nu k^\lambda k^\rho}{[k^2-L]^n} &= \frac{i}{(4\pi)^{\frac{D}{2}}}(-)^n\frac{\Gamma\left(n-2-\frac{D}{2}\right)}{\Gamma(n)} \\
&\quad\times\frac{1}{4}\left(g^{\mu\nu}g^{\lambda\rho}+g^{\mu\lambda}g^{\nu\rho}+g^{\mu\rho}g^{\nu\lambda}\right)L^{\frac{D}{2}+2-n}\ , \\
\int \frac{d^Dk}{(2\pi)^D}k^\mu k^\nu f\left(k^2\right) &= \frac{g^{\mu\nu}}{D}\int\frac{d^Dk}{(2\pi)^D}k^2 f\left(k^2\right)\ .
\end{aligned}$$

B.3 SU(N) Generators

The SU(N) Generators $T^a (a = 1, 2, \ldots, N^2 - 1)$ are hermitian and traceless matrices, which generate the closed SU(N) algebra.

$$\left[T^a, T^b\right] = if^{abc}T^c \ .$$

The fundamental representation is N-dimensional where T^a satisfy an additional relation

$$\left\{T^a, T^b\right\} = \frac{1}{N}\delta_{ab} + d^{abc}T^c \ ,$$

which is consistent with the normalization

$$\mathrm{Tr}\left(T^a T^b\right) = \frac{1}{2}\delta_{ab} \ .$$

Here d^{abc} is totally symmetric in a, b and c.
It's given by

$$d^{abc} = 2\mathrm{Tr}\left[\{T^a, T^b\}T^c\right] \ .$$

According to above equations we get following relation.

$$T^a T^b = \frac{1}{2N}\delta_{ab} + \frac{1}{2}d^{abc}T^c + \frac{1}{2}if^{abc}T^c \ .$$

The SU(N) structure constants satisfy following relation.

$$f^{ade}f^{bef}f^{cfd} = \frac{N}{2}f^{abc} \ .$$

and Jacobi Identities

$$\begin{aligned} f^{abe}f^{cde} + f^{cbe}f^{dae} + f^{dbe}f^{ace} &= 0 \ , \\ f^{abe}d^{cde} + f^{cbe}d^{dae} + f^{dbe}d^{ace} &= 0 \ . \end{aligned}$$

For The SU(3) Generators and structure constants are explicitly written down as follows.

$$\begin{aligned} \lambda_1 &= \begin{pmatrix} 0 & 1 & 0 \\ 1 & 0 & 0 \\ 0 & 0 & 0 \end{pmatrix} , \lambda_2 = \begin{pmatrix} 0 & -i & 0 \\ i & 0 & 0 \\ 0 & 0 & 0 \end{pmatrix} , \\ \lambda_3 &= \begin{pmatrix} 1 & 0 & 0 \\ 0 & -1 & 0 \\ 0 & 0 & 0 \end{pmatrix} , \lambda_4 = \begin{pmatrix} 0 & 0 & 1 \\ 0 & 0 & 0 \\ 1 & 0 & 0 \end{pmatrix} , \end{aligned}$$

$$\lambda_5 = \begin{pmatrix} 0 & 0 & -i \\ 0 & 0 & 0 \\ i & 0 & 0 \end{pmatrix}, \lambda_6 = \begin{pmatrix} 0 & 0 & 0 \\ 0 & 0 & 1 \\ 0 & 1 & 0 \end{pmatrix},$$

$$\lambda_7 = \begin{pmatrix} 0 & 0 & 0 \\ 0 & 0 & -i \\ 0 & i & 0 \end{pmatrix}, \lambda_8 = \frac{1}{\sqrt{3}} \begin{pmatrix} 1 & 0 & 0 \\ 0 & 1 & 0 \\ 0 & 0 & -2 \end{pmatrix},$$

where $T^a = \frac{\lambda^a}{2}$.

Non-zero components of structure constants are

$$\begin{aligned} f^{123} &= 1 , \\ f^{147} &= -f^{156} = f^{246} = f^{257} = f^{345} = -f^{367} = \frac{1}{2} , \\ f^{458} &= f^{678} = \frac{\sqrt{3}}{2} . \end{aligned}$$

Now we can get some formulae, of course these formulae are independent of the explicit representation of SU(N) Generators and structure constants.

$$\begin{aligned} (T^c T^c)_{ij} &= C_2(R)\delta_{ij} , \\ T^c T^a T^c &= \left[-\frac{1}{2}C_2(G) + C_2(R)\right] T^a , \\ \mathrm{Tr}\left[T^a T^b\right] &= \frac{1}{2}\delta^{ab} , \\ \mathrm{Tr}\left[T^a T^b T^c\right] &= \frac{1}{4}(d^{abc} + if^{abc}) , \\ \mathrm{Tr}\left[T^a T^b T^c T^d\right] &= \frac{1}{4N}\delta^{ab}\delta^{cd} + \frac{1}{8}(d^{abe} + if^{abe})(d^{cde} + if^{cde}) , \\ f^{abc} T^b T^c &= \frac{i}{2} f^{abc} f^{bcd} T^d \\ &= \frac{i}{2} C_2(G) T^a . \end{aligned}$$

$$\begin{aligned} C_2(R) &= \frac{N^2 - 1}{2N} \\ f^{acd} f^{bcd} &= C_2(G)\delta^{ab} = N\delta^{ab} . \end{aligned}$$

Appendix C

Feynman Rule

C.1 QED Lagrangian

$$\mathcal{L}_{\rm QED} \;=\; \mathcal{L}_{class} \;+\; \mathcal{L}_{gauge}\;.$$

$$\begin{aligned}
\mathcal{L}_{class} &= \bar{\psi}\,(i\;\not{D}\;-\;m)\,\psi\;-\;\frac{1}{4}F_{\mu\nu}F^{\mu\nu}\;,\\
\mathcal{L}_{gauge} &= -\frac{1}{2\alpha}\,(\partial^{\mu}A_{\mu})^{2}\;.
\end{aligned}$$

- Covariant Derivative and Field Strength Tensor:

$$\begin{aligned}
D_{\mu} &\equiv \partial_{\mu}\;-\;ieA_{\mu}\;,\\
F_{\mu\nu} &\equiv \partial_{\mu}A_{\nu}-\partial_{\nu}A_{\mu}\;,
\end{aligned}$$

We split up the above Lagrangian into the free part $\mathcal{L}_0$ and the interaction part $\mathcal{L}_I$.

$$\begin{aligned}
\mathcal{L}_{\rm QED} &\equiv \mathcal{L}_0\;+\;\mathcal{L}_I\;,\\
\mathcal{L}_0 &= \bar{\psi}(i\not{\partial}\;-\;m)\psi-\frac{1}{4}(\partial_{\mu}A_{\nu}-\partial_{\nu}A_{\mu})(\partial^{\mu}A^{\nu}-\partial^{\nu}A^{\mu})\\
&- \frac{1}{2\alpha}(\partial^{\mu}A_{\mu})^{2}\;,\\
\mathcal{L}_I &= e\;\bar{\psi}\gamma^{\mu}\psi A_{\mu}.
\end{aligned}$$

C.2 QED Feynman Rules

- Fermion Propagator:

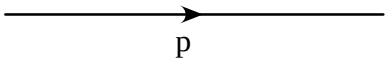

$$\frac{i}{\not{p} - m + i\varepsilon}$$

- Photon Propagator:

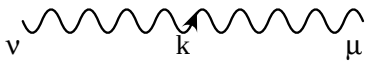

$$\frac{-i}{k^2 + i\varepsilon}\left[g_{\mu\nu} - (1-\alpha)\frac{k_\mu k_\nu}{k^2 + i\varepsilon}\right]$$

- Photon - Fermion Vertex:

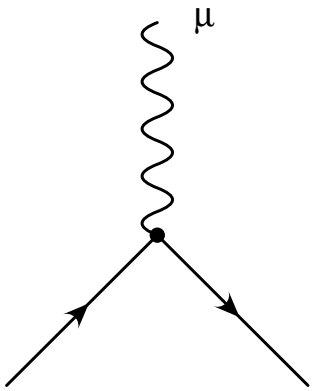

$$ie\gamma_\mu$$

C.3 QCD Lagrangian

$$\mathcal{L}_{\rm QCD} \;=\; \mathcal{L}_{class} \;+\; \mathcal{L}_{gauge} \;+\; \mathcal{L}_{ghost}\;,$$

$$\begin{aligned}
\mathcal{L}_{class} &= \bar{\psi}\,(i\not{D} \;-\; m)\,\psi \;-\; \frac{1}{4}F^a_{\mu\nu}F^{\mu\nu,a}\;,\\
\mathcal{L}_{gauge} &= -\frac{1}{2\alpha}\left(G^\mu A^a_\mu\right)^2\;,\\
\mathcal{L}_{ghost} &= (\partial^\mu\chi^{*a})\,D^{ab}_\mu\chi^b\;.
\end{aligned}$$

- χ, χ^* represent ghost and anti-ghost field.
- G^μ is given following,
  1. Coulomb Gauge: $\cdots\; G^\mu = (0, \nabla)$
  2. Covariant Gauge: $\cdots\; G^\mu = \partial^\mu$
     (a) Feynman Gauge: $\cdots \alpha = 1$
     (b) Landau Gauge: $\cdots \alpha = 0$
  3. Axial Gauge: $\cdots\; G^\mu = n^\mu$ (Light-cone Vector)
  4. Temporal Gauge: $\cdots\; G^\mu = (1,\;\; \mathbf{0}\;)$
- Covariant Derivative and Field Strength Tensor:

$$\begin{aligned}
D_\mu &\equiv \partial_\mu \;-\; ig_s A^a_\mu T^a\;,\\
F_{\mu\nu} &\equiv \partial_\mu A_\nu - \partial_\nu A_\mu - ig_s\,[A_\mu, A_\nu]\\
&= \left(\partial_\mu A^a_\nu - \partial_\nu A^a_\mu + g_s f^{abc} A^b_\mu A^c_\nu\right) T^a\;.
\end{aligned}$$

We split up the above Lagrangian into the free part $\mathcal{L}_0$ and the interaction part $\mathcal{L}_I$.

$$\begin{aligned}
\mathcal{L}_{\rm QCD} &\equiv \mathcal{L}_0 \;+\; \mathcal{L}_I\;,\\
\mathcal{L}_0 &= \bar{\psi}(i\not{\partial} \;-\; m)\psi - \frac{1}{4}(\partial_\mu A^a_\nu - \partial_\nu A^a_\mu)(\partial^\mu A^{a\nu} - \partial^\nu A^{a\mu})\\
&- \;\frac{1}{2\alpha}(\partial^\mu A^a_\mu)^2 \;+\; (\partial_\mu\chi^{*a})(\partial^\mu\chi^a)\;,\\
\mathcal{L}_I &= g_s\bar{\psi}\gamma^\mu T^a\psi A^a_\mu \;-\; \frac{g_s}{2}f^{abc}(\partial_\mu A^a_\nu - \partial_\nu A^a_\mu)A^{\mu b}A^{\nu c}\\
&- \;\frac{g_s^2}{4}f^{abc}f^{ade}A^b_\mu A^c_\nu A^{\mu d}A^{\nu e} \;-\; g_s f^{abc}(\partial^\mu\chi^{*a})\chi^b A^{\mu c}\;.
\end{aligned}$$

C.4 Notation and Conventions

- Covariant Derivative:

$$\begin{aligned} D_{\mu,ij}[A] &\equiv \partial_\mu \delta_{ij} - i g_s A^a_\mu [T^a]_{ij} , \\ D^{ab}_\mu [A] &\equiv \partial_\mu \delta^{ab} - g_s f^{abc} A^c_\mu . \end{aligned}$$

- Field Strength:

$$\begin{aligned} [D_\mu, D_\nu]_{ij} &\equiv -i g_s F^a_{\mu\nu} [T^a]_{ij} , \\ [D_\mu, D_\nu]^{ab} &\equiv -i g_s F^c_{\mu\nu} [T^c]^{ab} \\ &= -g_s f^{abc} F^c_{\mu\nu} , \\ F^a_{\mu\nu} &= \partial_\mu A^a_\nu - \partial_\nu A^a_\mu + g_s f^{abc} A^b_\mu A^c_\nu . \end{aligned}$$

- Dual Tensor:

$$\begin{aligned} \tilde{F}^{\mu\nu} &\equiv \frac{1}{2} \varepsilon^{\mu\nu\rho\sigma} F_{\rho\sigma} , \\ \tilde{F}^{\mu\nu a} &= \frac{1}{2} \varepsilon^{\mu\nu\rho\sigma} \left(\partial_\rho A^a_\sigma - \partial_\sigma A^a_\rho + g_s f^{abc} A^b_\rho A^c_\sigma \right) . \end{aligned}$$

- Bianchi Identity:

$$[D_\mu, [D_\nu, D_\rho]] + [D_\nu, [D_\rho, D_\mu]] + [D_\rho, [D_\mu, D_\nu]] = 0 .$$

  Thus we get follow identity.

$$\varepsilon^{\mu\nu\rho\sigma} [D_\mu, [D_\nu, D_\rho]] = 0 .$$

C.5 QCD Feynman Rules

- Fermion Propagator:

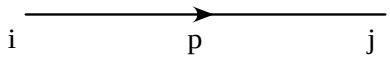

$$\frac{i\delta^{ij}}{\not{p} - m + i\varepsilon}$$

- Gluon Propagator:

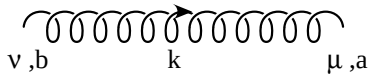

$$\frac{-i\delta_{ab}}{k^2 + i\varepsilon}\left[g_{\mu\nu} - (1-\alpha)\frac{k_\mu k_\nu}{k^2 + i\varepsilon}\right]$$

- Ghost Propagator:

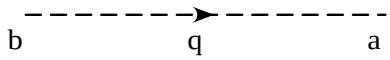

$$\frac{-i\delta_{ab}}{q^2 + i\varepsilon}$$

- Gluon - Fermion Vertex:

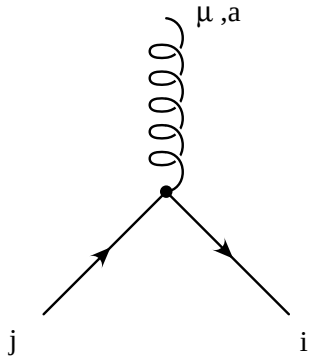

$$ig_s\gamma_\mu T^a_{ij}$$

- Gluon 3-point Vertex:

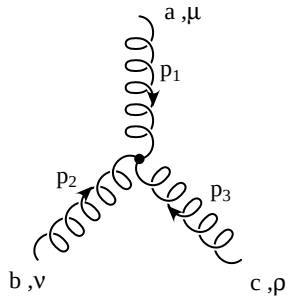

$$g_s f^{abc}\left[g_{\mu\nu}(p_1-p_2)_\rho + g_{\nu\rho}(p_2-p_3)_\mu + g_{\rho\mu}(p_3-p_1)_\nu\right]$$

- Gluon - Ghost Vertex:

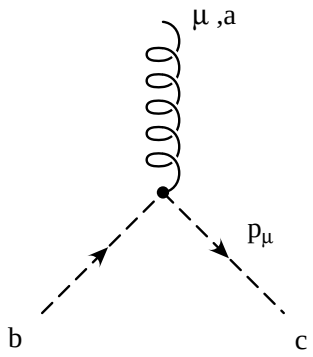

$$- g_s f^{abc} p_\mu$$

- Gluon 4-point Vertex:

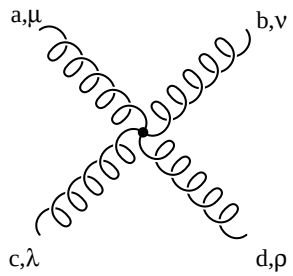

$$\begin{aligned} - \quad & i g_s^2 f^{abe} f^{cde} \left(g_{\mu\lambda} g_{\nu\rho} - g_{\mu\rho} g_{\nu\lambda}\right) \\ - \quad & i g_s^2 f^{ace} f^{bde} \left(g_{\mu\nu} g_{\lambda\rho} - g_{\mu\rho} g_{\nu\lambda}\right) \\ - \quad & i g_s^2 f^{ade} f^{cbe} \left(g_{\mu\lambda} g_{\nu\rho} - g_{\mu\nu} g_{\rho\lambda}\right) \end{aligned}$$

C.6 Electro-Weak Feynman Rule

- Z^0 Boson Propagator:

$$\frac{-i}{k^2 - M_Z^2 + i\varepsilon}\left[g_{\mu\nu} - (1-\alpha_Z)\frac{k_\mu k_\nu}{k^2 - \alpha_Z M_Z + i\varepsilon}\right]$$

- W Boson Propagator:

$$\frac{-i}{k^2 - M_W^2 + i\varepsilon}\left[g_{\mu\nu} - (1-\alpha_W)\frac{k_\mu k_\nu}{k^2 - \alpha_W M_W + i\varepsilon}\right]$$

- Photon - Fermion Vertex:

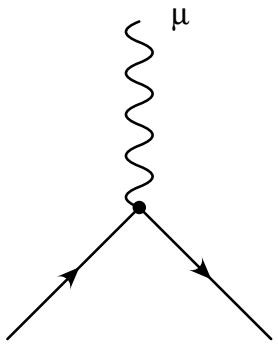

$$ieQ_\gamma(f)\gamma^\mu$$

- Z^0 Boson - Fermion Vertex:

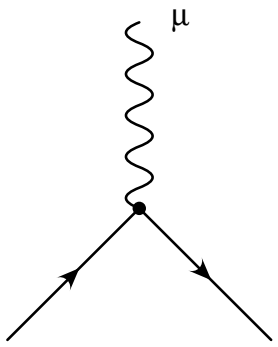

$$ie\left[Q_Z^R(f)\gamma_R^\mu + Q_Z^L(f)\gamma_L^\mu\right]$$

- Coefficients $Q_\gamma(f), Q_Z^{R,L}(f)$:

  When "f" stands for lepton (e^-, μ^- and τ^-), then coefficients $Q_\gamma(f),\ Q_Z^R(f)$ and $Q_Z^L(f)$ are

$$Q_\gamma(f) \ = \ -1\ ,\ Q_Z^R(f) \ = \ \frac{\sin\theta_w}{\cos\theta_w},\ Q_Z^L(f) \ = \ \frac{2\sin^2\theta_w - 1}{2\sin\theta_w\cos\theta_w}\ .$$

  While "f" stands for Quark, we get

$$\begin{aligned} Q_\gamma(\mathrm{U}) \ &= \ \frac{2}{3},\ Q_Z^R(\mathrm{U}) \ = \ \frac{-2\sin\theta_w}{3\cos\theta_w},\ Q_Z^L(\mathrm{U}) \ = \ \frac{3 - 4\sin^2\theta_w}{6\sin\theta_w\cos\theta_w}, \\ Q_\gamma(\mathrm{D}) \ &= \ -\frac{1}{3},\ Q_Z^R(\mathrm{D}) \ = \ \frac{\sin\theta_w}{3\cos\theta_w},\ Q_Z^L(\mathrm{D}) \ = \ \frac{-3 + 2\sin^2\theta_w}{6\sin\theta_w\cos\theta_w}\ , \end{aligned}$$

  where the suffices U, D mean up-type (u, c, t) and down-type (d, s, b) quarks.

- W Boson - Fermion Vertex:

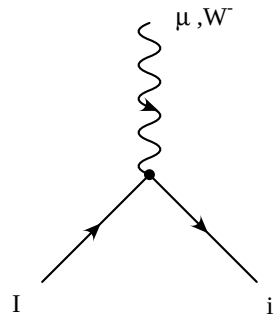

$$-i\frac{e}{\sqrt{2}\sin\theta_W}C_{iI}\gamma^{\mu}_{L}.$$

Coefficients C_{iI}:

When "$i,\ I$" stand for leptons ($e^-,\ \mu^-,\ \tau^-$ and ($\nu_e,\ \nu_\mu,\ \nu_\tau$), then coefficients $C_{iI} = 1$. While "$i,\ I$" stand for Quark, we get $C_{iI} = V_{iI}$, where V_{iI} is Cabbibo-Kobayashi-Maskawa mixing parameter.

Appendix D

Spinor Helicity Method

D.1 Notation and Convention

- Pseudo-scalar, Axial-vector:

$$\begin{aligned} \gamma_R &\equiv \frac{1}{2}(1+\gamma_5)\ ,\ \gamma_L \equiv \frac{1}{2}(1-\gamma_5)\ , \\ \gamma_R^\mu &\equiv \gamma^\mu \frac{1+\gamma_5}{2}\ ,\ \gamma_L^\mu \equiv \gamma^\mu \frac{1-\gamma_5}{2}\ . \end{aligned}$$

- Massless Helicity States:

$$\begin{aligned} u(p,+) &= \gamma_R u(p) \equiv |p+\rangle\ , \\ u(p,-) &= \gamma_L u(p) \equiv |p-\rangle\ . \end{aligned}$$

- Dirac Equation:

$$\hat{p}\,|p\pm\rangle = \langle p\pm|\,\hat{p} = 0, (\hat{p} \equiv \gamma^\mu p_\mu).$$

- Chirality Conditions:

$$\begin{aligned} (1\pm\gamma_5)\,|p\mp\rangle &= 0, \\ \langle p\pm|\,(1\pm\gamma_5) &= 0. \end{aligned}$$

- Normalization and Completeness:

$$\begin{aligned} \langle p\pm|\,\gamma^\mu\,|p\pm\rangle &= 2p^\mu, \\ |p+\rangle\langle p+| + |p-\rangle\langle p-| &= \hat{p}. \end{aligned}$$

- Massless Spinor Relations:

$$\begin{aligned}
|p\pm\rangle\langle p\pm| &= \frac{1\pm\gamma_5}{2}\hat{p}, \\
\langle p+|q+\rangle &= \langle p-|q-\rangle = 0, \\
\langle p-|q+\rangle &= -\langle q-|p+\rangle, \\
\langle p-|p+\rangle &= \langle p+|p-\rangle = 0.
\end{aligned}$$

- Fiertz rearrangement theorem:

$$\begin{aligned}
\langle p\pm|\gamma^\mu|q\pm\rangle\gamma_\mu\frac{1\pm\gamma_5}{2} &= 2|p\mp\rangle\langle q\mp| \ , \\
\langle p\pm|\gamma^\mu|q\pm\rangle\gamma_\mu\frac{1\mp\gamma_5}{2} &= 2|q\pm\rangle\langle p\pm| \ , \\
\langle A+|\gamma^\mu|B+\rangle\langle C-|\gamma_\mu|D-\rangle &= 2\langle A+|D-\rangle\langle C-|B+\rangle \ , \\
\langle p-|q+\rangle\gamma_R &= |q+\rangle\langle p-| - |p+\rangle\langle q-| \ , \\
\langle A-|B+\rangle\langle C-|D+\rangle &= \langle A-|D+\rangle\langle C-|B+\rangle + \langle A-|C+\rangle\langle B-|D+\rangle \ .
\end{aligned}$$

- Properties:

$$\begin{aligned}
\langle A\mp|B\pm\rangle &= -\langle B\mp|A\pm\rangle \ , \\
\langle A\pm|\gamma_\mu|B\pm\rangle &= \langle B\mp|\gamma_\mu|A\mp\rangle \ , \\
\langle p\pm|\gamma_{\mu_1}\cdots\gamma_{\mu_n}|q\mp\rangle &= -\langle 1\pm|\gamma_{\mu_1}\cdots\gamma_{\mu_n}|p\mp\rangle \ (n \text{ even}), \\
\langle p\pm|\gamma_{\mu_1}\cdots\gamma_{\mu_n}|q\pm\rangle &= \langle p\pm|\gamma_{\mu_1}\cdots\gamma_{\mu_n}|p\pm\rangle \ (n \text{ odd}).
\end{aligned}$$

- Polarization Vectors:

$$\begin{aligned}
\varepsilon^\mu_\mp(k) &= \pm\frac{1}{\sqrt{2}}\frac{\langle k\pm|\gamma^\mu|p\pm\rangle}{\langle p\mp|k\pm\rangle} \ , \\
\varepsilon^\mu_\mp(k)\gamma_\mu &= \pm\frac{\sqrt{2}}{\langle p\mp|k\pm\rangle}\left(|k\mp\rangle\langle p\mp| + |p\pm\rangle\langle k\pm|\right) \ .
\end{aligned}$$

- Properties of Polarization Vector:

$$\begin{aligned}
\varepsilon_\pm(k)\cdot k &= 0 \ , \\
\varepsilon^\mu_\mp(k) &= [\varepsilon^\mu_\pm(k)]^* \ , \\
\varepsilon_\lambda(k)\cdot\varepsilon^*_{\lambda'}(k) &= -\delta_{\lambda\lambda'} \ (\lambda,\lambda' \in (\pm,0)) \ , \\
\varepsilon_\lambda(k)\cdot k &= 0, \\
\sum_{\lambda=\pm,0}\varepsilon^\mu_\lambda(k)\varepsilon^{\nu *}_\lambda(k) &= -g^{\mu\nu} + \frac{k^\mu k^\nu}{m^2} \ .
\end{aligned}$$

- Massive Spinor States: The massive fermions with momentum p and anti-fermion with momentum $\bar{p}$

$$\begin{aligned}
u(p,\uparrow) &= |p_1+\rangle + |p_2-\rangle \frac{\langle p_2\ p_1\rangle}{m}, \\
u(p,\downarrow) &= |p_1-\rangle + |p_2+\rangle \frac{[p_2\ p_1]}{m}, \\
\bar{u}(p,\uparrow) &= \langle p_1+| + \frac{[p_1\ p_2]}{m} \langle p_2-|, \\
\bar{u}(p,\downarrow) &= \langle p_1-| + \frac{\langle p_1\ p_2\rangle}{m} \langle p_2+|, \\
v(\bar{p},\uparrow) &= |\bar{p}_1-\rangle - |\bar{p}_2+\rangle \frac{[\bar{p}_2\ \bar{p}_1]}{m}, \\
v(\bar{p},\downarrow) &= |\bar{p}_1+\rangle - |\bar{p}_2-\rangle \frac{\langle \bar{p}_2\ \bar{p}_1\rangle}{m}, \\
\bar{v}(\bar{p},\uparrow) &= \langle \bar{p}_1-| - \frac{\langle \bar{p}_1\ \bar{p}_2\rangle}{m} \langle \bar{p}_2+|, \\
\bar{v}(\bar{p},\downarrow) &= \langle \bar{p}_1+| - \frac{[\bar{p}_1\ \bar{p}_2]}{m} \langle \bar{p}_2-|,
\end{aligned}$$

with light like momenta p_1, p_2, $\bar{p}_1$ and $\bar{p}_2$,

$$\begin{aligned}
p_1 &\equiv \frac{p+ms_p}{2}, \quad p_2 \equiv \frac{p-ms_p}{2}, \\
\bar{p}_1 &\equiv \frac{\bar{p}+ms_{\bar{p}}}{2}, \quad \bar{p}_2 \equiv \frac{\bar{p}-ms_{\bar{p}}}{2},
\end{aligned}$$

where s_p is spin vector of the massive fermion, and $s_{\bar{p}}$ is spin vector of the massive anti-fermion.

- Polarization Vectors for Massive Boson:

  Three polarization vectors $\varepsilon^\mu_\lambda(k)$ are given in terms of two light-like vectors,

$$\begin{aligned}
k_1^\mu &= \frac{k^\mu - ms^\mu}{2}, \\
k_2^\mu &= \frac{k^\mu + ms^\mu}{2}.
\end{aligned}$$

  The polarization vectors for the incoming gauge boson:

$$\begin{aligned}
\varepsilon^\mu_\pm &= \frac{\langle k_1\pm| \gamma^\mu |k_2\pm\rangle}{\sqrt{2}m}, \\
\varepsilon^\mu_0 &= \frac{\langle k_1+| \gamma^\mu |k_1+\rangle - \langle k_2+| \gamma^\mu |k_2+\rangle}{2m} = \frac{k_1^\mu - k_2^\mu}{m}.
\end{aligned}$$

Appendix E

Phase space integrals over y and z

The phase space integrals necessary to derive the cross section are summarized in this Appendix. Although many of them have already appeared in the literatures [20], we will list all of them below for the convenience of the reader. After the integration over the angular variables, we are left with the following four types of integrals:

$$\begin{aligned} J_i &= \int dydz f_i(y,z) \ , \qquad N_i = \int \frac{dydz}{\sqrt{(1-y)^2-a}} f_i(y,z) \ , \\ L_i &= \int \frac{dydz}{(1-y)^2-a} f_i(y,z) \ , \quad K_i = \int \frac{dydz}{\{(1-y)^2-a\}^{3/2}} f_i(y,z) \ . \end{aligned}$$

The infrared divergences are regularized by the small gluon mass λ and $\beta = \sqrt{1-a} = \sqrt{1-4m^2/s}$. For the type L_i integrals, a shorthand notation $\omega = \sqrt{(1-\sqrt{a})/(1+\sqrt{a})}$ is used. The K_i integrals have a spurious singularity at the upper bound of the y integral, $y_+ = 1-\sqrt{a}$. Since this singularity turns out to be canceled out in the cross section, we regularize each integrals by deforming the integration region as $y_+ \to 1-\sqrt{a}-\epsilon$ [20]. Li_2 is the Spence function.

Class $\boldsymbol{J}$ Integrals:

$$\begin{aligned} J_1 &= \int dy\, dz \ = \ \frac{1}{2}\beta\left(1+\frac{1}{2}a\right) - \frac{1}{2}a\left(1-\frac{1}{4}a\right)\ln\left(\frac{1+\beta}{1-\beta}\right) \\ J_2 &= \int dy\, dz \ \frac{y}{z} \ = \ \int dy\, dz \ \frac{z}{y} \\ &= -\frac{1}{4}\beta\left(5-\frac{1}{2}a\right) + \frac{1}{2}\left(1+\frac{1}{8}a^2\right)\ln\left(\frac{1+\beta}{1-\beta}\right) \\ J_3 &= \int dy\, dz \ \frac{1}{y} \ = \ \int dy\, dz \ \frac{1}{z} = -\beta + \left(1-\frac{1}{2}a\right)\ln\left(\frac{1+\beta}{1-\beta}\right) \end{aligned}$$

$$
\begin{aligned}
J_4 &= \int dy\,dz\ \frac{y}{z^2} = \int dy\,dz\ \frac{z}{y^2} = \frac{2}{a}\beta - \ln\left(\frac{1+\beta}{1-\beta}\right) \\
J_5 &= \int dy\,dz\ \frac{1}{y^2} \ = \ \int dy\,dz\ \frac{1}{z^2} \\
&= -\frac{2\beta}{a}\left(\ln\frac{\lambda^2}{s} + 2\ln a - 4\ln\beta - 4\ln 2 + 2\right) + 2\left(1-\frac{3}{a}\right)\ln\left(\frac{1+\beta}{1-\beta}\right) \\
J_6 &= \int dy\,dz\ \frac{1}{yz} \\
&= \left(-\ln\frac{\lambda^2}{s} - \ln a + 4\ln\beta + 2\ln 2\right)\ln\left(\frac{1+\beta}{1-\beta}\right) \\
&\quad +2\left[\mathrm{Li}_2\left(\frac{1+\beta}{2}\right) - \mathrm{Li}_2\left(\frac{1-\beta}{2}\right)\right] + 3\left[\mathrm{Li}_2\left(-\frac{2\beta}{1-\beta}\right) - \mathrm{Li}_2\left(\frac{2\beta}{1+\beta}\right)\right]
\end{aligned}
$$

Class $\boldsymbol{N}$ Integrals:

$$
\begin{aligned}
N_1 &= \int \frac{dy\,dz}{\sqrt{(1-y)^2-a}} \ = 1 - \sqrt{a} - \frac{1}{2}a\ln\left(\frac{2-\sqrt{a}}{\sqrt{a}}\right) \\
N_2 &= \int \frac{dy\,dz}{\sqrt{(1-y)^2-a}}\ \frac{z}{y} = -\frac{1}{2}\ln a + \ln\left(2-\sqrt{a}\right) + \frac{2}{2-\sqrt{a}} - 2 \\
N_3 &= \int \frac{dy\,dz}{\sqrt{(1-y)^2-a}}\ \frac{y}{z} \\
&= 2\beta\ln\left(\frac{1-\beta}{1+\beta}\right) - \ln\left(\frac{1+\beta}{2}\right)\ln\left(\frac{1-\beta}{2}\right) + \left(2-\frac{a}{2}\right)\ln\left(\frac{2-\sqrt{a}}{\sqrt{a}}\right) \\
&\quad + \frac{1}{4}\ln^2\frac{a}{4} - \sqrt{a} + 1 + \mathrm{Li}_2\left(\frac{1+\beta}{2}\right) + \mathrm{Li}_2\left(\frac{1-\beta}{2}\right) - 2\,\mathrm{Li}_2\left(\frac{\sqrt{a}}{2}\right) \\
N_4 &= \int \frac{dy\,dz}{\sqrt{(1-y)^2-a}}\ \frac{y^2}{z^2} = \frac{2}{a}\left(1-\sqrt{a}\right)^2 \\
N_5 &= \int \frac{dy\,dz}{\sqrt{(1-y)^2-a}}\ y \\
&= \frac{1}{16}\left[-a^2\ln a + 2\,a^2\ln(2-\sqrt{a}) + 4(2-\sqrt{a})^2 - 4\left(2-a^{\frac{3}{2}}\right)\right] \\
N_6 &= \int \frac{dy\,dz}{\sqrt{(1-y)^2-a}}\ z \\
&= \frac{1}{32}\left[12 - (2+a)^2 - \frac{2+\sqrt{a}}{2-\sqrt{a}}\,a^2 + 2(8-a)a\,\ln\frac{\sqrt{a}}{2-\sqrt{a}}\right] \\
N_7 &= \int \frac{dy\,dz}{\sqrt{(1-y)^2-a}}\ \frac{y^2}{z}
\end{aligned}
$$

$$
\begin{aligned}
&= \left(1+\frac{1}{2}a\right)\left[\mathrm{Li}_2\left(\frac{1+\beta}{2}\right)+\mathrm{Li}_2\left(\frac{1-\beta}{2}\right)-2\,\mathrm{Li}_2\left(\frac{1}{2}\sqrt{a}\right)+\frac{1}{4}\ln^2\left(\frac{1}{4}a\right)\right.\\
&\quad\left.-\ln\left(\frac{1+\beta}{2}\right)\ln\left(\frac{1-\beta}{2}\right)\right]+3v\ln\left(\frac{1-\beta}{1+\beta}\right)+\frac{1}{8}(18+a)\\
&\quad-\frac{1}{8}(20-a)\sqrt{a}+\left(3-a+\frac{1}{16}a^2\right)\ln\left(\frac{2-\sqrt{a}}{\sqrt{a}}\right)\\
N_8 &= \int\frac{dy\,dz}{\sqrt{(1-y)^2-a}}\;\frac{1}{y}=2\ln\left(\frac{2-\sqrt{a}}{\sqrt{a}}\right)\\
N_9 &= \int\frac{dy\,dz}{\sqrt{(1-y)^2-a}}\;\frac{1}{z}\\
&= \mathrm{Li}_2\left(\frac{1+\beta}{2}\right)+\mathrm{Li}_2\left(\frac{1-\beta}{2}\right)+2\,\mathrm{Li}_2\left(-\frac{\sqrt{a}}{2-\sqrt{a}}\right)+\frac{1}{4}\ln^2 a\\
&\quad+\ln^2\left(\frac{2-\sqrt{a}}{2}\right)-\ln(1+\beta)\ln(1-\beta)\\
N_{10} &= \int\frac{dy\,dz}{\sqrt{(1-y)^2-a}}\;\frac{y}{z^2}=\frac{4}{a}\left(1-\sqrt{a}\right)\\
N_{11} &= \int\frac{dy\,dz}{\sqrt{(1-y)^2-a}}\;\frac{1}{y^2}\\
&= \frac{2}{a}\left[-\ln\frac{\lambda^2}{s}+\ln a+2\ln(1-\sqrt{a})-4\ln(2-\sqrt{a})+2\ln 2-2\right]\\
N_{12} &= \int\frac{dy\,dz}{\sqrt{(1-y)^2-a}}\;\frac{1}{z^2}\\
&= \frac{2}{a}\left[-\ln\frac{\lambda^2}{s}-\ln a+2\ln(1-\sqrt{a})-\frac{1+\beta^2}{\beta}\ln\left(\frac{1+\beta}{1-\beta}\right)+2\ln 2\right]\\
N_{13} &= \int\frac{dy\,dz}{\sqrt{(1-y)^2-a}}\;\frac{1}{yz}\\
&= \frac{1}{\beta}\ln\left(\frac{1-\beta}{1+\beta}\right)\left[\ln\frac{\lambda^2}{s}+\frac{1}{2}\ln a+4\ln(2-\sqrt{a})-4\ln(2\beta)-2\ln\left(\frac{1-\beta}{1+\beta}\right)\right]\\
&\quad+\frac{1}{\beta}\ln^2\left(\frac{(1-\beta)^2}{\sqrt{a}(2-\sqrt{a})}\right)+\frac{2}{\beta}\ln\left(\frac{\sqrt{a}(2-\sqrt{a})}{2}\right)\ln\left(\frac{2\sqrt{a}(1-\sqrt{a})}{(1-\sqrt{a}-\beta)^2}\right)\\
&\quad+\frac{2}{\beta}\left[\mathrm{Li}_2\left(\frac{\sqrt{a}(2-\sqrt{a})}{(1+\beta)^2}\right)-\mathrm{Li}_2\left[\left(\frac{1-\beta}{1+\beta}\right)^2\right]+\mathrm{Li}_2\left(\frac{(1-\beta)^2}{\sqrt{a}(2-\sqrt{a})}\right)\right]\\
&\quad+\frac{1}{\beta}\left[\mathrm{Li}_2\left(\frac{1+\beta}{2}\right)+\mathrm{Li}_2\left(-\frac{2\beta}{1-\beta}\right)-(\beta\to-\beta)-\frac{\pi^2}{3}\right]
\end{aligned}
$$

Class $\boldsymbol{L}$ Integrals:

$$
\begin{aligned}
L_1 &= \int \frac{dy\,dz}{(1-y)^2-a} \;= 2\,\frac{1-a}{4-a}\ln\left(\frac{1+\beta}{1-\beta}\right) \\
L_2 &= \int \frac{dy\,dz}{(1-y)^2-a}\;\frac{z}{y} \\
&= \left(-1+\frac{12}{4-a}-\frac{24}{(4-a)^2}\right)\ln\left(\frac{1+\beta}{1-\beta}\right)-\frac{2\beta}{4-a} \\
L_3 &= \int \frac{dy\,dz}{(1-y)^2-a}\;\frac{y}{z} \\
&= \frac{1}{2}\ln\left(\frac{1+\beta}{1-\beta}\right)\left[\frac{1}{2}\ln a+\ln(2+\sqrt{a})-\ln(1+\sqrt{a})-2\ln 2\right] \\
&\quad +\frac{1-\sqrt{a}}{\sqrt{a}}\left[\mathrm{Li}_2(\omega)+\mathrm{Li}_2\left(\frac{2+\sqrt{a}}{2-\sqrt{a}}\,\omega\right)-(\omega\to-\omega)\right] \\
&\quad +\left[\mathrm{Li}_2\left(\frac{1+\omega}{2}\right)+\mathrm{Li}_2\left((2+\sqrt{a})\frac{1+\omega}{4}\right)+\mathrm{Li}_2\left(\frac{2\sqrt{a}}{(2+\sqrt{a})(1+\omega)}\right)\right. \\
&\qquad\qquad \left.-(\omega\to-\omega)\right] \\
L_4 &= \int \frac{dy\,dz}{(1-y)^2-a}\;\frac{y^2}{z^2} = \frac{2}{a}\left[\ln\left(\frac{1+\beta}{1-\beta}\right)-2\beta\right] \\
L_5 &= \int \frac{dy\,dz}{(1-y)^2-a}\;y = -\left(1+\frac{1}{2}a-\frac{6}{4-a}\right)\ln\left(\frac{1+\beta}{1-\beta}\right)-\beta \\
L_6 &= \int \frac{dy\,dz}{(1-y)^2-a}\;z = -\frac{3a}{4-a}\left(1-\frac{2}{4-a}\right)\ln\left(\frac{1+\beta}{1-\beta}\right)+\frac{2\beta}{4-a} \\
L_7 &= \int \frac{dy\,dz}{(1-y)^2-a}\;\frac{1}{z} = \frac{1}{\sqrt{a}}\left[\mathrm{Li}_2(\omega)+\mathrm{Li}_2\left(\frac{2+\sqrt{a}}{2-\sqrt{a}}\,\omega\right)-(\omega\to-\omega)\right] \\
L_8 &= \int \frac{dy\,dz}{(1-y)^2-a}\;\frac{y}{z^2} = \frac{2}{a}\ln\left(\frac{1+\beta}{1-\beta}\right)
\end{aligned}
$$

Class $\boldsymbol{K}$ Integrals:

$$
\begin{aligned}
K_1 &= \int \frac{dy\,dz}{\{(1-y)^2-a\}^{3/2}} \\
&= \frac{2(1-\sqrt{a})}{\sqrt{a}(2-\sqrt{a})^2}\ln\frac{2\sqrt{a}(1-\sqrt{a})}{\epsilon(1+\sqrt{a})}-\frac{4a}{(4-a)^2}\ln\frac{(1+\sqrt{a})(2-\sqrt{a})^2}{2\sqrt{a}a} \\
K_2 &= \int \frac{dy\,dz}{\{(1-y)^2-a\}^{3/2}}\;y \\
&= \frac{2(1-\sqrt{a})^2}{\sqrt{a}(2-\sqrt{a})^2}\ln\frac{2\sqrt{a}(1-\sqrt{a})}{\epsilon(1+\sqrt{a})}+\frac{a^2}{(4-a)^2}\ln\frac{(1+\sqrt{a})(2-\sqrt{a})^2}{2\sqrt{a}a)}
\end{aligned}
$$

$$
\begin{aligned}
& + \ln \frac{2\sqrt{a}}{(1+\sqrt{a})} \\
K_3 &= \int \frac{dy\,dz}{\{(1-y)^2-a\}^{3/2}}\ z \\
&= \frac{2(1-\sqrt{a})^2}{(2-\sqrt{a})^3} \ln \frac{2\sqrt{a}(1-\sqrt{a})}{\epsilon(1+\sqrt{a})} + \frac{a(a^2+20a-32)}{2(4-a)^3} \ln \frac{(1+\sqrt{a})(2-\sqrt{a})^2}{2\sqrt{a}a} \\
& - \frac{1}{2} \ln \frac{2\sqrt{a}}{(1+\sqrt{a})} + \frac{2a(1-\sqrt{a})}{(4-a)(2-\sqrt{a})^2} \\
K_4 &= \int \frac{dy\,dz}{\{(1-y)^2-a\}^{3/2}}\ yz \\
&= \frac{2(1-\sqrt{a})^3}{(2-\sqrt{a})^3} \ln \frac{2\sqrt{a}(1-\sqrt{a})}{\epsilon(1+\sqrt{a})} + \frac{a^2(12-7a)}{2(4-a)^3} \ln \frac{(1+\sqrt{a})(2-\sqrt{a})^2}{2\sqrt{a}a} \\
& - \frac{1}{2} \ln \frac{2\sqrt{a}}{(1+\sqrt{a})} + \frac{2}{(4-a)} \left[a \frac{(1-\sqrt{a})^2}{(2-\sqrt{a})^2} + \sqrt{a} - 1 \right] \\
K_5 &= \int \frac{dy\,dz}{\{(1-y)^2-a\}^{3/2}}\ \frac{y}{z} \\
&= \frac{2(1-\sqrt{a})}{a(2-\sqrt{a})} \ln \frac{2\sqrt{a}(1-\sqrt{a})}{\epsilon(1+\sqrt{a})} + \frac{(4-3a)}{a(4-a)} \ln \frac{(1+\sqrt{a})(2-\sqrt{a})^2}{2\sqrt{a}a} \\
& - \frac{1}{a} \ln \frac{2\sqrt{a}}{(1+\sqrt{a})} + \frac{4(1-\sqrt{a})}{a(2-\sqrt{a})} - \frac{2\beta}{a} \ln \left(\frac{1+\beta}{1-\beta} \right) \\
K_6 &= \int \frac{dy\,dz}{\{(1-y)^2-a\}^{3/2}}\ \frac{1}{z} \\
&= \frac{2}{a(2-\sqrt{a})} \ln \frac{2\sqrt{a}(1-\sqrt{a})}{\epsilon(1+\sqrt{a})} + \frac{(4+a)}{a(4-a)} \ln \frac{(1+\sqrt{a})(2-\sqrt{a})^2}{2\sqrt{a}a} \\
& - \frac{1}{a} \ln \frac{2\sqrt{a}}{(1+\sqrt{a})} + \frac{4}{a(2-\sqrt{a})} - \frac{2}{a\beta} \ln \left(\frac{1+\beta}{1-\beta} \right) \\
K_7 &= \int \frac{dy\,dz}{\{(1-y)^2-a\}^{3/2}}\ \frac{y}{z^2} = \frac{2}{a\sqrt{a}} \ln \frac{2\sqrt{a}(1-\sqrt{a})}{\epsilon(1+\sqrt{a})} \\
K_8 &= \int \frac{dy\,dz}{\{(1-y)^2-a\}^{3/2}}\ \frac{y^2}{z^2} \\
&= \frac{2(1-\sqrt{a})}{a\sqrt{a}} \ln \left(\frac{2\sqrt{a}(1-\sqrt{a})}{\epsilon(1+\sqrt{a})} \right) + \frac{4}{a} \ln \left(\frac{2\sqrt{a}}{1+\sqrt{a}} \right)
\end{aligned}
$$

Appendix F

Total cross section

Let us examine the unpolarized total cross section including the top quark pairs using our formulae. It is given by

$$\sigma_T(e^-e^+ \to t+\bar{t}+X) = \frac{1}{4}\left[\sigma_T(e_L^-e_R^+ \to t+\bar{t}+X) + \sigma_T(e_R^-e_L^+ \to t+\bar{t}+X)\right] \ .$$

Note that only $k = 0, 2$ and $l, m, n = 0$ terms in Eq.(4.43) contribute to the total cross section. Integrating over the angle θ, we get

$$\begin{aligned}
&\sigma_T(e_L^-e_R^+ \to t+\bar{t}+X) \\
&= \frac{\pi\alpha^2}{s}\beta\Bigg[(f_{LL}+f_{LR})^2\left(3-\beta^2\right) \\
&\qquad \times \left(1+\hat{\alpha}_s\left\{V_I - \frac{6}{3-\beta^2}V_{II} + \frac{2}{\beta}J_{IR}^1 - \frac{8}{\beta}J_3 + \frac{8}{\beta(3-\beta^2)}J_2\right\}\right) \\
&\quad + 2\left(f_{LL}-f_{LR}\right)^2\beta^2 \\
&\qquad \times \left(1+\hat{\alpha}_s\left\{V_I + 2V_{II} + \frac{2}{\beta}J_{IR}^1 - \frac{8}{\beta}J_3 + \frac{2(3-\beta^2)}{\beta^3}J_2 + \frac{2a}{\beta^3}J_1\right\}\right)\Bigg].
\end{aligned}$$

The cross section for the process $e_R^-e_L^+$ is obtained by interchanging the coupling constant $L \leftrightarrow R$ in the above expression. Parametrizing the total cross section as

$$\begin{aligned}
R_t(s) &\equiv \left(\frac{1}{\sigma_{\rm pt}}\right)\sigma_T(e^-e^+ \to t+\bar{t}+X) \\
&= R_t^{(0)}(s) + \frac{\alpha_s(s)}{\pi}C_2(R)R_t^{(1)}(s) + \cdots \ ,
\end{aligned}$$

where $\sigma_{\rm pt} = 4\pi\alpha^2/3s$, we get the following numerical results at the CM energies $\sqrt{s} =$ 400 , 500 , 800 , 1000 , 1500 GeV.

$\sqrt{s}$ (GeV)	$R_t^{(0)}(s)$	$C_2(R)R_t^{(1)}(s)$
400	1.0083	8.9963
500	1.4190	6.0267
800	1.6864	3.3999
1000	1.7317	2.8422
1500	1.7714	2.2911

These are consistent with the results in Ref. [44].

Appendix G

Numerical Tables

We have shown the numerical tables for $e^-_{L/R}e^+ \to tX(\bar{t}$ or $\bar{t}g)$ process in the previous Chapters and Sections. In this Appendix, we present the numerical tables, we used to analyze the spin correlations because of its usefulness.

Now we show the numerical value of the coefficients C_{klmn}, D_{klmn} using following inputs.

$$\begin{aligned} m &= 175 \qquad (\text{GeV}) \\ M_z &= 91.187 \qquad (\text{GeV}) \\ \alpha &= 1/128 \\ \alpha_s(M_z^2) &= 0.118 \\ \sin^2\theta_W &= 0.2315 \end{aligned}$$

The multiplicative enhancement, κ_L/κ_L, the top quark speed β, and QCD strong coupling constant α_s, $\hat{\alpha}_s \equiv C_2(R)/(4\pi)\alpha_s$.

$\sqrt{s}$	400 GeV	500 GeV	800 GeV	1000 GeV	1500 GeV	4000 GeV
$\kappa(L)$	0.2778	0.1283	0.05747	0.04574	0.03474	0.02593
$\kappa(R)$	0.2799	0.1316	0.06023	0.04790	0.03599	0.02618
β	0.4841	0.7141	0.8992	0.9368	0.9723	0.9962
α_s	0.09804	0.09564	0.09096	0.08890	0.08539	0.07794
$\hat{\alpha}_s$	0.01040	0.01015	0.009652	0.009433	0.009060	0.008270

G.1 $e_L^- e^+ \to t_\uparrow + X$

Now we define coefficients $D^0_{klmn}, D^1_{klmn}, S_{klmn}, S^1_{klmn}$ and S^2_{klmn}.

$$\frac{d\sigma}{d\cos\theta}(e_L^- e_R^+ \to t_\uparrow X) = \frac{3\pi\alpha^2}{4s}\sum_{klmn}(D_{klmn} + \hat{\alpha}_s C_{klmn})\cos^k\theta\sin^l\theta\cos^m\xi\sin^n\xi \ ,$$

with

$$D_{klmn} \equiv D^0_{klmn} + D^1_{klmn}.$$

$$\begin{aligned}
D^0_{0000} &= \beta[f_{LL}^2 + f_{LR}^2 + 2a f_{LL} f_{LR}], \\
D^0_{2000} &= \beta^3(f_{LL}^2 + f_{LR}^2), \\
D^0_{1000} &= 2\beta^2(f_{LL}^2 - f_{LR}^2), \\
D^0_{0010} &= \beta^2(f_{LL}^2 - f_{LR}^2), \\
D^0_{2010} &= \beta^2(f_{LL}^2 - f_{LR}^2), \\
D^0_{1010} &= \beta[(f_{LL} + f_{LR})^2 + \beta^2(f_{LL} - f_{LR})^2], \\
D^0_{0101} &= \frac{\beta}{\sqrt{a}} a(f_{LL} + f_{LR})^2, \\
D^0_{1101} &= \frac{\beta^2}{\sqrt{a}} a(f_{LL}^2 - f_{LR}^2).
\end{aligned}$$

$$\begin{aligned}
D^1_{0000} &= \beta[f_{LL}^2 + f_{LR}^2 + 2a f_{LL} f_{LR}](\hat{\alpha}_s V_I) \\
&\qquad -\beta[2(f_{LL} + f_{LR})^2 - \beta^2(f_{LL} - f_{LR})^2]\hat{\alpha}_s V_{II} \ , \\
D^1_{2000} &= \beta^3(f_{LL}^2 + f_{LR}^2)(\hat{\alpha}_s V_I) + \beta^3(f_{LL} - f_{LR})^2\hat{\alpha}_s V_{II} \ , \\
D^1_{1000} &= 2\beta^2(f_{LL}^2 - f_{LR}^2)(\hat{\alpha}_s V_I) \ , \\
D^1_{0010} &= \beta^2(f_{LL}^2 - f_{LR}^2)(\hat{\alpha}_s V_I) \ , \\
D^1_{2010} &= \beta^2(f_{LL}^2 - f_{LR}^2)(\hat{\alpha}_s V_I) \ , \\
D^1_{1010} &= \beta[(f_{LL} + f_{LR})^2 + \beta^2(f_{LL} - f_{LR})^2](\hat{\alpha}_s V_I) \\
&\qquad -2\beta[(f_{LL} + f_{LR})^2 - \beta^2(f_{LL} - f_{LR})^2]\hat{\alpha}_s V_{II} \ , \\
D^1_{0101} &= \frac{\beta}{\sqrt{a}}(f_{LL} + f_{LR})^2[a(\hat{\alpha}_s V_I) - (1+a)\hat{\alpha}_s V_{II}] \ , \\
D^1_{1101} &= \frac{\beta^2}{\sqrt{a}}(f_{LL}^2 - f_{LR}^2)[a(\hat{\alpha}_s V_I) - (1-a)\hat{\alpha}_s V_{II}] \ .
\end{aligned}$$

$$\begin{aligned}\frac{d\sigma^{SGA}}{d\cos\theta}(e_L^- e_R^+ \to t_\uparrow \bar{t}) &= \frac{3\pi\alpha^2}{4s}\sum_{klmn} B_{klmn}\cos^k\theta\sin^l\theta\cos^m\xi\sin^n\xi \ , \\ &= \frac{3\pi\alpha^2}{4s}\sum_{klmn}\left(D^0_{klmn}+B^1_{klmn}\right)\cos^k\theta\sin^l\theta\cos^m\xi\sin^n\xi \ ,\end{aligned}$$

with

$$\begin{aligned}B^1_{0000} &= \beta[f_{LL}^2+f_{LR}^2+2af_{LL}f_{LR}]S_I \\ &\qquad -\beta[2(f_{LL}+f_{LR})^2-\beta^2(f_{LL}-f_{LR})^2]S_{II} \ , \\ B^1_{2000} &= \beta^3(f_{LL}^2+f_{LR}^2)S_I+\beta^3(f_{LL}-f_{LR})^2S_{II} \ , \\ B^1_{1000} &= 2\beta^2(f_{LL}^2-f_{LR}^2)S_I \ , \\ B^1_{0010} &= \beta^2(f_{LL}^2-f_{LR}^2)S_I \ , \\ B^1_{2010} &= \beta^2(f_{LL}^2-f_{LR}^2)S_I \ , \\ B^1_{1010} &= \beta[(f_{LL}+f_{LR})^2+\beta^2(f_{LL}-f_{LR})^2]S_I \\ &\qquad -2\beta[(f_{LL}+f_{LR})^2-\beta^2(f_{LL}-f_{LR})^2]S_{II} \ , \\ B^1_{0101} &= \frac{\beta}{\sqrt{a}}(f_{LL}+f_{LR})^2[aS_I-(1+a)S_{II}] \ , \\ B^1_{1101} &= \frac{\beta^2}{\sqrt{a}}(f_{LL}^2-f_{LR}^2)[aS_I-(1-a)S_{II}]\end{aligned}$$

$$\begin{aligned}D_{klmn}+\hat{\alpha}_s C_{klmn} &\equiv D^0_{klmn}+S_{klmn} \\ &\equiv (1+\kappa)D^0_{klmn}+S^1_{klmn} \qquad \cdots \text{Full} \\ &\equiv (1+\kappa)D^0_{klmn}+S^2_{klmn} \qquad \cdots \text{S.G.A}\end{aligned}$$

Therefore, S_{klmn}, S^1_{klmn} and S^2_{klmn} are given by

$$\begin{aligned}S_{klmn} &= D^1_{klmn}+\hat{\alpha}_s C_{klmn} \\ S^1_{klmn} &= D^1_{klmn}+\hat{\alpha}_s C_{klmn}-\kappa D^0_{klmn} \\ S^2_{klmn} &= B^1_{klmn}-\kappa D^0_{klmn} \ .\end{aligned}$$

$$\begin{aligned}R^{Full}_{klmn} &= \frac{S^1_{klmn}}{(1+\kappa)D^0_{klmn}} \\ R^{SGA}_{klmn} &= \frac{S^2_{klmn}}{(1+\kappa)D^0_{klmn}}\end{aligned}$$

- $\mathcal{O}(\alpha_s)$ Analysis

$\sqrt{s}$	400 GeV	500 GeV	800 GeV	1000 GeV	1500 GeV	4000 GeV
C_{0000}	−11.66	−30.13	−58.68	−71.01	−94.84	−167.3
C_{2000}	−1.872	−12.07	−44.72	−61.57	−92.84	−175.3
C_{1000}	−6.010	−25.83	−74.58	−98.212	−142.3	−263.3
C_{0010}	−2.988	−12.72	−36.28	−47.68	−69.09	−128.7
C_{2010}	−3.023	−13.14	−38.56	−50.97	−74.00	−136.2
C_{1010}	−13.60	−42.69	−105.4	−135.4	−191.9	−349.5
C_{0101}	−11.28	−26.85	−39.76	−40.73	−38.70	−27.28
C_{1101}	−2.637	−9.126	−16.75	−17.79	−17.47	−12.60
D_{0000}	1.630	2.025	2.289	2.374	2.542	3.048
D_{2000}	0.2675	0.8100	1.671	1.949	2.332	3.012
D_{1000}	0.8650	1.760	2.858	3.194	3.674	4.626
D_{0010}	0.4325	0.8799	1.429	1.597	1.837	2.313
D_{2010}	0.4325	0.8799	1.429	1.597	1.837	2.313
D_{1010}	1.890	2.835	3.960	4.324	4.874	6.060
D_{0101}	1.563	1.753	1.439	1.241	0.9196	0.4246
D_{1101}	0.3770	0.6100	0.6139	0.5475	0.4185	0.1969

$\sqrt{s}$	400 GeV	500 GeV	800 GeV	1000 GeV	1500 GeV	4000 GeV
D^0_{0000}	1.183	1.528	1.629	1.625	1.614	1.603
D^0_{2000}	0.1882	0.5960	1.174	1.323	1.475	1.583
D^0_{1000}	0.6111	1.299	2.010	2.169	2.325	2.431
D^0_{0010}	0.3056	0.6497	1.005	1.085	1.163	1.215
D^0_{2010}	0.3056	0.6497	1.005	1.085	1.163	1.215
D^0_{1010}	1.371	2.124	2.802	2.948	3.089	3.185
D^0_{0101}	1.137	1.331	1.040	0.8652	0.5978	0.2294
D^0_{1101}	0.2674	0.4548	0.4397	0.3797	0.2712	0.1063
S_{0000}	0.3260	0.1910	0.09417	0.07918	0.06780	0.06193
S_{2000}	0.05993	0.09144	0.06577	0.04599	0.01608	−0.02013
S_{1000}	0.1913	0.1984	0.1278	0.09841	0.05992	0.01786
S_{0010}	0.09583	0.1012	0.07363	0.06265	0.04874	0.03378
S_{2010}	0.09548	0.09688	0.05161	0.03170	0.004244	−0.02836
S_{1010}	0.3852	0.2775	0.1408	0.09893	0.04598	−0.01484
S_{0101}	0.3092	0.1488	0.01564	−0.008947	−0.02875	−0.03045
S_{1101}	0.08220	0.06263	0.01257	0.00001984	−0.01105	−0.01366

	400 GeV	500 GeV	800 GeV	1000 GeV	1500 GeV	4000GeV
$(1+\kappa)D^0_{0000}$	1.511	1.724	1.722	1.700	1.671	1.644
$(1+\kappa)D^0_{2000}$	0.2404	0.6724	1.241	1.383	1.526	1.624
$(1+\kappa)D^0_{1000}$	0.7809	1.466	2.126	2.269	2.406	2.494
$(1+\kappa)D^0_{0010}$	0.3905	0.7330	1.063	1.134	1.203	1.247
$(1+\kappa)D^0_{2010}$	0.3905	0.7330	1.063	1.134	1.203	1.247
$(1+\kappa)D^0_{1010}$	1.751	2.396	2.963	3.083	3.197	3.268
$(1+\kappa)D^0_{0101}$	1.452	1.502	1.100	0.9048	0.6186	0.2353
$(1+\kappa)D^0_{1101}$	0.3416	0.5131	0.4650	0.3970	0.2807	0.1091
S^1_{0000}	−0.002552	−0.005000	0.0005645	0.004836	0.01172	0.02039
S^1_{2000}	0.007655	0.01500	−0.001682	−0.01450	−0.03516	−0.06116
S^1_{1000}	0.02154	0.03170	0.01224	−0.0008102	−0.02085	−0.04516
S^1_{0010}	0.01094	0.01785	0.01586	0.01304	0.008357	0.002274
S^1_{2010}	0.01059	0.01356	−0.006158	−0.01791	−0.03614	−0.05987
S^1_{1010}	0.004433	0.005069	−0.02030	−0.03590	−0.06134	−0.09742
S^1_{0101}	−0.006564	−0.02193	−0.04413	−0.04852	−0.04952	−0.03639
S^1_{1101}	0.007920	0.004308	−0.01270	−0.01734	−0.02047	−0.01642

	400 GeV	500 GeV	800 GeV	1000 GeV	1500 GeV	4000 GeV
R^{Full}_{0000}	−0.001689	−0.002900	0.0003278	0.002845	0.007014	0.01240
R^{Full}_{2000}	0.03184	0.02231	−0.001356	−0.01048	−0.02304	−0.03767
R^{Full}_{1000}	0.02758	0.02163	0.005757	−0.0003571	−0.008667	−0.01811
R^{Full}_{0010}	0.02803	0.02435	0.01492	0.01150	0.006948	0.001823
R^{Full}_{2010}	0.02711	0.01849	−0.005793	−0.01579	−0.03004	−0.04802
R^{Full}_{1010}	0.0025310	0.002115	−0.006849	−0.01165	−0.01919	−0.02981
R^{Full}_{0101}	−0.004520	−0.01460	−0.04013	−0.05362	−0.08005	−0.15465
R^{Full}_{1101}	0.02318	0.008395	−0.02731	−0.04369	−0.07294	−0.15050

- Soft Gluon App.

  We define the ω_{max} to satisfy the following relation.

$$\int_{-1}^{1} d\cos\theta \sum_{s=\uparrow,\downarrow} \frac{d\sigma_{T,L/R}}{d\cos\theta}(e^-_{L/R}e^+ \to t_s X(\bar{t} \text{ or } \bar{t}g))$$
$$= \int_{-1}^{1} d\cos\theta \sum_{s=\uparrow,\downarrow} \frac{d\sigma_{SGA,L/R}}{d\cos\theta}(e^-_{L/R}e^+ \to t_s\bar{t})$$

	400 GeV	500 GeV	800 GeV	1000 GeV	1500 GeV	4000 GeV
ω_{max}	13.49	38.60	106.7	149.7	254.8	775.9
B_{0000}	1.508	1.718	1.716	1.695	1.668	1.644
B_{2000}	0.2482	0.6903	1.258	1.397	1.534	1.625
B_{1000}	0.8023	1.499	2.151	2.288	2.416	2.496
B_{0010}	0.4011	0.7495	1.075	1.144	1.208	1.248
B_{2010}	0.4011	0.7495	1.075	1.144	1.208	1.248
B_{1010}	1.757	2.408	2.975	3.092	3.202	3.269
B_{0101}	1.446	1.486	1.0749	0.8790	0.5962	0.2235
B_{1101}	0.3496	0.5187	0.4593	0.3889	0.2717	0.1037
B^1_{0000}	0.3259	0.1900	0.08785	0.06979	0.05347	0.04103
B^1_{2000}	0.06009	0.09431	0.08469	0.07414	0.05908	0.04258
B^1_{1000}	0.1911	0.1996	0.1407	0.1183	0.09133	0.06506
B^1_{0010}	0.09556	0.09979	0.07034	0.05916	0.04567	0.03253
B^1_{2010}	0.09556	0.09979	0.07034	0.05916	0.04567	0.03253
B^1_{1010}	0.3860	0.2843	0.1725	0.1439	0.1126	0.08361
B^1_{0101}	0.3099	0.1540	0.03373	0.01373	−0.001588	−0.005863
B^1_{1101}	0.08219	0.06395	0.01957	0.009227	0.0004544	−0.002634

	400 GeV	500 GeV	800 GeV	1000 GeV	1500 GeV	4000 GeV
S^2_{0000}	−0.002607	−0.005957	−0.005747	−0.004551	−0.002615	−0.0005169
S^2_{2000}	0.007821	0.01787	0.01724	0.01365	0.007846	0.001551
S^2_{1000}	0.02134	0.03293	0.02514	0.01910	0.01057	0.002038
S^2_{0010}	0.01067	0.01646	0.01257	0.009549	0.005284	0.001019
S^2_{2010}	0.01067	0.01646	0.01257	0.009549	0.005284	0.001019
S^2_{1010}	0.005214	0.01191	0.01149	0.009101	0.005231	0.001034
S^2_{0101}	−0.005870	−0.01676	−0.02604	−0.02585	−0.02235	−0.01181
S^2_{1101}	0.007915	0.005621	−0.005706	−0.008136	−0.008968	−0.005391
R^{SGA}_{0000}	−0.001725	−0.003455	−0.003337	−0.002677	−0.001566	−0.0003144
R^{SGA}_{2000}	0.03253	0.02658	0.01389	0.009870	0.005141	0.0009552
R^{SGA}_{1000}	0.02733	0.02246	0.01183	0.008418	0.004393	0.0008172
R^{SGA}_{0010}	0.02733	0.02246	0.01183	0.008418	0.004393	0.0008172
R^{SGA}_{2010}	0.02733	0.02246	0.01183	0.008418	0.004393	0.0008172
R^{SGA}_{1010}	0.002977	0.004972	0.003879	0.002952	0.001636	0.0003164
R^{SGA}_{0101}	−0.004042	−0.01115	−0.02368	−0.02857	−0.03614	−0.05018
R^{SGA}_{1101}	0.02317	0.01096	−0.01227	−0.02049	−0.03195	−0.04941

- SGA I

$\sqrt{s}$	400 GeV	500 GeV	800 GeV	1000 GeV	1500 GeV	4000 GeV
ω_{max}	10 GeV	30 GeV	90 GeV	130 GeV	230 GeV	730 GeV
B_{0000}	1.498	1.690	1.675	1.653	1.629	1.610
B_{2000}	0.2466	0.6794	1.228	1.363	1.498	1.592
B_{1000}	0.7970	1.475	2.099	2.232	2.360	2.444
B_{0010}	0.3984	0.7376	1.050	1.116	1.180	1.222
B_{2010}	0.3984	0.7376	1.050	1.116	1.180	1.222
B_{1010}	1.745	2.370	2.903	3.017	3.127	3.201
B_{0101}	1.436	1.461	1.047	0.8566	0.5817	0.2187
B_{1101}	0.3472	0.5104	0.4480	0.3790	0.2651	0.1015
B^1_{0000}	0.3157	0.1621	0.04600	0.02769	0.01430	0.007045
B^1_{2000}	0.05846	0.08341	0.05453	0.03989	0.02330	0.009018
B^1_{1000}	0.1858	0.1758	0.08901	0.06213	0.03493	0.01351
B^1_{0010}	0.09292	0.08791	0.04451	0.03107	0.01746	0.006754
B^1_{2010}	0.09292	0.08791	0.04451	0.03107	0.01746	0.006754
B^1_{1010}	0.3742	0.2455	0.1005	0.06758	0.03760	0.01606
B^1_{0101}	0.3000	0.1297	0.007001	−0.008684	−0.01609	−0.01073
B^1_{1101}	0.07988	0.05563	0.008266	−0.0006056	−0.006126	−0.004889

G.2 $e_R^- \, e^+ \to t_\downarrow + X$

- $\mathcal{O}(\alpha_s)$ Analysis

$\sqrt{s}$	400 GeV	500 GeV	800 GeV	1000 GeV	1500 GeV	4000 GeV
C_{0000}	−5.088	−13.73	−28.17	−34.56	−46.82	−83.45
C_{2000}	−0.9132	−5.943	−22.22	−30.66	−46.31	−87.57
C_{1000}	−3.387	−14.68	−42.75	−56.41	−81.91	−151.7
C_{0010}	−1.684	−7.227	−20.80	−27.39	−39.76	−74.14
C_{2010}	−1.704	−7.467	−22.11	−29.27	−42.59	−78.47
C_{1010}	−6.033	−19.91	−51.38	−66.60	−95.22	−174.4
C_{0101}	−4.816	−11.64	−17.53	−18.03	−17.21	−12.20
C_{1101}	−1.486	−5.187	−9.600	−10.22	−10.05	−7.263
D_{0000}	0.7129	0.9271	1.104	1.159	1.257	1.521
D_{2000}	0.1308	0.3992	0.8305	0.9708	1.164	1.505
D_{1000}	0.4875	1.000	1.638	1.835	2.115	2.666
D_{0010}	0.2438	0.5001	0.8192	0.9174	1.057	1.333
D_{2010}	0.2438	0.5001	0.8192	0.9174	1.057	1.333
D_{1010}	0.8437	1.3263	1.9343	2.130	2.420	3.025
D_{0101}	0.6679	0.7616	0.6364	0.5506	0.4097	0.1897
D_{1101}	0.2125	0.3467	0.3520	0.3145	0.2408	0.1135

$\sqrt{s}$	400 GeV	500 GeV	800 GeV	1000 GeV	1500 GeV	4000 GeV
D^0_{0000}	0.5167	0.6982	0.7840	0.7927	0.7978	0.7995
D^0_{2000}	0.09176	0.2932	0.5829	0.6583	0.7357	0.7905
D^0_{1000}	0.3444	0.7385	1.152	1.246	1.338	1.401
D^0_{0010}	0.1722	0.3692	0.5762	0.6231	0.6690	0.7004
D^0_{2010}	0.1722	0.3692	0.5762	0.6231	0.6690	0.7004
D^0_{1010}	0.6085	0.9915	1.367	1.451	1.534	1.590
D^0_{0101}	0.4856	0.5786	0.4598	0.3840	0.2663	0.1025
D^0_{1101}	0.1507	0.2585	0.2521	0.2181	0.1561	0.06128
S_{0000}	0.1433	0.08952	0.04786	0.04071	0.03479	0.03117
S_{2000}	0.02954	0.04566	0.03323	0.02331	0.008236	−0.01002
S_{1000}	0.1078	0.1127	0.07325	0.05653	0.03448	0.01029
S_{0010}	0.05401	0.05750	0.04221	0.03599	0.02805	0.01947
S_{2010}	0.05381	0.05506	0.02959	0.01821	0.002443	−0.01634
S_{1010}	0.1725	0.1328	0.07156	0.05096	0.02413	−0.007143
S_{0101}	0.1322	0.06490	0.007412	−0.003494	−0.01250	−0.01371
S_{1101}	0.04633	0.03560	0.007208	0.000011398	−0.006358	−0.007873

$\sqrt{s}$	400 GeV	500 GeV	800 GeV	1000 GeV	1500 GeV	4000 GeV
$(1+\kappa)D^0_{0000}$	0.6613	0.7901	0.8313	0.8307	0.8266	0.8204
$(1+\kappa)D^0_{2000}$	0.1174	0.3318	0.6180	0.6899	0.7622	0.8112
$(1+\kappa)D^0_{1000}$	0.4408	0.8357	1.222	1.306	1.386	1.437
$(1+\kappa)D^0_{0010}$	0.2204	0.4178	0.6109	0.6529	0.6931	0.7187
$(1+\kappa)D^0_{2010}$	0.2204	0.4178	0.6109	0.6529	0.6931	0.7187
$(1+\kappa)D^0_{1010}$	0.7787	1.122	1.449	1.521	1.589	1.632
$(1+\kappa)D^0_{0101}$	0.6216	0.6547	0.4875	0.4024	0.2759	0.1052
$(1+\kappa)D^0_{1101}$	0.1929	0.2925	0.2673	0.2285	0.1617	0.06289
S^1_{0000}	−0.001287	−0.002358	0.0006297	0.002742	0.006079	0.01024
S^1_{2000}	0.003862	0.007074	−0.001884	−0.008222	−0.01824	−0.03072
S^1_{1000}	0.01143	0.01556	0.003835	−0.003159	−0.01367	−0.02639
S^1_{0010}	0.005814	0.008914	0.007500	0.006143	0.003972	0.001128
S^1_{2010}	0.005612	0.006475	−0.005121	−0.01164	−0.02164	−0.03468
S^1_{1010}	0.002248	0.002290	−0.01078	−0.01854	−0.03107	−0.04878
S^1_{0101}	−0.003764	−0.01122	−0.02028	−0.02189	−0.02208	−0.01640
S^1_{1101}	0.004154	0.001587	−0.007977	−0.01043	−0.01198	−0.009478

$\sqrt{s}$	400 GeV	500 GeV	800 GeV	1000 GeV	1500 GeV	4000 GeV
R^{Full}_{0000}	−0.001947	−0.002985	0.0007576	0.003301	0.007354	0.01248
R^{Full}_{2000}	0.03289	0.02132	−0.003048	−0.01192	−0.02393	−0.03787
R^{Full}_{1000}	0.02593	0.01862	0.003139	−0.002419	−0.009864	−0.01836
R^{Full}_{0010}	0.02638	0.02133	0.01228	0.009409	0.005731	0.001570
R^{Full}_{2010}	0.02546	0.01550	−0.008382	−0.01782	−0.03122	−0.04826
R^{Full}_{1010}	0.002886	0.002041	−0.007438	−0.01219	−0.01955	−0.02989
R^{Full}_{0101}	−0.006056	−0.01714	−0.04161	−0.05439	−0.08003	−0.1559
R^{Full}_{1101}	0.02154	0.005427	−0.02984	−0.04566	−0.07406	−0.1507

- Soft Gluon App.

  We define the ω_{max} to satisfy the following relation.

$$\int_{-1}^{1} d\cos\theta \sum_{s=\uparrow,\downarrow} \frac{d\sigma_{T,R}}{d\cos\theta}(e^-_{L/R}e^+ \to t_s X(\bar{t} \text{ or } \bar{t}g))$$
$$= \int_{-1}^{1} d\cos\theta \sum_{s=\uparrow,\downarrow} \frac{d\sigma_{SGA,R}}{d\cos\theta}(e^-_{L/R}e^+ \to t_s\bar{t})$$

	400 GeV	500 GeV	800 GeV	1000 GeV	1500 GeV	4000 GeV
ω_{max}	13.55	38.84	107.2	150.2	255.2	776.1
B_{0000}	0.6600	1.719	1.717	1.696	1.668	1.644
B_{2000}	0.1214	0.6906	1.259	1.397	1.535	1.625
B_{1000}	0.4522	1.500	2.152	2.289	2.417	2.496
B_{0010}	0.2261	0.7498	1.076	1.144	1.209	1.248
B_{2010}	0.2261	0.7498	1.076	1.144	1.209	1.248
B_{1010}	0.7814	2.409	2.976	3.094	3.203	3.269
B_{0101}	0.6181	1.486	1.074	0.879	0.5964	0.2235
B_{1101}	0.1970	0.5189	0.4596	0.3891	0.2718	0.1037
B^1_{0000}	0.1433	0.1907	0.08886	0.07067	0.05405	0.04117
B^1_{2000}	0.02964	0.09457	0.08541	0.07486	0.05962	0.04272
B^1_{1000}	0.1078	0.2002	0.1419	0.1195	0.09217	0.06527
B^1_{0010}	0.05388	0.1001	0.07096	0.05975	0.04609	0.03264
B^1_{2010}	0.05388	0.1001	0.07096	0.05975	0.04609	0.03264
B^1_{1010}	0.1729	0.2853	0.1743	0.1455	0.1137	0.08389
B^1_{0101}	0.1325	0.1546	0.03437	0.01420	−0.001372	−0.005843
B^1_{1101}	0.04635	0.06415	0.01984	0.009433	0.0005521	−0.002624

	400 GeV	500 GeV	800 GeV	1000 GeV	1500 GeV	4000 GeV
S^2_{0000}	−0.001319	−0.0103680	−0.009239	−0.007183	−0.002033	−0.0003753
S^2_{2000}	0.003957	0.01615	0.01473	0.01151	0.008378	0.001691
S^2_{1000}	0.01137	0.02918	0.02083	0.01558	0.01141	0.002253
S^2_{0010}	0.005683	0.01459	0.01042	0.007792	0.005703	0.001126
S^2_{2010}	0.005683	0.01459	0.01042	0.007792	0.005703	0.001126
S^2_{1010}	0.002638	0.005783	0.005487	0.004327	0.006345	0.001315
S^2_{0101}	−0.003445	−0.02060	−0.02827	−0.02725	−0.02214	−0.011790
S^2_{1101}	0.004170	0.004308	−0.006649	−0.008751	−0.008870	−0.005381
R^{SGA}_{0000}	−0.001994	−0.005996	−0.005351	−0.004217	−0.001217	−0.0002282
R^{SGA}_{2000}	0.03369	0.02395	0.01183	0.008305	0.005490	0.001041
R^{SGA}_{1000}	0.02578	0.01984	0.009774	0.006855	0.004741	0.0009033
R^{SGA}_{0010}	0.02578	0.01984	0.009774	0.006855	0.004741	0.0009033
R^{SGA}_{2010}	0.02578	0.01984	0.009774	0.006855	0.004741	0.0009033
R^{SGA}_{1010}	0.003387	0.002406	0.001847	0.001401	0.001985	0.0004025
R^{SGA}_{0101}	−0.005543	−0.01367	−0.02564	−0.03005	−0.03579	−0.05010
R^{SGA}_{1101}	0.02162	0.008372	−0.01426	−0.02200	−0.03161	−0.04932

- SGA I

$\sqrt{s}$	400 GeV	500 GeV	800 GeV	1000 GeV	1500 GeV	4000 GeV
ω_{max}	10 GeV	30 GeV	90 GeV	130 GeV	230 GeV	730
B_{0000}	0.6554	0.7741	0.8080	0.8077	0.8057	0.8031
B_{2000}	0.1206	0.3350	0.6106	0.6787	0.7476	0.7950
B_{1000}	0.4492	0.8384	1.2035	1.282	1.358	1.4086
B_{0010}	0.2246	0.4192	0.6017	0.6409	0.6791	0.7043
B_{2010}	0.2246	0.4192	0.6017	0.6409	0.6791	0.7043
B_{1010}	0.7760	1.109	1.419	1.486	1.553	1.598
B_{0101}	0.6138	0.6349	0.4629	0.3802	0.2592	0.09768
B_{1101}	0.1957	0.2901	0.2568	0.2177	0.1526	0.05847
B^1_{0000}	0.1388	0.07592	0.02394	0.01493	0.007892	0.003678
B^1_{2000}	0.02883	0.04174	0.02772	0.02035	0.01190	0.004559
B^1_{1000}	0.1047	0.09992	0.05103	0.03569	0.02010	0.007784
B^1_{0010}	0.05237	0.04996	0.02552	0.01784	0.01005	0.003892
B^1_{2010}	0.05237	0.04996	0.02552	0.01784	0.01005	0.003892
B^1_{1010}	0.1676	0.1177	0.05166	0.03528	0.01979	0.008237
B^1_{0101}	0.1282	0.05634	0.003095	−0.003854	−0.007169	−0.004792
B^1_{1101}	0.04502	0.03162	0.004739	−0.0003479	−0.003526	−0.002817

G.3 Off-Diagonal Basis

$$\sigma\left(e_L^- e^+ \to t_\uparrow + X\right)/\sigma_{T,L}$$

$\sqrt{s}$	400 GeV	500 GeV	800 GeV	1000 GeV	1500 GeV
Tree	0.99876	0.99255	0.97350	0.96514	0.95345
$\mathcal{O}(\alpha_s)$	0.99850	0.99093	0.96815	0.95833	0.94480
SGA	0.99871	0.99225	0.97276	0.96434	0.95275

$$\sigma\left(e_L^- e^+ \to t_\downarrow + X\right)/\sigma_{T,L}$$

$\sqrt{s}$	400 GeV	500 GeV	800 GeV	1000 GeV	1500 GeV
Tree	0.00124	0.00745	0.02650	0.03486	0.04655
$\mathcal{O}(\alpha_s)$	0.00150	0.00907	0.03185	0.04167	0.05520
SGA	0.00129	0.00775	0.02724	0.03566	0.04725

$$\sigma\left(e_R^- e^+ \to t_\downarrow + X\right)/\sigma_{T,R}$$

$\sqrt{s}$	400 GeV	500 GeV	800 GeV	1000 GeV	1500 GeV
Tree	0.99833	0.99371	0.98141	0.97619	0.96897
$\mathcal{O}(\alpha_s)$	0.99786	0.99184	0.97615	0.96958	0.96057
SGA	0.99809	0.99318	0.98065	0.97545	0.96837

$$\sigma\left(e_R^- e^+ \to t_\uparrow + X\right)/\sigma_{T,R}$$

$\sqrt{s}$	400 GeV	500 GeV	800 GeV	1000 GeV	1500 GeV
Tree	0.00167	0.00629	0.01859	0.02381	0.03103
$\mathcal{O}(\alpha_s)$	0.00214	0.00816	0.02385	0.03042	0.03943
SGA	0.00191	0.00682	0.01935	0.02455	0.03163

G.4 Helicity Basis

$$\sigma\left(e_L^- e^+ \to t_L + X\right)/\sigma_{T,L}$$

$\sqrt{s}$	400 GeV	500 GeV	800 GeV	1000 GeV	1500 GeV
Tree	0.66359	0.75084	0.83177	0.84997	0.86797
$\mathcal{O}(\alpha_s)$	0.66814	0.75658	0.83500	0.85160	0.86712
SGA	0.66809	0.75657	0.83579	0.85299	0.86962

$$\sigma\left(e_L^- e^+ \to t_R + X\right)/\sigma_{T,L}$$

$\sqrt{s}$	400 GeV	500 GeV	800 GeV	1000 GeV	1500 GeV
Tree	0.33641	0.24916	0.16823	0.15003	0.13203
$\mathcal{O}(\alpha_s)$	0.33187	0.24342	0.16500	0.14840	0.13288
SGA	0.33191	0.24343	0.16421	0.14701	0.13038

$$\sigma\left(e_R^- e^+ \to t_R + X\right)/\sigma_{T,R}$$

$\sqrt{s}$	400 GeV	500 GeV	800 GeV	1000 GeV	1500 GeV
Tree	0.70979	0.80926	0.89267	0.91039	0.92758
$\mathcal{O}(\alpha_s)$	0.71528	0.81541	0.89546	0.91145	0.92608
SGA	0.71524	0.81550	0.89660	0.91327	0.92913

$$\sigma\left(e_R^- e^+ \to t_L + X\right)/\sigma_{T,R}$$

$\sqrt{s}$	400 GeV	500 GeV	800 GeV	1000 GeV	1500 GeV
Tree	0.29021	0.19074	0.10733	0.08961	0.072419
$\mathcal{O}(\alpha_s)$	0.28472	0.18459	0.10454	0.08855	0.073918
SGA	0.28476	0.18450	0.10340	0.08673	0.07087

G.5 Beamline Basis

$$\sigma\left(e_L^- e^+ \to t_\uparrow + X\right)/\sigma_{T,L}$$

$\sqrt{s}$	400 GeV	500 GeV	800 GeV	1000 GeV	1500 GeV
Tree	0.98811	0.96769	0.93097	0.91822	0.90218
$\mathcal{O}(\alpha_s)$	0.98851	0.96784	0.92922	0.91565	0.89853
SGA	0.98869	0.96889	0.93210	0.91913	0.90272

$$\sigma\left(e_L^- e^+ \to t_\downarrow + X\right)/\sigma_{T,L}$$

$\sqrt{s}$	400 GeV	500 GeV	800 GeV	1000 GeV	1500 GeV
Tree	0.01189	0.03231	0.06903	0.08178	0.09782
$\mathcal{O}(\alpha_s)$	0.01149	0.03216	0.07078	0.08435	0.10147
SGA	0.01131	0.03111	0.06790	0.08087	0.09728

$$\sigma\left(e_R^- e^+ \to t_\downarrow + X\right)/\sigma_{T,R}$$

$\sqrt{s}$	400 GeV	500 GeV	800 GeV	1000 GeV	1500 GeV
Tree	0.99436	0.98432	0.96581	0.95934	0.95119
$\mathcal{O}(\alpha_s)$	0.99470	0.98437	0.96400	0.95666	0.94727
SGA	0.99490	0.98545	0.96693	0.96025	0.95174

$$\sigma\left(e_R^- e^+ \to t_\downarrow + X\right)/\sigma_{T,R}$$

$\sqrt{s}$	400 GeV	500 GeV	800 GeV	1000 GeV	1500 GeV
Tree	0.00564	0.01568	0.03419	0.04066	0.04881
$\mathcal{O}(\alpha_s)$	0.00530	0.01563	0.03600	0.04334	0.05273
SGA	0.00510	0.01455	0.03307	0.03975	0.04826

Bibliography

[1] H. Fritzsh, M. Gell-Mann and H. Leutwyler, *Phys. Lett.* **B47** (1973) 365.

[2] S.L. Glashow,*Nucl. Phys.* **22** (1961)579; S. Weinberg, *Phys. Rev. Lett* **19** (1967) 1264; A. Salam, in: N. Svartholm (Ed.), *Elementary particle Theory* Almqvistand Wiksells, Stockholm, (1968).

[3] P.W.Higgs, *Phys. Rev. Lett.* **12** (1964) 132; *Phys. Rev.* **145** (1966) 1156; F. Englert and R. Brout, *Phys. Rev. Lett.* **13** (1964) 321; G.S. Guralnik, C.R. Hagen and T.W. Kibble, *Phys. Rev. Lett.* **13** (1964) 585.

[4] F. Abe et al., CDF Collaboration, *Phys. Rev. Lett.* **74** (1995) 2626.

[5] S. Abachi et al., D0 Collaboration, *Phys. Rev. Lett.* **74** (1995) 2632.

[6] C. Caso et al, *The European Physical Journal* **C3** (1998) 1.

[7] See, for example,
W. Bernreuther, O. Nachtmann, P. Overmann and T. Schröder, *Nucl. Phys.* **B388** (1992) 53-80;
erratum *Nucl. Phys.* **B406** (1993) 516;
S. Y. Choi and K. Hagiwara, *Phys. Lett.* **B359** (1995) 369-374;
B. Grządkowski and Z. Hioki, *Nucl. Phys.* **B484** (1997) 17-32, and references therein.

[8] J. H. Kühn, *Nucl. Phys.* **B237** (1984) 77.

[9] I. Bigi, Y. Dokshizer, V. Khoze, J. Kühn and P. Zerwas, *Phys. Lett.* **B181** (1986) 157.

[10] M. Jezabek, J. H. Kühn and T. Teubner, *Z. Phys.* **C56** (1992) 653.
M. Jezabek and J. H. Kühn, *Phys. Lett.* **B329** (1994) 317.

[11] V. Barger, J. Ohnemus and R.J.N Phillips, *Int. J. Mod. Phys.* **A4** (1989) 617.

[12] G. L. Kane, J. Pumplin and W. Repko, *Phys. Rev. Lett.* **41** (1978) 1689.
G. L. Kane, G. A. Ladinsky and C. -P. Yuan, *Phys. Rev.* **D45** (1992) 124.

[13] M. Anselmino, P. Kroll and B. Pire, *Phys. Lett.* **B167** (1986) 113.
D. Atwood and A. Soni, *Phys. Rev.* **D45** (1992) 2405.
C. - P. Yuan, *Phys. Rev.* **D45** (1992) 318.
G. A. Ladinsky, *Phys. Rev.* **D46** (1992) 3789.
W. Bernreuther, O. Nachtmann, P. Overmann and T. Schröder, *Nucl. Phys.* **B388** (1992) 53; erratum **B406** (1993) 516.
M. E. Peskin, in *Physics and Experiments at Linear Colliders*, R. Orava, P. Eeorla and M. Nordberg, eds. (World Scientific, 1992).
T. Arens and L. M. Seghal, *Nucl. Phys.* **B393** (1993) 46.
F. Cuypers and S. D. Rindani, *Phys. Lett.* **B343** (1995) 333.
P. Poulose and S. D. Rindani, *Phys. Lett.* **B349** (1995) 379.

[14] C. R. Schmidt and M. E. Peskin, *Phys. Rev. Lett.* **69** (1992) 410.
D. Atwood, A. Aeppli and A. Soni, *Phys. Rev. Lett.* **69** (1992) 2754.
Y. Hara, *Prog. Theo. Phys.* **86** (1991) 779.
W. Bernreuther and A. Brandenburg, *Phys. Rev.* **D49** (1994) 4481.

[15] G. Mahlon and S. Parke, *Phys. Rev.* **D53** (1996) 4886, *Phys. Lett.* **B411** (1997) 173.

[16] S. Parke and Y. Shadmi, *Phys. Lett.* **B387** (1996) 199.

[17] G. Grunberg, Y. J. Ng and S. -H. H. Tye, *Phys. Rev.* **D21** (1980) 62.
J. Jersák, E. Laermann and P. Zerwas, *Phys. Rev.* **D25** (1982) 1218.

[18] S. Groote, J. G. Körner and J. A. Leyva, hep-ph/9801255.

[19] C. R. Schmidt, *Phys. Rev.* **D54** (1996) 3250.

[20] S. D. Rindani and M. M. Tung, *Phys. Lett.* **B424** (1998) 125.
S. Groote, J. G. Körner and M. M. Tung, *Z. Phys.* **C70** (1996) 281.
M. M. Tung, J. Bernabeu and J. Penarrocha, *Nucl. Phys.* **B470** (1996) 41.
M. M. Tung, *Phys. Rev.* **D52** (1995) 1353.
J. G. Körner, A. Pilaftsis and M. M. Tung, *Z. Phys.* **C63** (1994) 575.

[21] W. Bernreuther, J.P. Ma and T. Schröder, *Phys. Lett.* **B297** (1992) 318-326, S. Groorte and J.G. Körner, *Z. Phys.* **C72** (1996) 199.

[22] R. Harlander, M. Jezabek, J.H. Kuhn and T. Teubner, *Phys. Lett.* **B346** (1995) 137-142, R. Harlander, M. Jezabek, J.H. Kühn and M. Peter, *Z. Phys.* **C73** (1997) 477-494.

[23] J.D. Bjorken and M.C. Chen, *Phys. Rev.* **154** (1966) 1335.

[24] P. de Causmaecker, R. Gastmans, W. Troost, and T.T. Wu, *Phys. Lett.* **105B** (1981) 215; *Nucl. Phys.* **B206** (1982) 53; F. A. Berends, R. Kleiss, P. De Causmaecker, R. Gastmans, W. Troost, and T. T. Wu, *Nucl. Phys.* **B206** (1982) 61; *ibid.* **B239** (1984) 382; *ibid.* **B239** 395; *ibid.* **B264** (1986) 243; *ibid.* **B266** 265.

[25] Z. Xu, D.-H. Zhang and L. Chang, *Nucl. Phys.* **B291** (1987) 392.

[26] S. J. Parke and T. R. Taylor, *Phys. Lett.* **157B** (1985) 81;*Nucl. Phys.* **B269** (1986) 410.

[27] M.L. Mangano and S.J. Parke, *Phys. Rep.* **200** (1991) 301.

[28] F.A. Berends, P.H. Daverveldt and R. Kleiss, *Nucl. Phys.* **B253** (1985) 441; R. Kleiss and W.J. Stirling, *Nucl. Phys.* **B262** (1985) 235; C. Mana and M. Martinez, *Nucl. Phys.* **B287** (1987) 601.

[29] Howard E. Haber, *preprint* SCIPP-93-49, NSF-ITP-94-30 (1994).

[30] J. Bjorken and S. Drell, *Relativistic Quantum Mechanics*, (McGraw-Hill Book Company, New York, 1964).

[31] J. Kodaira and S. Parke, in private communication.

[32] G. Mahlon and S. Parke, *Phys. Rev.* **D58** (1998) 054015. (1991) 301.

[33] J.H. Kühn, A. Reiter and P.M. Zerwas, *Nucl. Phys* **B272** (1986) 560, M. Anselmino, P. Kroll adn B. Pire, *Phys. Lett* **B167** (1986) 113.

[34] S. Parke, *preprint* hep-ph/9802279, FERMILAB-Conf-98/056-T (1998).

[35] I. Bigi, Y. Dokshitzer, V. Khoze, J. Kühn and P. Zerwas, *Phys. Lett.* **B181** (1986) 157.

[36] M. Jeżabek and J. H. Kühn, *Phys. Lett.* **B329** (1994) 317-324, and references therein.

[37] J. H. Kühn, *Nucl. Phys.* **B237** (1984) 77-85.

[38] G. Mahlon and S. Parke, *Phys. Rev.* **D53** (1996) 4886-4896; *Phys. Lett.* **B411** (1997) 173-179.

[39] S. Parke, *preprint* hep-ph/9807573, FERMILAB-Conf-98/212-T (1998).

[40] M. Hori, Y. Kiyo and T. Nasuno, *Phys. Rev.* **D58** (1998) 014005.

[41] J. Kodaira, T. Nasuno and S. Parke, *Physical Review* **D 59** (1999) 014023.

[42] M. Hori, Y. Kiyo, J. Kodaira, T. Nasuno and S. Parke *preprint* hep-ph/9801370, HUPD-9801, FERMILAB-Conf-98/022-T (1998).

[43] G. Bhattacharyya and R.N. Mohapatra, *Phys. Rev.* **D54** (1996) 4204; J.F. Gunion, D.W. McKay and H. Pois, *Phys. Rev.* **D53** (1996) 1616; M. Carena, H.E. Habar and E. Nardi, *Phys. Lett.* **B355** (1995) 199.

[44] R. Harlander and M. Steinhauser, *Eur. Phys. J.* **C2** (1998) 151.

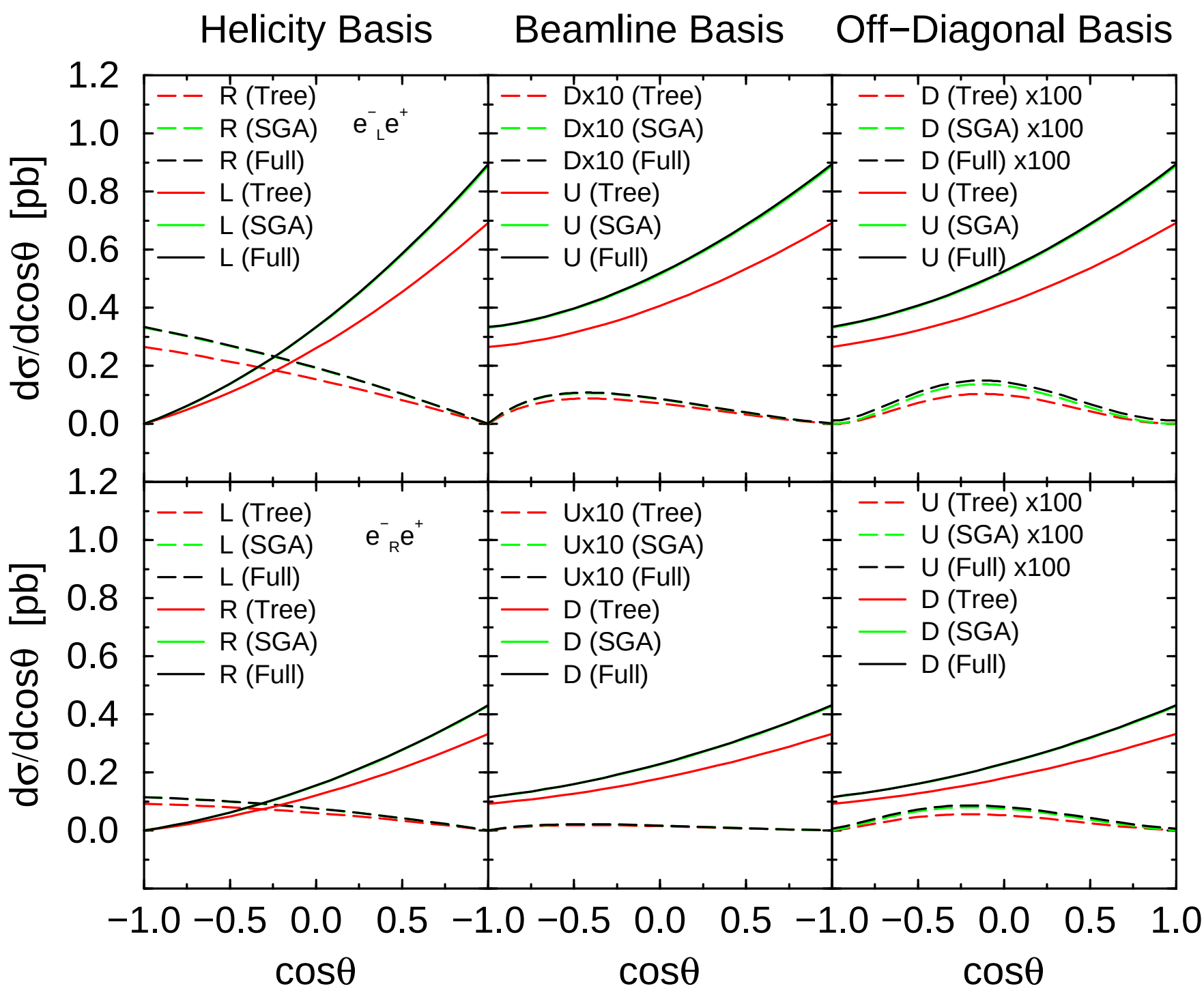
Helicity Basis
Beamline Basis
Off−Diagonal Basis
dσ/dcosθ [pb]
cosθ
R (Tree)
R (SGA)
R (Full)
L (Tree)
L (SGA)
L (Full)
e⁻Le+
Dx10 (Tree)
Dx10 (SGA)
Dx10 (Full)
U (Tree)
U (SGA)
U (Full)
D (Tree) x100
D (SGA) x100
D (Full) x100
U (Tree)
U (SGA)
U (Full)
L (Tree)
L (SGA)
L (Full)
R (Tree)
R (SGA)
R (Full)
e⁻Re+
Ux10 (Tree)
Ux10 (SGA)
Ux10 (Full)
D (Tree)
D (SGA)
D (Full)
U (Tree) x100
U (SGA) x100
U (Full) x100
D (Tree)
D (SGA)
D (Full)

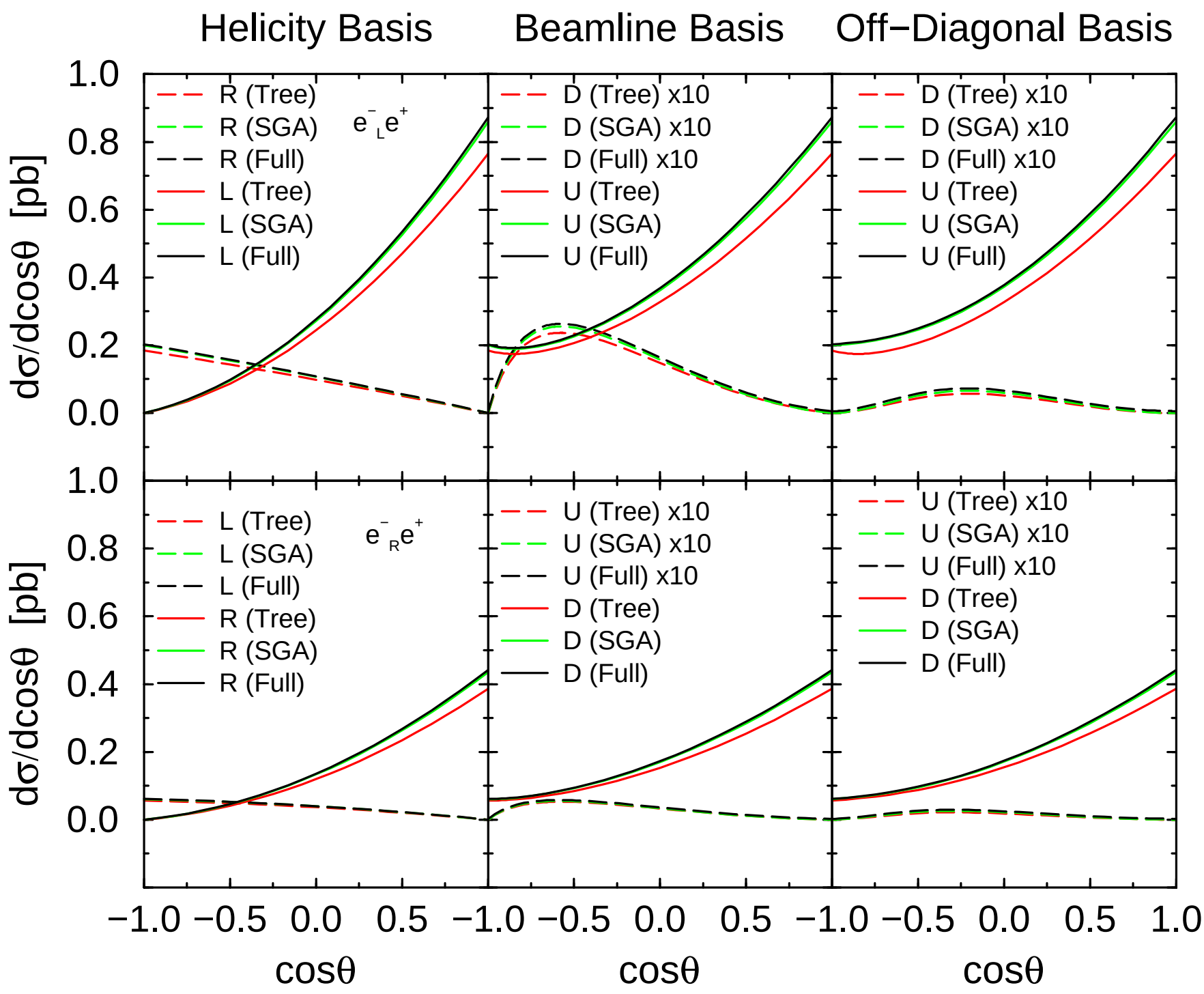
Helicity Basis
Beamline Basis
Off−Diagonal Basis
dσ/dcosθ [pb]
cosθ
R (Tree)
R (SGA)
R (Full)
L (Tree)
L (SGA)
L (Full)
e⁻Le⁺
D (Tree) x10
D (SGA) x10
D (Full) x10
U (Tree)
U (SGA)
U (Full)
L (Tree)
L (SGA)
L (Full)
R (Tree)
R (SGA)
R (Full)
e⁻Re⁺
U (Tree) x10
U (SGA) x10
U (Full) x10
D (Tree)
D (SGA)
D (Full)
1.0
0.8
0.6
0.4
0.2
0.0
−1.0
−0.5
0.0
0.5
1.0

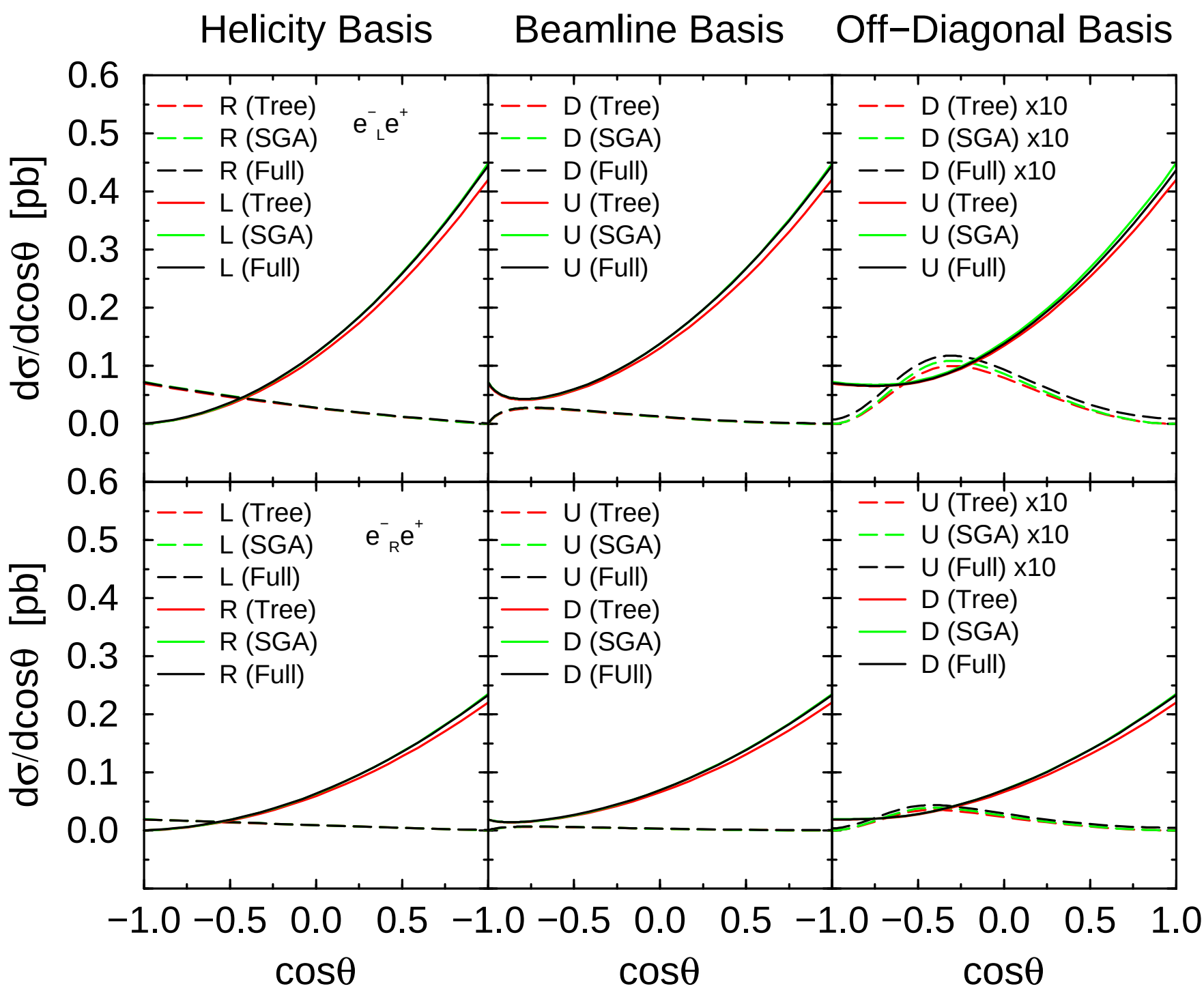
Helicity Basis
Beamline Basis
Off−Diagonal Basis
dσ/dcosθ [pb]
cosθ
R (Tree)
R (SGA)
R (Full)
L (Tree)
L (SGA)
L (Full)
e⁻Le+
D (Tree)
D (SGA)
D (Full)
U (Tree)
U (SGA)
U (Full)
D (Tree) x10
D (SGA) x10
D (Full) x10
U (Tree) x10
U (SGA) x10
U (Full) x10
e⁻Re+
D (FUll)

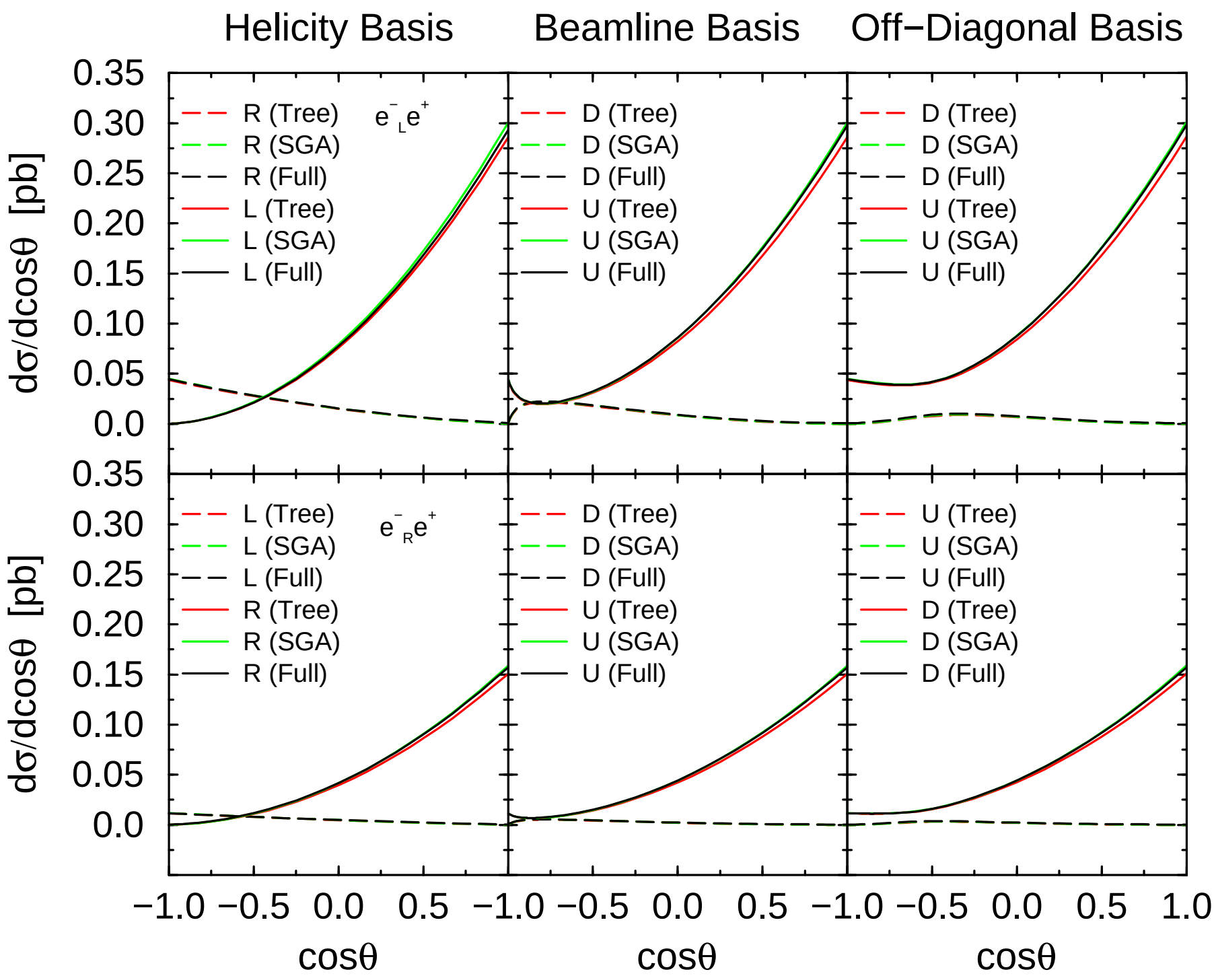
Helicity Basis
Beamline Basis
Off−Diagonal Basis
dσ/dcosθ [pb]
cosθ
e⁻L e⁺
e⁻R e⁺
R (Tree)
R (SGA)
R (Full)
L (Tree)
L (SGA)
L (Full)
D (Tree)
D (SGA)
D (Full)
U (Tree)
U (SGA)
U (Full)
0.35
0.30
0.25
0.20
0.15
0.10
0.05
0.0
−1.0
−0.5
0.0
0.5
1.0

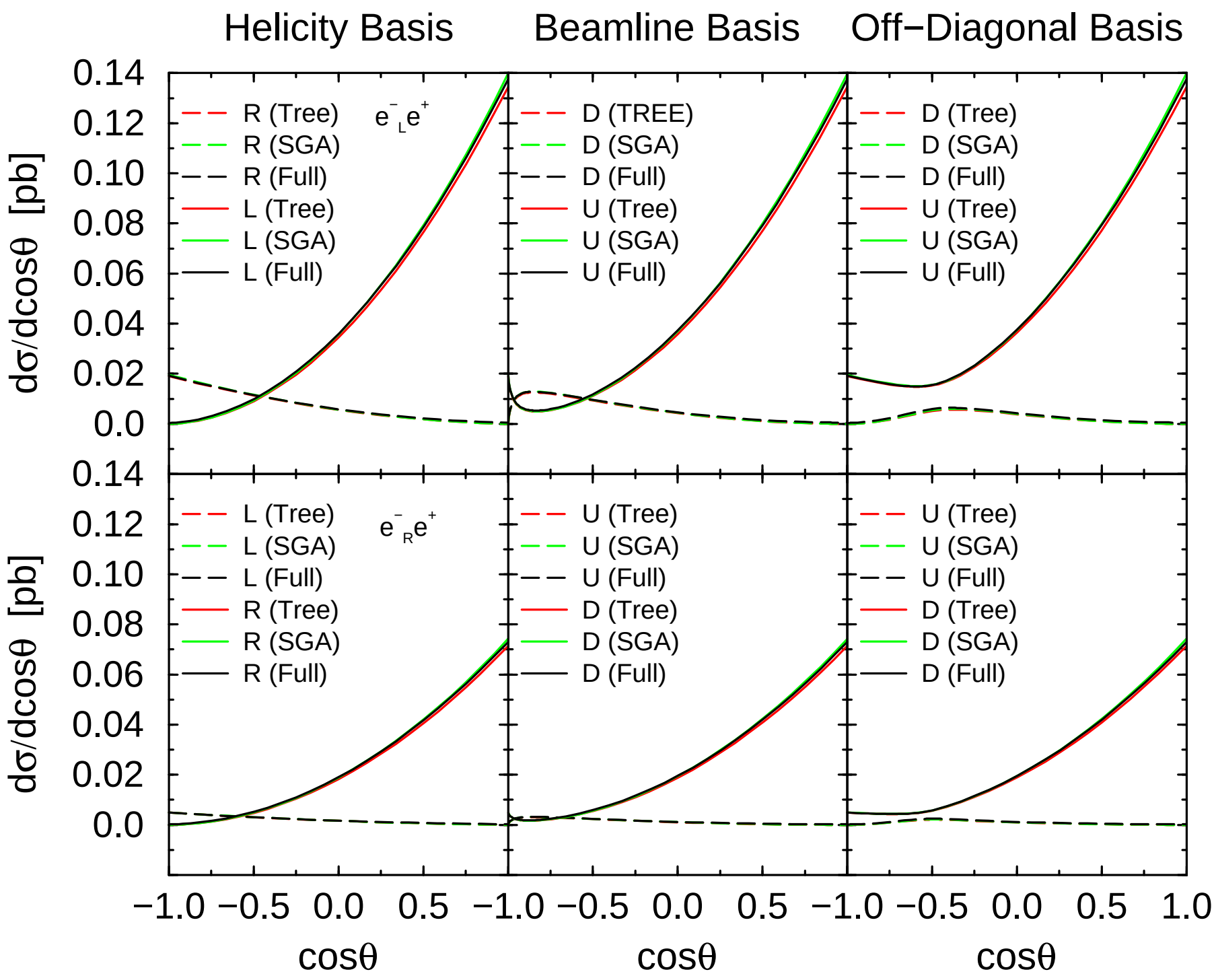
Helicity Basis
Beamline Basis
Off−Diagonal Basis
dσ/dcosθ [pb]
0.14
0.12
0.10
0.08
0.06
0.04
0.02
0.0
R (Tree)
R (SGA)
R (Full)
L (Tree)
L (SGA)
L (Full)
e⁻Le+
D (TREE)
D (SGA)
D (Full)
U (Tree)
U (SGA)
U (Full)
D (Tree)
D (SGA)
D (Full)
U (Tree)
U (SGA)
U (Full)
L (Tree)
L (SGA)
L (Full)
R (Tree)
R (SGA)
R (Full)
e⁻Re+
U (Tree)
U (SGA)
U (Full)
D (Tree)
D (SGA)
D (Full)
U (Tree)
U (SGA)
U (Full)
D (Tree)
D (SGA)
D (Full)
−1.0 −0.5 0.0 0.5 1.0
cosθ

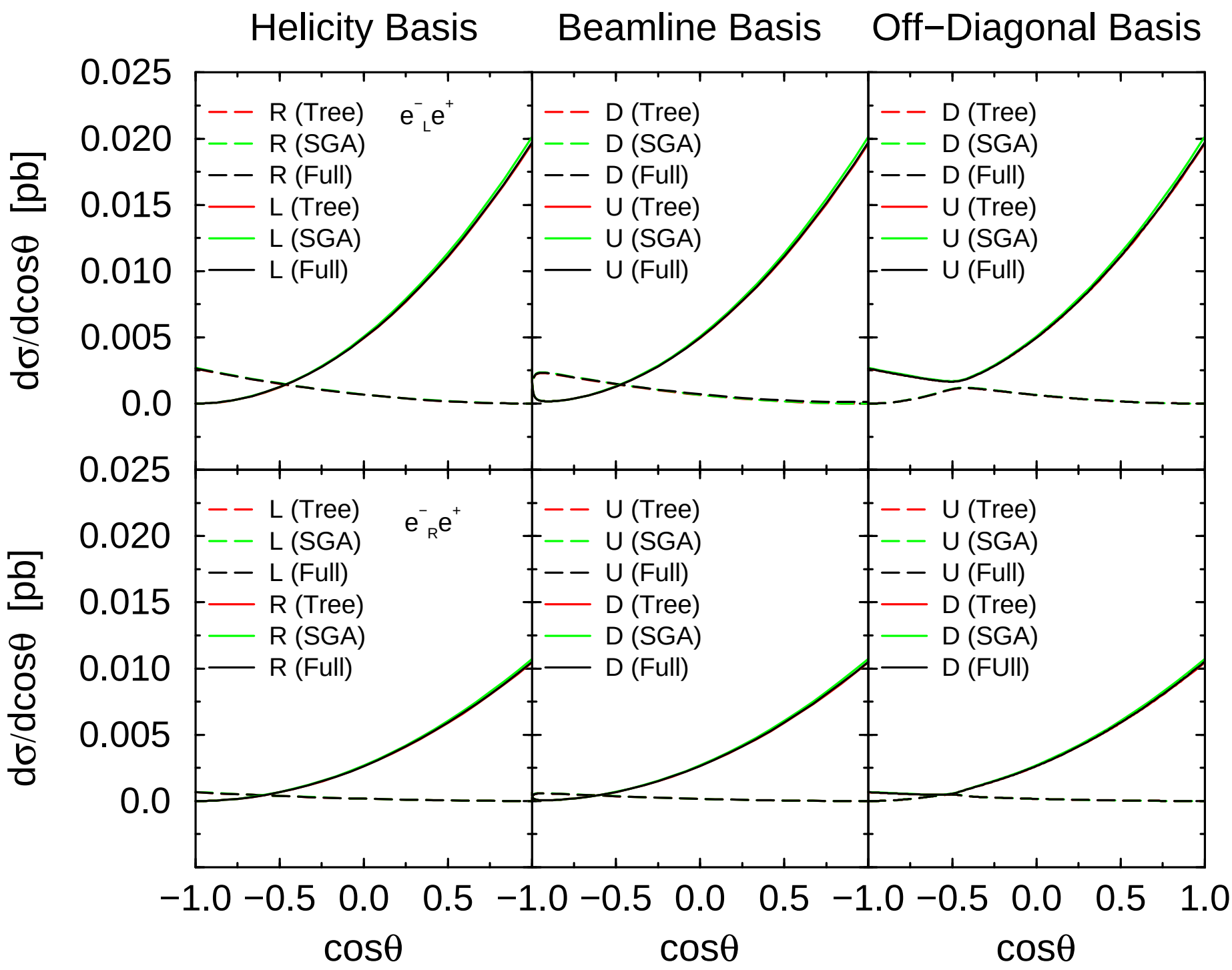
Helicity Basis
Beamline Basis
Off−Diagonal Basis
dσ/dcosθ [pb]
0.025
0.020
0.015
0.010
0.005
0.0
R (Tree)
R (SGA)
R (Full)
L (Tree)
L (SGA)
L (Full)
e⁻Le⁺
D (Tree)
D (SGA)
D (Full)
U (Tree)
U (SGA)
U (Full)
D (Tree)
D (SGA)
D (Full)
U (Tree)
U (SGA)
U (Full)
L (Tree)
L (SGA)
L (Full)
R (Tree)
R (SGA)
R (Full)
e⁻Re⁺
U (Tree)
U (SGA)
U (Full)
D (Tree)
D (SGA)
D (Full)
U (Tree)
U (SGA)
U (Full)
D (Tree)
D (SGA)
D (FUll)
−1.0 −0.5 0.0 0.5 1.0
cosθ

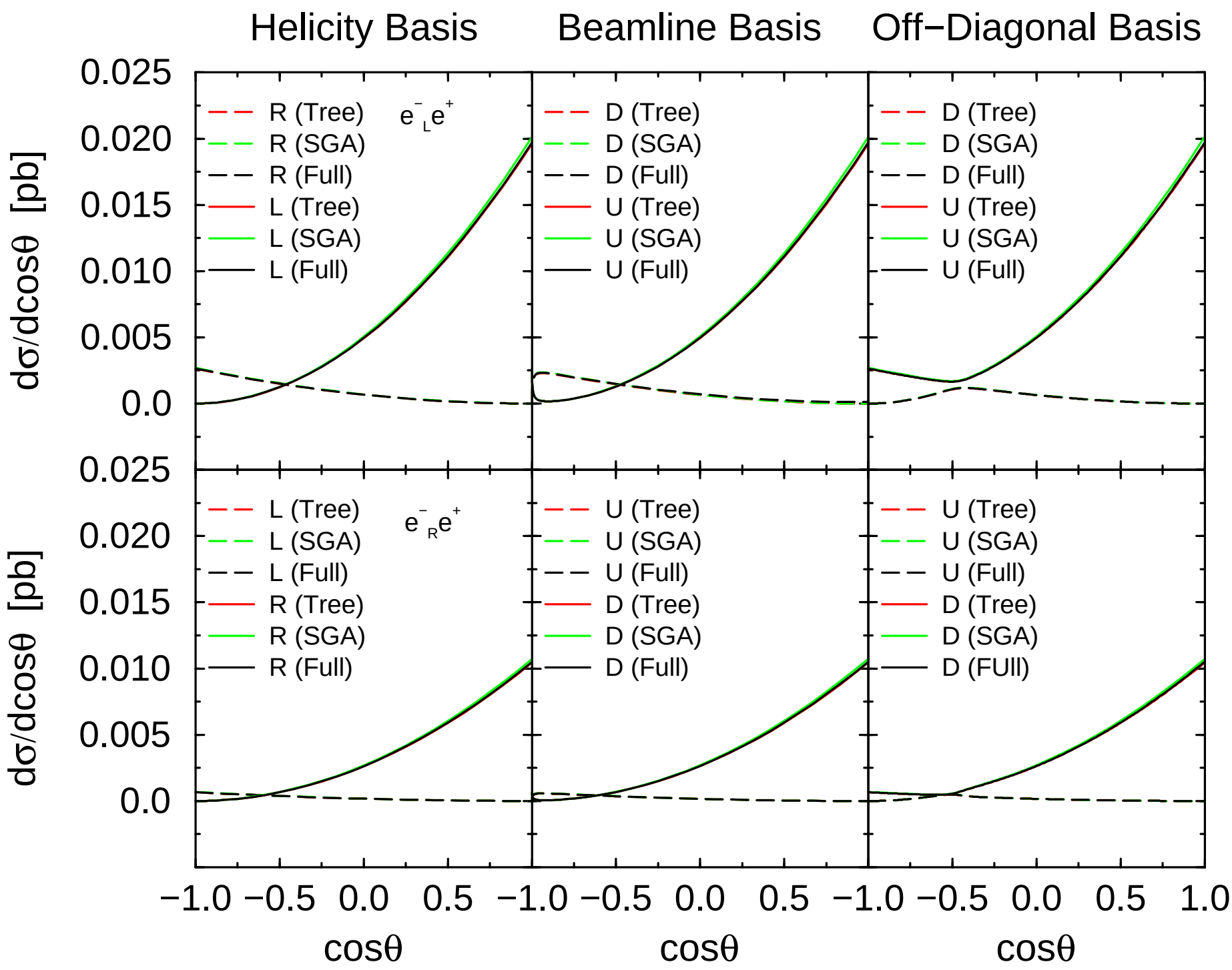
Helicity Basis
Beamline Basis
Off−Diagonal Basis
dσ/dcosθ [pb]
0.025
0.020
0.015
0.010
0.005
0.0
R (Tree)
R (SGA)
R (Full)
L (Tree)
L (SGA)
L (Full)
e⁻Le⁺
D (Tree)
D (SGA)
D (Full)
U (Tree)
U (SGA)
U (Full)
D (Tree)
D (SGA)
D (Full)
U (Tree)
U (SGA)
U (Full)
L (Tree)
L (SGA)
L (Full)
R (Tree)
R (SGA)
R (Full)
e⁻Re⁺
U (Tree)
U (SGA)
U (Full)
D (Tree)
D (SGA)
D (Full)
U (Tree)
U (SGA)
U (Full)
D (Tree)
D (SGA)
D (FUll)
−1.0 −0.5 0.0 0.5 1.0
cosθ

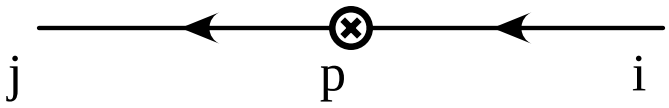
j
p
i

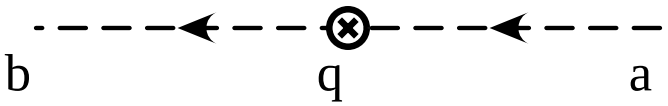
b
q
a

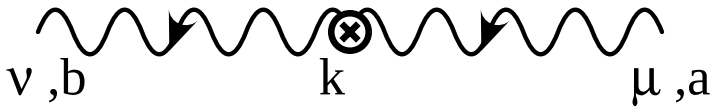
ν ,b
k
μ ,a

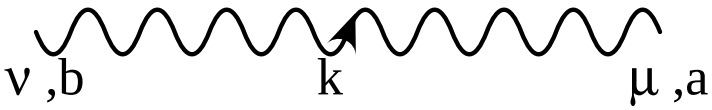
ν ,b
k
μ ,a

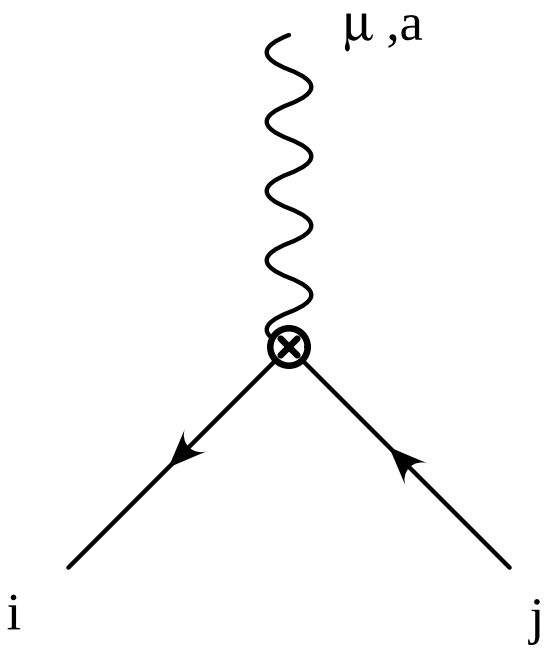
μ ,a
i
j

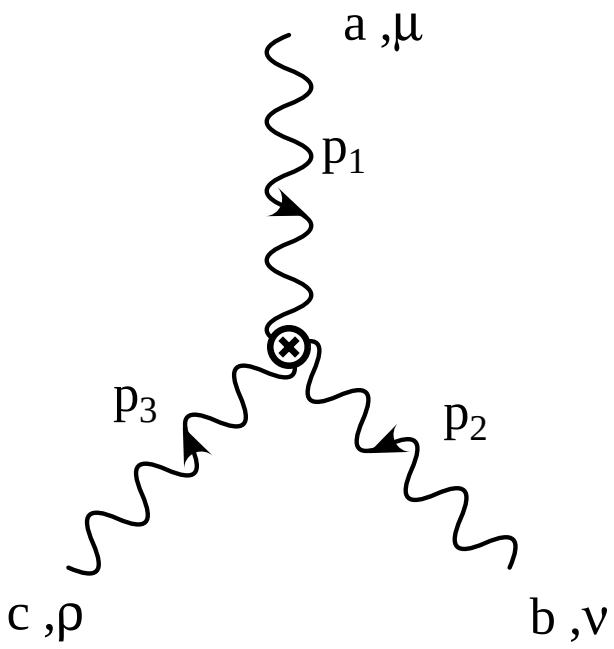
a ,μ
p1
p3
p2
c ,ρ
b ,ν

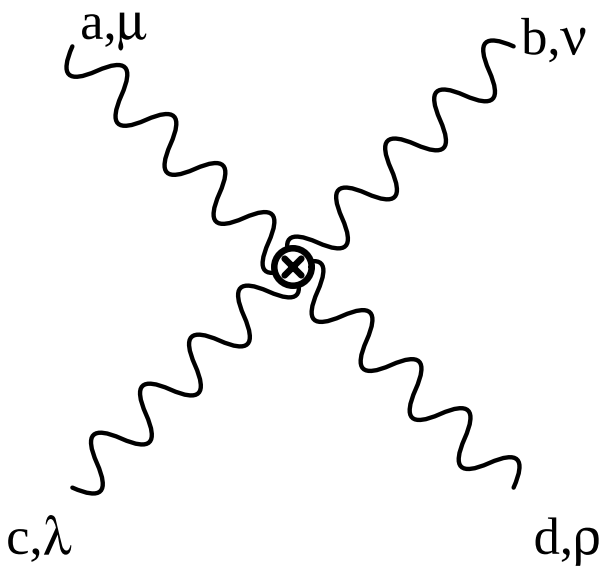
a,μ
b,ν
c,λ
d,ρ

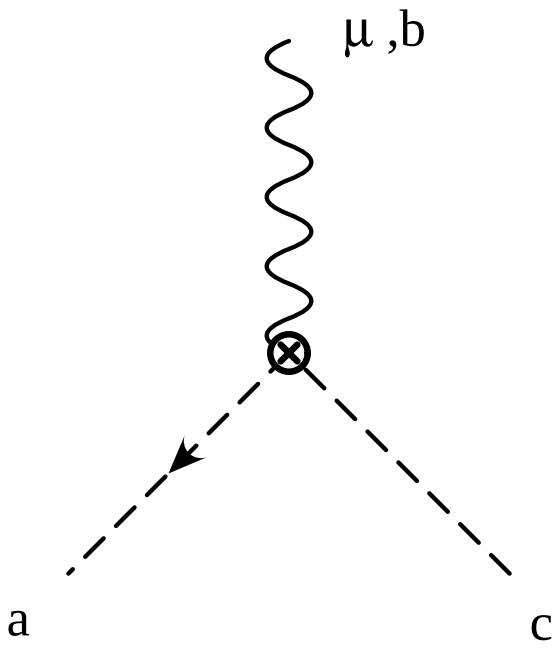
μ ,b
a
c